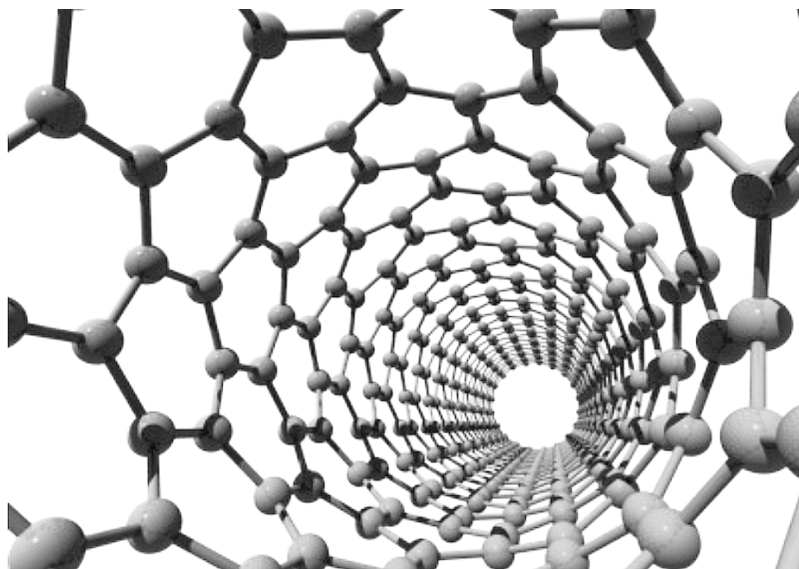


第 61 回
フラーレン・ナノチューブ・グラフェン
総合シンポジウム

The 61st Fullerenes–Nanotubes–Graphene
General Symposium



講演要旨集

Abstracts

2021 年 9 月 1 日(水) ~ 3 日(金)
オンラインバーチャルシンポジウム
Online Virtual Symposium

主催 フラーレン・ナノチューブ・グラフェン学会
The Fullerenes, Nanotubes and Graphene Research Society

共催 ・ **後援**
日本化学会

The Chemical Society of Japan

協賛

日本物理学会
応用物理学会
高分子学会
電気化学会

The Physical Society of Japan
The Japan Society of Applied Physics
The Society of Polymer Science, Japan
The Electrochemical Society of Japan

インテル® oneAPI 2021 ベース & HPC ツールキット

さまざまな解析処理、シミュレーションを高速化

振動解析、強度解析、熱流体解析や、それらのシミュレーションを高速化するには、プロセッサの性能を最大限に引き出すように開発する必要があります。

「インテル® oneAPI ベース & HPC ツールキット」は、多様なアーキテクチャに対応するコンパイラ、最適化済みライブラリ、性能解析ツール、デバッガなどを含む最新のツールスイートで、インテルの CPU、GPU、FPGA を含む、最新のプロセッサの性能を最大限に引き出すアプリケーションの開発を強力に支援します。インテル® Parallel Studio XE で開発したコードも活用できます。

■ CPU、GPU、FPGA で共通のプログラミング

現在の標準 C++ と Khronos SYCL* に拡張機能を加えた標準ベースのクロスアーキテクチャ言語、データ並列 C++ (DPC++) により、これまでの C/C++ プログラムから始めて、インテルの CPU、GPU、FPGA 向けに効率よく動作させることが可能なプログラムを作成できます。

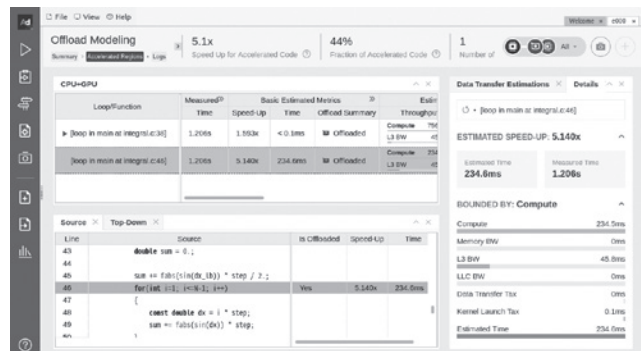
DPC++ 対応のインテル® oneAPI DPC++/C++ コンパイラ、OpenMP* ディレクティブによるオフロード機能でインテルの GPU を利用可能なベータ版インテル® Fortran コンパイラに加えて、従来のインテル® C++/Fortran コンパイラも含まれます。

すでに CUDA* で記述されたコードがある場合は、DPC++ への移行を支援するツールを利用できます。

対応ハードウェアがない場合も、インテルの開発サンドボックス環境、oneAPI 向けインテル® DevCloud (devcloud.intel.com/oneapi) (英語) を利用してインテルの GPU および FPGA 向けの開発をすぐに試せます。

■ 高速化の可能性と効果を検証

さまざまな性能解析 / デバッグツールにより、関数ごとの処理時間や、時系列の CPU と GPU、メモリー帯域幅の利用率など、調整個所の特定や対応方法の検討に役立つ情報が得られます。



インテル® Advisor で現在のプログラムの動作を分析し、代わりに GPU を演算に使う場合に予想される高速化について表示

「将来の高度なコンピューティングには、エクサスケール・クラスのワークロードに必要な演算能力を最大化するヘテロジニアス・ハードウェアが必要です。インテルが主導している oneAPI 業界イニシアチブにより、多様な計算アーキテクチャにおけるプログラミングは大幅に簡素化されるでしょう。」

アルゴンヌ国立研究所 計算機科学、環境科学、ライフサイエンス アソシエイト・ラボラトリー・ディレクター
シカゴ大学 コンピューター・サイエンス教授
Rick Stevens 博士

製品詳細、評価利用はこちらから
www.xlsoft.com/intel/fntg



高速化のための無料セミナー実施中
www.xlsoft.com/intel/seminar



製品の詳細に関するお問い合わせ先：

Abstract of The 61st Fullerenes-Nanotubes-Graphene General Symposium

Sponsored by: The Fullerenes, Nanotubes and Graphene Research Society

Co-Sponsored by: The Chemical Society of Japan

Supported by: The Physical Society of Japan
The Japan Society of Applied Physics
The Society of Polymer Science, Japan
The Electrochemical Society of Japan

Date: September 1st (Wed.) –3rd (Fri.), 2021

Place: Online Virtual Symposium

Presentation Time: Special Lecture (25 min presentation + 5 min discussion)
Invited Lecture (15 min presentation + 5 min discussion)
General Lecture (10 min presentation + 5 min discussion)
Poster Preview (1 min presentation without discussion)

第 61 回フラーレン・ナノチューブ・グラフェン総合シンポジウム 講演要旨集

主催: フラーレン・ナノチューブ・グラフェン学会

共催・後援: 日本化学会

協賛: 日本物理学会、応用物理学会、高分子学会、電気化学会

日時: 2021 年 9 月 1 日(水) ~ 9 月 3 日(金)

場所: オンラインバーチャルシンポジウム

発表時間: 特別講演 (発表 25 分 + 質疑応答 5 分)
招待講演 (発表 15 分 + 質疑応答 5 分)
一般講演 (発表 10 分 + 質疑応答 5 分)
ポスタープレビュー (発表 1 分・質疑応答 なし)

展示団体御芳名 (五十音順、敬称略)

santec(株)

テレダイ・ジャパン(株)

(株)日本レーザー

広告掲載団体御芳名 (五十音順、敬称略)

アイクストロン(株)

エクセルソフト(株)

(株)セントラル科学貿易

テレダイ・ジャパン(株)

日本電子(株)

(株)日本レーザー

フィルジェン(株)

Contents

Timetable	i
Chairpersons	ii
Program.....	iii
Abstracts	
Special Lecture	1
Invited Lecture	13
General Lecture	17
Poster.....	45
Author Index.....	133

目次

早見表	i
座長一覧	ii
プログラム	iii
講演予稿	
特別講演	1
招待講演	13
一般講演	17
ポスター発表.....	45
発表者索引	133

Timetable

Sep. 1 (Wed)

09:00 **Opening**
 09:05 **Poster preview I**
 09:50 **Poster session I**
 11:35 **Lunch**
 13:00 **Poster preview II**
 13:45 **Poster session II**
 15:30 **Poster preview III**
 16:15 **Poster session III**
 (18:00)

Special Lecture:

Presentation 25min
 Discussion 5min

Invited Lecture:

Presentation 15min
 Discussion 5min

General Lecture:

Presentation 10min
 Discussion 5min

Poster Preview:

Presentation 1min

Sep. 2 (Thu)

09:00 **CNT 30th Anniversary Session I**
 09:05 **Special lecture**
Sumio Iijima
 09:35 **Special lecture**
Lian-Mao Peng
 10:05 **Special lecture**
Riichiro Saito
 10:35 **Special lecture**
Shigeo Maruyama
 11:05 **Coffee break**
 11:20 **CNT 30th Anniversary Session II**
 11:25 **Invited lecture**
Takeshi Tanaka
 11:45 **Invited lecture**
Suguru Noda
 12:05 **Invited lecture**
Tsuyohiko Fujigaya
 12:25 **Lunch**
 13:20 **Award ceremony**
 13:45 **General meeting**
 14:15 **Coffee break**
 14:30 **Special lecture**
Cedric Huyghebaert
 15:00 **Special lecture**
Kaoru Toko
 15:30 **Oral session**
Graphene and 2D materials:
 - Applications
 - Others
 16:15 **Coffee break**
 16:30 **Special lecture**
Christophe Bichara
 17:00 **Oral session**
Carbon nanotubes:
 - Synthesis and growth
 18:30 **Banquet**
 (20:30)

Sep. 3 (Fri)

09:00 **Oral session - Osawa Award / Iijima Award Nominees**
Carbon nanotubes:
 - Chemistry
 - Applications
Graphene and 2D materials:
 - Optical property
 10:00 **Coffee break**
 10:15 **Special lecture**
Yuichiro K. Kato
 10:45 **Oral session**
Carbon nanotubes:
 - Applications
 - Transport property
 12:15 **Lunch**
 13:15 **Oral session**
Others:
 - Synthesis and growth
Fullerenes:
 - Chemistry
 13:45 **Special lecture**
Masato Sakano
 14:15 **Oral session**
Graphene and 2D materials:
 - Electronic structure
 - Others
 - Applications
 15:00 **Coffee break**
 15:15 **Special lecture**
Takao Sasagawa
 15:45 **Oral session**
Graphene and 2D materials:
 - Electronic structure
 - Transport property
 - Optical property
 16:30 **Coffee break**
 16:45 **Special lecture**
Yukiko Yamada-Takamura
 17:15 **Oral session**
Graphene and 2D materials:
 - Electronic structure
 - Synthesis and growth
 18:00 **Closing**
 (18:05)

座長一覧 (Chairpersons)

9月1日(水)

(敬称略)

セッション	時間	座長
ポスタープレビュー I	9:05 ~ 9:50	上野 裕 桐谷 乃輔
ポスタープレビュー II	13:00 ~ 13:45	田中 直樹 Hao-sheng Lin
ポスタープレビュー III	15:30 ~ 16:15	Lim Hong En 福島 知宏

9月2日(木)

セッション	時間	座長
CNT30周年記念セッション I	9:00 ~ 11:05	宮本 良之
CNT30周年記念セッション II	11:20 ~ 12:25	湯田坂 雅子
特別講演 (Cedric Huyghebaert)	14:30 ~ 15:00	吾郷 浩樹
特別講演 (都甲薫)	15:00 ~ 15:30	齋藤 理一郎
一般講演	15:30 ~ 16:15	蓬田 陽平
特別講演 (Christophe Bichara)	16:30 ~ 17:00	丸山 茂夫
一般講演	17:00 ~ 18:00	杉目 恒志

9月3日(金)

セッション	時間	座長
一般講演	9:00 ~ 10:00	若林 知成
特別講演 (加藤雄一郎)	10:15 ~ 10:45	齋藤 理一郎
一般講演	10:45 ~ 12:15	藤ヶ谷 剛彦
一般講演	13:15 ~ 13:45	岡田 晋
特別講演 (坂野昌人)	13:45 ~ 14:15	長汐 晃輔
一般講演	14:15 ~ 15:00	有江 隆之
特別講演 (笹川崇男)	15:15 ~ 15:45	長汐 晃輔
一般講演	15:45 ~ 16:30	竹延 大志
特別講演 (高村由起子)	16:45 ~ 17:15	長汐 晃輔
一般講演	17:15 ~ 18:00	若林 克法

Sep. 1 (Wed)

09:00~09:05 Opening

09:05~09:50 Poster preview I

1P-1 ~ 1P-29

09:50~11:35 Poster session I

1P-1 ~ 1P-29

9:50~ Odd number posters

10:45~ Even number posters

☆: Candidates for the Young Scientist Poster Award

Carbon nanotubes: Applications

☆**1P-1** Fabrication and hierarchical structure control of carbon nanotube electron field emitter for X-ray tube 45
**Kotaro Yasui, Hisashi Sugime, Hayato Ochi, Yuichi Nishikiori, Suguru Noda*

Carbon nanotubes: Electronic structure

☆**1P-2** Fabrication of nanostructures incorporating carbon nanotubes and one-dimensional confinement of charged excitons 46
**Haruna Nakajima, Taiki Inoue, Shohei Chiashi, Shigeo Maruyama, Keiji Ueno, Kenji Watanabe, Takashi Taniguchi, Ryo Kitaura*

Carbon nanotubes: Optical property

☆**1P-3** Efficient and Narrow-Linewidth Photoluminescence Devices Based on Single-Walled Carbon Nanotubes and Silicon Photonics 47
**Ryohei Imafuku, Naoto Higuchi, Hiroto Niiyama, Kenta Nakagawa, Hideyuki Maki*

Carbon nanotubes: Others

☆**1P-4** Machine learning assisted control of nanocarbon dispersion for optimal material and process design of electronics 48
**Shun Muroga, Ying Zhou, Takeo Yamada, Toshiya Okazaki, Kenji Hata*

Carbon nanotubes: Transport property

- ☆**1P-5** Air-Stable n-type of Single-Walled Carbon Nanotubes by Organic Boron Compounds 49
**Aoi Hamasuna, Naoki Tanaka, Tsuyohiko Fujigaya*

Fullerenes: Chemistry

- ☆**1P-6** Systematic structural study of cation-ordered pentavalent fullerides 50
**Keisuke Matsui, Kosmas Prassides*

Graphene and 2D materials: Electronic structure

- ☆**1P-7** Electron states tuning of bilayer graphene by intercalation and adsorption of corannulene 51
**Mina Maruyama, Susumu Okada*

Graphene and 2D materials: Optical property

- ☆**1P-8** The strain effect on van der Waals heterostructure 52
**Rei Usami*
- ☆**1P-9** Optical properties of transition metal dichalcogenides with microspherical optical cavity 53
**Mikio Kobayashi, Keisuke Shinokita, Naoki Wada, Takahiko Endo, Yasumitsu Miyata, Kazunari Matsuda*

Graphene and 2D materials: Transport property

- ☆**1P-10** Electrical Transport Properties of W₆Te₆ Nanowire Network Films 54
**Iori Kikuchi, Hiroshi Shimizu, Hong En Lim, Takahiko Endo, Yusuke Nakanishi, Yasumitsu Miyata, Jiang Pu, Taishi Takenobu*

Carbon nanotubes: Applications

- 1P-11** Antibody-conjugated polymer wrapped single-walled carbon nanotube for photothermal therapy via near-infrared light 55
**Yukiko Nagai, Kenta Nakamura, Jun Ohno, Tsuyohiko Fujigaya*
- 1P-12** Effect of dispersant on supported state and electrocatalytic properties of Pt nanoparticles on single-walled carbon nanotubes 56
**Yuho Abe, Hironori Ogata*

Carbon nanotubes: Synthesis and growth

- 1P-13** Catalyst-Free Synthesis of Highly-Crystalline Free-Standing Boron Nitride Nanotube Films 57
**Shuhui Wang, Ming Liu, Ya Feng, Keigo Otsuka, Esko I Kauppinen, Shohei Chiashi, Rong Xiang, Shigeo Maruyama*

1P-14	Influence of carbon source pyrolysis on high-temperature CNT growth from solid carbon growth seeds <i>*Mengyue Wang, Michiharu Arifuku, Noriko Kiyoyanagi, Masamitsu Satake, Taiki Inoue, Yoshihiro Kobayashi</i>	58
1P-15	Highly crystalline single-walled carbon nanotubes by microplasma-assisted gas-phase chemical vapor deposition <i>*Guohai Chen, Takashi Tsuji, Yoshiki Shimizu, Jaeho Kim, Hajime Sakakita, Kenji Hata, Don N. Futaba, Shunsuke Sakurai</i>	59
Carbon nanotubes: Transport property		
1P-16	Current-induced electrical path formation in random SWCNTs networks <i>*Naoki Koga, Yuuma Matsuura, Masaki Ozawa</i>	60
1P-17	Temperature Dependence of the Thermoelectric Conductivity L_{12} in Semiconducting SWCNTs with Controlled Chemical Potential <i>*Yota Ichinose, Akari Yoshida, Manaho Matsubara, Shigeki Saito, Kan Ueji, Yohei Yomogida, Takahiro Yamamoto, Kazuhiro Yanagi</i>	61
1P-18	Heat and charge-carrier flows in single-walled carbon nanotube film during a vertical electrolyte-gating <i>*Nobuhiro Muto, Kan Ueji, Yuya Matsuoka, Yota Ichinose, Yohei Yomogida, Takashi Yagi, Jana Zaumseil, Kazuhiro Yanagi</i>	62
Carbon nanotubes: Others		
1P-19	Dry Functionalization of Carbon Nanotubes While Retaining Intrinsic Properties <i>*Dewu Lin, Don Futaba, Kazufumi Kobashi, Kenji Hata</i>	63
1P-20	Aromaphilicity: the affinity for graphene and carbon nanotubes determined by experiments and simulations <i>*Atsushi Hirano, Tomoshi Kameda, Momoyo Wada, Takeshi Tanaka, Hiromichi Kataura</i>	64
Graphene and 2D materials: Applications		
1P-21	Photo-enhanced Responses of Gas Sensor Based on MoS ₂ Monolayers to Various Biogas Species <i>*Taishi Goto, Ryota Inao, Hiroshi Tabata, Osamu Kubo, Mitsuhiro Katayama</i>	65
Graphene and 2D materials: Electronic structure		
1P-22	Geometric structure and piezoelectric polarization of MoS ₂ nanoribbons under uniaxial strain <i>*Susumu Okada, Yanlin Gao, Mina Maruyama</i>	66

Graphene and 2D materials: Optical property

1P-23 Raman spectroscopy of Weyl semimetal $\text{Co}_3\text{Sn}_2\text{S}_2$ 67
**Kenya Tanaka, Akira Takakura, Yasumoto Segawa, Taishi Nishihara, Kazunari Matsuda, Yuhei Miyauchi*

1P-24 Helicity resolved Raman spectroscopy in MoS_2 68
**Hirofumi Nema, Yasuhiro Fujii, Shogo Saito, Eiichi Oishi, Akitoshi Koreeda*

Graphene and 2D materials: Transport property

1P-25 Quasi-ballistic heat transport in graphene elucidated by isotopic interface 69
**Yoshito Hata, Kuniharu Takei, Seiji Akita, Takayuki Arie*

1P-26 Switching speed of optically-generated spin current at the graphene edge 70
**Yuan Tian, M. Shoufie Ukhtary, Saito Riichiro*

Graphene and 2D materials: Synthesis and growth

1P-27 Metal Deposition on a Suspended Graphene Surface 71
**Yuta Kawase, Kenta Matsushima, Juntaro Doi, Shinichiro Mouri, Tsutomu Araki*

Others: Synthesis and growth

1P-28 Synthesis of Boron Nitride Nanotubes Using Solid Boron, Water Vapor, and Ammonia 72
**Takazumi Kaida, Hiromu Takahashi, Toshio Osawa, Hisashi Sugime, Suguru Noda*

1P-29 Indium intercalation in bundles of WTe atomic wires 73
**Hiroshi Shimizu, Zheng Liu, Hong En Lim, Yusuke Nakanishi, Takahiko Endo, Yasumitsu Miyata*

11:30~13:00 Lunch

13:00~13:45 Poster preview II

1P-30 ~ 1P-58

13:45~15:30 Poster session II

1P-30 ~ 1P-58

13:45~ Odd number posters

14:35~ Even number posters

☆: Candidates for the Young Scientist Poster Award

Carbon nanotubes: Applications

☆**1P-30** Carbon nanotube and boron nitride nanotube make battery lighter and safer 74
**Kentaro Kaneko, Keisuke Hori, Suguru Noda*

☆**1P-31** Chemically-enriched and integrated carbon nanotube 75
photo-thermoelectric scanners for non-sampling, source and label-free
chemical monitoring
**Kou Li, Yukio Kawano*

Carbon nanotubes: Optical property

☆**1P-32** Photoluminescence property changes of aryl-modified locally 76
functionalized single-walled carbon nanotubes by ortho-substituent effects
**Sadahito Naka, Tsuyohiko Fujigaya, Tomohiro Shiraki*

☆**1P-33** Pure and Efficient Single-Photon Sources by Shortening and 77
Functionalizing Air-Suspended Carbon Nanotubes
**Shuma Oya, Rintaro Kawabe, Hiroshi Takaki, Takayuki Ibi, Yutaka
Maeda, Kenta Nakagawa, Hideyuki Maki*

Carbon nanotubes: Synthesis and growth

☆**1P-34** In situ XAFS analysis of growth mechanism of single-walled carbon 78
nanotubes from Co-catalyst
**Shusaku Karasawa, Daiki Yamamoto, Kamal Sharma, Takahiro Saida,
Shigeya Naritsuka, Takahiro Maruyama*

Carbon nanotubes: Transport property

☆**1P-35** Comparison of anisotropic thermal conductivities in bundles of SWCNTs 79
at different temperature regions
**Hiromu Hamasaki, Takumi Kawase, Kaori Hirahara*

Graphene and 2D materials: Applications

- ☆**1P-36** Designing of self-assembled peptides as a molecular scaffold for graphene biosensor 80
**Shun Shimizu, Chishu Honma, Yoshiaki Sugizaki, Hideyuki Tomizawa, Yuhei Hayamizu*

Graphene and 2D materials: Electronic structure

- ☆**1P-37** Kelvin probe force microscopy study of MoS₂/MoSe₂ in-plane heterostructures 81
**Kazuki Hashimoto, Hong En Lim, Yusuke Nakanishi, Takahiko Endo, Yasumitsu Miyata*

Graphene and 2D materials: Optical property

- ☆**1P-38** Electrolyte-based transition metal dichalcogenide light-emitting devices with microcavity 82
**Soma Suzuki, Tomohiro Ogura, Takahiko Endo, Yasumitsu Miyata, Kenichi Yamashita, Jiang Pu, Taishi Takenobu*

Graphene and 2D materials: Others

- ☆**1P-39** Stacking angle-dependent intercalation in bilayer graphene 83
**Yuji Araki, Pablo Solís-Fernández, Kenji Kawahara, Hiroki Ago*

Carbon nanotubes: Applications

- 1P-40** Organic solar cells with semiconducting carbon nanotubes in the hole transport layer 84
**Daisuke Miyata, Yutaka Matsuo, Hao-sheng Lin, Soma Ishikawa, Takeshi Hashimoto, Satoru Hashimoto*

- 1P-41** Electrical characterization of carbon-nanotube thin film transistor based on direct deposition method 85
**Shugo Kogure, Ryo Mizuno, Hiromichi Kataura, Yutaka Ohno*

- 1P-42** Fabrication of SWCNT-BNNT field-effect transistors and evaluation of contact resistance 86
**Taiki Sugihara, Satoru Matsushita, Shu Sato, Keigo Otsuka, Taiki Inoue, Shohei Chiashi, Shigeo Maruyama*

Carbon nanotubes: Chemistry

- 1P-43** Modulating selectivity of 1,3-dipolar cycloaddition by carbon nanotube confinements: A dispersion-corrected density functional theory study 87
**Shuta Fukuura, Takashi Yumura*

Carbon nanotubes: Synthesis and growth

- 1P-44** Growth of high-density CNT forest by a self-assembled monolayer of iron oxide nanoparticles 88
**Yuga Kono, Kento Tabata, Takayuki Nakano, Yoku Inoue*
- 1P-45** Chemical vapor deposition growth of carbon layers on boron nitride nanotubes 89
**Taiki Inoue, Masakiyo Kato, Yungkai Chou, Yoshihiro Kobayashi*
- 1P-46** Double-walled carbon nanotube transparent conductor overcoming performance–yield tradeoff 90
**Jeong-Seok Nam, Qiang Zhang, Jiye Han, Sukanta Datta, Nan Wei, Er-Xiong Ding, Aqeel Hussain, Saeed Ahmad, Taher Khan, Yong-Ping Liao, Tavakkoli Mohammad, Bo Peng, Shigeo Maruyama, Hua Jiang, Il Jeon, Esko I. Kauppinen*
- 1P-47** Molecular Dynamics Simulation of Single-Walled Carbon Nanotube Growth from Metal Carbide Nanoparticles 91
**Ikuma Kohata, Ryo Yoshikawa, Kaoru Hisama, Keigo Otsuka, Shohei Chiashi, Shigeo Maruyama*

Fullerenes: Applications

- 1P-48** Synthesis of g-C₂N₂-[C₆₀] fullerene nanowhisker composites and their photocatalytic activity for degradation of rhodamine B 92
**Jeong Won Ko, Se Hwan Park, Sugyeong Jeon, Weon Bae Ko*

Fullerenes: Chemistry

- 1P-49** Synthesis and Characterization of Li-Encapsulated PCBM (Li@PCBM): the First Li@C₆₀ Derivative 93
**Hiroshi Ueno, Daiki Kitabatake, Hao-Sheng Lin, Yue Ma, Il Jeon, Fuminori Misaizu, Shigeo Maruyama, Yutaka Matsuo*

Fullerenes: Optical property

- 1P-50** Molecular IR emission of C₆₀ and C₇₀ thin plates 94
**Tomonari Wakabayashi, Kazuki Wakebe, Miho Hatanaka, Takeshi Kodama*

Graphene and 2D materials: Applications

- 1P-51** Spin current generation by edge plasmon in graphene ribbon 95
**Muhammad Shoufie Ukhtary, Yuan Tian, Riichiro Saito*
- 1P-52** One-step synthesis of Mo₂C composite film on Mo substrate and evaluation of HER catalytic activities 96
**Shunsuke Numata, Hironori Ogata*

1P-53	Schottky barrier height control by reducing Fermi level pinning effect between the single-layer WS ₂ and ITO electrodes for high-performance transparent solar cells <i>*Xing He, Toshiro Kaneko, Toshiaki Kato</i>	97
Graphene and 2D materials: Chemistry		
1P-54	Confinement of Hydrogen Nanobubble between Graphene and Au Surface by Electrocatalytic Hydrogen Evolution Reaction <i>*Tomohiro Fukushima, Takaha Komai, Ruifeng Zhou, Kei Murakoshi</i>	98
Graphene and 2D materials: Synthesis and growth		
1P-55	Lateral growth of twisted graphene on graphene/SiC template in a continuous vacuum environment <i>*Yao Yao, Taiki Inoue, Royta Negishi, Makoto Takamura, Yoshitaka Taniyasu, Yoshihiro Kobayashi</i>	99
1P-56	Wire-to-Ribbon Conversion in Transition Metal Chalcogenides <i>*Hong En Lim, Zheng Liu, Jiang Pu, Hiroshi Shimizu, Takahiko Endo, Yusuke Nakanishi, Taishi Takenobu, Yasumitsu Miyata</i>	100
Others: Synthesis and growth		
1P-57	Improved synthesis of WS ₂ nanotubes with relatively small diameters by tuning sulfurization timing and reaction temperature <i>*Md. Ashiqur Rahman, Yohei Yomogida, Mai Nagano, Ryoga Tanaka, Yasumitsu Miyata, Kazuhiro Yanagi</i>	101
1P-58	Molecular dynamics study on open-edge growth of boron nitride nanotubes from single-walled carbon nanotube template <i>*Kaoru Hisama, Ksenia Bets, Nitant Gupta, Yongjia Zheng, Rong Xiang, Keigo Otsuka, Shohei Chiashi, Boris Yakobson, Shigeo Maruyama</i>	102

15:30~16:15 Poster preview III

1P-59 ~ 1P-87

16:15~18:00 Poster session III

1P-59 ~ 1P-87

16:15~ Odd number posters

17:10~ Even number posters

☆: Candidates for the Young Scientist Poster Award

Carbon nanotubes: Optical property

☆**1P-59** Avidin-biotin interactions on locally functionalized single-walled carbon nanotubes for photoluminescence wavelength shifts 103

**Yoshiaki Niidome, Rie Wakabayashi, Masahiro Goto, Tsuyohiko Fujigaya, Tomohiro Shiraki*

☆**1P-60** Circular dichroism spectra of Helicity-sorted Single-wall Carbon Nanotubes with Controlled Chemical Potential 104

**Yuuya Hosokawa, Yohei Yomogida, Kazuhiro Yanagi*

Carbon nanotubes: Synthesis and growth

☆**1P-61** Growth mechanism and handedness relation of 1D SWCNT-BNNT van der Waals heterostructures 105

**Yongjia Zheng, Akihito Kumamoto, Kaoru Hisama, Keigo Otsuka, Yuta Sato, Taiki Inoue, Shohei Chiashi, Daiming Tang, Qiang Zhang, Anton Anisimov, Esko I. Kauppinen, Kazu Suenaga, Yuichi Ikuhara, Rong Xiang, Shigeo Maruyama*

Carbon nanotubes: Transport property

☆**1P-62** Electrical conductivity and magnetoresistance of SWCNT thin films under ionic-liquid gating 106

**Hiroki Date, Takenori Fujii, Taiki Inoue, Esko Kauppinen, Shigeo Maruyama, Shohei Chiashi*

Graphene and 2D materials: Optical property

☆**1P-63** Optical Spin Hall Effect in Few-Layered NbSe₂: Spin Hall Angle and Temperature Effect 107

**Ren Habara, Katsunori Wakabayashi*

☆**1P-64** Anomalous Photovoltaic Effect in Strained Monolayer WS₂ 108

**Takahashi Togo, Jiang Pu, Takahiko Endo, Yasumitsu Miyata, Taishi Takenobu*

Graphene and 2D materials: Chemistry

- ☆**1P-65** Controlled surface etching of multilayer hBN 109
**Hsin Yi, Pablo Solís-Fernández, Hiroki Ago*

Graphene and 2D materials: Synthesis and growth

- ☆**1P-66** Nano ~ sub-nanometer-width one-dimensional quantum wells embedded 110
in two-dimensional semiconductors
**Nanami Ichinose, Liu Zheng, Takashi Taniguchi, Kenji Watanabe, Ryo Kitaura*

Graphene and 2D materials: Transport property

- ☆**1P-67** N-type polar transition of p-type MoS₂ by chemical doping 111
**Hiroto Ogura, Yoshiyuki Nonoguchi, Shaochun Zhang, Yusuke Nakanishi, Hong En Lim, Ryo Kitaura, Kosuke Nagashio, Yasumitsu Miyata*
- ☆**1P-68** Nonlinear anomalous Hall effect in trigonal superconductor PbTaSe₂ 112
**Yuki Itahashi, Toshiya Ideue, Shintaro Hoshino, Chihiro Goto, Hiromasa Namiki, Takao Sasagawa, Yoshihiro Iwasa*

Carbon nanotubes: Applications

- 1P-69** Thermal properties of MWNT coatings for solar collector 113
**Hiroshi Furuta, Shimon Honda, Md. Saiful Islam, Akimitsu Hatta*
- 1P-70** Electrical and mechanical property of homogeneous CNT/Cu composite 114
wire made from copper nanoparticles decorated spin capable CNT forest
**Kosuke Tanaka, Takayuki Nakano, Yoku Inoue*

Carbon nanotubes: Optical property

- 1P-71** Spectroscopic ellipsometry on single-chirality-enriched carbon nanotube 115
membranes
**Hengkai Wu, Taishi Nishihara, Akira Takakura, Kazunari Matsuda, Takeshi Tanaka, Hiromichi Kataura, Yuhei Miyauchi*
- 1P-72** Comparison between high harmonic generation in metallic single-walled 116
carbon nanotubes and graphene
**Hiroyuki Nishidome, Kohei Nagai, Kento Uchida, Kenji Kawahara, Junko Eda, Hitomi Okubo, Yohei Yomogida, Hiroki Ago, Koichiro Tanaka, Kazuhiro Yanagi*
- 1P-73** Near infrared photoluminescence from locally functionalized 117
single-walled carbon nanotubes synthesized using bisaryl modifiers with
short linkage structures
**Tomohiro Shiraki, Haruka Aoki, Tsuyohiko Fujigaya*

Carbon nanotubes: Synthesis and growth

- 1P-74** Growth of single-walled carbon nanotubes from Ir catalyst on alumina buffer layer prepared by dip-coating process 118
**Shu Kondo, Daiki Yamamoto, Kamal Sharma, Takahiro Saida, Shigeya Naritsuka, Takahiro Maruyama*
- 1P-75** Comparison of single-walled carbon nanotube growth with Ir catalyst on SiO₂ layer prepared by different methods: Sputtering method vs thermal oxidation 119
**Daiki Yamamoto, Shu kondo, Kamal Sharma, Takahiro Saida, Shigeya Narituka, Takahiro Maruyama*
- 1P-76** Quantitative crystallinity investigation of carbon nanotubes produced by plasma-assisted gas-phase synthesis using far-infrared spectroscopy 120
**Takashi Tsuji, Kazufumi Kobashi, Guohai Chen, Jaeho Kim, Hajime Sakakita, Yoshiki Shimizu, Kenji Hata, Don Futaba, Shunsuke Sakurai*
- 1P-77** The effect of oxidants on SWCNT growth analyzed by isotope labeling technique 121
**Ryoya Ishimaru, Keigo Otsuka, Taiki Inoue, Shohei Chiashi, Shigeo Maruyama*

Fullerenes: Others

- 1P-78** Production of atom-encapsulated C₆₀ by ns laser induced breakdown 122
**Moeno Maejima, Haruo Shiromaru, Tomonari Wakabayashi, Koichi Kikuchi, Yohji Achiba, Takeshi Kodama*
- 1P-79** Study of magnetic properties of Er-dimetallofullerene anions 123
**Naoya Fujita, Aichi Yamashita, Yoshikazu Mizuguchi, Koichi Kikuchi, Yohji Achiba, Takeshi Kodama*
- 1P-80** The cage dependence of single molecule magnet properties of Tb-dimetallofullerene anions: [Tb₂@C₈₀(I_h)]⁻ and [Tb₂@C₇₈(D_{3h})]⁻ 124
**Kazuki Yamagishi, Aichi Yamashita, Yoshikazu Mizuguchi, Ryuji Higashinaka, Yuji Aoki, Koichi Kikuchi, Yohji Achiba, Takeshi Kodama*

Graphene and 2D materials: Applications

- 1P-81** Modulation of electronic states in two-dimensional semiconductors by bowl-shaped molecules. 125
**Shotaro Yotsuya, Akito Fukui, Akihiro Tsurusaki, Takeshi Yoshimura, Norifumi Fujimura, Daisuke Kiriya*
- 1P-82** Diffusion of Oxygen Atom on Single Layer of Graphene Sheet with Atomic Vacancy V6 for Graphene Oxide as ReRAM devices 126
**Takazumi Kawai*

Graphene and 2D materials: Transport property

- 1P-83** Modulation of electronic properties of graphene by B⁺ / N⁺ beam irradiation 127
**Takumi Hidaka, Yasushi Ishiguro, Kosuke Nakamura, Tomoaki Nishimura, Kazuyuki Takai*
- 1P-84** Application of the energy exchange eHEX algorithm to thermal transport 128
in 2 layers hBN system in molecular dynamics calculations
**Tatiana Zolotoukhina, Yusuke Michisuji, Wataru Yuhara*

Others: Others

- 1P-85** Aggregates of Elementary Diamond Nanoparticles in Their Aqueous 129
Colloidal Solutions Induced by Trace Ions
**Masaya Nemoto, Toshihiko Tanaka, Yasuhiro F. Miura, Tetsuya Aoyama, Kazunori Miyamoto, Atsuya Muranaka, Masanobu Uchiyama, Eiji Osawa*

Others: Synthesis and growth

- 1P-86** Synthesis and properties of fluorescent carbon quantum dots using lignin 130
**Takaki Yoda, Hironori Ogata*
- 1P-87** Synthesis of Boron Nitride Nanotubes Using Mist of Boric Acid Aqueous 131
Solution as a Low-Cost Boron Source
**Sota Ebisu, Tetsuro Sawada, Toshio Osawa, Hisashi Sugime, Suguru Noda*

Sep. 2 (Thu)

09:00~10:35	CNT 30th Anniversary Session I	
09:00~09:05	Introduction <i>Yoshiyuki Miyamoto</i>	
09:05~09:35	Special lecture	
2S-1	Discovery of carbon nanotubes <i>*Sumio Iijima</i>	1
09:35~10:05	Special lecture	
2S-2	Carbon Nanotube based high performance CMOS and RF devices operating in terahertz regime <i>*Lian-Mao Peng</i>	2
10:05~10:35	Special lecture	
2S-3	30 years of nanotubes with FNTG Society <i>*Riichiro Saito</i>	3
10:35~11:05	Special lecture	
2S-4	Perspective of carbon nanotubes research celebrating the 30th Anniversary <i>*Shigeo Maruyama</i>	4
11:05~11:20	Coffee break	
11:20~12:25	CNT 30th Anniversary Session II	
11:20~11:25	Introduction <i>Masako Yudasaka</i>	
11:25~11:45	Invited lecture	
2I-1	Separation of single-wall carbon nanotubes by polysaccharide gels and their applications. <i>*Takeshi Tanaka</i>	13

11:45~12:05	Invited lecture	
2I-2	Progresses and future challenges of carbon nanotube production <i>*Suguru Noda</i>	14
12:05~12:25	Invited lecture	
2I-3	Developments of the Carbon Nanotube Applications based on Molecular Adsorption <i>*Tsuyohiko Fujigaya</i>	15
12:25~13:20	Lunch	
13:20~13:45	Award ceremony	
13:45~14:15	General meeting	
14:15~14:30	Coffee break	
Graphene and 2D materials: Applications		
14:30~15:00	Special lecture	
2S-5	2D Materials: Integration Challenges for Future Electronics <i>*Cedric Huyghebaert</i>	5
Graphene and 2D materials: Synthesis and growth		
15:00~15:30	Special lecture	
2S-6	Layer-exchange synthesis of multilayer graphene for flexible battery anodes <i>*Kaoru Toko</i>	6
Graphene and 2D materials: Applications		
15:30~15:45		
2-1	Cationic nitrogen-doped graphene as a p-type modifier for high-performance PEDOT:PSS hole transporters in organic solar cells <i>*Hao-Sheng Lin, Takuhei Kaneko, Soma Ishikawa, Sangwoo Chae, Takumi Yana, Nagahiro Saito, Yutaka Matsuo</i>	17

Graphene and 2D materials: Others

15:45~16:00

- 2-2** “Ultramixing”: A Simple and Effective Method to Obtain Controlled and Stable Dispersions of Graphene Oxide in Cell Culture Media 18
**Giacomo Reina, Amalia Ruiz, Diane Murera, Yuta Nishina, Alberto Bianco*

Graphene and 2D materials: Applications

16:00~16:15

- 2-3** pH dependence of electrical response in graphene biosensors functionalized by self-assembled peptides 19
**Chishu Homma, Yoshiaki Sugizaki, Hideyuki Tomizawa, Yuhei Hayamizu*

16:15~16:30 Coffee break

Carbon nanotubes: Synthesis and growth

16:30~17:00 Special lecture

- 2S-7** Nucleation and growth of SWNTs are driven by the dynamics of their edge 7
**Christophe Bichara*

17:00~17:15

- 2-4** Single chirality separation of metallic single-wall carbon nanotubes using gel-column chromatography 20
**Hiromichi Kataura, Mayumi Tsuzuki, Takeshi Tanaka*

17:15~17:30

- 2-5** Design of multi-step gas-phase CVD reactor for the synthesis of high-quality single-walled carbon nanotube 21
**Shunsuke Sakurai, Takashi Tsuji, Guohai Chen, Maho Yamada, Jaeho Kim, Hajime Sakakita, Yoshiki Shimizu, Kenji Hata, Don Futaba*

17:30~17:45

- 2-6** O₂ assisted growth of small-diameter vertically-aligned SWCNTs using Os catalyst 22
**Kamal Prasad Sharma, Masaya Kobayashi, Daiki Yamamoto, Takahiro Maruyama*

17:45~18:00

- 2-7** Synthesis and Characterization of Various One-dimensional van der Waals Heterostructures 23
**Wanyu Dai, Yongjia Zheng, Keigo Otsuka, Shohei Chiashi, Rong Xiang, Shigeo Maruyama*

Sep. 3 (Fri)

9:00~10:00 Osawa Award / Iijima Award Nominees

Carbon nanotubes: Chemistry

09:00~09:20

- ◆3-1** Chirality isolation of single-walled carbon nanotubes by the phase transition of a thermoresponsive polymer 24
*Eriko Shimura, Tomomi Tanaka, Yuki Kuwahara, Takeshi Saito, Toshiki Sugai, *Shota Kuwahara*

Carbon nanotubes: Applications

09:20~09:40

- ◆3-2** Patterning and Photo-thermal Sensing Applications of Suspended, 2D, Micro-scale CNT film array 25
**Daichi Suzuki, Nao Terasaki*

Graphene and 2D materials: Optical property

09:40~10:00

- ◆3-3** Novel excitonic features of moiré exciton in twisted van der Waals heterostructures 26
**Keisuke Shinokita, Yuhei Miyauchi, Kenji Watanabe, Takashi Taniguchi, Kazunari Matsuda*

10:00~10:15 Coffee break

Carbon nanotubes: Optical property

10:15~10:45 Special lecture

- 3S-1** Deterministic transfer of optical-quality carbon nanotubes for atomically defined technology 8
*Keigo Otsuka, Nan Fang, Daiki Yamashita, Takashi Taniguchi, Kenji Watanabe, *Yuichiro K. Kato*

Carbon nanotubes: Applications

10:45~11:00

- 3-4** Controlled Removal of Surfactants from Double-Walled Carbon Nanotubes for Stronger p-Doping Effect and its Demonstration in Perovskite Solar Cells 27
**Jeong-Seok Nam, Ahmed Shawky, Seungju Seo, Rong Xiang, Yutaka Matsuo, Shigeo Maruyama, Il Jeon*

11:00~11:15

- 3-5** Carbon Nanotube Mask Filters and their Hydrophobic Barrier and Hyperthermic Antiviral Effects on SARS-CoV-2 28
**Sangsu Lee, Jeong-Seok Nam, Jiye Han, Qiang Zhang, Esko I. Kauppinen, Il Jeon*

11:15~11:30

- 3-6** Output power enhancement of stretchable, transparent triboelectric nanogenerator by charge trapping layer 29
**Masahiro Matsunaga, Jun Hirotsu, Yutaka Ohno*

11:30~11:45

- 3-7** Improvement in Thermal Diffusivity of CNT/Polymer Composite Films via Orienting CNTs by Robotic Dispenser 30
**Nikita Kumari, Ryo Abe, Naofumi Okamoto, Manish Pandey, Masakazu Nakamura*

Carbon nanotubes: Transport property

11:45~12:00

- 3-8** Hall effect in gated single-wall carbon nanotube films 31
**Yohei Yomogida, Kanako Horiuchi, Ryotaro Okada, Hideki Kawai, Yota Ichinose, Hiroyuki Nishidome, Kan Ueji, Natsumi Komatsu, Weilu Gao, Junichiro Kono, Kazuhiro Yanagi*

12:00~12:15

- 3-9** Intuitive Correlations between Heat and Charge-Carrier Flows in Vertical Devices Using Single-Walled Carbon Nanotube Films 32
**Kan Ueji, Nobuhiro Muto, Yuya Matsuoka, Yota Ichinose, Yohei Yomogida, Takashi Yagi, Jana Zaumseil, Kazuhiro Yanagi*

12:15~13:15 Lunch

Others: Synthesis and growth

13:15~13:30

- 3-10** Dispersed 2.6nm quasi-spherical diamond particles: A versatile starting material in nanotechnology 33
**Eiji Osawa, Toshihiko Tanaka, Amanda Barnard*

Fullerenes: Chemistry

13:30~13:45

- 3-11** Self-Assembled Organofullerene Nano- and Microspheres Containing Inorganic and Biological Nanoparticles 34
**Koji Harano, Ryosuke Sekine, Prince Ravat, Haruaki Yanagisawa, Chao Liu, Masahide Kikkawa, Eiichi Nakamura*

Graphene and 2D materials: Electronic structure

13:45~14:15 Special lecture

- 3S-2** Direct observation of the layer-number-dependent electronic structure in few-layer WTe₂ 9
**Masato Sakano*

14:15~14:30

- 3-12** Carrier density tuning of Nb-doped WSe₂ by an external electric field 35
**Kaoru Hisama, Yanlin Gao, Mina Maruyama, Ryo Kitaura, Susumu Okada*

Graphene and 2D materials: Others

14:30~14:45

- 3-13** Enhancement of the Thermal Conductance on Artificially Stacked MoS₂ by Intercalation 36
*Wenyu Yuan, Kan Ueji, Takashi Yagi, Takahiko Endo, Hong En Lim, Yasumitsu Miyata, Yohei Yomogida, *Kazuhiro Yanagi*

Graphene and 2D materials: Applications

14:45~15:00

- 3-14** Edge States of Graphene Oxide Observed by Field Emission and Field Ion Microscopy 37
**Yahachi Saito, Yuta Nishina*

15:00~15:15 Coffee break

Graphene and 2D materials: Electronic structure

15:15~15:45 Special lecture

- 3S-3** Post/Beyond Graphene: from Topological to 2.5-Dimensional Quantum Materials 10
**Takao Sasagawa*

15:45~16:00

- 3-15** Energetics of bilayer hexagonal boron nitride nanoflakes: A nucleation process of a second layer on a substrate layer 38
**Mina Maruyama, Susumu Okada*

Graphene and 2D materials: Transport property

16:00~16:15

- 3-16** Efficient fabrication of graphene nanoribbon quantum dot devices with temperature-stable orbital-level spacing 39
**Naofumi Sato, Takahito Kitada, Mizuki Seo, Toshiro Kaneko, Tomohiro Otuka, Toshiaki Kato*

Graphene and 2D materials: Optical property

16:15~16:30

- 3-17** Activation of single-photon emitter on CVD-hBN treated with thermal process 40
**Yusuke Adachi, Takayuki Arie, Kuniharu Takei, Seiji Akita*

16:30~16:45 Coffee break

Graphene and 2D materials: Synthesis and growth

16:45~17:15 Special lecture

- 3S-4** Novel two-dimensional materials stabilized on substrates 11
**Yukiko Yamada-Takamura*

Graphene and 2D materials: Electronic structure

17:15~17:30

- 3-18** Spiro-graphene: New two-dimensional C allotropes comprising fenestratetraene and cyclooctatetraene 41
**Susumu Okada, Nguyene Thanh Cuong, Yanlin Gao, Mina Maruyama*

Graphene and 2D materials: Synthesis and growth

17:30~17:45

- 3-19** Insulating properties of h-BN film synthesized by sputtering method 42
**Daiyu Kondo, Kenjiro Hayashi, Masako Kataoka, Shintaro Sato*

17:45~18:00

- 3-20** Precipitation of graphite layer with smooth and large domain on c-plane 43
sapphire using crystallized Ni catalyst
**Shigeya Naritsuka, Asato Nakashima, Tomoaki Murahashi, Tatsuya
Kashio, Yasuhiro Fukunishi, Kazuki Mita, Takahiro Maruyama*

18:00~18:05 Closing

特別講演
Special Lecture

2S - 1 ~ 2S - 7

3S - 1 ~ 3S - 4

Discovery of carbon nanotubes

Sumio Iijima

*Member of Japan Academy and University Professor, Meijo University, Nagoya
468-8502, Japan*

The name became so well known that it was introduced in high school chemistry textbooks. The number of Google Citations in this treatise is 53,678 (August 2021), which is still increasing and a wide range of research is underway. For example, a dentist's three-dimensional X-ray imaging device (using CNTs as an electron beam source) approved by the US FDA (Food and Drug Administration) in July this year has been commercialized. Development of the favorite CNT device is also being strengthened in the United States and China (Japan?).

The discovery of CNT can be said to be serendipity, as is known from many inventions and discoveries. However, it can be said that the discovery was inevitable. The discovery of CNTs would not be possible without a high resolution electron microscope. The relationship between this measuring device and me began when I was a graduate student, and the discovery of CNT was about 30 years later. That long research experience has led to discovery.

Corresponding Author: S.Iijima

Tel: +81-52-834-4001, Fax: +81-52-834-4001,

E-mail: ijimas@meijo-u.ac.jp

Carbon Nanotube based high performance CMOS and RF devices operating in terahertz regime

Lian-Mao Peng

Department of Electronics, Peking University, Beijing 100871, China

Carbon nanotube (CNT)-based electronics has been considered one of the most promising candidates to replace Si complementary metal-oxide-semiconductor (CMOS) technology, which will soon meet its performance limit. In particular CNTs have been investigated for various electronic and optoelectronic device applications, such as sub-10nm CMOS devices which outperform that of state-of-the-art Si based CMOS devices in both speed and power consumption [1-5], as well as idea material for monolithic optoelectronic integration with complementary MOS-compatible signal processing circuit [6-8].

High performance CNT-based electronics requires scalable production of dense and electronically pure semiconducting CNT arrays on wafers. A multiple dispersion and sorting process have been developed that resulted in extremely high semiconducting purity and a dimension-limited self-alignment procedure for preparing well-aligned CNT arrays with a tunable density of 100 to 200 CNTs per micrometer on a 10-centimeter silicon wafer. Top-gate field-effect transistors (FETs) fabricated on the CNT array show better performance than that of commercial silicon MOS FETs with similar gate length, while maintaining a low room-temperature subthreshold swing of <90 millivolts per decade. Batch-fabricated top-gate five-stage ring oscillators exhibited high maximum oscillating frequency of >8 gigahertz [9].

The development of next-generation wireless communication technology requires integrated RF devices capable of operating at frequencies greater than 90 GHz. Radiofrequency transistors operating in terahertz regime have been developed using high-purity carbon nanotube arrays. The nanotube arrays exhibit a high carrier mobility of over $1,500 \text{ cm}^2 \text{ V}^{-1} \text{ s}^{-1}$ and a saturation velocity of up to $3.0 \times 10^7 \text{ cm s}^{-1}$. Transistors with a 50 nm gate length show current-gain and power-gain cutoff frequencies of up to 540 and 306 GHz, demonstrating potential operation at millimetre-wave and terahertz frequencies [10].

- [1] C. Qiu *et al.* *Science*, **255**, 271 (2017).
- [2] C. Qiu *et al.* *Science*, **361**, 387 (2018).
- [3] D.L. Zhong *et al.* *Nature Electronics*, **1**, 40 (2018).
- [4] L.-M. Peng *et al.* *Nature Electronics*, **1**, 158 (2018).
- [5] L. Xiang *et al.* *Nature Electronics*, **1**, 273 (2018).
- [6] L.J. Yang *et al.* *Nature Photonics*, **5**, 672 (2011).
- [7] Y. Liu *et al.* *Nature Communication*, **8**, 15649 (2017).
- [8] Y. Liu *et al.* *Science Advances*, **3**, e170145 (2017).
- [9] L. Liu *et al.* *Science*, **368**, 850 (2020).
- [10] H. Shi *et al.* *Nature Electronics*, **4**, 405 (2021).

Corresponding Author: L.-M. Peng

Tel: +86-01-62764967

E-mail: lmpeng@pku.edu.cn

30 years of nanotubes with FNTG Society

○Riichiro Saito¹

¹ *Department of Physics, Tohoku University, Sendai 980-8578, Japan*

Since the first paper by S. Iijima, 30 years have passed for nanotube research. In this presentation, we would like to overview the history of carbon nanotubes and summarize a perspective which has been discussed in the FNTG society.

Carbon nanotube is a rolled-up graphene sheet into a cylinder. A typical size of a single wall carbon nanotube (SWNT) is 1-3nm in diameter and 100nm-10cm in length and thus a SWNT is one-dimensional material. The structure of a SWNT is defined by two integers (n,m), which is called as chirality. Depending on the chirality of SWNT, a SWNT can be either metal or semiconductor. In particular, an energy gap of a semiconducting SWNT is inversely proportional to the diameter of the SWNT, which gives chirality-dependent physical properties such as optical properties, thermo-electronic properties and transport properties. On the other hand, as an extension of carbon fiber, we expect an exceptional mechanical and thermal properties of SWNTs or multi-wall carbon nanotubes (MWNTs).

Since the early times of 1990's, electron-microscopy measurement and solid state physics of SWNTs have been reported and discussed, respectively. However, we should wait for a large synthesis of carbon nanotube that appears in the end of the last century to measure and apply SWNTs. Chemical vapor deposition (CVD) in which the gas of molecule that contains carbon atoms is decomposed by the metal catalyst such as Fe, Co, and Ni, at a high temperature from 500 to 1000C, succeeded to a large synthesized SWNTs. Optimizing the condition of CVD, the synthesis of SWNTs is industrialized, which accelerates the measurement of physical properties of SWNTs as a function of (n,m) in 2020's and the application of SWNTs in 2010's.

One of application of SWNTs is to make a semiconductor device. Since the size of Si semiconductor devices has been decreasing up to several nm, people say that the Moore's law will be finished within a decade. A SWNT has a size of 1nm and thus incorporating SWNTs in the integrated circuit would be a solution for 1nm devices. In 2000's, single nanotube field effect transistor is fabricated. However, the technique was in the laboratory level. SWNT devices have some merits such as high melting point, flexible, chemically stable. On the other hand, there are many challenges for making a device. For example, (1) synthesis of single (n,m) (2) process technique of putting a SWNT on the device. In a SWNT, it is also known that electron-electron interaction is crucial for transport properties even at the room temperature. Thus quantum properties of devices are necessary to discuss the new operation of devices at the room temperature.

In the current situation in 2021, the applications of SWNTs are based on the following three kinds of SWNT materials; (1) the randomly oriented or aligned sheet of SWNTs, which can be used for transparent conducting sheet, solar cell, neural network device, and thermal-conducting sheet. (2) a yarn of SWNTs, which can be used for a strong fiber or artificial muscle, and (3) independent SWNT separated by surfactant in the water, which can be used for biological marker at far infrared region. In the presentation, we would like to introduce corresponding techniques that support the applications.

Saito acknowledges Professor Mildred S. Dresselhaus, Professor Gene F. Dresselhaus and all collaborators for giving me the life of carbon nanotubes.

Corresponding Author: R. Saito

Tel: +81-22-795-7754, Fax: +81-22-795-6447,

E-mail: rsaito@flex.phys.tohoku.ac.jp

Web: <http://flex.phys.tohoku.ac.jp>

Perspective of carbon nanotubes research celebrating the 30th Anniversary

○Shigeo Maruyama¹

¹ *Department of Mechanical Engineering, The University of Tokyo, Tokyo 113-8656, Japan*

It is a great pleasure to celebrate 30th Anniversary of carbon nanotube research since the land-mark paper by Professor Sumio Iijima [1]. A family of nano-carbon materials such as fullerenes, carbon nanotubes, graphene, and other 2D materials (shown in Fig. 1) has attracted many researchers in science, engineering and application fields. We can witness through the recent 60th anniversary of FNTG research society [2] and 20th anniversary of NT conferences [3]. Especially, single-walled carbon nanotubes (SWCNTs) with the diverse optical and electronic properties (metallic or semiconducting) depending on chiral indices (n, m) have been the remarkable key material. I will discuss the future perspective of carbon nanotube research with the emphasis on one-dimensional (1D) van der Waals (vdW) hetero structures [4] based on SWCNT as shown in Fig. 2 [5]. We can further extend 1D vdW hetero structures as shown in Fig. 3 [6] including the controlled modulation of properties by employing the inner space of the SWCNTs to encapsulate various materials.

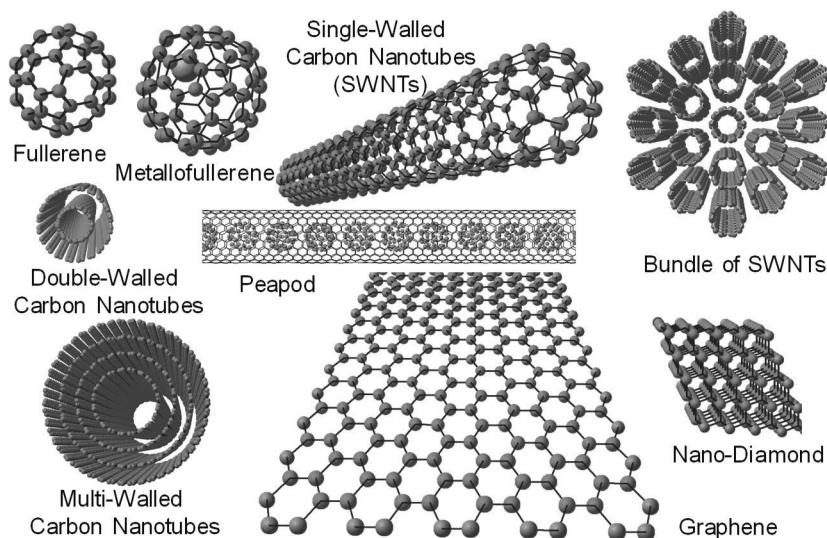


Fig. 1 Structure of typical nano-carbon materials.

- [1] S. Iijima, *Nature*, **354**, 56 (1991).
 [2] The Fullerenes, Nanotubes and Graphene (FNTG) Research Society, <https://fntg.jp/>.
 [3] International Conference on Science and Application of Nanotubes and Low-Dimensional Materials (NT conferences), <http://www.photon.t.u-tokyo.ac.jp/nt/>.
 [4] R. Xiang *et al.*, *Science*, **367**, 537 (2020).
 [5] R. Xiang, S. Maruyama, *Small Sci.*, **1**, 2000039 (2021).
 [6] S. Cambré, M. Liu, D. Levshov, K. Otsuka, S. Maruyama, R. Xiang, *Small*, 2102585 (2021).

Corresponding Author: S. Maruyama,
 Tel: +81-3-5841-6421, Fax: +81-3-5800-6983
 E-mail: maruyama@photon.t.u-tokyo.ac.jp

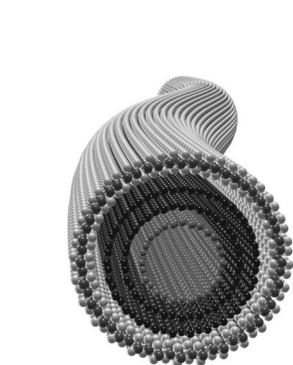


Fig. 2 One-dimensional hetero structures [5],
 SWCNT@BNNT@MoS₂NT.

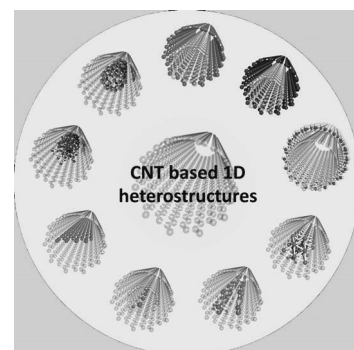


Fig. 3 Extended 1D hetero structures based on CNT [6].

2D Materials : Integration Challenges for Future Electronics

Cedric Huyghebaert for the 2D team of imec

At imec we explore the challenges of wafer scale integration of 2D materials. In this talk, we will report on wafer level integrated graphene-based modulators and double gated WS₂ transistors with gate length down to 18 nm on 300mm wafers in our Si fab.

We will address the challenges linked to the growth, the transfer and the encapsulation of 2D materials in a semiconductor environment. We built an integration vehicle where the impact of each process step can be understood and developed accordingly to enhance device performance. The work presented here paves the way towards industrial adoption of 2D materials.

Layer-exchange synthesis of multilayer graphene for flexible battery anodes

○Kaoru Toko¹,

¹ *Institute of Applied Physics, University of Tsukuba, Tsukuba 305-8573, Japan*

Low-temperature synthesis of multilayer graphene (MLG) on insulators is the key to incorporating MLG-based functional thin films, including transparent electrodes, low-resistance wiring, heat spreaders, and battery anodes in advanced electronic devices. In the field of semiconductor thin films, layer exchange phenomenon is known as a type of reaction between semiconductor and metal layers [1]. In 2017, we discovered the layer exchange between carbon and metals [2], which is based on a principle different from that of conventional carbon precipitation methods. The layer exchange enables low-temperature synthesis and control of film thickness and position of MLG on arbitrary substrates. In particular, Ni-induced layer exchange allows for the MLG anode electrode structure on a plastic substrate, which will be useful for fabricating flexible rechargeable batteries.

In the presentation, the following topics will be introduced:

1. The mechanism and basic properties of layer exchange.
2. The important factors for layer exchange of MLG: metal species [3], annealing conditions [4], interlayer insertion [5,6], and thickness [7].
3. The electrical properties [7] and battery anode application [8].

[1] K. Toko and T. Suemasu, *J. Phys. D. Appl. Phys.* **53**, 373002 (2020).

[2] H. Murata *et al.*, *Appl. Phys. Lett.* **110**, 033108 (2017).

[3] Y. Nakajima *et al.*, *ACS Appl. Mater. Interfaces* **10**, 41664 (2018).

[4] H. Murata *et al.*, *App. Phys. Express* **13**, 055502 (2020).

[5] H. Murata *et al.*, *Appl. Phys. Lett.* **111**, 243104 (2017).

[6] H. Murata *et al.*, *CrystEngComm* **22**, 3106 (2020).

[7] H. Murata *et al.*, *Sci. Rep.* **9**, 4068 (2019).

[8] H. Murata *et al.*, *ACS Appl. Energy Mater.* **3**, 8410 (2020).

Corresponding Author: K. Toko

Tel: +81-29-853-5472, Fax: +81-29-853-5205,

E-mail: toko@bk.tsukuba.ac.jp

Nucleation and growth of SWNTs are driven by the dynamics of their edge

Christophe Bichara

CINaM, CNRS and Aix-Marseille University, Marseille, France

In classical crystal growth, the interaction of the growing object with its support and the energies of the different facets determine the growth mode and the resulting crystalline structures. The synthesis of carbon nanotubes by chemical vapor deposition poses somewhat similar yet more complex issues. The catalytic particle is both a support and a reactive interface with the growing tube, and many properties are altered because of the nanometric size of the objects.

In this context, we have identified different growth modes driven by the thermodynamic properties of the interface [1, 2] and developed a model of the interface [3], emphasizing the importance of the configurational entropy of the nanotube edge to stabilize chiral tubes and to account for the temperature dependence of tube helicity distributions. This simple lattice model is pushed further to account for more general interface structures and kinetic Monte Carlo (KMC) simulations are developed [4] to study the growth mechanisms and kinetics, and analyze growth rates in relation with the chiral selectivity of the synthesis.

We also present new *in situ* measurements of individual CNT growth rates by homodyne polarization microscopy [5] with better temporal and statistical resolution than previous studies [6]. The growth patterns are surprisingly complex and exhibit growth instabilities characterized by stochastic alternations of growth, etching, stops and sometimes restarts. These events occur with or without changes in the structure of single-walled nanotubes. To understand the first, fascinating case, we perform KMC simulations and propose a model emphasizing the role of the tube/catalyst interface dynamics.

[1] Fiawoo M.-F. C. *et al.*, Phys. Rev. Lett. **108**, 195503 (2012).

[2] He M. *et al.*, Nanoscale **10**, 6744, (2018)

[3] Magnin Y. *et al.*, Science **362**, 212–215 (2018)

[4] Förster G. D., *et al.*, AIP Adv. **11**, 045306 (2021).

[5] Pimonov V., *et al.*, *submitted to Nano Letters*

[6] Koyano B. *et al.*, Carbon **155**, 635–642 (2019)

Deterministic transfer of optical-quality carbon nanotubes for atomically defined technology

K. Otsuka¹, N. Fang¹, D. Yamashita², T. Taniguchi³, K. Watanabe⁴, ○Y. K. Kato^{1,2}

¹*Nanoscale Quantum Photonics Laboratory, RIKEN Cluster for Pioneering Research, Saitama 351-0198, Japan*

²*Quantum Optoelectronics Research Team, RIKEN Center for Advanced Photonics, Saitama 351-0198, Japan*

³*International Center for Materials Nanoarchitectonics, National Institute for Materials Science, Ibaraki 305-0044, Japan*

³

Research Center for Functional Materials, National Institute for Materials Science, Ibaraki 305-0044, Japan

When continued device scaling reaches the ultimate limit imposed by atoms, technology based on atomically precise structures is expected to emerge. Device fabrication will then require building blocks with identified atomic arrangements and assembly of the components without contamination. Here we report on a versatile dry transfer technique for deterministic placement of optical-quality carbon nanotubes [1]. Single-crystalline anthracene is used as a medium which readily sublimates by mild heating, leaving behind clean nanotubes and thus enabling bright photoluminescence. We are able to position nanotubes of a desired chirality with a sub-micron accuracy under in-situ optical monitoring, thereby demonstrating deterministic coupling of a nanotube to a photonic crystal nanobeam cavity. A cross junction structure is also designed and constructed by repeating the nanotube transfer, where intertube exciton transfer is observed. Our results represent an important step towards development of devices consisting of atomically precise components and interfaces.

Parts of this study are supported by JSPS (KAKENHI JP20H02558, JP19J00894, JP20K15137), MIC (SCOPE 191503001), and MEXT (Nanotechnology Platform JPMXP09F19UT0075). Growth of hexagonal boron nitride crystals is supported by the Element Strategy Initiative conducted by the MEXT (JPMXP0112101001), JSPS (KAKENHI JP20H00354), and JST (CREST JPMJCR15F3). K.O. and D.Y. are supported by JSPS (Research Fellowship for Young Scientists). N.F. is supported by RIKEN Special Postdoctoral Researcher Program. We thank T. Inoue, S. Maruyama, and K. Nagashio for help in the material preparation, as well as the Advanced Manufacturing Support Team at RIKEN for technical assistance.

[1] K. Otsuka, N. Fang, D. Yamashita, T. Taniguchi, K. Watanabe, Y. K. Kato, *Nat. Commun.* **12**, 3138 (2021).

Corresponding Author: Y. K. Kato
Tel: +81-48-462-1449
E-mail: yuichiro.kato@riken.jp
<https://katogroup.riken.jp/>

Direct observation of the layer-number-dependent electronic structure in few-layer WTe₂

Masato Sakano

Quantum-Phase Electronics Center and Department of Applied Physics, The University of Tokyo, Bunkyo-ku, Tokyo, 113-8656, Japan

The physical property in the atomically-thin two-dimensional (2D) material drastically changes as the number of layers decreases to the monolayer limit. The quantization of band dispersions along the stacking direction, as well as the reduction of symmetry compared to the infinite bulk crystal can strongly modify the electronic structures of 2D materials, resulting in the peculiar physical phenomena. WTe₂, the material we focused on in our study, is one of the representative materials. Bulk WTe₂ is a charge-compensated polar semimetal [1] predicted as an inversion-symmetry-broken type-II Weyl semimetal [2]. In contrast, mono- and 2-layer WTe₂ are known as insulators with small bandgaps [3-5]. In terms of the structural symmetry, although the monolayer WTe₂ is centrosymmetric, the stacking order of layers breaks the inversion-symmetry in few-layer WTe₂, leading to the unique phenomena related to Berry-curvature dipole [4-8]. The abovementioned studies on thin-flake WTe₂ have been mostly proceeded by comparing the transport properties on micro-devices with the band calculations. Due to the limited size (typically $\sim 10 \mu\text{m}$) and volume of the samples as well as the difficulty in handling, many of the physical property measurements established in bulk systems are not available. Nevertheless, the precise investigation of the electronic structure is extremely important, especially considering that the property related to Berry-curvature is determined by the electronic band dispersions in the reciprocal space.

In our study, by using micro-focused laser angle-resolved photoemission spectroscopy (ARPES) in combination with the 2D materials manufacturing system (2DMMS) [9] that can freely stack atomic layers by image recognition, machine learning, and robotic assembly, we developed an efficient procedure for investigating the band dispersions of atomically thin micro-flakes. We prepared 2D WTe₂ flake samples for ARPES by using the Graphite / hBN as a substrate and by encapsulating with graphene. We successfully observed the thickness-dependent band structures of the atomically thin WTe₂ flakes [Fig.1(a)-(d)]. It clearly revealed the insulator–semimetal transition realized between the 2- and 3-layer, and the striking even–odd effect in the layer-number dependence of the spin-band splitting [10].

- [1] M. N. Ali, *et al.*, Nature **514**, 205, (2014).
- [2] A. A. Soluyanov, *et al.*, Nature **527**, 495 (2015).
- [3] Z. Fei, *et al.*, Nat. Phys. **13**, 677 (2017).
- [4] Z. Fei, *et al.*, Nature **560**, 336 (2018).
- [5] I. Cucchi, *et al.*, Nano Lett. **19**, 554 (2019).
- [6] K. Kang, *et al.*, Nat. Mater. **18**, 324 (2019).
- [7] H. Wang and X. Qian, npj Comput. Mater. **5**, 119 (2019).
- [8] J. Xiao, *et al.*, Nat. Phys. **16**, 1028 (2020).
- [9] S. Masubuchi, *et al.*, npj 2D Mater. Appl. **4**, 3 (2020).
- [10] M. Sakano *et al.*, arXiv:2103.11885 (2021).

Corresponding Author: M. Sakano,

Tel: +81-3-5841-7903, Fax: +81-3-5841-7903

E-mail: sakano@ap.t.u-tokyo.ac.jp

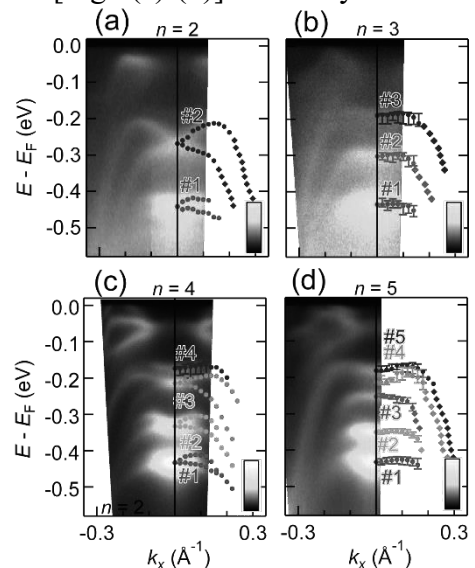


Fig. 1(a)-(d) ARPES images for 2-5 layer WTe₂.

Post/Beyond Graphene: from Topological to 2.5-Dimensional Quantum Materials

○Takao Sasagawa

Laboratory for Materials and Structures, Tokyo Institute of Technology, Kanagawa 226-8503, Japan

We are exploring solid-state materials with exotic electronic states and novel properties such as topological insulators, topological semimetals, and topological superconductors [1-11]. Most of them have layer-stacking crystal structures, and their single crystals show good cleavage properties, as similar to graphene. Therefore, their exfoliated nanosheets could be promising building blocks for 2.5-dimensional quantum materials [12,13]. Keeping “post/beyond graphene” in mind, the properties, potential applications, and future prospects of the topological and associated 2.5-dimensional quantum materials will be discussed.

- [1] R. Noguchi, T. Sasagawa, T. Kondo *et al.*, *Nature Materials* **20**, 473 (2021).
- [2] T. Machida, T. Hanaguri, T. Sasagawa *et al.*, *Nature Materials* **18**, 811 (2019).
- [3] R. Noguchi, T. Sasagawa, T. Kondo *et al.*, *Nature* **566**, 518 (2019).
- [4] M.S. Bahramy, T. Sasagawa, P.D.C. King *et al.*, *Nature Materials* **17**, 21 (2018).
- [5] K. Iwaya, T. Hanaguri, T. Sasagawa *et al.*, *Nature Commun.* **8**, 976 (2017).
- [6] Y.-S. Fu, T. Hanaguri, T. Sasagawa *et al.*, *Nature Commun.* **7**, 10829 (2016).
- [7] J. M. Riley, T. Sasagawa, P.D.C. King *et al.*, *Nature Nanotech.* **10**, 1043 (2015).
- [8] M. Sakano, T. Sasagawa, K. Ishizaka *et al.*, *Nature Commun.* **6**, 8595 (2015).
- [9] Y.-S. Fu, T. Hanaguri, T. Sasagawa *et al.*, *Nature Physics* **10**, 815 (2014).
- [10] Y.L. Chen, Z.-X. Shen, T. Sasagawa *et al.*, *Nature Physics* **9**, 704 (2013).
- [11] Y.L. Chen, T. Sasagawa, Z.-X. Shen *et al.*, *Science* **329**, 659 (2010).
- [12] S. Masubuchi, T. Sasagawa, T. Machida *et al.*, *NPJ 2D Mater. Appl.* **4**, 3 (2020).
- [13] K. Takeyama, R. Moriya, T. Sasagawa, T. Machida *et al.*, *Nano Lett.* **21**, 3929 (2021).

Corresponding Author: T. Sasagawa

Tel & Fax: +81-45-924-5366

E-mail: sasagawa@msl.titech.ac.jp

Novel two-dimensional materials stabilized on substrates

○Yukiko Yamada-Takamura

*School of Materials Science, Japan Advanced Institute of Science and Technology (JAIST),
Ishikawa 923-1292, Japan*

New two-dimensional (2D) materials stabilized only on substrates, so far, will be introduced.

The first example is a 2D Ge lattice having a “bitriangular” structure. Our theoretical study on freestanding bitriangular lattice demonstrated that the flat band of a kagome lattice can be embedded in this very different-looking structure [1]. In parallel, we have grown $\text{ZrB}_2(0001)$ thin films on Ge(111) substrates and found that Ge atoms segregate and crystallize into such bitriangular lattice on the ZrB_2 film surface (see Fig.1) [2], unlike when the film is grown on Si(111) substrate forming a honeycomb lattice of Si, “silicene” [3].

The second example is a new polymorph “trigonal anti-prismatic” phase of monolayer GaSe which is a semiconducting monochalcogenide (see Fig.2b). Bulk GaSe is known to crystallize in four polytypes which differ in how layers shown in Fig.2a are stacked via van der Waals interaction, but no polymorph has been reported based on experimental study, including other layered monochalcogenides sharing the same crystal structure, such as GaS or InSe. Through cross-sectional scanning transmission electron microscopy of GaSe thin films grown on Ge(111) substrates, we found that monolayer GaSe with trigonal anti-prismatic structure (Fig.2b) exist near the film-substrate interface [4]. Our first-principles study [5] implies that the new phase is metastable, and can be stabilized by tensile strain.

These findings add new families of materials to be explored in the ever-emerging field of 2D materials.

- [1] C.-C. Lee, A. Fleurence, Y. Yamada-Takamura, and T. Ozaki, *Phys. Rev. B*, **100**, 045150 (2019).
 [2] A. Fleurence *et al.*, *Phys. Rev. B*, **95**, 201102(R) (2020).
 [3] Y. Yamada-Takamura and R. Friedlein, *Sci. Technol. Adv. Mater.*, **15**, 064404 (2014).
 [4] T. Yonezawa *et al.*, *Surf. Interface Anal.*, **51**, 95-99 (2019).
 [5] H. Nitta, T. Yonezawa, A. Fleurence, Y. Yamada-Takamura, and T. Ozaki, *Phys. Rev. B*, **102**, 235407 (2020).

Corresponding Author: Y. Yamada-Takamura
 Tel: +81-761-51-1570, Fax: +81-761-51-1149,
 E-mail: yukikoyt@jaist.ac.jp

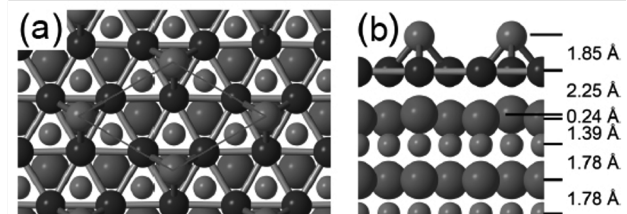


Fig.1 (a) Top view and (b) side view of ball-and-stick model of Ge atoms crystallized with bitriangular structure on Zr-terminated ZrB_2 revealed by total reflection high energy positron diffraction [2].

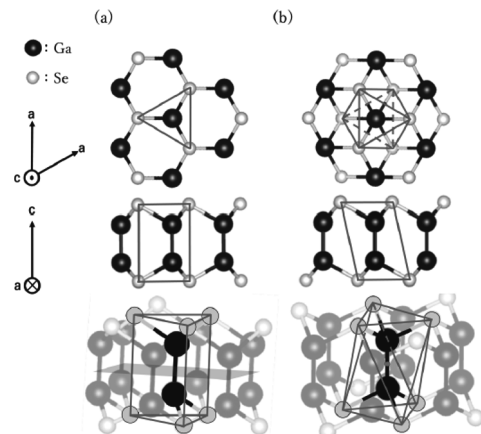


Fig.2 (a) Trigonal prismatic and (b) trigonal anti-prismatic phases of monolayer GaSe [5].

招待講演
Invited Lecture

2 I-1 ~ 2 I-3

Separation of single-wall carbon nanotubes by polysaccharide gels and their applications.

○Takeshi Tanaka

Nanomaterials Research Institute, National Institute of Advanced Industrial Science and Technology (AIST), Tsukuba, Ibaraki 305-8565, Japan

Metallic/semiconducting (M/S) separation and chirality separation of single-wall carbon nanotubes (SWCNTs) are very important for their electrical and optical applications. We have studied the separations using polysaccharide gels for 15 years. In this presentation, I will summarize the gel separation and show the recent progress of the separation including defectless/defective SWCNTs separation and single chirality M-SWCNT separation. First we used agarose gel and then dextran-based Sephacryl gel to separate M/S and single-chirality SWCNTs with sodium dodecyl sulfate as a dispersant [1]. Triple-mixed surfactant system on Sephacryl gel chromatography improved the purities of chirality separation of S-SWCNTs and enantiomer separation of S-SWCNTs [2,3]. When we introduced highly hydrophobic cholate derivative, sodium lithocholate, to the mixed surfactant system, further improvement of the separation could be archived [4]. Now we can separate SWCNTs with difference in defect introduction and also single chirality M-SWCNTs. The separated SWCNTs enabled us to investigate photoluminescence quantum yield of SWCNTs corrected for the photon reabsorption [5]. The separated semiconducting SWCNTs were also used for various applications, such as ethylene gas sensor [6], photodynamic therapy [7], and luminescence of SWCNTs by luciferin/luciferase reaction [8]. Details will be discussed in the presentation.

- [1] T.T., H. Liu, S. Fujii, and H. Kataura, *Phys. Status Solidi RRL* **9**, 301 (2011).
- [2] Y. Yomogida, T.T., M. Zhang, M. Yudasaka, X. Wei, and H. Kataura, *Nature Commun.*, **7**, 12056 (2016).
- [3] X. Wei, T.T., Y. Yomogida, N. Sato, R. Saito, and H. Kataura, *Nature Commun.*, **7**, 12899 (2016).
- [4] Y. Yomogida, T.T., M. Tsuzuki, X. Wei, H. Kataura, *ACS Appl. Nano Mater.* **3**, 11289 (2020).
- [5] X. Wei, T.T., S. Li, M. Tsuzuki, G. Wang, Z. Yao, L. Li, Y. Yomogida, A. Hirano, H. Liu, H. Kataura, *Nano Lett.* **20**, 410 (2020).
- [6] S. Ishihara, A. Bahuguna, S. Kumar, V. Krishnan, J. Labuta, T. Nakanishi, T.T., H. Kataura, Y. Kon, D. Hong, *ACS Sens.* **5**, 1405 (2020).
- [7] R. Fukuda, T. Umeyama, M. Tsujimoto, F. Ishidate, T.T., H. Kataura, H. Imahori, T. Murakami, *Carbon* **161**, 718 (2020).
- [8] T.T., M. Higuchi, A. Hiratsuka, H. Kataura, The 58th FNTG general symposium, 1-3 (2020).

Corresponding Author: T. Tanaka

Tel: +81-29-861-2903, Fax: +81-29-861-2786,

E-mail: tanaka-t@aist.go.jp

Progresses and future challenges of carbon nanotube production

○Suguru Noda^{1,2,*}

¹Department of Applied Chemistry, ²Waseda Research Institute for Science and Engineering, Waseda University, Tokyo 169-8555, Japan

Carbon nanotubes (CNTs) enable various devices by using carbon, an abundant chemical element. They can be synthesized from various carbon sources via both physical vapor deposition (PVD) and chemical vapor deposition (CVD). Owing to the moderate reaction temperature and gaseous carbon sources, CVD is considered more practical for low-cost and large-scale production. Metal nanoparticles are crucially important as catalyst for promoting reaction and as template for controlling CNT structure. Catalyst can be either suspended in gas or supported on solid and can be fed in either 2D or 3D (Fig. 1). Significant progress has been made for production in the past decades. Production method should be selected, appropriately considering characteristics of each method, for each application target (Fig. 2).

Floating catalyst CVD (Fig. 1a) yields high-quality CNTs [1] because CNTs grow freely from buckling due to the crowding effect. Such CNTs are suitable for thin film applications including transparent electrodes and solar cells [2]. However the low catalyst density in the reactor is a bottleneck for mass production. Flame-assisted CVD enables nucleation of catalyst particles at high density and synthesis of single-wall CNTs downstream the flame [3].

On-substrate CVD using supported catalyst (Fig. 1c) yields long and pure CNTs with controlled ensemble structure [4], thus is suitable for direct implementation of CNTs in various devices. H₂O vapor at ppmv level enhances catalyst lifetime [4], and less active CO₂ at percent level provides the same effect for large scale [5].

Catalyst supported on powder (Fig. 1b) enables low-cost and large-scale production of CNTs in 3D processes such as fluidized bed [6]. By using ceramic beads with smooth surface, submillimeter-long, >99 wt% pure CNTs can be produced at high yield [7]. Such CNTs enable light-weight rechargeable batteries without using polymeric binders nor metal foils [8].

To realize wide application of CNTs, environmental burden such as greenhouse gas emission for their production, use, and disposal should also be assessed and reduced [9].

[1] T. Saito, et al., *J. Phys. Chem. B* 110, 5849 (2006). [2] R. Xie, et al., *Carbon* 175, 519 (2021). [3] S. Okada, et al., *Carbon* 138, 1 (2018). [4] K. Hata, et al., *Science* 306, 1362 (2004). [5] T. Sato, et al., *Carbon* 136, 143 (2018). [6] Q. Zhang, et al., *ChemSusChem* 4, 864 (2011). [7] Z. Chen, et al., *Carbon* 80, 339 (2014). [8] K. Hasegawa and S. Noda, *J. Power Sources* 321, 155 (2016). [9] H.Y. Teah, et al., *ACS Sustainable Chem. Eng.* 8 (4), 1730 (2020).

Corresponding Author: S. Noda Tel&Fax: +81-3-5286-2769, E-mail: noda@waseda.jp

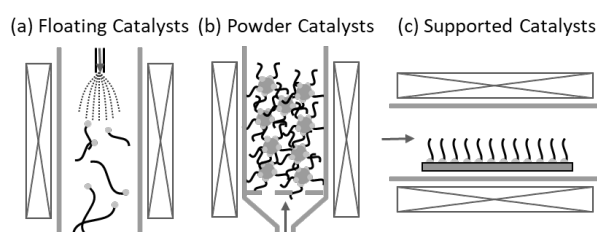


Fig. 1. Various CVD processes.

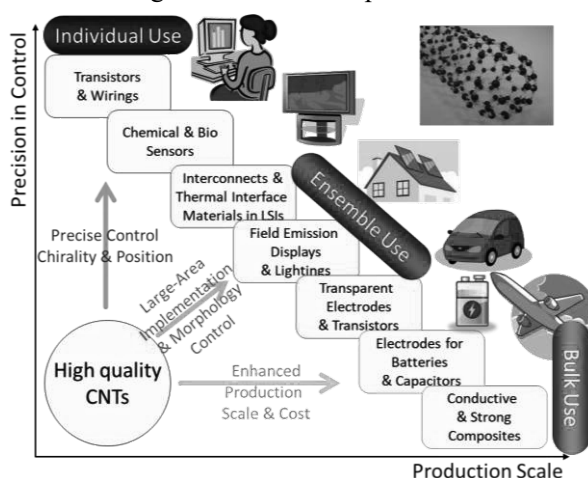


Fig. 2. Map of CNT applications.

Developments of the Carbon Nanotube Applications based on Molecular Adsorption

○Tsuyohiko Fujigaya^{1,2,3}

¹*Department of Applied Chemistry, Faculty of Engineering, Kyushu University, 819-0395, Japan.*

²*WPI I²CNER, Kyushu University, 819-0395, Japan.*

³*Center for Molecular Systems, Kyushu University, 819-0395, Japan.*

Nano-carbon materials such as fullerenes, carbon nanotubes, graphene, and so on are attractive materials for optical, electronic, mechanical, and biological applications due to their unique physical properties based on their low dimensionality. In many of these applications, modifications of these nano-carbons with organic molecules and polymers are effective way to tune or to add their functions or properties, in which proper molecular design, type of modification (i.e. non-covalent or covalent), geometry and amount are key parameter to finely control the functions and/or properties.

We have been developed polymer-wrapped or molecular-doped nano-carbons based on non-covalent modifications for biological [1-3], thermoelectric [4,5], fuel cell [6-8] and reinforcement [9] applications. In this presentation, preparation, characterization, and effect of the polymer-based or molecular-based modifications for these applications will be introduced. Polymer-wrapping and molecular-doping enable the increases of the catalyst efficiency of the fuel cell, catalyst durability of fuel cell, doping stability in the thermoelectric materials and effective load transfer in the filler reinforced plastics.

- [1] T. Fujigaya *et al.* ACS Appl. Bio Mater., **4**, 5049–5056 (2021).
- [2] T. Fujigaya *et al.* ACS Appl. Nano Mater, **2**, 4703-4710 (2019).
- [3] T. Fujigaya, *et al.* J. Am. Chem. Soc. **140**, 8544-8550 (2018).
- [4] T. Fujigaya *et al.* J. Mater. Chem. A, **9**, 12188–12195 (2021).
- [5] T. Fujigaya, *et al.* Synthetic Metals, **225**, 76-80 (2016).
- [6] T. Fujigaya *et al.* J. Power Source **496**, 229855 (2021).
- [7] T. Fujigaya, *et al.* Sci. Rep. **5**, art. No.16711 (2015).
- [8] T. Fujigaya, *et al.* Adv. Mater., **25**, 1666-1681 (2013).
- [9] T. Fujigaya, *et al.* Polym. J. **51**, 921–927 (2019).

Corresponding Author: T. Fujigaya
Tel: +81-92-802-2842, Fax: +81-92-802-2842,
E-mail: fujigaya.tsuyohiko.948@m.kyushu-u.ac.jp

一般講演
General Lecture

2-1 ~ 2-7

3-1 ~ 3-20

Cationic nitrogen-doped graphene as a p-type modifier for high-performance PEDOT:PSS hole transporters in organic solar cells

○Hao-Sheng Lin,¹ Takuhei Kaneko,¹ Soma Ishikawa,¹ Sangwoo Chae,¹ Takumi Yana,¹ Nagahiro Saito,¹ Yutaka Matsuo^{1,*}

Department of Chemical System Engineering, Graduate School of Engineering, Nagoya University, Furo-cho, Chikusa-ku, Nagoya 464-8603, Japan

Hole transporting layer (HTL), a significant constituent positioned between the anode and the active layer in organic solar cells (OSCs), that selectively conducting holes and simultaneously blocking out the unwanted electrons from triggering the charge recombination for a better power conversion efficiency (PCE). Among the long list of organic HTLs, poly(3,4-ethylenedioxythiophene)-poly(styrenesulfonate) (PEDOT:PSS) has been mostly applied in both lab-scale and industrial OSCs owing to its easily scalable production, outstanding optical properties and good electricidal properties. However, non-modified PEDOT:PSS commonly suffers from the low conductivity because of the insulating PSS component, the mismatched HOMO energy level, and the electrical inhomogeneities, which implies an additional space for promoting the hole-transport performance. As a consequence, plenty of p-type dopants have been investigated to resolve above-mentioned issues to achieve the high-performance OSCs by using doped-PEDOT:PSS.

Recently, we successfully achieved highly efficient and facile synthesis of a cationic nitrogen-doped graphene (CNG), which afforded nitrogen a p-type property [1]. Therefore, we investigated the developed CNG to OSCs as HTL and the p-type overcoat in PEDOT:PSS, respectively. When CNG-coated PEDOT:PSS was applied in OSCs, the PCE was dramatically promoted to 2.76% thanks to substantial enhancement in open-circuit voltage (V_{OC}) and short-circuit current density (J_{SC}) [2].

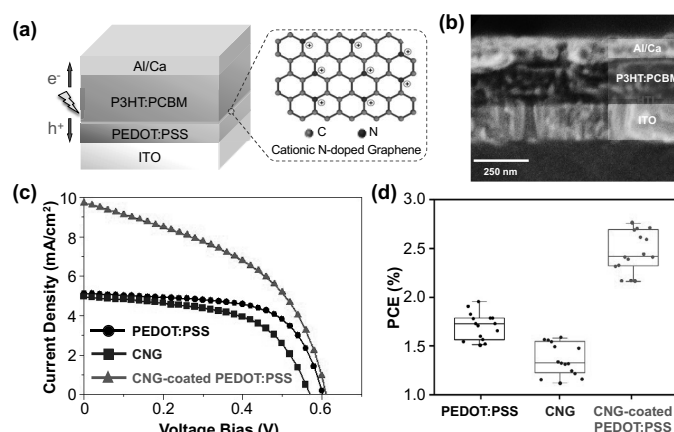
References

- [1] S. Ghae, G. Panomsuwan, M. A. Bratescu, K. Teshima, N. Saito, *ACS Appl. Nano Mater.* **2019**, *2*, 1350.
 [2] H.-S. Lin, T. Kaneko, S. Ishikawa, I. Jeon, S. Chae, T. Yana, N. Saito, Y. Matsuo, *Jpn. J. Appl. Phys.*, **2021**, *60*, 070902.

Corresponding Author: Y. Matsuo

Tel: +81-3-5841-6408

E-mail: matsuo@photon.t.u-tokyo.ac.jp



“Ultramixing”: A Simple and Effective Method to Obtain Controlled and Stable Dispersions of Graphene Oxide in Cell Culture Media

Giacomo Reina^{1,‡}, Amalia Ruiz¹, Diane Murera¹, Yuta Nishina², Aberto Bianco¹

¹ *University of Strasbourg, CNRS, Immunology, Immunopathology and Therapeutic Chemistry, UPR 3572, 67000 Strasbourg, France*

² *Graduate School of Natural Science and Technology, Research Core for Interdisciplinary Sciences, Okayama University, Tsushimanaka, Okayama 700-8530, Japan*

[‡] *Present address: Graduate School of Human and Environmental Studies, Kyoto University, Kyoto 606-8501, Japan*

The last decade has seen an increase in the application of graphene oxide (GO) in biomedicine. GO has been successfully exploited for its ability to deliver many kinds of drugs into target cells. However, GO toxicity assessment is still controversial. Several studies have demonstrated that GO protein coating is able to alleviate the material’s toxicity.[1] Besides, coronation leads to the formation of big agglomerates, reducing the cellular uptake of the material and thus its therapeutic efficiency. In this work, we propose a method to control the

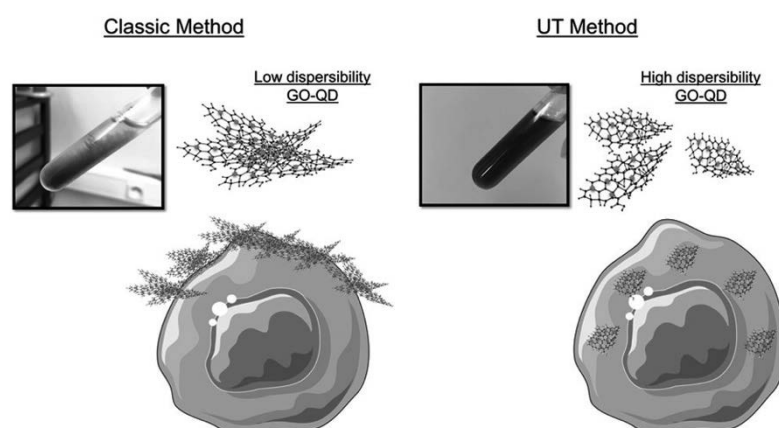


Fig. 1 The effect on “ultramixing” on colloidal stability and cell uptake.

corona formation by reducing the degree of flake agglomeration. This is achieved by premixing GO with the serum proteins using a high circumferential speed disperser ultra-turrax (UT). We compared the UT technique with the “classic” mixing of the material with the biological media. Using the UT protocol, we were able to reduce GO agglomeration in the presence of proteins and obtain stable GO dispersions in cell culture media (Fig. 1). By labelling GO with luminescent nanoparticles (quantum dots), we studied the GO internalization kinetic and efficiency. Comparing the “classic” and UT protocols, we found that the latter allows faster and more efficient internalization both in macrophages and HeLa cells without affecting cell viability. The same strategy has been applied also for functionalization obtaining highly stable flakes in cell culture media with higher performances in gene delivery.[2] We believe that the use of UT protocol will be interesting and suitable for the preparation of the next-generation GO-based drug-delivery platforms.

[1] Reina *et al.* *ACS Appl. Mater. Interfaces*, **11**, 456 (2019).

[2] Reina *et al.* *Appl. Mater. Today*, *Submitted*.

Corresponding Author: G. Reina

Tel: +81-75-753-6833, Fax: +81-75-753-6833,

E-mail: reina.giacomo.25u@st.kyoto-u.ac.jp

pH dependence of electrical response in graphene biosensors functionalized by self-assembled peptides

○Chishu Homma¹, Yoshiaki Sugizaki², Hideyuki Tomizawa, Yuhei Hayamizu¹

¹ Department of Materials Science and Engineering, School of Materials and Chemical Technology, Tokyo Institute of Technology, 2-12-1 Ookayama, meguro-ku, Tokyo, Japan

² Corporate Research & Development Center, Toshiba Corporation, 1, Komukai-Toshiba-cho, Saiwai-ku, Kawasaki, Japan

Graphene biosensor has been studied due to its high sensitivity arising from excellent electronic properties and high surface area. The sensitivity and selectivity of these biosensors relies on bio-probe molecules immobilized on graphene surface. Thus, it is necessary to develop a way to immobilize variety of bio-probes on graphene. Peptides are known to physically adsorb onto graphene surfaces and form uniform self-assembled structures [1]. And, they can be used as molecular scaffolds to immobilize bio-probes on graphene in a non-covalent manner. In fact, previous works demonstrated self-assembled peptides as a molecular scaffold for biosensing [2]. To develop more stable molecular scaffolds by using peptides, the conditions for self-assembly of peptides on graphene surface is still needed to be optimized. In this study, we aim to investigate the effect of solution pH on the electrical response of graphene field effect transistors (GFETs) functionalized with self-assembled peptides. The stability of the self-assembled structures and their impact on the graphene conductivity should exhibit a correlation with the amino acid sequence of peptides.

Three kinds of peptides with different amino acids at both ends were employed: (1) RY5, (2) EY5, and (3) QY5. All these peptides have a repeated sequence of glycine and alanine with the charged amino acids (R, E, and Q) at the both ends, and form β -sheet structure on graphene. It was demonstrated in a previous work that their self-assembled structures remained even after washing with deionized water [3]. In this work, each peptide was immobilized at various pH condition such as pH 2.7, 7, and 12.3, and their influence on the electrical conductivity of GFETs were examined. Fig. 1 shows a schematic diagram of a GFET and peptide self-assembly. Electrical measurements of GFETs revealed that charge neutral point varied depending on pH. On the other hand, the mobility of GFETs had a less influence by pH.

This work was supported by the Cabinet Office (CAO), Cross ministerial Strategic Innovation Promotion Program (SIP), “Intelligent Processing Infrastructure of Cyber and Physical Systems” (funding agency: NEDO).

[1] Y. Hayamizu, et al., Scientific reports, 2016, 6.1: 1-9.

[2] D. Khatayevich, et al. Langmuir, 2012, 28 (23).

[3] P. Li, et al. ACS Appl. Mater. Interfaces 2019 (11).

Corresponding Author: Y. Hayamizu

Tel: +81-03-5734-3651 E-mail: honma.c.aa@m.titech.ac.jp

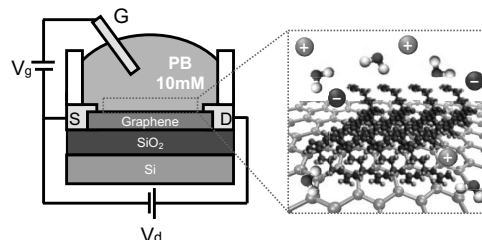


Fig. 1 Schematic diagram of GFET and self-assembled peptides on graphene.

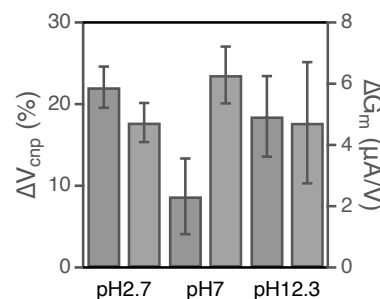


Fig. 2 Change of charge neutral point and mobility of GFETs modulated by RY5 adsorption at different pH.

Single chirality separation of metallic single-wall carbon nanotubes using gel-column chromatography

○Hiromichi Kataura¹, Mayumi Tsuzuki¹, Takeshi Tanaka¹

¹ *Nanomaterials Research Institute, AIST, Tsukuba Ibaraki 305-8565, Japan*

It is obvious that obtaining single-chirality single-wall carbon nanotubes (SWCNTs) is very important for understanding their physical properties and developing suitable applications. Many reports on the structural sorting of SWCNTs have been reported so far. However, most reports focus on semiconducting SWCNTs rather than metallic SWCNTs probably due to their high importance in electronic device applications and easiness of sorting. This report shows a single-chirality separation of metallic SWCNTs using gel-column chromatography.

At the beginning stage of SWCNT sorting using gel medium, it was thought that only semiconducting SWCNTs would be adsorbed on the polysaccharide gels when sodium dodecyl sulfate was used as a dispersant. This selective adsorption resulted in metal/semiconductor separation. However, adsorption mechanism was not well understood at that time. Today, we have a better understanding of the adsorption mechanism and have more precise control over the adsorption process. In this study, we succeeded in adsorbing metallic SWCNTs in the gel column. When the metallic SWCNTs were adsorbed on the column, interestingly, the elution behaved very much like the semiconducting SWCNTs. Diameter selective elution can be achieved simply by stepwise increasing concentration of the surfactant. As a result, six metallic species such as (5,5), (7,4), (8,2), (8,5), (9,3), and (6,6) could be sorted from SG65i, CoMoCAT. This method can be applied to other SWCNT sources such as HiPco. Fig. 1 shows optical absorption spectra of armchair SWCNTs, (5,5), (6,6), and (7,7). Since the armchair species show similar spectral shapes except E_{11} wavelength, assignment is very easy. For the chiral metallic SWCNTs, however, the assignment is not easy, because we cannot use photoluminescence mapping that has been a powerful tool for the chirality assignment of semiconducting SWCNTs. We will discuss resonance Raman results where the anomalous overtone series of radial breathing modes were observed in chiral metallic SWCNTs.

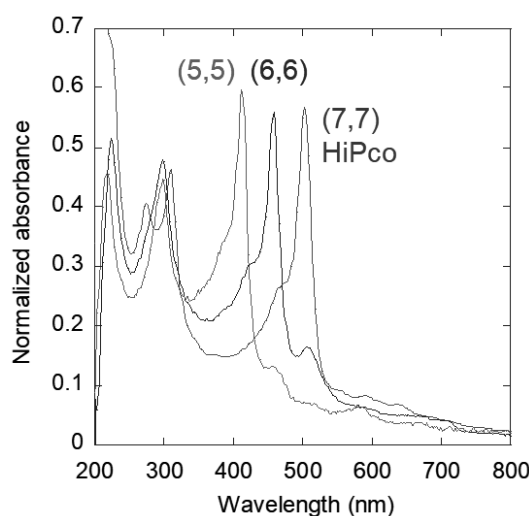


Fig. 1 Optical absorption spectra of armchair SWCNTs (5,5), (6,6), and (7,7).

Acknowledgements

This work was supported by JSPS KAKENHI, grant No. 20H05668, Japan and JST CREST, grant No. JPMJCR18I5, Japan.

Corresponding Author: H. Kataura

Tel: +81-29-861-2551, E-mail: h-kataura@aist.go.jp

Design of multi-step gas-phase CVD reactor for the synthesis of high-quality single-walled carbon nanotube

○Shunsuke Sakurai¹, Takashi Tsuji¹, Guohai Chen¹, Maho Yamada¹, Jaeho Kim²,
Hajime Sakakita², Yoshiki Shimizu^{3,4}, Kenji Hata¹, Don N. Futaba¹

¹ CNT-Application Research Center, AIST, Tsukuba, Ibaraki 305-8565, Japan

² Innovative Plasma Processing Group, Research Institute for Advanced electronics and Photonics, AIST, Tsukuba, Ibaraki 305-8568, Japan

³ Nanomaterials Research Institute, AIST, Tsukuba, Ibaraki 305-8565, Japan

⁴ AIST-UTokyo Advanced Operando-Measurement Technology Open Innovation Laboratory (OPERANDO-OIL), AIST, Kashiwa, Chiba 227-8589, Japan

Among various production techniques of the carbon nanotube (CNT), chemical vapor deposition using floating catalyst (FCCVD) has been extensively studied, especially for electronic applications based on the excellent performances of high crystalline CNTs. FCCVD consists of two processes: the formation of catalyst nanoparticle (NP) aerosol and the following CVD of CNT on the pre-formed catalyst NP, and in the most cases the above two processes are carried out spontaneously in the one thermal reactor chamber. Although various attempts to separately pre-form catalyst NPs by widespread methods such as spark, microplasma, flame, and colloid injection has been also reported, the control on the aggregation among pre-formed NPs is commonly required, especially when the number density of NPs are huge.

Recently, we reported a tiny gas-phase CNT synthesis reactor utilizing microplasma which enables the localized deposition of high quality CNTs [1,2]. In this study, a novel design of multi-step gas-phase CVD reactor utilizing microplasma for the pre-formation of catalyst NP is demonstrated to realize fast mixing with carbon feedstock within a few milliseconds to avoid aggregation. Specifically, a microplasma reactor (inner diameter of 0.8 mm) has been inserted into a thermal reactor at high temperature up to 1100 °C (Fig. 1a). Importantly, both catalyst NP and the pre-heated carbon feedstock have been supplied to the confined space ($\phi=5$ mm) designed by the fluid dynamics simulation to enable the fast mixing (Fig. 1b and c). Successfully, high-crystalline single-walled CNT has been synthesized (Fig. 1d).

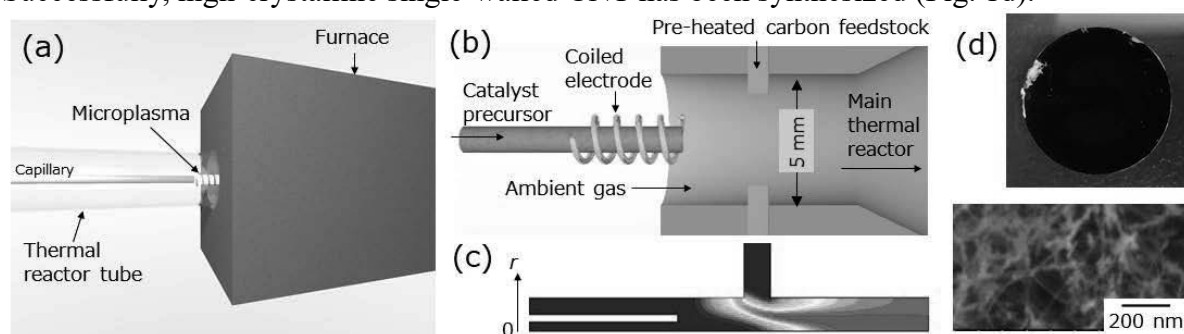


Fig. 1 (a) Schematic illustration of the reactor. (b) Conceptual design of gas mixing between catalyst NP and carbon feedstock. (c) Typical simulation result showing the distribution of catalyst multiplied by carbon feedstock concentration. (d) Photograph (upper) and SEM image (lower) of the synthesized CNT.

[1] T. Tsuji, S. Sakurai *et al.* Carbon, **173**, 448-453 (2020).

[2] T. Tsuji, S. Sakurai *et al.* ACS Omega, DOI: 10.1021/acsomega.1c01822.

Corresponding Author: S. Sakurai

Tel: +81-29-861-6205, Fax: +81-29-861-4851

E-mail: shunsuke-sakurai@aist.go.jp

O₂ assisted growth of small-diameter vertically-aligned SWCNTs using Os catalyst

○ Kamal P Sharma^{1,2}, Masaya Kobayashi¹, Daiki Yamamoto¹, Takahiro Maruyama^{1,2}
¹Department of Applied Chemistry, ²Nanomaterials Research Center, Meijo University

Single-walled carbon nanotube (SWCNT) is realized as a promising material for fore frontier application due to its superior chemical, electrical and optical properties (1). The band gap of semiconducting SWCNTs increases on decreasing diameter, and a band gap of larger than 1 eV is achievable by SWCNTs of diameter smaller than 1 nm (2,3) which is highly desirable for electronic application. Recently, we have reported an efficient technique for the synthesis of small-diameter vertically-aligned SWCNTs (VA-SWCNTs) by alcohol catalytic chemical vapor deposition (ACCVD) (4,5). In this research, we challenged to improve the growth rate of VA-SWCNTs.

An ultrahigh vacuum (UHV) ACCVD system with a nozzle in the proximity of substrate though which ethanol is supplied as a chemical vapor was used as a growth chamber as reported elsewhere (4). A variable leak valve is employed to supply O₂, which is mixed with ethanol prior to effuse through the nozzle onto substrate. 0.2 nm Os catalysts-deposited SiO₂/Si were utilized as growth substrates. 10⁻¹ Pa ethanol vapor over the 10⁻⁶ Pa base pressure was supplied for 60 min at 800 °C. As synthesized SWCNTs under our optimized condition were analyzed by Raman spectroscopy, FESEM, and XPS.

Figure 1 (a) and **(b)** show the Raman spectra of VA-SWCNTs grown for 60 min at 800°C without and with mixing O₂ respectively by keeping other conditions unchanged. It is clearly observable that small diameter distributed SWCNTs grown in O₂ assisted technique with significant improved in growth rate (see FESEM images) compared to that observed in O₂ free technique. **Figure 1 (e)** shows Os retained its metallic state during annealing and after growth of SWCNTs. The nominal amount of O₂ mixed with ethanol helped to improve the growth rate.

Acknowledgement: This work was partially supported by the MEXT supported program “the Meijo University Research Branding Project for Cultivation and Invention of New Nanomaterials”

- [1] R. H. Baughman, et al. *Science*, 297, 787 (2002).
 [2] P. Avouris, et al. *Chem. Phys.* 281, 429 (2002).
 [3] Y. Matsuda, et al. *J. Phys. Chem. Lett.* 1, 2946 (2010).

- [4] T. Maruyama et al. *Appl. Surf. Sci.* 509, 145340 (2020).
 [5] T. Maruyama et al. *Diam. Relat. Mater.* 117, 108501 (2021).

Corresponding Author: takamaru@meijo-u.ac.jp (T.M.), kamalprasads@gmail.com (K.P.S.)

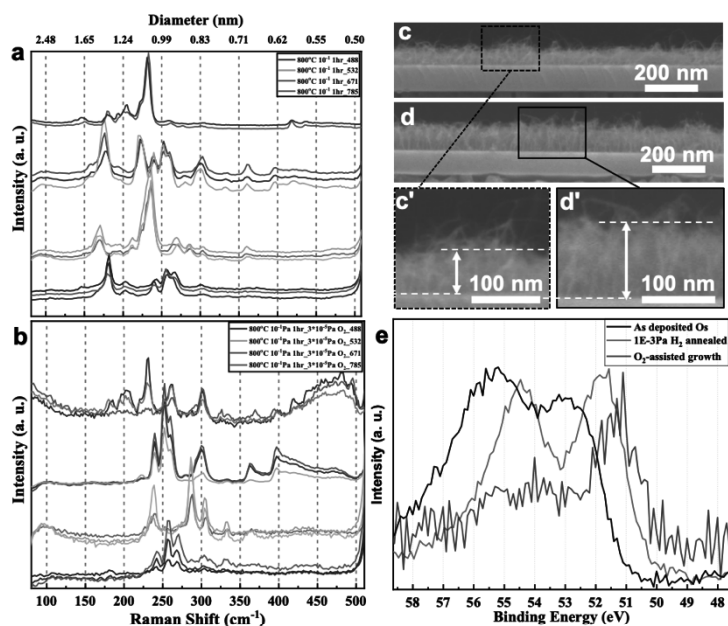


Figure 1. Raman spectra of SWCNTs grown onto SiO₂/Si by ACCVD technique **(a)** without, and **(b)** with O₂ assisted growth at 800°C for 1 h, and **(c)** and **(d)** show their respective cross-sectional FESEM images (**(c')**, **(d')** show their magnified images). **(e)** XPS spectra of Os 4f_{7/2} observed using samples from different stages of ACCVD process.

Synthesis and Characterization of Various One-dimensional van der Waals Heterostructures

○Wanyu Dai¹, Yongjia Zheng¹, Keigo Otsuka¹, Shohei Chiashi¹, Rong Xiang¹, Shigeo Maruyama¹

¹*Department of Mechanical Engineering, The University of Tokyo, Tokyo 113-8656, Japan*

We recently presented the experimental synthesis of one-dimensional (1D) van der Waals (vdW) heterostructures which includes single-walled carbon nanotubes (SWCNTs), boron nitride nanotubes (BNNTs) and molybdenum disulfide nanotubes (MoS₂NTs) [1]. Further, the nucleation and crystal growth behaviors over these highly curved nanotube surfaces were investigated [2]. The atomic model, TEM image, and EELS mapping of the SWCNT-BNNT-MoS₂NT heterostructure are shown in Fig. 1 [2]. By using film samples, we have demonstrated the strong photoluminescence (PL) from monolayer MoS₂NT and quenching of PL by SWCNT through thin BNNT [3]. Furthermore, by using a micro-meter long single heterostructure, we have demonstrated that naturally *p*-doped SWCNT and *n*-type MoS₂NT becomes a radial semiconductor–insulator–semiconductor (S-I-S) tunneling heterojunction diode [4]. We can imagine various optical and electronic devices with such 1D heterostructures [5]. The 1D heterostructures which synthesized by shell-by-shell growth process have the freedom to alter the shell combination [2], while great numbers of transition metal dichalcogenides (TMDCs) nanotubes might be synthesized following similar strategies to MoS₂ growth [6]. Hence, the controlled synthesis process of 1D vdW heterostructures with different shell combination are of fundamental research interest [7]. Here we present the chemical vapor deposition (CVD) synthesis of 1D vdW heterostructures based on tungsten disulfide (WS₂) and niobium disulfide (NbS₂). Also, synthesis process of MoS₂ based 1D vdW heterostructures was re-optimized. From observations with transmission electron microscopy (TEM), all the TMDC shells in these heterostructures are verified being highly crystallized. This work indicates that CVD may be a universal synthesis method for 1D vdW heterostructures, and could be applied for a wide variety of TMDCs.

Part of this work was supported by JSPS KAKENHI Grant Number JP20H00220 and by JST, CREST Grant Number JPMJCR20B5, Japan.

- [1] R. Xiang, *et al.*, *Science*, **367**, 537 (2020).
 [2] Y. Zheng, *et al.*, *PNAS*, (2021), submitted.
 [3] M. Liu, *et al.*, *ACS Nano*, **15**, 8418 (2021).
 [4] Y. Feng *et al.*, *ACS Nano*, **15**, 5600 (2021).
 [5] R. Xiang, *et al.*, *Small Sci.*, **1**, 2000039 (2021).
 [6] J. Zhou, *et al.*, *Nature*, **556**, 355 (2018).
 [7] S. Cambre, *et al.*, *Small*, (2021), in press.

Corresponding Author: S. Maruyama
 Tel: +81-3-5841-6421, Fax: +81-3-5800-6983
 E-mail: maruyama@photon.t.u-tokyo.ac.jp

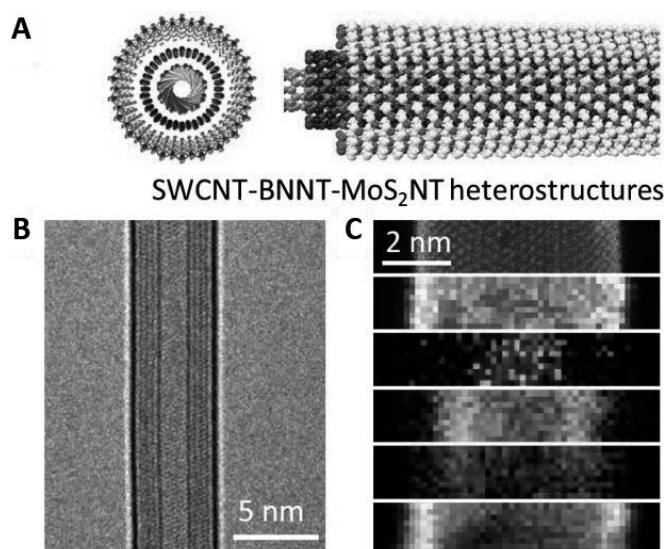


Fig. 1 (A) Atomic model, (B) TEM image and (C) EELS mapping of a SWCNT-BNNT-MoS₂NT hetero-structure (green, blue, red, yellow indicate the elemental distribution of carbon, boron, nitride, sulfur, respectively) [2].

Chirality isolation of single-walled carbon nanotubes by the phase transition of a thermoresponsive polymer

Eriko Shimura¹, Tomomi Tanaka¹, Yuki Kuwahara², Takeshi Saito², Toshiki Sugai¹,
○Shota Kuwahara¹

¹ Department of Chemistry, Toho University, Funabashi, Chiba 274-8510, Japan

² Nanomaterials Research Institute, National Institute of Advanced Industrial Science and Technology (AIST), Tsukuba, 305-8565, Japan

Recently, we demonstrated the sorting of chirality-selective semiconducting single-walled carbon nanotubes (SWCNTs), which is highly attractive for creating nanocircuits and thin film transistors from nanomaterials, by exploiting the phase transition of poly(*N*-isopropyl acryl amide) (PNIPAM), a well-known thermoresponsive polymer (Fig. 1a) [1]. Although the simple procedure and continuous use of PNIPAM have a high potential for the mass production of SWCNTs with a specific electronic structure, knowledge of efficient single-chirality sorting methods with mixed surfactant systems is not applicable since the available surfactant is limited to bile acid for the phase transition of PNIPAM. In this work, regarding the chiral isolation of SWCNTs, we explored experimental conditions by controlling the interaction among PNIPAM, sodium cholate (SC) and SWCNTs [2].

A dispersion of SWCNTs in aqueous SC solution was added to PNIPAM solution with additive. Then, the mixed solution was heated to 45 °C and incubated for 15 minutes. The obtained liquid phase was collected, and characterized by UV-vis-NIR spectrophotometer (SHIMADZU, UV-3600) and a Shimadzu NIR-PL system (CNT-RF).

After optimizing the PNIPAM and SC concentrations, tetraborate buffer solution was used for the additive. As shown in Fig. 1b, the sorting solution exhibited a bright PL peak that showed an S₁₁ emission at 883 nm and an S₂₂ excitation at 590 nm, which corresponded to (6,4) nanotubes. The PNIPAM sorting mechanism was explained by the difference in the micelle configuration on SWCNTs and the hydrophobic collapse of PNIPAM in the presence of a sodium salt.

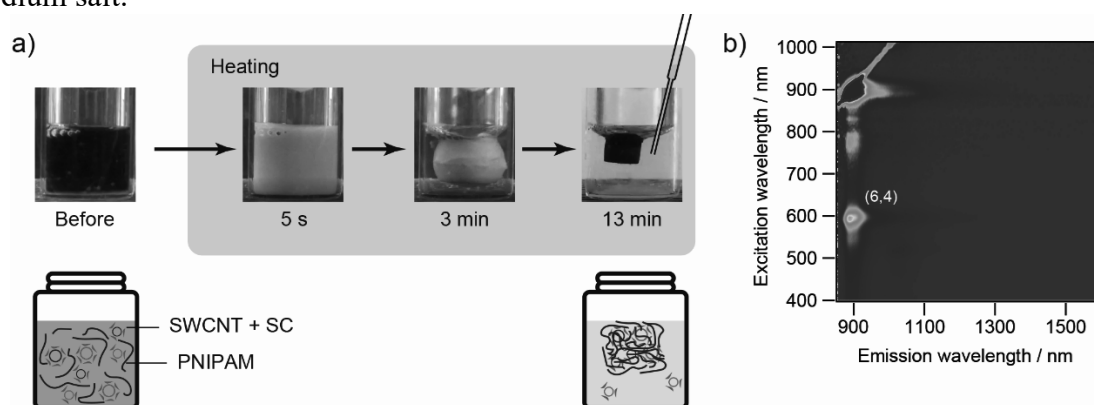


Fig. 1 (a) Images displaying the evolution of the aggregation and shrinkage of PNIPAM, including the dispersion of SWCNTs and SC. (b) PL excitation map for the sorting solution in the presence of a tetraborate buffer solution in D₂O.

[1] E. Shimura *et al.* Chem. Commun., **54**, 3026 (2018). [2] E. Shimura *et al.* RSC Adv., **10**, 24570 (2020).

Corresponding Author: S. Kuwahara

Tel: +81-47-472-4442, Fax: +81-47-472-4442, E-mail: syouta.kuwahara@sci.toho-u.ac.jp

Patterning and Photo-thermal Sensing Applications of Suspended, 2D, Micro-scale CNT film array

○Daichi Suzuki, Nao Terasaki

Sensing System Research Center, AIST, Saga 841-0052, Japan

Research and development of soft sensors is a core objective toward the realization of Society 5.0 centered around human augmentation and soft robotics. The advantages of a carbon nanotube (CNT) film compared to other soft materials are the ultra-wideband light absorption ranging from the millimeter wave band to the near infrared band due to the plasmon resonance, and the high conversion efficiency of the absorbed light (heat) to an electrical signal. By utilizing the photo-thermo-electric effect of a CNT film, we previously have developed a terahertz (THz) soft sensor and have demonstrated non-destructive quality inspections (Fig. 1) [1, 2]. This time, we report our recent results of a self-aligned filtration process for a suspended, 2D, micro-scale CNT film array and which applications as a THz camera patch sheet that can be cut freely and be attached according to the shapes of the measured objects [3].

The point of this filtration process is to directly form CNT films according to the pattern, instead of a top-down processing after the CNT film formation. First, holes are formed in a polyimide film, which is the support substrate of the CNT film, by laser ablation processing. By filtrating a CNT dispersion through a composite of the patterned polyimide film and a membrane filter, CNTs are filtrated only at the holes on the polyimide film in a self-aligned manner, and thereby CNT films are formed according to the pattern. After forming and drying the CNT films, when the membrane filter is peeled off, the suspended CNT films supported with the edges of the holes of the polyimide film is formed. The size and array position of the suspended CNT film can be freely adjusted in micro to centimeter size according to laser processing. This technique can be applied to variety of applications, i.e., THz cameras by 2D sensor arrays (Fig. 2), thermoelectric power generators with micro-scale thermocouples connected in series, and optical components such as array antennas and polarizers. We thus expect that this technique can widely advance the CNT device research progress.

[1] D. Suzuki *et al.* Nat. Photon., **10**, 809–813 (2016).

[2] D. Suzuki *et al.* Carbon, **162**, 13–24 (2020).

[3] D. Suzuki *et al.* Adv. Funct. Mater., **31**, 2008931 (2021).

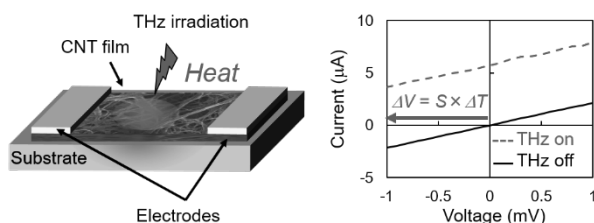


Fig. 1. THz soft sensor with a CNT film. The photo-thermo-electric voltage ΔV is generated, where S is the Seebeck coefficient of the CNT film and ΔT is the thermal gradient induced by THz irradiation, respectively.

Corresponding Author: D. Suzuki

Tel: +81-942-81-3620, Fax: +81-942-81-4018, E-mail: daichi.suzuki@aist.go.jp

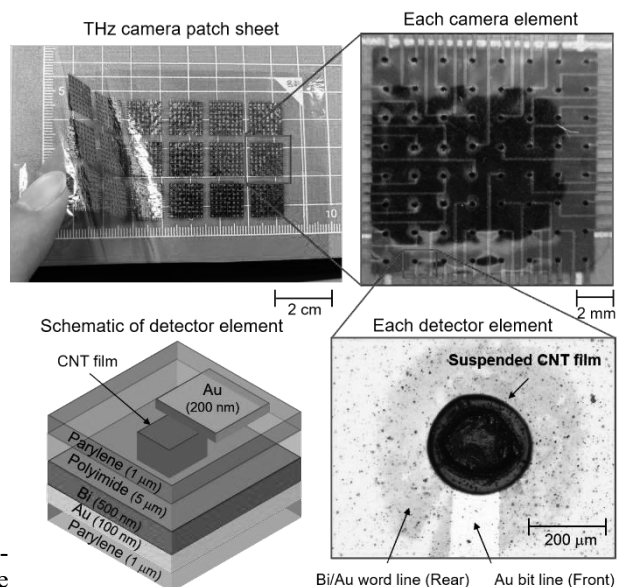


Fig. 2. THz camera patch sheet with a suspended, 2D, micro-scale CNT film array. A few tens of camera elements are combined in a single flexible sheet.

Novel excitonic features of moiré exciton in twisted van der Waals heterostructures

○Keisuke Shinokita¹, Yuhei Miyauchi¹, Kenji Watanabe², Takashi Taniguchi³, and Kazunari Matsuda¹

¹ Institute of Advanced Energy, Kyoto University, Uji 611-0011, Japan

² Research Center for Functional Materials, NIMS, Tsukuba 305-0044, Japan

³ International Center for Materials Nanoarchitectonics, NIMS, Tsukuba 305-0044, Japan

Atomically thin transition metal dichalcogenides (TMDs) is ideal two-dimensional system and possesses intriguing optical properties related to valley degrees of freedom [1]. Van der Waals heterostructures composed of TMDs are a fascinating platform to engineer the optically generated excitonic properties through moiré patterns towards novel quantum phenomena. The moiré pattern as a periodic trap potential can give rise to spatially ordered ensembles of zero-dimensional exciton (moiré exciton), which offers the possibility for dense coherent quantum emitters and quantum simulation of many-body physics [2].

Here we studied the novel moiré exciton properties in a twisted WSe₂/MoSe₂ heterobilayer based on near-resonant photoluminescence excitation (PLE) spectroscopy. Figure 1(a) shows the photoluminescence (PL) spectra with different excitation energies of 1.356 and 1.366 eV. Several peaks observed in the PL spectra reflect the response of the interlayer exciton trapped with the moiré potential, or moiré exciton. The PL spectral shape strongly depends on the excitation energy, suggesting highly selective excitation of a specific moiré exciton under resonance excitation conditions. The resonance behavior is clearly shown in the 2D color map of excitonic emissions as a function of excess energy in Fig. 1(b). The specific moiré exciton emission was enhanced under excitation with ~ 24 and ~ 48 meV excess energy, while the PL intensities are significantly weak under off-resonance conditions. The energy difference of 24 meV observed in the PLE resonance is close to the energy of the A₁' phonon mode in MoSe₂ and A₁' + E' phonon modes in WSe₂ at 30 meV (~ 240 cm⁻¹), suggesting that phonon resonances are candidates to explain the resonance features. The slight smaller energy of 24 meV compared with Raman signal of 30 meV would reflect the zero-dimensionality of moiré exciton [3].

[1] K. Shinokita *et al.*, Adv. Funct. Mater. **29**, 190260 (2019).

[2] K. Seyler *et al.*, Nature **66**, 567 (2019).

[3] K. Shinokita *et al.*, Nano Lett. *in press*.

Corresponding Author: K. Shinokita

Tel: +81-774-38-3465 Fax: +81-774-38-3467,

E-mail: shinokita.keisuke.4r@kyoto-u.ac.jp

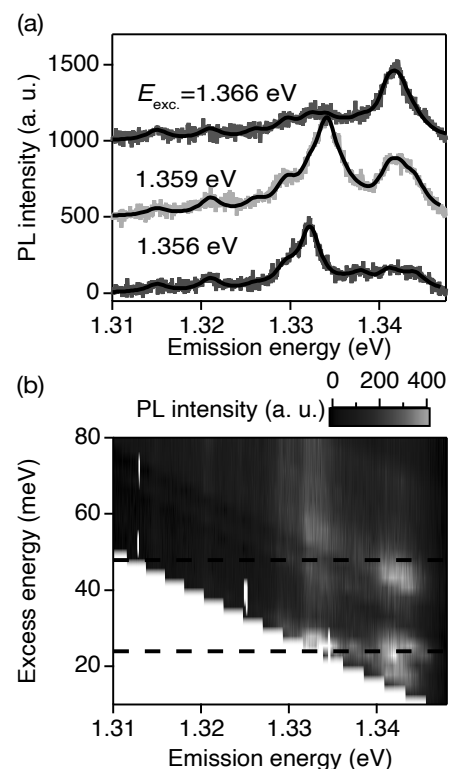


Fig. 1. (a) PL spectrum obtained under near-resonant excitation from $E_{\text{exc}}=1.356$ to 1.366 eV. The black lines are fitted with multiple Lorentz functions. (b) 2D color map of PL intensity as a function of excess energy. The black dashed lines show excess energy of 24 and 48 meV.

Controlled Removal of Surfactants from Double-Walled Carbon Nanotubes for Stronger *p*-Doping Effect and its Demonstration in Perovskite Solar Cells

○ Jeong-Seok Nam¹, Ahmed Shawky², Seungju Seo², Rong Xiang², Yutaka Matsuo², Shigeo Maruyama², Il Jeon¹

¹ Department of Chemical Materials, Pusan National University, Busan 46241, Republic of Korea

² Department of Mechanical Engineering, School of Engineering, The University of Tokyo, Tokyo 113-8656, Japan

Double-walled carbon nanotubes (DWNTs) have shown the potential as a promising alternative to conventional transparent electrodes owing to solution-processability as well as high conductivity and transparency.[1] However, their DC to optical conductivity ratio is limited by surrounding surfactants preventing *p*-doping of the carbon nanotubes.[2] To maximize the doping effectiveness, the surfactants are removed from double-walled carbon nanotubes with negligible damage to the nanotubes by calcinating in Ar atmosphere. The effective removal of the surfactants was evidenced by various analyses and the results show that 400 °C is the optimal temperature. The conductivity improvement of the double-walled carbon nanotube films by triflic acid increased from 31.9% to 59.7% after the removal of the surfactants. Using the surfactant-removed *p*-doped solution-processed transparent electrodes, inverted-type perovskite solar cells are fabricated and a power conversion efficiency of 17.7% without hysteresis is displayed. This work advances the transparent conductor application of double-walled carbon nanotubes as the efficiency is highest among the reported carbon nanotube electrode-based perovskite solar cells and solution-processable transparent electrode-based solar cells to date.

[1] I. Jeon, *et al.* J. Phys. Chem. Lett, **8**, 5395 (2017)

[2] I. Jeon, *et al.* Adv. Energy Mater, **9**, 1901204 (2019)

Corresponding Author: I. Jeon

E-mail: il.jeon@spc.oxon.org

Carbon Nanotube Mask Filters and their Hydrophobic Barrier and Hyperthermic Antiviral Effects on SARS-CoV-2

○Sangsu Lee¹, Jeong-Seok Nam¹, Jiye Han¹, Qiang Zhang², Esko I. Kauppinen², Il Jeon¹

¹ Department of Chemical Materials, Pusan National University, Busan 46241, Republic of Korea

² Department of Applied Physics, Aalto University School of Science, Aalto FI-00076, Finland

COVID-19, caused by SARS-CoV-2, is extremely serious as it mutates naturally over a short period of time. This disease infection spreads via airborne saliva droplets, and mask filters can effectively block these particles. While the vaccine against the SARS-CoV-2 has been developed recently, the mutations are far from being resolved. Therefore, experts from many organizations, including the WHO, have stated that wearing a face mask is the one of the most effective methods of preventing COVID-19 both before and after vaccination. Targeting protection against SARS-CoV-2, our investigation and discussion focus on five key aspects: 1) industrial viability, 2) hydrophobicity, 3) breathability, 4) anti-viral effect and 5) reusability.

In this study, commercially available spunbonded/melt-blown/spunbonded polypropylene (SMS) filter-based face masks are used as the control sample. Owing to the roll-to-roll processability of the CNT film, the CNT filter could be added on top of the SMS filter or replace one of the existing layers without a significant increase in production cost. The CNT filter exhibited stronger hydrophobicity uniformly across the area of the filter compared with the conventional SMS filter. The average water contact angle of the CNT filter ($131.7^\circ \pm 0.87^\circ$) was approximately 7° greater than that of the SMS filters ($124.6^\circ \pm 3.07^\circ$), and 75% of the CNT filter area exhibited a water contact angle above 130° . In addition, the CNT filter displayed a long durability of greater than 5 d without reduction in hydrophobicity under constant application of the water droplets, owing to the exceptional mechanical strength of the nanotubes. OTR showed that the addition of a CNT filter does not undermine breathability, while demonstrating a better blocking effect against the intruding airborne saliva droplets.

The physical porosity of the CNT filter observed by scanning electron microscopy (SEM) shows that the CNT network has a smaller pore size of less than 100 nm on average compared with the SMS filters. Considering that the size of a single SARS-CoV-2 varies between 100 nm and 200 nm, it can easily be inferred that the CNT filter also blocks the intrusion of the virus. The high thermal conductivity of the CNT filter induced a hyperthermal anti-viral effect, as evidenced by the swift temperature rise to 65°C in less than 5 min when the situation of the mask being worn outside was simulated. Inactivation of the viruses on the heated CNTs was confirmed by both SEM and transmission electron microscopy (TEM) imaging of denatured viruses. It transpires hyperthermic antiviral effects, which offers stronger protection against the virus, as well as reusability.

In brief, we are positive that aerosol-synthesized CNTs can be viable on an industrial level within a short time. Its effectiveness in protecting against SARS-CoV-2 in every key aspect of the face mask proves that the CNT material has promising potential when used solely or in combination with conventional face masks according to the results of this work. The aerosol-synthesized carbon nanotube filter warrants its viability, reinforcing the fight against the COVID-19 pandemic.

Corresponding Author: I. Jeon, E. Kauppinen

E-mail: il.jeon@spc.oxon.org (I.J.), esko.kauppinen@aalto.fi (E.K.)

Output power enhancement of stretchable, transparent triboelectric nanogenerator by charge trapping layer

○Masahiro Matsunaga¹, Jun Hirotsu², Yutaka Ohno^{1,2}

¹ *Institute of Materials and Systems for Sustainability, Nagoya University, Nagoya 464-8601, Japan*

² *Department of Electronics, Nagoya University, Nagoya 464-8603, Japan*

Triboelectric nanogenerator (TENG), a kind of mechanical energy harvester, is a promising candidate for self-powered electronics because of its outstanding features such as simple structure, high-output capability, and diverse material selection [1]. Previously, we have reported stretchable and transparent TENG using carbon nanotube thin film as a transparent electrode for wearable self-powered electronics [2]. High-output power of 8 W/m² with hand tapping was obtained by modifying the electronegativity of the elastomer surface with CF₄ plasma treatment. However, further enhancement of the output power is required for the realization of self-powered electronics. In this study, we introduced a charge trapping layer to enhance the output power.

Figure 1 shows a schematic of the TENG with a charge trapping layer. The charge trapping layer captures the charges generated by the triboelectrification, so that, total charge density at the surface of the TENG is increased. The charge trapping layer was formed by polydimethylsiloxane (PDMS) / SWNT mixture and inserted into the top elastomer layer. The simultaneous output power density as a function of the external load resistance was shown in Fig. 2. Here, the external mechanical force of 5 N at 2 Hz was applied using a linear motor. The output power density was enhanced from 28 mW/m² to 51 mW/m² by introducing the charge trapping layer. We also obtained a high output power density of 13.6 W/m² by hand tapping (approximately 70 N, 2 Hz). The detail will be discussed in the presentation.

[1] Z. L. Wang, *Mater. Today* **20**, 74 (2017).

[2] M. Matsunaga, et al., *Nano Energy* **67**, 104297 (2020).

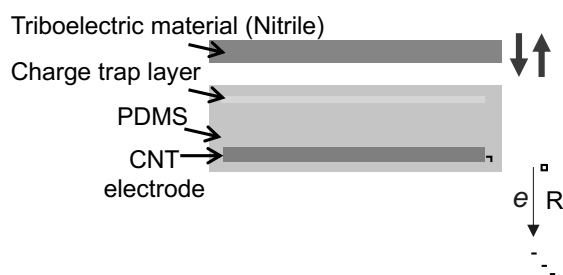


Fig. 1 Schematic of TENG with charge trapping layer.

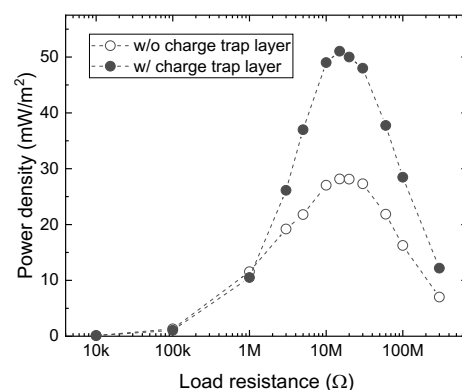


Fig. 2 Power density as a function of the load resistance.

Corresponding Author: M. Matsunaga

Phone: +81-52-789-5230, Fax: +81-52-789-5455

E-mail: matsunaga.masahiro@i.mbox.nagoya-u.ac.jp

Improvement in Thermal Diffusivity of CNT/Polymer Composite Films via Orienting CNTs by Robotic Dispenser

○Nikita Kumari, Ryo Abe, Naofumi Okamoto, Manish Pandey, Masakazu Nakamura

Division of Material Science, Nara Institute of Science and Technology, 8916-5 Takayama-cho, Ikoma, Nara 630-0192, Japan

Studies reveal that isolated Carbon Nanotubes (CNTs) exhibit very high and anisotropic mechanical, electrical, and thermal characteristics. However, bulk fabrication of aligned CNT networks is preferred for their practical applications. In bulk, CNTs are entangled due to their mechanical flexibility and strong van der Waals interactions. Therefore, to utilize their optimum potentiality, film fabrication with uniaxially aligned CNTs are significant. Recently, we have reported a method for fabricating oriented CNT/polymer composite films through a programmable robotic dispenser, as shown in Fig. 1 (a) [1]. Here the ink is extruded through a narrow needle, and ribbon-like films can be prepared on any substrates up to any length.

In this work, the CNT/polymer composite films were fabricated. The degree of CNT alignment in ribbon-like films was characterized by mapping the G-band intensity ratio of polarized Raman spectra, Fig. 1 (b – d). CNT orientation was found to be along the drawing direction. Here the orientation was sensitive to casting parameters such as dispensing parameters, wettability of the ink to the substrate, and ink composition, and their optimization will be reported in detail.

The effect of CNT alignment on the thermal diffusivity was also studied, and more than four-fold increment in thermal diffusivity was obtained compared to the isotropic films.

In addition to this, the effect of CNT length was also crucial for obtaining the optimum thermal transport. The

impact of various other parameters concerning dispersion and ink composition as well as film fabrication will be discussed in detail.

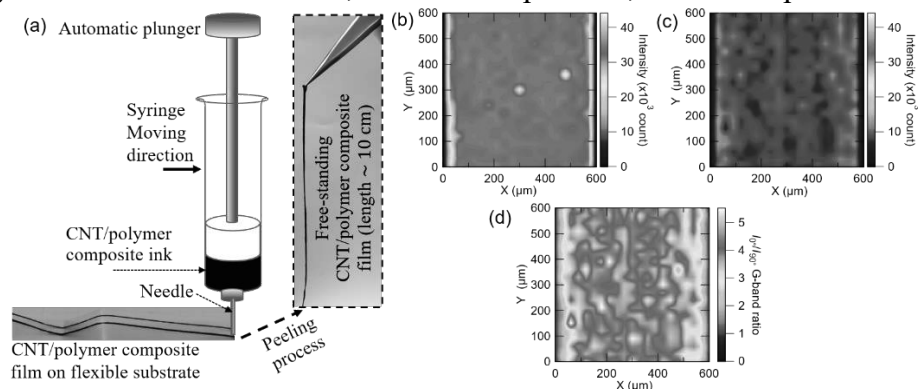


Fig. 1. (a) Schematic for film casting by robotic dispenser and digital image of representative films. Polarized Raman mapping of G-band intensity with laser polarized (b) along (I_{00}) and (c) orthogonal (I_{900}) to casting direction. (c) I_{00}/I_{900} corresponds to CNT orientation in the film. X- and Y-axis are along the ribbon width and length.

Reference:

[1] M. Pandey et al., Appl. Phys. Express 13, 065503 (2020)

Acknowledgment:

This work was supported by JST CREST Grant Number JPMJCR18I3, Japan.

Corresponding Author: M. Nakamura

Tel: +81-743-72-6031, Fax: +81-743-72-6047,

E-mail: mnakamura@ms.naist.jp

Hall effect in gated single-wall carbon nanotube films

○Yohei Yomogida¹, Kanako Horiuchi¹, Ryotaro Okada¹, Hideki Kawai¹, Yota Ichinose¹, Hiroyuki Nishidome¹, Kan Ueji¹, Natsumi Komatsu², Weilu Gao³, Junichiro Kono^{2,4,5}, Kazuhiro Yanagi¹

¹*Department of Physics, Tokyo Metropolitan University, Hachioji, Tokyo 192-0397, Japan*

²*Department of Electrical and Computer Engineering, Rice University, Houston, Texas 77005, USA*

³*Department of Electrical and Computer Engineering, University of Utah, Salt Lake City, UT 84112, USA*

⁴*Department of Physics and Astronomy, Rice University, Houston, Texas 77005, USA*

⁵*Department of Materials Science and NanoEngineering, Rice University, Houston, Texas 77005, USA*

Hall-effect measurements are fundamental methods to evaluate the type and density of charge carriers in crystalline materials. However, it is known that Hall measurements can lead to erroneous carrier types and densities when hopping carriers dominantly contributed to the charge transport [1]. Therefore, in hopping conduction systems, it is essential to compare the carrier types and density with those obtained by other methods such as field-effect transistor (FET) measurements. Thin films composed of single-wall carbon nanotubes (SWCNTs), which are important for fundamental research and device applications, are also known to be hopping conduction systems. Thus, in interpreting Hall effect in SWCNT films, one must carefully assess the contribution of hopping carriers. However, these issues have not been addressed in previous Hall-effect studies of SWCNT films. In this study, we evaluate the validity of the Hall effect in SWCNT films by comparing the results of Hall effect with those of FETs.

Transistors with standard Hall bar configuration were fabricated using films of different SWCNTs, such as metallic, semiconducting, and unsorted SWCNTs. The carrier types and density were controlled by ionic liquid gating. Figure 1 shows transfer characteristics of the metallic SWCNT device. We observed clear n- and p-type conduction. Hall measurements were performed on such gated sample. Figure 1 shows the measured Hall voltage of the metallic SWCNT device in the n-type and p-type regions. The magnetic field dependence corresponds to the doped carriers, indicating that the type of carrier can be correctly estimated by the Hall effect. On the other hand, regarding the carrier density, the Hall-determined carrier densities ($\sim 10^{17} \text{ cm}^{-2}$) were significantly overestimated compared to the FET-determined carrier densities ($\sim 10^{15} \text{ cm}^{-2}$). This overestimation behavior was observed in all samples, and the degree of overestimation varied among the samples.

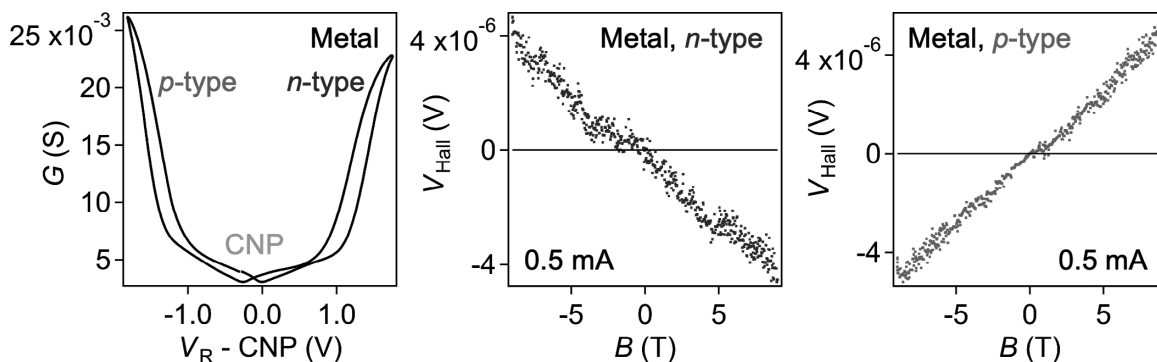


Fig. 1 (left) Transfer characteristics of the metallic SWCNT device. Channel conductance G is plotted as a function of reference voltage V_R . (center, right) Hall voltages V_{Hall} of the metallic SWCNT device, plotted as a function of magnetic field. Data in the n-type (center) and p-type regions (right) are shown.

[1] T. Uemura et al., Phys. Rev. B 85, 035313 (2012), H. T. Yi et al., Sci. Rep. 6, 23650 (2016).

Intuitive Correlations between Heat and Charge-Carrier Flows in Vertical Devices Using Single-Walled Carbon Nanotube Films

○Kan Ueji¹, Nobuhiro Muto¹, Yuya Matsuoka¹, Yota Ichinose¹,
Yohei Yomogida¹, Takashi Yagi², Jana Zaumseil³, Kazuhiro Yanagi¹

¹ Department of Physics, Tokyo Metropolitan University, Tokyo 192-0372, Japan

² National Metrology Institute of Japan, National Institute of Advanced Industrial Science and Technology, Tsukuba, Ibaraki 305-8563, Japan

³ Institute for Physical Chemistry and Centre for Advanced Materials, Universität Heidelberg, D-69120 Heidelberg, Germany

Flexible devices composed of carbon or organic materials have attracted attention because the Internet-of-Things society utilizes flexible devices as ubiquitous sensors, electronics, and thermoelectric generators. However, flexible materials are more intractable than inorganic materials for fabricating ultrafine structures on the same plane. To handle this issue, one approach is to use a transistor with a vertical channel, *i.e.*, the film thickness of the flexible material is regarded as the channel direction in the device design. This vertical design using flexible materials was first proposed in 1994 [1] and has recently been shown to have equivalent performance to conventionally lateral transistors.

Single-walled carbon nanotubes (SWCNTs) are promising for thermoelectric phenomena based on the Seebeck effect because of their low dimensionality [2] and high chemical stability. To evaluate the thermoelectric figure-of-merit, a measurement technique is required for the Seebeck coefficient, electrical conductivity (σ), and thermal conductivity (κ). We have demonstrated the evaluation of the σ - κ relationship of the semiconducting SWCNT film depending on its Fermi-level tuning by electrolyte gating and time-domain thermoreflectance (TDTR) [3]. However, the measurement directions are different: σ and κ correspond to the lateral and vertical directions, respectively. To overcome this direction problem, we employ a vertical electrolyte-gated transistor by which the semiconducting SWCNT film is doped overall [4]. We also conducted trial investigations on the σ - κ relationships of two kinds of SWCNT films in vertical devices without electrolytes. The first involves semiconducting SWCNTs separated from the arc-discharge CNTs using an ultracentrifuge; moreover, the film was transferred to the device (sample No.1). The second is a (6,5) CNT separated from CoMoCAT by the polymer wrapping method, where the film was fabricated by aerosol printing (sample No.2).

The vertical devices and TDTR systems reveal that both films have low κ and low σ (No.1: $0.1 \text{ Wm}^{-1}\text{K}^{-1}$, $5 \times 10^{-2} \text{ Sm}^{-1}$; No.2: $0.04 \text{ Wm}^{-1}\text{K}^{-1}$, $8 \times 10^{-6} \text{ Sm}^{-1}$), thus indicating that the dominant heat flows in both films are by phonon transport. Furthermore, the κ of No.1 is more than twice that of No.2, suggesting that the method used to fabricate the film affects its internal structure. The details of this study will be further discussed during the presentation.

[1] Y. Yang *et al.*, *Nature* **372**, 344 (1994). [2] L. D. Hicks *et al.*, *Phys. Rev. B*, **47**, 16631 (1993)

[3] K. Ueji *et al.*, *APL*, **117**, 133104. (2020). [4] M. Rother *et al.*, *ACS Appl. Nano Mater.* **1**, 3616 (2018)

Corresponding Author: K. Ueji and K. Yanagi

E-mail: kueji@tmu.ac.jp (K.U.), yanagi-kazuhiro@tmu.ac.jp (K.Y.)

Dispersed 2.6nm Quasi-Spherical Diamond Particles : A Versatile Starting Material in Nanotechnology

○Eiji Ōsawa¹, Toshihiko Tanaka² and Amanda Barnard³

¹NanoCarbon Research Institute Limited, AREC, Dept. Fiber Sci. Eng., Shinshu University, Ueda, Nagano 386-8567, Japan. ²Department of Chemistry and Biochemistry, National Institute of Technology, Fukushima College, Iwaki, Fukushima, 970-8034, Japan. ³Australian National University, Research School of Computer Science, Acton ACT 2601, Australia.

As nanotechnology keeps expanding, and fullerenes and carbon nanotubes have been exhaustively worked out, it is desirable to have a few more new nanoparticles that are readily available and can be used as our common starting material [1]. Actually, many of us regarded *detonation nanodiamonds* (DND) an ideal material for this purpose and studied them extensively. However, we found that DNDs could be further split into 4~5nm particles with large excess of 30 μ m zirconia beads in a commercial beads-milling setup in 2005 [2]. However, then it took very long time for us to reach the true PPDND: we had to solve quite a few new problems and phenomena unique to nanoparticles. In the meantime, we observed remarkable increase in the toughness of solid matrices when trace amounts of PPDND were dispersed in them. In view of the brittle fracture in practically all of the artificial solid materials including plastics and ceramics, the toughening effect of PPDND suggests tremendous usefulness that we can even think of replacing iron with PPDND-dispersed PET. All these details will be reported herein and also in the forthcoming papers.

Synthesis. DND agglomerates were dispersed in water to 4% concentration to give fairly stable suspension. Beads-milling of the suspension with an Ultra Apex Mill (made in Kotobuki Giken Kogyo Co.) easily disintegrated DND into its PPs to give translucent black aqueous solution! It takes 2 hours to process 20g of DND into the PP solution in quantitative yield.

Size and Shape of PPDND. Average hydrodynamic size of 2.6 \pm 0.5nm proved close to one-half of the initially given DND size of 4 to 5nm. The dimer bonds must have been abnormally strong. As the diamonds are well known for their rich metamorphic varieties, which should have close stabilities, the final black PPDND solution must contain considerable number of isomers of PPDND. For convenience, we chose one intermediate as the representative structure (Fig. 1).



Fig. 1. A favored candidate for a representative structure of PPDND. Left: Line drawing of truncated rhombicuboctahedron. Center: Computed surface charge distribution. Right: Wire mesh model. Surface is virtually graphitized. Core diamond is partially visible (in black).

Surface and Internal Structure of PPDND.

Extensive graphitization of the top layer of PPDND must have caused enormous strain to localize below the surface. As a consequence, at least the top layer of core diamond is likely disordered, but the rest remained as the initial cubic diamond structure.

[1] V. Danilenko, O. A. Shenderova, 'Advances in synthesis of nanodiamond particles,' in '*Ultrananocrystalline diamond, 2nd edition*,' O. A. Shenderova, D. M. Gruen (eds.), Chapt. 5, p. 133-164.

[2] A. Krüger, *et al.* "Unusually tight aggregation in detonation nanodiamond: identification and disintegration," *Carbon* **2005**, 43, 1722-1730.

Corresponding Author: E. Ōsawa, Tel: +81-0268-75-8381, E-mail: osawa@nano-carbon.jp

Self-Assembled Organofullerene Nano- and Microspheres Containing Inorganic and Biological Nanoparticles

○Koji Harano¹, Ryosuke Sekine¹, Prince Ravat¹, Haruaki Yanagisawa², Chao Liu¹, Masahide Kikkawa², Eiichi Nakamura¹

¹ Department of Chemistry, The University of Tokyo, Tokyo 113-0033, Japan

² Department of Cell Biology and Anatomy, Graduate School of Medicine, The University of Tokyo, Tokyo 113-0033, Japan

Multiple-component nano- and microspheres represented by core-shell particles continue to be the subject of research and applications in diverse fields, and their preparation is likewise diverse requiring a meticulous choice of conditions depending on the size, the nature of the core particles, and their use. For example, the synthesis of archetypal organic microspheres includes the coating of a particle with a monomer emulsified by a surfactant followed by polymerization that converts the noncovalent monomer assembly to a covalently bonded shell. The covalent network that guarantees stability, however, requires chemical transformations and hence imposes limitations on the range of core particles that can be inside. We have explored for some time the diversity of nanostructures created by self-assembly of conical fullerene amphiphiles in water or buffer such as vesicles, micelles, Langmuir-Blodgett films, and anisotropic nanostructures, and conjectured on self-assembly of the fullerene molecules into a spherical solid (fullersphere, FS) containing nanoparticles (NPs) inside. Herein, we describe an approach via self-assembly to robust core-shell particles via in situ conversion of a water-soluble anion, (4-heptylphenyl)₅C₆₀⁻K⁺ (**C7K**), to amorphous nano- to microspheres of (4-heptylphenyl)₅C₆₀H (**C7H-FS**) (Figure 1). Scanning electron microscopy indicates a perfectly spherical FS of narrow size distribution. The key enabler is the higher acidity of **C7H** than water (estimated to be less than 13) that allows gradual protonation of **C7K** by neutral to alkali water to in situ generate water-insoluble **C7H**. This process ensures uniform nucleation of NPs and hence the spherical shape and uniform diameter. The diameter of FS can be tuned from 30 nm to 2.5 μm by changing the mixing rate and pH of the buffer. Using an aqueous solution of organic dye, inorganic NP, protein, and virus, we incorporated these entities in FS. FS is spherical, amorphous, thermally stable, and resistant to electron irradiation, and we found its unconventional utility as a container for electron tomography, where the specimen is tilted about a rotational axis for data collection from various directions to obtain three-dimensional structural information of NPs and biomaterials inside.

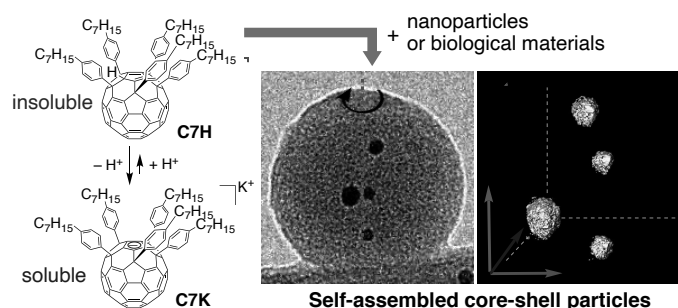


Fig. 1 Preparation and electron tomographic application of fullerspheres containing nanoparticles.

[1] R. Sekine *et al.* *J. Am. Chem. Soc.*, **143**, 2822 (2021).

Corresponding Authors: K. Harano and E. Nakamura

Tel: +81-3-5841-4369, Fax: +81-3-5841-4367,

E-mail: harano@chem.s.u-tokyo.ac.jp

Carrier density tuning of Nb-doped WSe₂ by an external electric field

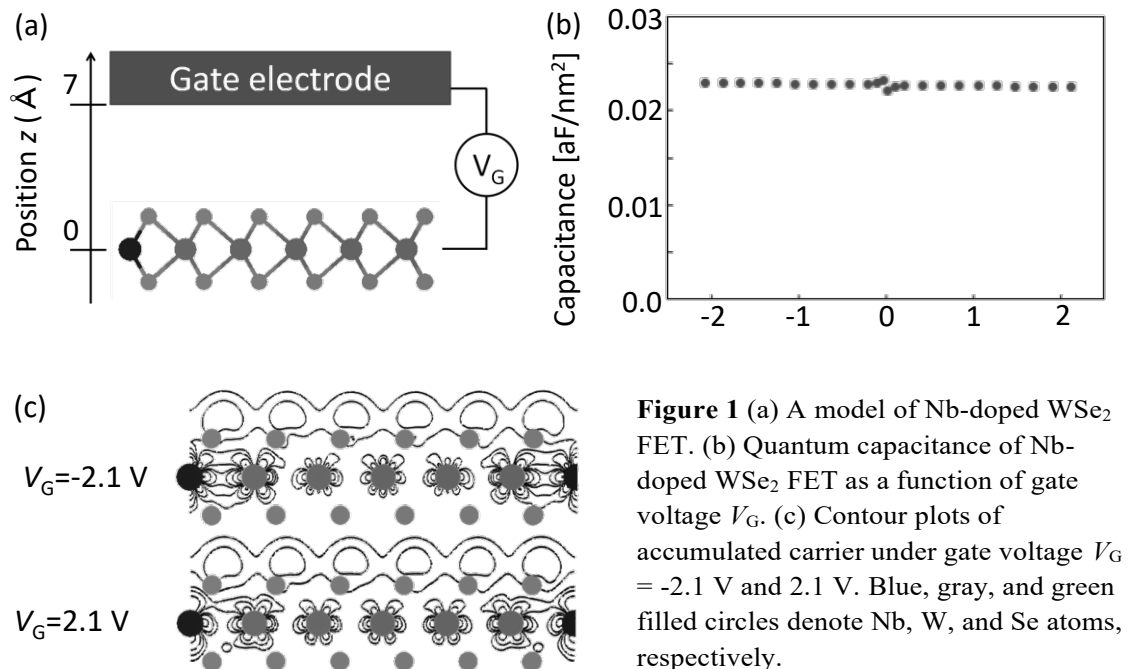
○Kaoru Hisama¹, Yanlin Gao¹, Mina Maruyama¹, Ryo Kitaura², and Susumu Okada¹

¹ Department of Physics, University of Tsukuba, Tsukuba 305-8571, Japan

² Department of Chemistry, Nagoya University, Nagoya 464-8602, Japan

Nb is a plausible dopant to inject hole into transition-metal dichalcogenides (TMDCs), making them p-type channel materials. The doped hole is extended throughout the sheet, because of a strong orbital hybridization between transition-metals and Nb. Although the intrinsic hole distribution in Nb-doped TMDCs is clarified, it is still uncertain whether the carrier density is controllable by the external electric field or not. Therefore, to clarify the possibility of the Fermi level tuning, we investigated the carrier density of Nb-doped WSe₂ implemented in a field effect transistor (FET) with a top gate electrode, using the density functional theory combined with the effective screening medium method [Fig. 1(a)].

Calculated quantum capacitance of the Nb-doped WSe₂ has approximately a constant value of 0.023 aF/nm² under gate voltage ranging from -2.1 to 2.1 V [Fig. 1(b)]. Carriers injected by the gate voltage are primarily distributed on S atomic sites located at the electrode side and extended through the surface [Fig. 1(c)]. Because of the constant capacitance and the extended carrier distribution, Nb-doped WSe₂ is a promising p-channel material where the Fermi level is tunable by the gate electric field.



Enhancement of the Thermal Conductance on Artificially Stacked MoS₂ by Intercalation

Wenyu Yuan¹, Kan Ueji¹, Takashi Yagi², Takahiko Endo¹, Hong En Lim¹,

Yasumitsu Miyata¹, Yohei Yomogida¹, ○Kazuhiro Yanagi^{1*}

¹Department of Physics, Tokyo Metropolitan University, Tokyo, Japan

²Department of Physics, Tokyo University of Science, Shinjuku, Tokyo, Japan

The ability to tune the thermal transport of solids is of increasing significance for advanced electronics and thermal energy harvesting. Over the past decade, various strategies have been demonstrated to tune the heat flow, in which the electrical manipulation by the applied voltage is highly desirable. The electronic structure can be altered through electric field, which includes the electrochemical intercalation, the injection of carriers, and the symmetry transformation, thereby ultimately affects the heat conduction. Conventional thermophysical theory suggests that the intercalation of heteroatoms into lattices or interlayers deservedly leads to the suppression of heat conduction due to the unavoidably enhanced phonon scattering. For instance, the intercalation of Li⁺ cations into various two-dimensional (2D) materials (e.g. MoS₂, black phosphorus) *decreases* the out-plane thermal conductivity [1]. Here, we report the *enhancement* of out-plane thermal conduction by intercalation in the artificially stacked van der Waals (vdW) structure, 5- or 4-layered MoS₂.

Multi-layered MoS₂ were prepared through multi-transfer technique using monolayer MoS₂ film synthesized via a conventional chemical vapor deposition. We investigated thermal conductance G of the sample using our home-build time domain thermoreflectance (TDTR) setup. In our TDTR setup, the gold electrode can be used as the transducer, and thus we can combine electrochemical intercalation technique and the TDTR measurements, and make us to investigate the G during intercalation using KClO₄ as electrolyte.

Figure 1 shows the change of TDTR phase signal as a function of delay time. As shown here, we observed clear change of TDTR signals as the shift of gate voltage. The G values at each gate voltage are derived from calculation fitting. Figure 2 shows the change of G , which is derived through fitting simulation, as the shift of gate voltage. We found the enhancement of G nearly two times by the shift of gate voltage.

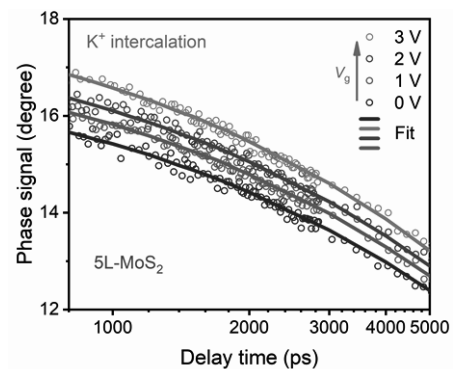


Figure 1: The change of the TDTR phase signal as the shift of gate voltage.

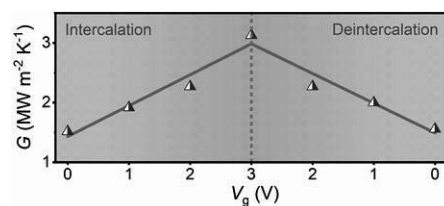


Figure 2: The change of G in 5L MoS₂ as the shift of gate voltage V_g

References:

- [1] J. S. Kang, et al., *Nano Lett.* **17**, 1431-1438 (2017). G. Zhu *et al.*, *Nat. Commun.* **7**, 13211 (2016).
Corresponding Author: K. Yanagi, +81-42-677-2494, yanagi-kazuhiro@tmu.ac.jp

Edge States of Graphene Oxide Observed by Field Emission and Field Ion Microscopy

○Yahachi Saito¹ and Yuta Nishina²

¹Toyota Physical and Chemical Research Institute, Nagakute 480-1192, Japan

²Research Core for Interdisciplinary Sciences, Okayama University, Okayama 700-8530, Japan

Electronic states at graphene edges exhibit peculiar properties, e.g., spin polarization at zigzag edge [1]. Field emission microscopy (FEM) of graphene edges shows a striped pattern (“lip pattern”), reflecting the symmetry of π orbitals at a graphene edge [2]. Field ion microscopy (FIM), being complementary to FEM, exhibits much fine images with atomic resolution. In our previous FIM study on few-layer graphene, arrays of paired spots being split on both side of a graphene plane, were observed [3]. According to the image formation mechanism of FIM, these dipole spots in the FIM images are surmised to reflect the spatial distribution of unoccupied π orbitals at the edges of graphene.

In the present study, FEM and FIM were applied to graphene oxide (GO) to reveal atomic structures and electronic states at the edges of GO. GO emitters were prepared by drop-and-dry of GO solution. Figure 1 shows a scanning electron micrograph of the edge of a prepared GO emitter. Figures 2 (a) and (b) are typical FEM and FIM images of a GO emitter, respectively. The FEM image (Fig. 2 (a)) exhibits a “lip pattern” characteristic to a graphene edge; an array of streaked double spots. The striation of spots perpendicular to the graphene layer is due to the strong anisotropy of magnification for two-dimensional material like graphene. The corresponding FIM image (Fig. 2 (b)), taken using Ne as imaging gas, reveals more detailed structures because of higher spatial resolution. An array of streaked, split spots (dipole spots), and race-track shaped spots, being very similar to those in FIM images of scratched graphene emitters [3]. Since the images in FIM represent the locations where imaging gas atoms are ionized by electron tunneling to unoccupied electronic states of the emitter, the observed FIM patterns (doublets, race-track shaped spots) reflect spatial distributions of the unoccupied π^* -orbitals at the edge of GO (and graphene).

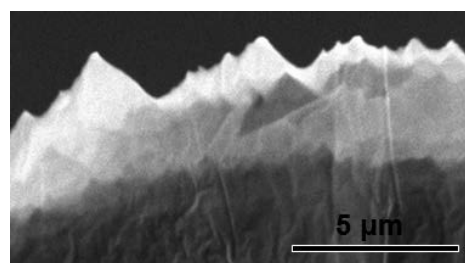


Fig. 1

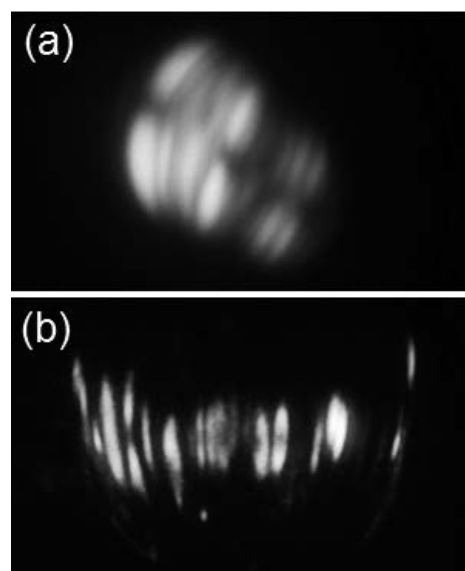


Fig. 2

[1] M. Fujita et al., *J. Phys. Soc. Jpn.* **65** (1996) 1920. [2] N. Yokoyama et al., *Surf. Interface Anal.* **48** (2016) 1217. [3] Y. Saito et al., *Abst. of the 57th FNTG Symp.* (Sept., 2019) p.27.

Corresponding Author: Y. Saito

Tel: +81- 561-57-9616, Fax: +81- 561-63-6302, E-mail: ysaito@toyotariken.jp

Energetics of bilayer hexagonal boron nitride nanoflakes: A nucleation process of a second layer on a substrate layer

○Mina Maruyama, Susumu Okada

Department of Physics, University of Tsukuba, Tsukuba 305-8571, Japan

Hexagonal boron nitride (hBN) is a key substrate material for other layered materials without modulating their physical and chemical properties. Therefore, it is important to synthesize high quality and large area hBN. Chemical vapor deposition (CVD) experiments reported that the nucleation of the second layer depends on the environmental conditions: Primarily two different nanoflake orientations have been observed on the substrate layer of hBN during CVD growth [1]. However, it is still uncertain the physical mechanism of the nucleation of the second layer of hBN. Therefore, in this work, we theoretically investigated energetic of bilayer hBN nanoflakes in terms of their mutual stacking arrangement, flake orientation, and edge termination using density functional theory with generalized gradient approximation including van der Waals correction.

Figure 1 shows calculation models in this work where the second layer of hBN nanoflakes with H edges are adsorbed on the large triangular hBN substrate with edge size of 2.3 nm. Our calculations demonstrated that the nucleation of the smallest triangular flake depend on the edge termination: Formation energy of the flake with N edges is lower than that with B edges irrespective of their orientation and position. We also found that the triangular flake prefers the center of the large hBN flake and the energy monotonically decreases with approaching the edge atomic sites. In contrast, the formation energy is insensitive to the mutual orientation of small flakes on the substrate layer.

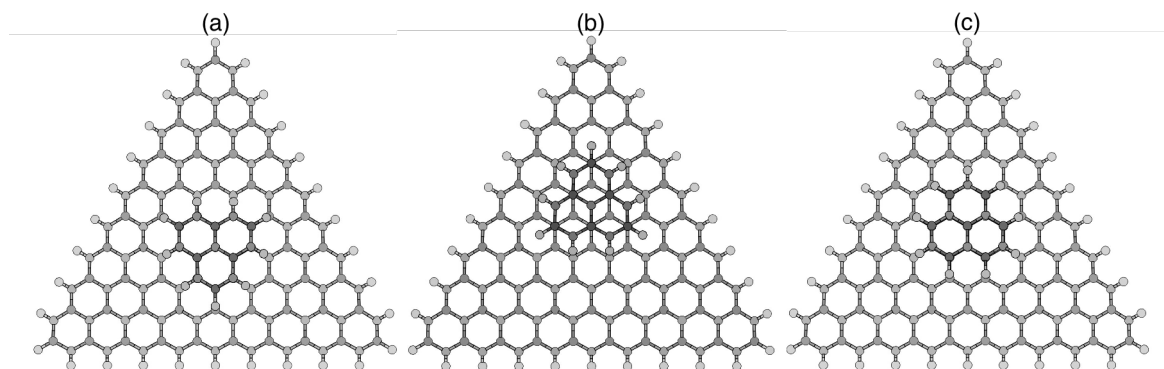


Fig. 1 A structural model of bilayer h-BN nanoflakes comprising a large triangular flake (2.3 nm) and the smallest triangular flakes with (a) N edge in AA' stacking, (b) N edge in AB stacking, and (c) B edge in AA' stacking. Blue, violet, and pink balls denote N, B, and H atoms, respectively.

[1] Y. Uchida, et al., *Phys. Chem. Chem. Phys.* **19** (2017) 8230-8235.

Corresponding Author: M. Maruyama

Tel: +81-29-853-5921, Fax: +81-29-853-5924, E-mail: mmaruyama@comas-tsukuba.jp

Efficient fabrication of graphene nanoribbon quantum dot devices with temperature-stable orbital-level spacing

○Naofumi Sato¹, Takahito Kitada², Mizuki Seo¹, Toshiro Kaneko¹, Tomohiro Otuka², Toshiaki Kato¹

¹ Graduate School of Engineering, Tohoku University, Sendai 980-8579, Japan

² Research Institute of Electrical Communication, Tohoku University, Sendai 980-8577, Japan

In recent years, graphene nanoribbon (GNR), strips of two-dimensional (2D) graphene into one-dimensional (1D) structure gather intense attentions because of their superior electrical features.

Until now, we have developed a novel method based on the advanced plasma CVD with nanoscale Ni catalyst (Ni nanobar) for directly fabricating suspended GNR devices [1, 2]. In this study, we have demonstrated the scalable fabrication of GNR-based quantum dot devices by adjusting GNR structures and growth conditions in our plasma CVD.

Systematic investigation revealed that fine structures are formed at the middle of the GNRs (Fig. 1), which can be considered as the origin of the quantum-dot features in our GNRs. Detailed measurements at cryogenic temperatures revealed that clear orbital-level spacings ($\Delta V_{ds,ex}$) between the ground state (GS) and excited states (ES) exist in our GNR-based quantum-dot device (Fig. 2). Furthermore, the orbital levels were found to be very stable even at high-temperature conditions (~ 20 K), which can be explained by the very fine structures formed in the middle of the GNR and relatively light effective mass of the GNR. More than 18% of devices fabricated within the same substrate showed orbital levels, indicating that integration of GNR-based quantum-dot devices is possible with our method. These findings further the fundamental study of GNR-based quantum devices toward practical applications.

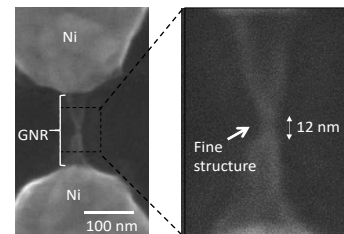


Fig. 1. SEM images of suspended GNR with fine structures grown by our plasma CVD.

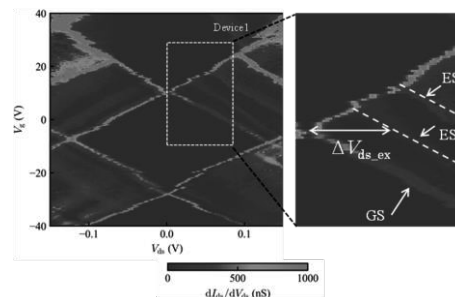


Fig. 2. Large Coulomb diamonds observed from our GNR-QD device. The dashed lines highlight ESs parallel to the edges of the diamonds (GS).

[1] T. Kato and R. Hatakeyama, *Nature Nanotechnology*, **7**, 651-656 (2012).

[2] H. Suzuki, T. Kaneko, Y. Shibuta, M. Ohno, Y. Maekawa, T. Kato, *Nature Communications*, **7**, 11797-1-10 (2016).

Corresponding Author: N. Sato

Tel: +8122-795-7046, Fax: +8122-263-9225,

E-mail: naofumi.sato.s2@dc.tohoku.ac.jp

Activation of single-photon emitter on CVD-hBN treated with thermal process

○Yusuke Adachi, Takayuki Arie, Kuniharu Takei, Seiji Akita

Department of Physics and Electronics, Osaka Prefecture University, Sakai 599-8531, Japan

Recently, hexagonal boron nitride (hBN) is expected to play an important role in various fields such as single photon emitters (SPEs) or nano-electro-mechanical components. The SPEs in hBN are bright and operate in room-temperature. Therefore, the hBN is considered to be promising components for quantum information and communication technology. However, there is room for improvement in emission purity or intensity. In this work, we investigate the light emission from multi-layer CVD-hBN treated with thermal annealing process [1].

The multilayer CVD-hBN on copper foil purchased from “SixCarbon Technology” was transferred to the substrate by typical wet transfer method. Transferred samples were put into a electric tube furnace and annealed at 850 °C for 30 min under 1 torr of argon. The sample was than cooled to room-temperature overnight.

We observed light emission from CVD-hBN at ambient condition. Fig.1(a) is the bright field image of CVD-hBN under the irradiation of LED light with the center wavelength of 530 nm. Fig.1(b) is the photoluminescence (PL) image of CVD-hBN under the irradiation of same LED light as in BF image. The PL image was taken through a 550 nm LPF. In the center of the PL image, there is a light emitting spot with a diameter of about 2 μm on the hBN film. Note that the PL emission from the hBN without thermal treatment has rarely observed.

Fig.1(c) shows a PL spectrum from the emission site on the CVD-hBN shown in Fig. 1 (b) measured at room temperature, where the 532 nm laser was used for excitation. The clear peak around 620 nm was observed corresponding to the zero phonon line.[1] Moreover, the spectrum shows a phonon side band doublet with well-resolved peak at 670 nm.[1] Thus, the thermal treatment around 850 °C is efficient for the activation of single photon emission site even for the multilayer CVD-hBN.

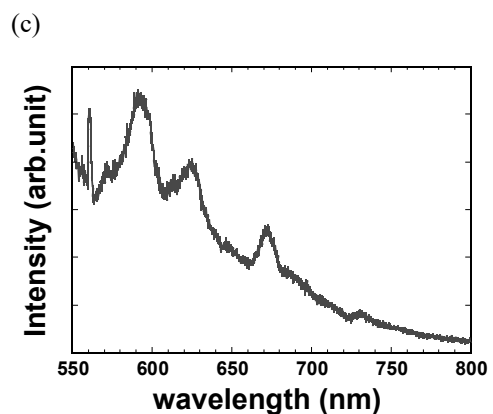
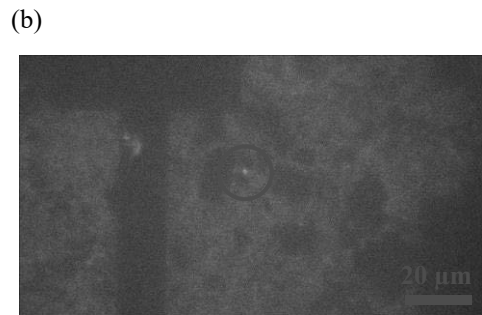
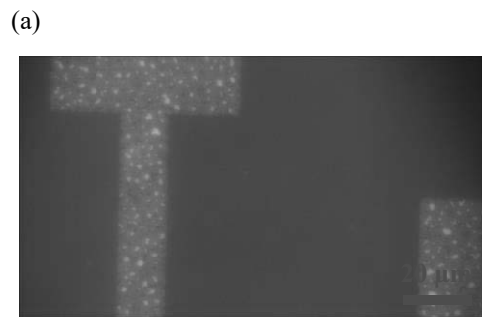


Fig.1: (a) BF image of the multilayer CVD-hBN when irradiated 530 nm light. (b) PL image of same hBN in BF image. (c) The PL spectrum of CVD-hBN excited by 532 nm laser at room temperature.

References

[1] T. T. Tran *et al.*, *Nat. Nanotechnol.* **11**, 37 (2016).

Corresponding Author: Y. Adachi

Tel: +81-72-254- 9261, E-mail: adachi-4@pe.osakafu-u.ac.jp

Spiro-graphene: New two-dimensional C allotropes comprising fenestratetraene and cyclooctatetraene

○Susumu Okada, Nguyen Thanh Cuong, Yanlin Gao, Mina Maruyama

Department of Physics, University of Tsukuba, Tsukuba 305-8571, Japan

Topological design of sp^2 C atoms provided an additional degree of freedom to tune the electronic structure of carbon-based nanoscale materials because the covalent network topologies of sp^2 C atoms tightly correlated with their electronic structure. Polymerization of small hydrocarbon molecules is one of plausible procedure for synthesizing covalent networks of C atoms whose structures are precisely controlled. This procedure benefits from the ability to design the electronic structures of resultant covalent networks by assembling and polymerizing appropriate molecules.

In this work, we aim to investigate the geometric and electronic structure of two-dimensional covalent networks of fused pentagons with structural rippling using density functional theory (DFT) with generalized gradient approximation because the pentagonal rings and polymeric structure of hydrocarbon molecules lead to a peculiar electronic structure. We focus on a fenestratetraene (four pentagons sharing their edges and one vertex) and a cyclooctatetraene (C_8H_8) as constituent unit of the networks (Fig. 1). Our DFT calculations revealed that the network is a metastable phase of a metallic carbon allotrope with relatively high total energy and remarkable thermal stability. This spiro-graphene comprising fenestratetraene and cyclooctatetraene is a metal where two dispersive bands cross at the Fermi level. In addition, this structure undergoes structural phase transition resulting in a space structure which possesses spin polarized states as its ground state.

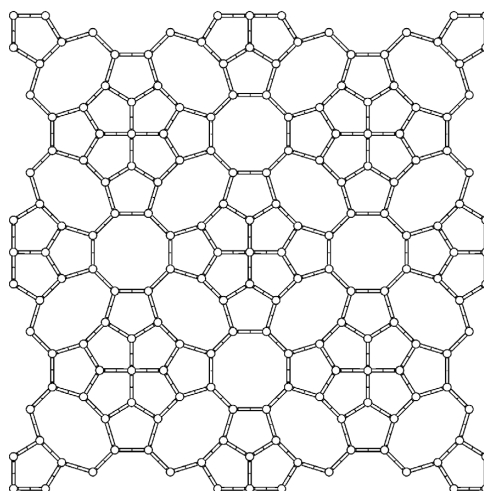


Fig.1 Geometric structure of spiro-graphene consisting of fenestratetraene and cyclooctatetraene.

Corresponding Author: Susumu Okada
 TEL: +81-29-853-5921, FAX: +81-29-853-5924
 E-mail: sokada@comas-tsukuba.jp

Insulating properties of h-BN film synthesized by sputtering method

○Daiyu Kondo¹ Kenjiro Hayashi¹, Masako Kataoka¹ and Shintaro Sato¹

¹ *Fujitsu Research, Fujitsu Limited,
10-1 Morinosato-Wakamiya, Atsugi 243-0198, Japan*

Hexagonal boron nitride (h-BN) is well known as a prominent candidate for an insulation and passivation layer of graphene-based devices [1]. Extremely high field effect mobility has been reported for a graphene-channel sandwiched between h-BN layers [2]. Generally, h-BN films are obtained by exfoliation from bulk h-BN. Therefore, one can easily imagine that it is difficult to prepare large-area h-BN for industrial use. Here, we propose synthesis of few-layer h-BN films by the sputtering method, which is easily scalable for electronics applications.

The sputtering method was performed in a low-pressure chamber. Metal catalysts such as iron (Fe) and BN films were sputtered on a sapphire substrate with a temperature of 500°C. The thicknesses of Fe and BN films were 50 nm and 2-150 nm, respectively. The sputtering of 2-nm BN onto the catalyst film resulted in the formation of few-layer h-BN, as observed in a transmission electron microscopy (TEM) image of figure 1. On the other hand, h-BN with random structures was observed when the thicknesses of sputtered BN were increased above 2 nm. Furthermore, insulating properties of few-layer h-BN were measured with a conductive atomic force microscope. The 5-nm-thick h-BN structures obtained by the sputtering method were found to break down when a voltage of -15 V was applied. By assuming the parallel plate model, the breakdown strength of h-BN was estimated to be around 40 MV/cm, which is compellable with that for exfoliated h-BN reported previously [3].

Part of this work was conducted at the Nano-Processing Facility, supported by IBEC Innovation Platform. This research was partly supported by JST CREST Grant Number JPMJCR15F1, Japan.

[1] H. Yamada *et al.* Science, **123**, 456 (2020). A. Geim and K. Novoselov, Nature Mater. **6**, 183 (2007)

[2] C.R. Dean, A.F. Young, I. Meric, C. Lee, and L. Wang, *et al.*, Nature Nanotechl. **5**, 722 (2010)

[3] Y. Hattori, T. Taniguchi, K. Watanabe, and K. Nagashio, ACS Nano **9**, 916 (2015)

Corresponding Author: D. Kondo

Tel: +81-46-250-8238, Fax: +81-46-250-8844,

E-mail: kondo.daiyu@fujitsu.com

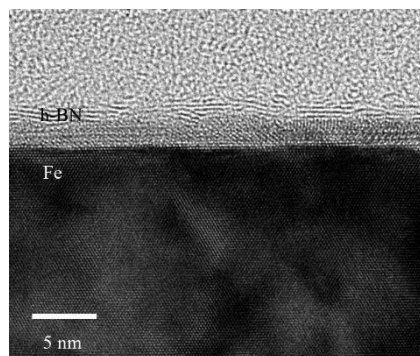


Fig. 1 Cross sectional TEM image of h-BN.

Precipitation of graphite layer with smooth and large domain on c-plane sapphire using crystallized Ni catalyst

○Shigeya Naritsuka¹, Asato Nakashima¹, Tomoaki Murahashi¹, Tatsuya Kashio¹,
Yasuhiro Fukunishi¹, Kazuki Mita¹, and Takahiro Maruyama²

¹ Department of Materials Science and Engineering, Faculty of Science and Technology, Meijo University, Nagoya 468-8502, Japan

² Department of Applied Chemistry, Faculty of Science and Technology, Meijo University, Nagoya 468-8502, Japan

Graphene was initially supplied by the exfoliation of highly-oriented pyroclitic graphite [1]. However, the size and the reproducibility was far inferior to the request of their applications. Chemical vapor deposition on copper foil is the regular routine to obtain graphene. On the other hand, we have been trying to produce a superior multi-layer graphene directly on substrates using precipitation method [2]. The high-quality multi-layer graphene, in other words, graphite is useful to use as a graphene source in the van der Waals engineering process of 2D materials [3]. Here, we show the result of graphite precipitation using crystallized Ni catalyst.

A 100 nm-thick MBE-grown Ni (111) layer was used to thermally crystallize a 300 nm-thick e-beam deposited Ni layer on a sapphire substrate. After the crystallization of the Ni catalyst, the sample was coated by nanodiamond, and heated at 900°C for 30min in a vacuum (10^{-4} – 10^{-3} Pa) using an infrared lamp apparatus. Then, the temperature was cooled down at a rate of 3°C/min. After the precipitation, the catalyst was removed using a diluted FeCl₃ solution to directly observe the graphene on the substrate.

Mapping of the Raman D/G peak ratios is shown in Fig. 1 along with a microscopy image of the sample area. It is evident from the figure that the ratio was reduced in the area with thick graphene islands. In addition, the boundaries where two graphene islands merged are shown by the broken lines in the image, and there is no associated increased in the D/G ratio in these regions. This result suggests that the islands are smoothly connected and so the boundaries had very few defects. This can likely be attributed to the precise alignment of the islands and to the smooth stitching. The perfect atomic arrangement of Ni atoms in the crystallized Ni layer also likely assisted in the superior alignment of the graphene islands.

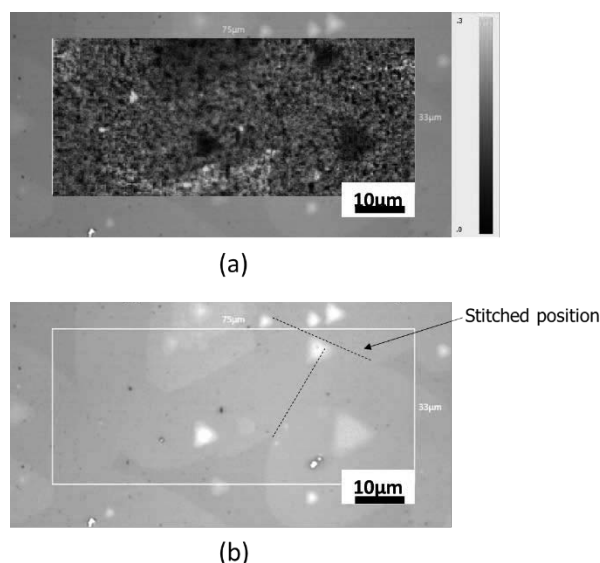


Fig. 1 (a) A Raman D/G ratio map of a precipitated graphene sample and (b) an N-DICM image of the corresponding area.

[1] K. S Novoselov et al., *Science* **306** (2004) 666.

[2] J. Yamada et al., *Jpn. J. Appl. Phys.* **55** (2016) 100302.

[3] S. Masubuchi et al., *Nature Comm.* **9** (2018) 1413.

Corresponding Author: S. Naritsuka

E-mail: narit@meijo-u.ac.jp

ポスター発表
Poster Preview

1P-1 ~ 1P-87

Fabrication and hierarchical structure control of carbon nanotube electron field emitter for X-ray tube

○Kotaro Yasui¹, Hisashi Sugime², Hayato Ochi³, Yuichi Nishikiori³, Suguru Noda^{1,2}

¹ Department of Applied Chemistry, Waseda University

² Waseda Research Institute for Science and Engineering, Waseda University

³ MEIDENSHA CORPORATION

Compared with thermal emitters, electron field emitters are effective for miniaturization and lowering energy consumption of X-ray tube which is expected for various uses such as medical and industrial uses. Carbon nanotube (CNT) which has high electric conductivity and high aspect ratio is one of the most promising material for electron field emitters, thus has been researched intensively [1]. In this research, field electron emitters were fabricated by controlling morphology of vertically aligned (VA) CNT variously via simple processes for X-ray tubes.

As shown in Fig. 1, the morphology of the VACNT was controlled, and the emitter performance was evaluated by applying electrical field with 2.5 kV/mm under $10^{-4} - 10^{-5}$ Pa for 1001 cycles. As can be seen in the current density at the 1001st cycle (Fig. 2), the morphology control of VACNT at the micrometer level had little effect on performance improvement (Sample B) while that at the sub-millimeter level significantly enhanced the field emission performance (Samples C and D).

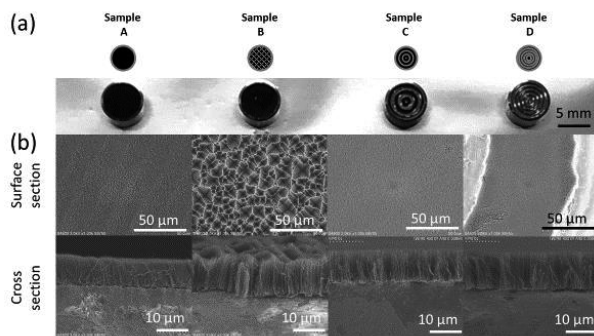


Fig. 1. (a) CNT emitters on Cu stages (Samples A, B, C, and D). (b) SEM Images of surface VACNTs morphology on emitters.

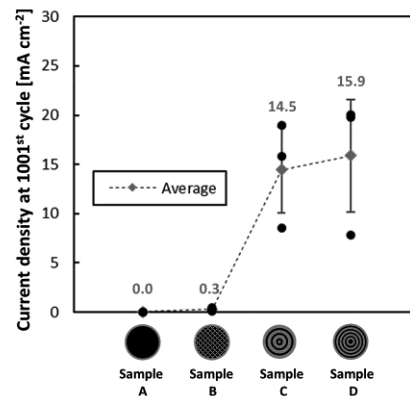


Fig.2, Current density at the 1001st cycle of the CNT emitters (Samples A, B, C, and D)

[1] Y. Cheng & O. Zhou, C.R. Physique, 4, 1021 (2003).

Corresponding Author: S. Noda
Tel&Fax: +81-3-5286-2769,
E-mail: noda@waseda.jp

Fabrication of nanostructures incorporating carbon nanotubes and one-dimensional confinement of charged excitons

○Haruna Nakajima¹, Taiki Inoue², Shohei Chiashi³, Shigeo Maruyama³, Keiji Ueno⁴, Kenji Watanabe⁵, Takashi Taniguchi⁵, Ryo Kitaura¹

¹ Department of Chemistry, & Institute for Advanced Research, Nagoya University, Nagoya 464-8602, Japan

² Department of Applied Physics, Graduate School of Engineering, Osaka University, Osaka 565-0871, Japan

³ Department of Mechanical Engineering, The University of Tokyo, Tokyo 113-8656, Japan

⁴ Department of Chemistry, Graduate School of Science and Engineering, Saitama University, Saitama 338-8570, Japan

⁵ National Institute of Materials Science, Tsukuba 305-0044, Japan

Functional heterostructures formed through assembling nanomaterials play a central role in nanoscience and nanotechnology. Carbon nanotubes (CNTs), ultrathin one-dimensional (1D) semiconductors/metals, are indispensable components for the functional heterostructures, providing ultimate thin semiconductor channels, local probes, and local gate electrodes, etc. In this research, aiming to establish a versatile construction method for nanostructures incorporating CNTs, we have developed a simple CNT transfer method by combining a polymer stamping and a micromanipulation machine. Also, we have applied the method to fabricate 1D-2D mixed-dimensional (1-2mD) structures and investigated their optical properties.

A schematic diagram of the experimental procedure developed is shown (Fig. 1). First, we prepare highly-oriented CVD-grown CNTs on silicon substrates. These CNTs are lifted by a dome-shaped polymer stamp and transferred onto another substrate. Through the controlling position of the stamp and orientation of the substrate, orientation-controlled CNTs are successfully placed on the substrate at the desired location. Furthermore, we have applied this method to fabricate 1-2mD structures, where a CNT and a 2D semiconductor (transition metal dichalcogenides, TMDs) are stacked (Fig. 2). Using the 1-2mD structures, TMDs can (1) locally be gated to realize 1D channels in 2D and (2) host 1D electronic states through local 1D strain. In the presentation, in addition to details of fabrication, I will discuss optical properties of these 1-2mD structures.

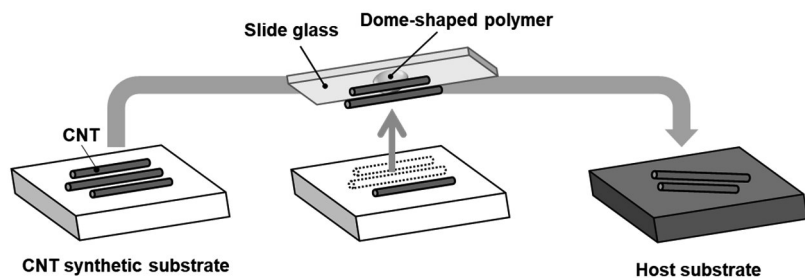


Fig 1. A schematic diagram of experimental procedure

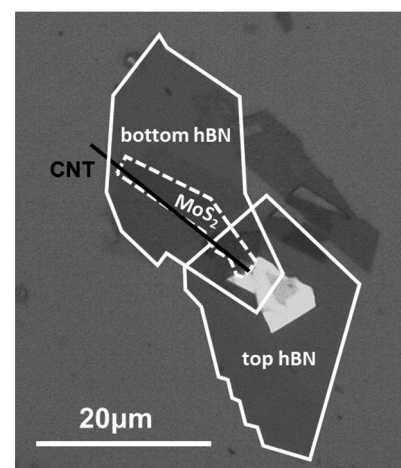


Fig.2 An optical microscope image of hBN / MoS₂ / hBN / CNT structure transferred on a SiO₂/Si substrate

Corresponding Author: R. Kitaura

Tel: +81-52-789-3660, Fax: +81-52-747-6442,

E-mail: r.kitaura@nagoya-u.jp

Efficient and Narrow-Linewidth Photoluminescence Devices Based on Single-Walled Carbon Nanotubes and Silicon Photonics

○Ryohei Imafuku¹, Naoto Higuchi¹, Hiroto Niiyama¹, Kenta Nakagawa^{1,2} and Hideyuki Maki^{1,3}

¹ Department of Applied Physics and Physico-Informatics, Keio University, Kanagawa 223-8522, Japan

² Kanagawa Institute of Industrial Science and Technology (KISTEC), Kanagawa 243-0435, Japan

³ Center for Spintronics Research Network (CSRN), Keio University, Kanagawa 223-8522, Japan

Nanocarbon materials are promising candidates for optoelectronic devices such as light sources [1-4] because they are easily formed on silicon substrates. In this study, we developed narrow-linewidth photoluminescence (PL) devices based on single-walled carbon nanotubes (SWNTs) and silicon photonics with micro-resonators and waveguides (Fig. 1(a)). Although most previous studies on SWNTs-silicon photonics devices managed either the excitation or emission light from the top of the device, our devices allow in-line operation by inputting and outputting light via the waveguide. As shown in Fig. 1(b), narrow-linewidth PL emission with a Q factor of ~ 3000 , whose linewidth is about 1/140 of that in free space, is observed from the ring resonator device. In addition, the PL emission is enhanced by a factor of approximately 34 due to confinement of the excitation light in the resonator. We also observed the excitation intensity dependence of the PL intensity and Q factor due to the saturable absorption of the SWNTs on the resonator. From the disk resonator device, PL emission with a high Q factor of 5700 and a narrow linewidth of 270 nm is obtained (Fig. 1(c)). This on-chip and in-line PL device can be applied for highly integrated silicon photonics and optoelectronics based on SWNTs in telecommunication band for optical communications, optical interconnects, quantum photonics, etc. This work was partially supported by PRESTO and A-STEP from JST and KAKENHI, KISTEC project, and NIMS Nanofabrication Platform in Nanotechnology Platform Project by MEXT.

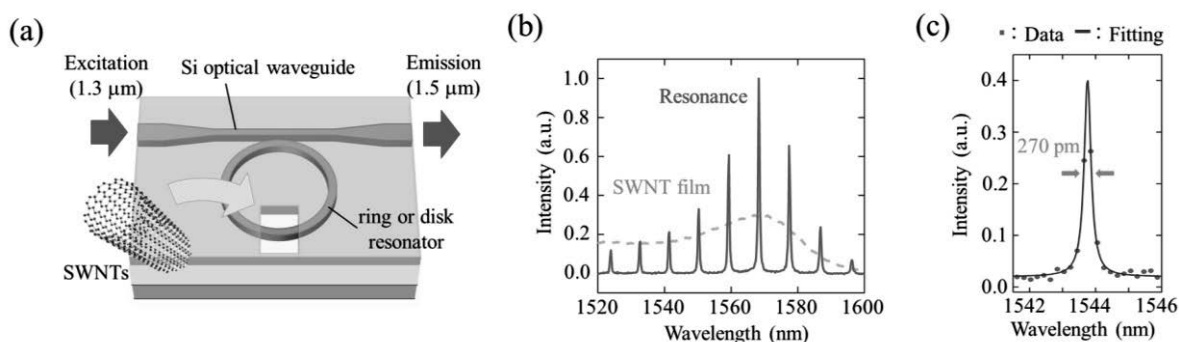


Fig. 1(a) A schematic of SWNTs light emitter. (b) PL spectrum under resonant excitation (continuous line). The dotted line shows the typical PL spectrum of the SWNT film on the SiO₂ substrate. (c) PL spectrum of disk resonator device.

[1] N. Higuchi, H. Niiyama, K. Nakagawa & H. Maki ACS Appl. Nano Mater. 3, 7678-7684 (2020).

[2] H. Takahashi, Y. Suzuki, N. Yoshida, K. Nakagawa & H. Maki J. Appl. Phys. 127, 16 (2020).

[3] R. Kawabe, H. Takaki, T. Ibi, Y. Maeda, K. Nakagawa & H. Maki ACS Appl. Nano Mater. 3, 682-690 (2020).

[4] T. Mori, Y. Yamauchi, S. Honda & H. Maki Nano. Lett. 14, 3277-3283(2014).

Corresponding Author: H. Maki

Tel: +81-45-566-1643, Fax: +81-45-566-1587, E-mail: maki@az.appi.keio.ac.jp

Machine learning assisted control of nanocarbon dispersion for optimal material and process design of electronics

○Shun Muroga, Ying Zhou, Takeo Yamada, Toshiya Okazaki, Kenji Hata

CNT-Application Research Center, National Institute of Advanced Industrial Science and Technology (AIST), Tsukuba 305-8565, Japan

Printable, lightweight, mechanically durable, and chemically stable electrodes are demanded for futures electronics, including stretchable devices, foldable displays, wearable devices, and flexible solar cells. Nanocarbons, especially carbon nanotube (CNT), has attracted strong interest due to their potential compared to metals and cost-effective to other nanomaterials [1,2]. Depending on the fabrication process, compositions of dispersion were under several constraints, which requires trial-and error for material and process design. We focused on machine learning techniques for shortening period for selecting and trying rational solvents depending on the process.

In this study, we developed a model for predicting degree of exfoliation of carbon nanotube in solvent using machine learning technique as shown in Fig. 1. Machine learning model was trained by chemical structures of solvent and degrees of exfoliation after dispersion to select rational solvent from predicted results. Here, the degree of exfoliation was defined as a logarithm of the ratio of average width of bundles before and after dispersion process. Highly crystalline single walled carbon nanotube (eDIPS, Meijo Nanocarbon) and polyacrylic acid (PAA) as a dispersant were used as model materials. Various solvents were used to disperse CNT with PAA to obtain exfoliated CNT dispersions. I/O of the machine learning model were the chemical descriptors from the Simplified Molecular Input Line Entry System (SMILES) of chemical structures of the solvents as inputs, and the degrees of exfoliation as outputs.

Machine learning model was constructed from a random forest regressor, resulting in a good relationship between measured degree of exfoliation and predicted values from the model. Fig. 2 shows the relationship of the predicted degree of exfoliation and solvent viscosity and boiling point. Large marker indicates the highly exfoliated dispersion in the solvent. The results represented that our model enabled to select rational solvent depending of processing with desired volatility and viscosity, e.g., applicability to select solvents in different situations, such as, spin coating, bar coating, screen printing, and inkjet printing.

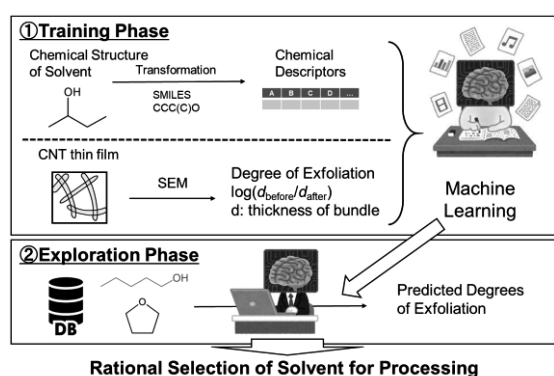


Fig. 1. Schematics of the machine learning.

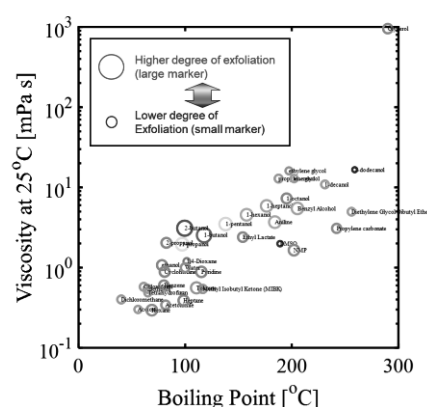


Fig. 2. Predicted degrees of exfoliation in various solvents.

[1] Y. Zhou *et al.* Appl. Phys. Exp., **114**, 213104 (2019). [2] Y. Zhou *et al.* Nanoscale, **11**, 3804-3813 (2019).

Corresponding Author: S. Muroga, Tel: +81-29-849-1534, Fax: +81-29-851-5424, E-mail: muroga-sh@aist.go.jp

Air-Stable n-type of Single-Walled Carbon Nanotubes by Organic Boron Compounds

○Hamasuna Aoi¹, Naoki Tanaka^{1,2}, Tsuyohiko Fujigaya^{1,2,3}

¹ Graduate School of Engineering, Kyushu University, Fukuoka 819-0395, Japan

² WPI- I²CNER, Kyushu University, Fukuoka 819-0385, Japan

³ Center for Molecular Systems (CMS), Kyushu University, Fukuoka 819-0395, Japan

Single-walled carbon nanotubes (SWCNTs) are promising materials for thermoelectric devices because of their remarkable electrical conductivity, flexibility, and light weight. For efficient thermoelectric generation, both p-type and n-type thermoelectric materials are required. However, SWCNTs act as p-type semiconductors owing to the hole doping by water and oxygen in the air. Therefore, many efforts to develop n-type SWCNTs have been performed mainly by chemical doping using electron donors. Recently, our group reported that pyridine boryl radicals generated by mix bis(pinacolate)diboron (B_2pin_2) and pyridine derivatives as a Lewis base can act as electron-dopants of SWCNTs [1]. However, the n-doped SWCNTs did not show long-term air stability. In this study, we demonstrated that n-doped SWCNTs using tetrahydroxydiboron ($B_2(OH)_4$) as boron source showed long-term n-type nature in air (Fig. 1).

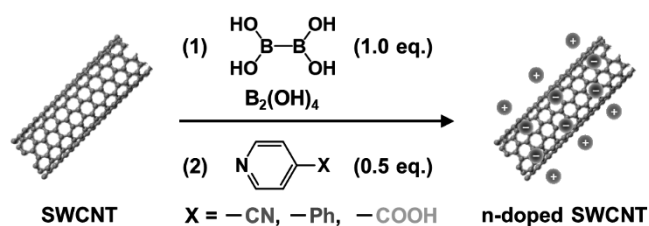


Fig. 1 Schematic image of n-doping of SWCNT using tetrahydroxydiboron ($B_2(OH)_4$) and pyridines.

The Seebeck coefficient of SWCNT sheets after immersing in a THF solution of mixing $B_2(OH)_4$ and pyridine derivatives with cyano, phenyl, and carboxy groups in the para position were negative, indicating that a n-type nature was generated by electron doping (Fig. 2). As the n-type stability of the three SWCNT sheets in air were evaluated, the SWCNT sheet using $B_2(OH)_4$ and 4-phenylpyridine showed n-type properties for more than 50 days under air.

[1] N. Tanaka, T. Fujigaya et al., *Chem. Commun.*, **2021**, 57, 6019-6022.

Corresponding Author: T. Fujigaya
Tel: +81-92-802-2842, Fax: +81-92-802-2842,
Web: <http://www.chem.kyushu-u.ac.jp/~fifth/jp/>
E-mail: fujigaya.tsuyohiko.948@m.kyushu-u.ac.jp

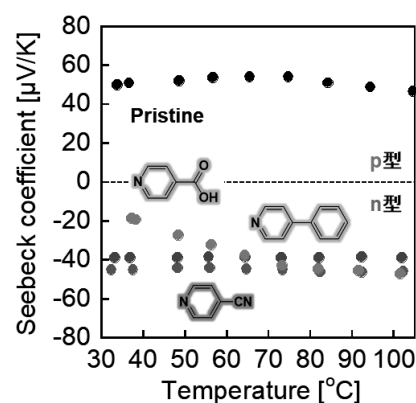


Fig. 2 Seebeck coefficient of pristine SWCNT sheet (black) and SWCNT sheets doped with $B_2(OH)_4$ and pyridines (4-cyanopyridine (red), 4-phenylpyridine (blue) and 4-carboxypyridine (pink)).

Systematic structural study of cation-ordered pentavalent fullerides

○Keisuke Matsui¹, Kosmas Prassides¹

¹ Department of Materials Science, Osaka Prefecture University, Osaka 599-8531, Japan

Buckminsterfullerene C₆₀ has high electron affinity that allows it to behave as an electron acceptor. For example, solid C₆₀ forms charge-transfer compounds with various metals (fullerides), which are established as molecule-based strongly correlated electron systems. The properties of fullerides dramatically change depending on the doping level, the nature of intercalants, and the charge states of C₆₀ (up to -12). One of the most interesting family is that of trivalent fullerides A₃C₆₀ (A = alkali metals) which show the highest superconducting transition temperature ($T_c \sim 38$ K) and critical magnetic field ($H_{c2} \sim 90$ T) for a molecular solid. In this system, T_c follows dome-like dependence as a function of U/W (U : on-site Coulomb energy, W : bandwidth) or equivalently unit cell volume in a wide range^[1] (Fig. 1).

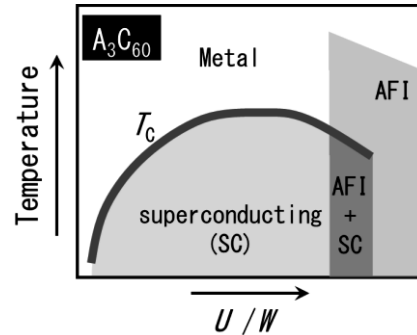


Fig. 1 Schematic phase diagram of trivalent fullerides A₃C₆₀. AFI stands for antiferromagnetic insulator.

On the other hand, pentavalent fullerides have not been experimentally well-studied except for non-superconducting Ba₂AC₆₀ (face-centered cubic, *fcc*)^{[1][2][3]} although theory suggests possible emergence of superconductivity. In this system, Ba²⁺ and A⁺ occupy small tetrahedral (T_d) and large octahedral (O_h) holes, respectively in the *fcc*-C₆₀ lattice^{[2][3]}. Another approach to access (C₆₀)⁵⁻ in the lithium fulleride Li_xCsC₆₀ ($x \approx 5$) has been also reported^[5], that revealed *fcc*-Li₅CsC₆₀ does not show superconductivity. In both cases, the unit cell volume varies very little in the approximate range 700 - 720 Å³ per C₆₀ molecule.

Here we present our syntheses and systematic structural study of cation-ordered M₂AC₆₀ fullerides by synchrotron X-ray diffraction. Diffraction profiles of these fullerides where Ba²⁺ ion is substituted by the smaller strontium/ytterbium ions showed the adoption of an orthorhombic lattice (Fig. 2), unlike isoelectronic *fcc*-Ba₂AC₆₀. Intriguingly, the cation doped into the tetrahedral holes are away from the center which has never been encountered in trivalent fullerides A₃C₆₀. Although superconductivity has not as yet been observed in these ternary systems, systematic control of the crystal structure at the fixed charge level (C₆₀)⁵⁻ has been established by chemical means.

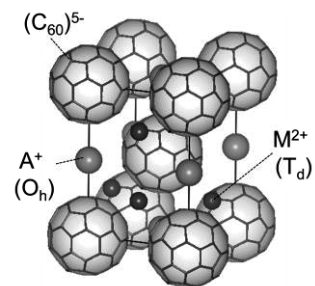


Fig. 2 Crystal structure of ternary fullerides M₂AC₆₀.

[1] Y. Takabayashi *et al.* Science, **323**, 1585 (2009).

[2] A. C. Duggan *et al.* Chem. Commun., **10**, 1191 (1996).

[3] T. Yildirim *et al.* Phys. Rev. B., **54**, 11981 (1996).

[4] K.-F. Their *et al.* Phys. Rev. B., **59**, 10536 (1999).

[5] M. Kosaka *et al.* Phys. Rev. B., **59**, R6628 (1999).

Corresponding Author: Kosmas Prassides

Tel: +81-72-254-6162

Electron states tuning of bilayer graphene by intercalation and adsorption of corannulene

○Mina Maruyama, Susumu Okada

Department of Physics, University of Tsukuba, Tsukuba 305-8571, Japan

Graphite occupies an important position in pure and applied sciences owing to its unique structural and electronic properties. A chemically inert honeycomb covalent network of C makes graphene a starting material to construct various hybrid structures with other layered materials and molecules. Graphite intercalation compound (GIC) is the representative example of such hybrid structures where atoms or molecules are intercalated into nanoscale spacing between graphene layers. Depending on the intercalated materials and their conformation between graphene layers, GICs exhibit interesting variation in their physical properties [1]. In this work, we considered the thinnest GIC consisting of bilayer graphene and corannulene molecule ($C_{20}H_{10}$) to explore a potential carbon-based intercalation compound with unique geometric and electronic structures, using density functional theory with generalized gradient approximation including van der Waals correction.

Our calculations show that their electronic structures strongly depend on corannulene conformations between graphene layers. Electrons and holes are redistributed in graphene layers located at the edge and convex regions of corannulene, respectively, owing to the dipole moment of corannulene. We further demonstrated that the bilayer graphene containing corannulene molecules act as the p/n junction by forming the border where corannulene direction is opposite each other. Figure 1 shows the projected density of states (pDOS) on atomic sites of graphene layers. Band bending occurs at the border between the bowl-up and bowl-down regions. We also found the similar band bending of valence and conduction band edges of bilayer graphene on which the corannulene layers are adsorbed. Therefore, the result implied that the bowl-shaped hydrocarbon molecules could control the local electronic structures of bilayer graphene in terms of their molecular conformations.

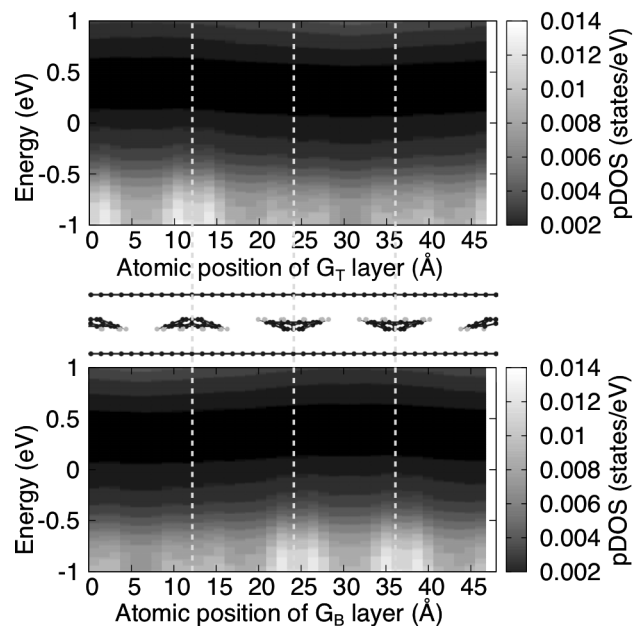


Fig. 1 Projected density of states (pDOS) on atomic sites belonging to top graphene layer (G_T) and to bottom graphene layer (G_B) of corannulene intercalated bilayer graphene. The energy is measured from that of the Fermi level.

[1] M. S. Dresselhaus and G. Dresselhaus, *Adv. Phys.* **30**, 139-326 (1981).

Corresponding Author: M. Maruyama

Tel: +81-29-853-5921, Fax: +81-29-853-5924, E-mail: mmaruyama@comas-tsukuba.jp

The strain effect on van der Waals heterostructure

○Rei Usami¹, Ryotaro Fukui¹, Takahiko Endo², Yasumitsu Miyata², Jiang Pu¹,
Souma Suzuki¹, Togo Takahashi¹, Ryo Kitaura³, Taishi Takenobu¹

¹Department of Applied Physics, Nagoya University, Nagoya 464-8603, Japan

²Department of Electrical Engineering, Tokyo Metropolitan University, Tokyo 192-0397, Japan

³Department of Science, Nagoya University, Nagoya 464-8603, Japan

Recently, transition metal dichalcogenide (TMDC) monolayers and their van der Waals heterostructures have been attracted intense attention because many unique properties such as interlayer exciton and Moiré pattern were realized [1-3]. In particular, Moiré pattern offered a platform to discover new physics and device functionalities [3]. However, Moiré patterns are created by manual exfoliation/lamination of monolayers and precise control of their relative layer angle is necessary. Therefore, it is still difficult to prepare the controlled Moiré patterns and researchers on Moiré pattern are still limited. Here, we propose a method to control Moiré patterns using strain effect, which can continuously tune photoluminescence (PL) properties and Moiré structure at the hetero interface.

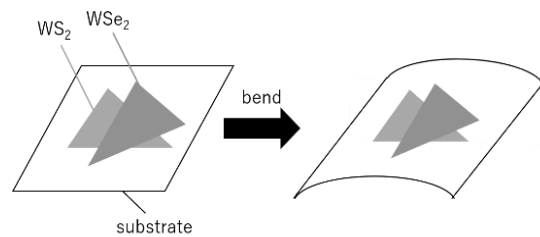


Fig. 1 Schematic drawing of transfer and measure.

Figure 1 schematically illustrates the fabrication and measurement of the strained heterostructure. First, CVD-grown WS₂ monolayer was transferred on a PEN substrate. Then, CVD-grown WSe₂ monolayer was transferred on the initial substrate. We evaluated PL spectra of each layer and interlayer exciton with additional strain. Figure 2 shows the strain dependences of PL peak energy with tensile and compressive strain. For WS₂ layer, the linear peak shift was observed, which attributes to the bandgap change *via* strain effects [4]. The peak shift of interlayer excitons was also linearly varied. This is first observation of strain tuning interlayer excitons in TMDC heterostructures. Most interestingly, for WSe₂ layer, the peak shift was changed non-linearly, meaning that the peak shift seemed to be smaller as increasing strains (Fig. 2). We expected that these inconsistent PL behaviors between WS₂ and WSe₂ was due to the different strain distributions. Therefore, our results suggest the continuous control of Moiré patterns in strained heterostructures. Furthermore, the proposed approach may enable to create unconventional Moiré structures offering possibilities for elucidating novel physical properties in the future.

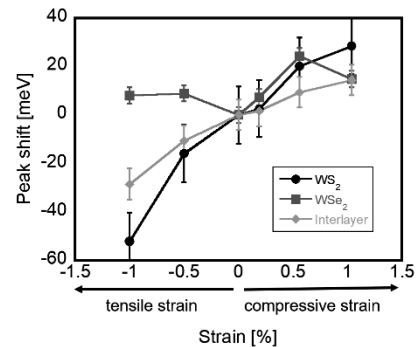


Fig.2 Strain dependence of the peak shift.

[1] Xiaoping Xue *et al.* Applied Surface Science 455 963-969 (2018)

[2] Kha Tran *et al.* Nature, VOL.567 7 March (2019)

[3] Y. Chandra *et al.* Computational Materials Science 177 109507 (2020)

[4] Sangyeon Pak *et al.* Nano Lett. 17, 5634-5640 (2017)

Corresponding Author: J. Pu, T. Takenobu

E-mail: jiang.pu@nagoya-u.jp, takenobu@nagoya-u.jp, Tel/Fax: +81-52-789-5165

Optical properties of transition metal dichalcogenides with microspherical optical cavity

○Mikio Kobayashi¹, Keisuke Shinokita¹, Naoki Wada², Takahiko Endo²,
Yasumitsu Miyata², Kazunari Matsuda¹

¹*Institute of Advanced Energy, Kyoto University, Uji 611-0011, Japan*

²*Department of Physics, Tokyo Metropolitan University, Hachioji, Tokyo 192-0397, Japan*

Atomically thin transition metal dichalcogenides (TMDs) have attracted much attention in recent years because of their excellent optical properties. Their strong light emission properties in its monolayer form could be applicable for next-generation optoelectronic devices as extremely thin optical gain medium. Recently several studies have tried to achieve lasing operations by integrating TMDs into optical microcavity such as Fabry-Perot, photonic crystal, microdisk, and microsphere cavities [1,2]. However, the detail properties and lasing operation of TMDs in the microcavity still remains to be reported. Here, we have investigated the optical properties of microspheres-coupled monolayer WSe₂ and WSe₂/WS₂ heterobilayer.

Figure 1(a) shows photoluminescence (PL) spectra of monolayer WSe₂ with and without polystyrene microsphere (diameter: 10 μm). Several sharp peaks observed in the PL spectra from intra-layer exciton suggest the strong confinement of emitted light in the microsphere and resonances originating from Whispering-gallery mode (WGM). The calculated Q -value is approximately 1000, suggests superior performance of microspherical optical cavity due to their smooth surface and total internal reflection repeated on the surface without optical loss. We also show the PL spectra of microsphere-coupled WSe₂/WS₂ heterobilayer in Fig. 1(b). The sharp resonance peaks both from intra-layer exciton above 1.7 eV and inter-layer exciton below 1.6 eV have been observed originating from WGM in the PL spectra. We will discuss the details of coupling to microsphere of out-of- and in-plane light emission from intra- and inter-layer exciton, respectively, based on finite-difference time domain (FDTD) simulation. Our results would pave the way for using this highly efficient coupling of microspherical optical cavity and TMDs towards on-chip low-threshold micro-lasers and optical circuits.

[1] S. Wu *et al.*, Nature **520**, 69 (2015).

[2] E. Y. Paik *et al.*, Nature **576**, 80 (2019).

Corresponding Author: K. Matsuda

Tel: +81-774-38-3460, Fax: +81-774-38-3467

E-mail: matsuda@iae.kyoto-u.ac.jp

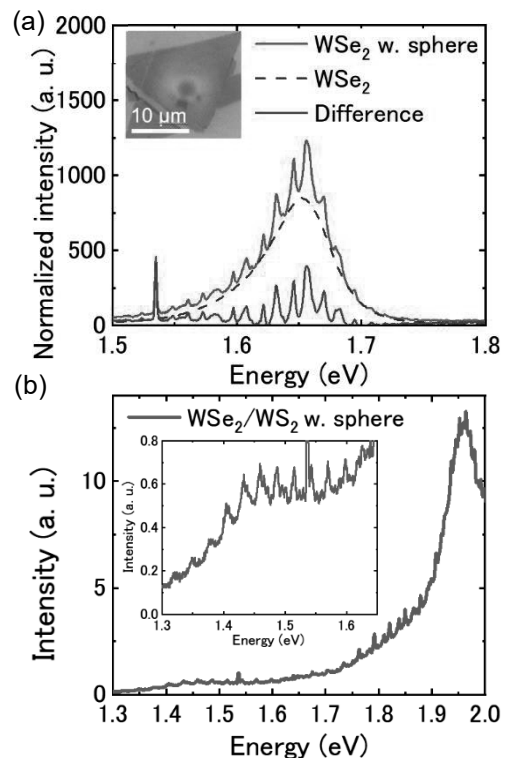


Figure 1. (a) PL spectra of 10 μm polystyrene coupled monolayer WSe₂. Inset shows optical image. (b) PL spectra microsphere coupled to WS₂/WSe₂ heterobilayer. Inset shows in inter-layer exciton region.

Electrical Transport Properties of W_6Te_6 Nanowire Network Films

○Iori Kikuchi¹, Hiroshi Shimizu², Hong En Lim², Takahiko Endo²,
Yusuke Nakanishi², Yasumitsu Miyata², Jiang Pu¹, Taishi Takenobu¹

¹Department of Applied Physics, Nagoya University, Nagoya 464-8603, Japan

²Department of Physics, Tokyo Metropolitan University, Tokyo 192-0397, Japan

Transition metal chalcogenide nanowires are one-dimensional (1D) van der Waals materials and, in principle, the absence of dangling bonds allows the formation of various shape nanostructures, such as 1D wires, 2D layers and 3D bundles. Indeed, a 1D transport behavior, Tomonaga-Luttinger liquid (TLL), have been reported by the top-down isolation of 1D wires from 3D single crystals [1]. However, the structural control was still difficult and the bottom-up method was strongly required. Recently, we established a CVD growth method of W_6Te_6 and realized the bottom-up control of nanostructure, such as 2D layers and 3D bundles (Fig. 1) [2]. Here, we challenged the systematic fine control of W_6Te_6 nanostructures from 3D bundles to 1D wires using air exposure. As shown in Fig. 1, the surface of bundles is covered by amorphous layer, which is caused by air due to the chemical instability of W_6Te_6 ; so that, we tried to tune the structure *via* gradual atmospheric exposure.

Two-terminal electrodes were formed on W_6Te_6 networks and we measured the temperature dependence of electrical resistance and magnetoresistance to investigate the air-exposure time dependences. As shown in Fig. 2, as-grown sample exhibited metallic temperature dependence at higher temperature and 2D weak anti-localization (WAL) at low temperature. However, the air exposure changed the network properties from metallic to insulator (Fig. 2) and the vanish of 2D WAL was also confirmed by magnetoresistance. Very importantly, the observed insulative behavior was explained by neither thermally active nor variable range hopping, and, finally, the current-voltage characteristics strongly indicate TLL. These results suggest the continuous tuning from 2D metallic to 1D TLL behavior, offering a new route to control morphologies and transport properties in W_6Te_6 network.

[1] Venkataraman, L. *et al. Phys. Rev. Lett.* **83**, 5334 (1999).

[2] Lim, H. E. *et al. Nano Lett.* **21**, 243 (2021).

Corresponding Author: T. Takenobu, Tel/Fax: +81-52-789-5173, E-mail: takenobu@nagoya-u.jp

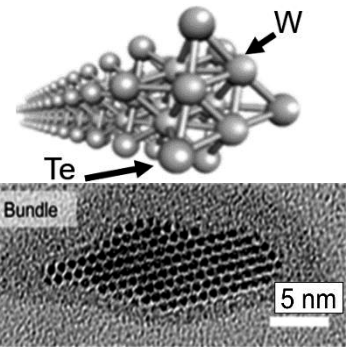


Fig.1 Structure and TEM of W_6Te_6 samples

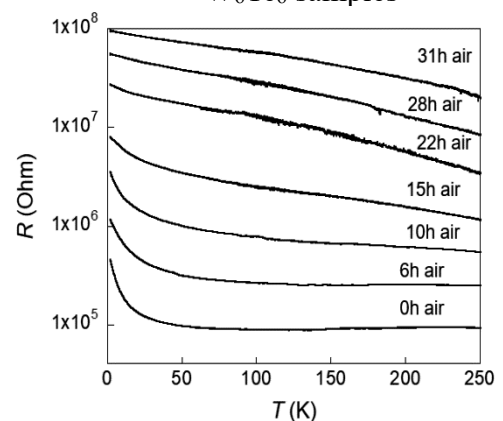


Fig.2 Temperature dependence of electrical resistance

Antibody-conjugated polymer wrapped single-walled carbon nanotube for photothermal therapy via near-infrared light

○Yukiko Nagai¹, Kenta Nakamura¹, Jun Ohno², Tsuyohiko Fujigaya^{1,3,4}

¹Department of Applied Chemistry, Graduate School of Engineering, Kyushu University, 744 Motoooka, Fukuoka, Japan. ²Center for Regenerative Medicine, Fukuoka Dental College, Fukuoka, Japan. ³WPI ICNER, Kyushu University. ⁴Center for Molecular Systems, Kyushu University.

Near-infrared (NIR) triggered photothermal therapy (PTT) is one of the attractive candidate for cancer treatment due to its non-invasiveness. Single-walled carbon nanotubes (SWCNTs) are promising materials for PTT owing to their strong absorption in NIR region as well as their high photothermal conversion efficiency and excellent photostability. To reduce potential side effects, the cancer cell selectivity is desirable, which requires SWCNTs to be able to bioconjugate with some type of targeting groups, such as an antibody, without losing unique SWCNT natures. Previously, we reported a unique method to coat SWCNT surface by a cross-linked polymer keeping intrinsic structure of SWCNTs through a process called CNT Micelle Polymerization[1] and successfully introduced maleimide groups, that allowed for the post-modification of thiol-containing molecules.[2] Importantly, the cross-linked polymer layer functions not only to conjugate the antibody but also to disperse SWCNTs so that no additional dispersant is necessary in our system. In this presentation, we demonstrate a conjugation of the antibody with maleimide-polymer coated SWCNTs, their selective recognition of cancer cells and killing of the cells via the PTT effect *in vitro*. [3] (**Fig.1**)

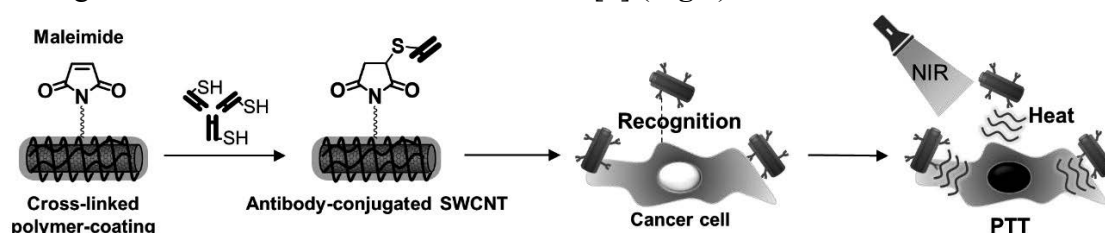


Fig. 1 Schematic illustration of the post-modification of single-walled carbon nanotubes (SWCNTs) with thiol-functionalized antibodies via maleimide groups and the use of the antibody-conjugated SWCNTs in the PTT-triggered killing of cancer cells.

Here, we conjugated maleimide-polymer-coated SWCNTs with an antibody against TRP-1, a melanoma specific protein, for the PTT of the B16F10 melanoma cell line. The B16F10 melanoma cells on the dish, which had been incubated with the anti-TRP-1 conjugated SWCNTs (TRP-SWCNTs), were irradiated with an NIR laser using an optical microscope. Two dyes, Calcein-AM and PI, were used to stain living cells and dead cells, respectively. Indeed, cells treated with TRP-SWCNTs showed a remarkable decrease in the fluorescence from the Calcein-AM after NIR irradiation (**Fig.2**, left panels), while the fluorescence from the PI staining could be clearly observed (**Fig.2**, right panels), which indicated that the PTT-triggered killing of the B16F10 melanoma cells via TRP-SWCNTs.

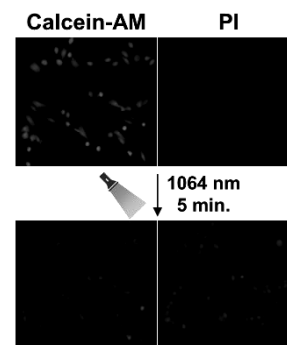


Fig. 2 Fluorescence microscopy images of B16F10 treated with TRP-SWCNTs (up) and following NIR irradiation (bottom).

[1] T. Fujigaya *et al.*, *RSC Adv.*, 4, 6318 (2014). [2] Y. Nagai *et al.*, *J. Am. Chem. Soc.*, 140, 8544 (2018). [3] Y. Nagai *et al.*, *ACS Appl. Bio Mater.* 4, 5049 (2021).

Corresponding Author: T. Fujigaya

Tel: +81-92-802-2842, Fax: +81-92-802-2842, E-mail: fujigaya.tsuyohiko.948@m.kyushu-u.ac.jp

Effect of dispersant on supported state and electrocatalytic properties of Pt nanoparticles on single-walled carbon nanotubes

○Yuho Abe¹ and Hironori Ogata^{1,2}

¹ *Department of Chemical Science and Technology, Hosei University*

² *Research Center for Micro-Nano Technology, Hosei University*

E-mail: hogata@hosei.ac.jp

A direct methanol fuel cells(DMFCs), which is a type of solid oxide fuel cell(SOFC), is expected as a next generation energy supply source. DMFCs are one of the most promising transportable power sources which can be used in mobiles, laptops, and small power generation. The basic operation principle of DMFCs involves methanol oxidation and oxygen reduction on the precious metal catalysts, which are carbon supports as well as catalyst particle size and shape plays a dominant role in the electrochemical performance for fuel cells. The most important advantage of DMFCs over other types of fuel cells is that methanol can integrate effectively with transmission and distribution systems that already exist. However, there are technological challenges for the commercialization of DMFCs that remain unsolved [1,2,3,4]. The basic operation principle of DMFCs involves methanol oxidation and oxygen reduction on the precious metal catalysts, which are loaded on the support surfaces. As is well-known, the dispersion of Pt-based nanoparticles on carbon supports as well as catalyst particle size and shape plays a dominant role in the electrochemical performance for DMFCs.

In this study, we investigated suitable dispersants for the purpose of improving the electrocatalytic activity of Pt-based nanoparticle-supported single-walled carbon nanotube s(SWNTs) films for the electrode of DMFCs fabricated by the liquid phase reduction method. In the dispersion of SWNTs, several kinds of aromatic molecules were used as dispersants, and the difference in the supported state of Pt-based nanoparticles and the effect on the electrocatalytic activity were systematically investigated.

The detailed results will be presented.

References:

- [1] N. Pongpichyakul *et al.*, *Springer Nature*, **50**, 51-62 (2019).
- [2] S.K.Kamarudin *et al.*, *Applied Catalysis B: Environmental*, Elsevier, **262**, 118217 (2019)
- [3] I. Martinalou *et al.*, *International Journal of Hydrogen Energy*, Elsevier, **34**, 6902-6916 (2009)
- [4] Zhipeng Wang, Mao Shoji and Hironori Ogata, *Appl. Surf. Sci.*, **259**, 219-224 (2012).

Corresponding Author: H.Ogata

Tel: +81-42-387-6229, Fax: +81-42-387-6229,

E-mail: hogata@hosei.ac.jp

Catalyst-Free Synthesis of Highly-Crystalline Free-Standing Boron Nitride Nanotube Films

○Shuhui Wang¹, Ming Liu¹, Ya Feng¹, Keigo Otsuka¹, Esko I. Kauppinen², Shohei Chiashi¹, Rong Xiang¹, Shigeo Maruyama¹

¹ *Department of Mechanical Engineering, The University of Tokyo, Tokyo 113-8656, Japan*

² *Department of Applied Physics, Aalto University School of Science, Espoo 15100, FI-00076 Aalto, Finland*

Boron nitride nanotube (BNNT) has attracted considerable attention in various scientific fields due to its outstanding optical, thermal, and electrical (dielectric and insulating) properties [1]. We have demonstrated a CVD synthesis of one-dimensional heterostructures, where single-walled carbon nanotube (SWCNT), BNNT and molybdenum disulfide nanotube (MoS₂NT) are coaxially nested [2]. The enhanced thermal conductance of the heterostructured SWCNT@BNNT films makes them a promising building block for thermal and optoelectronic applications [3]. We also achieved removing the inner SWCNT from SWCNT@BNNT films by an oxygen annealing process [4].

Based on our optimization of 2D hexagonal boron nitride (h-BN) growth on graphite [5], where the large size of monolayer h-BN with high quality was grown at higher temperature (1250 °C), we expect that higher growth temperature might help synthesize high-quality BNNTs. Thus, we studied the optical properties of SWCNT@BNNT film samples grown at different temperatures (1075 °C [2-4] and 1250 °C) as well as BNNT film samples by Raman spectroscopy, Fourier transformed infrared (FTIR) spectroscopy, and Ultraviolet-visible-near-IR (UV-vis-NIR) spectroscopy. Furthermore, the crystalline structure of BNNTs and by-products such as h-BN flakes were observed by high-resolution TEM. This study will help better understanding of the synthesis of high-quality BNNTs.

[1] D. Golberg *et al.* *Adv. Mater.*, **19**, 2413 (2007).

[2] R. Xiang *et al.* *Science*, **367**, 537 (2020).

[3] P. Wang *et al.* *ACS Nano*, **14**, 4298 (2020).

[4] M. Liu *et al.* *ACS Nano*, **15**, 5600 (2021).

[5] H. Arai *et al.* *Nanoscale*, **12**, 10399 (2020).

Corresponding Author: Shigeo Maruyama

Tel: +81-3-5841-6421, Fax: +81-3-5800-6983, E-mail: maruyama@photon.t.u-tokyo.ac.jp

Influence of carbon source pyrolysis on high-temperature CNT growth from solid carbon growth seeds

°Mengyue Wang¹, Michiharu Arifuku², Noriko Kiyoyanagi², Masamitsu Satake², Taiki Inoue¹, Yoshihiro Kobayashi¹

¹ Department of Applied Physics, Osaka University, Osaka 565-0871, Japan

² Nippon Kayaku, Tokyo 115-8588, Japan

Carbon source decomposition process in gas phase is one of factors that influence chemical vapor deposition (CVD) system for carbon nanotube (CNT) synthesis, especially in CNT growth from non-metallic growth seeds. Various gas phase pyrolysis pathways of carbon source species were studied [1, 2]. In our previous work [3], C₂H₄ was used as carbon feedstock for high-yield and high-quality CNT growth from solid carbon growth seeds through two-stage growth process, and carbon dioxide (CO₂) was used as the etchant to prevent deposition of amorphous carbon (a-C). Nevertheless, it lacks the illustration about carbon source pyrolysis behavior in gas phase as well as the explanation for the weaker etching result while using stronger etchant, water vapor (H₂O), in such growth system. In this work, we performed a comparative study of CNT growth by using different carbon feedstock (C₂H₂, C₂H₄) and etchants (H₂O, CO₂). Based on the obtained results, carbon source pyrolysis with and without etchant in CNT growth at high temperature is discussed.

Growth seeds were formed by heating nanodiamond at 1000°C in Ar for 1 hour. In the two-stage growth process, CNT growth behavior was compared with employing different carbon sources, C₂H₂ and C₂H₄. In the first stage for cap formation (1 min), temperature and carbon source partial pressure were adjusted to 850 °C and 1 Pa for C₂H₂, and 900 °C and 20 Pa for C₂H₄. Then, for the second growth stage, the temperature was increased to 1000°C for nanotube growth (30 min). The carbon source partial pressure was kept at 0.5 Pa for C₂H₂ and 5 Pa for C₂H₄. The quality (G and D bands) and yield (G band observation frequency) of the grown CNTs were characterized by Raman spectra using 633 nm excitation.

Raman spectra in Fig. 1 compare the growth behavior with different carbon feedstock utilized in two-stage growth and with/without etchant injection. The growth condition for these samples was optimized for high-quality CNT growth. When using C₂H₄ as the carbon feedstock (Fig. 1(b)), the intensity of D band, which represents the deposition of a-C in this case, did not show any distinct decrease even after the injection of H₂O. On the other hand, D band decreases a lot with CO₂ injection, in contrast to the case of C₂H₂ in Fig. 1(a). According to the milder etching effect presented in our previous study, C₂H₄ assisted high temperature CNT growth [3], CO₂ tends to prevent the formation of a-C before it is deposited on the surface of growth seeds, which means CO₂ is more likely to influence a-C deposition through gas phase reaction. The hydrocarbon pyrolysis reaction study [1] shows that, in the case of C₂H₄, formation rate of intermediate C₄ species is higher than further pyrolysis reaction rate. This causes the excessive C₄ species, which is easier to be eliminated by CO₂. In the case of C₂H₂, other excessive intermediates formed during pyrolysis process, which are easier to be eliminated by H₂O. This indicates that the species of intermediates formed by different carbon sources during pyrolysis process influence CNT growth efficiency at high temperature.

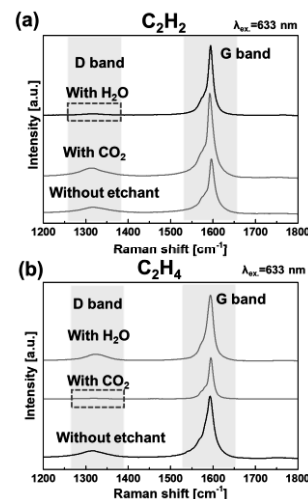


Fig. 1 Raman spectra of CNTs grown from C₂H₂ (a) and C₂H₄ (b) with or without the injection of etchant (water vapor or carbon dioxide) in the two-stage growth system.

[1] K. Norinaga et al., *Ind. Eng. Chem. Res.*, 46 (2007), 3547-3557. [2] N. Yang et al., *Carbon*, 130 (2018), 607-613. [3] M. Wang et al., *JSAP Autumn Meeting 2019*, 21a-PB1-1., M. Wang et al., *JSAP Spring Meeting 2020*, 8p-z29-1.

Corresponding Author: Y. Kobayashi, E-mail: kobayashi@ap.eng.osaka-u.ac.jp

Highly crystalline single-walled carbon nanotubes by microplasma-assisted gas-phase chemical vapor deposition

○Guohai Chen¹, Takashi Tsuji¹, Yoshiki Shimizu^{2,3}, Jaeho Kim⁴, Hajime Sakakita⁴, Kenji Hata¹, Don N. Futaba¹, Shunsuke Sakurai¹

¹ CNT-Application Research Center, National Institute of Advanced Industrial Science and Technology (AIST), Central 5, 1-1-1 Higashi, Tsukuba, Ibaraki 305-8565, Japan

² Nanomaterials Research Institute, National Institute of Advanced Industrial Science and Technology (AIST), Central 5, 1-1-1 Higashi, Tsukuba, Ibaraki 305-8565, Japan

³ AIST-UTokyo Advanced Operando-Measurement Technology Open Innovation Laboratory (OPERANDO-OIL), National Institute of Advanced Industrial Science and Technology (AIST), Kashiwa Research Complex, II 5-1-5, Kashiwanoha, Kashiwa, Chiba 227-8589, Japan

⁴ Innovative Plasma Processing Group, Research Institute for Advanced electronics and Photonics, National Institute of Advanced Industrial Science and Technology (AIST), Central 2, 1-1-1 Umezono, Tsukuba, Ibaraki 305-8568, Japan

Carbon nanotubes (CNTs) have attracted extensive attention due to their exceptional properties [1-3]. Among all the structural features of CNTs, crystallinity and length have been shown to be crucial for transferring the intrinsic properties of individual CNTs to the macroscopic scale. Despite great progress, the synthesis of single-walled CNTs (SWCNTs) with high crystallinity and long length remains a challenge [4].

In this presentation, we propose a microplasma-assisted, gas-phase synthesis of SWCNTs. The synthesis consists of two components: first, a microplasma to generate appropriately sized catalyst nanoparticles. Second, a carbon source to contact the catalyst nanoparticles at determined timing to nucleate CNTs (Fig. 1a). Therefore, this independent control of the catalyst nucleation and CNT nucleation/growth affords a unique control of the carbon feeding to the active nanoparticles. The CNTs were collocated onto a filter membrane and characterized by Raman, SEM and TEM, etc., which showed high crystallinity and a small average diameter about 1.32 nm. (Fig. 1b). The microplasma-assisted gas-phase process demonstrates the potential to synthesize high quality small diameter SWCNTs, which is expected to enable improved control over the diameter distribution and CNT length.

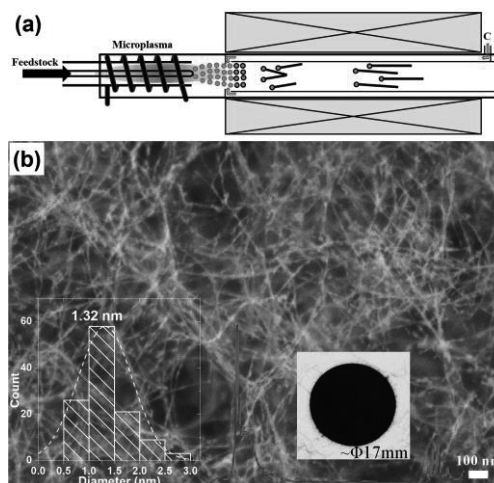


Fig. 1 (a) Schematic of microplasma-assisted CVD setup and (b) as-synthesized SWCNTs.

- [1] G. H. Chen *et al.* ACS Nano, **7**, 10218 (2013).
- [2] G.H. Chen *et al.* Carbon, **170**, 59 (2020).
- [3] G.H. Chen *et al.* ACS Applied Nano Materials, **4**, 869 (2021).
- [4] H. Kimura *et al.* J. Am. Chem. Soc. **134**, 9219 (2012).

Corresponding Author: G.H. Chen

Tel: +81-29-861-4416

Web: <https://unit.aist.go.jp/cnta/ja/member/Guohai.html>

E-mail: guohai-chen@aist.go.jp

Current-induced electrical path formation in random SWCNTs networks

○Naoki Koga, Yuuma Matsuura, Masaki Ozawa

Department of Applied Chemistry, Meijo University, Aichi 468-8502, Japan

Animals' traffic generates desire paths on a woodland, which changes depending on how much to be used. Likewise, signals travelling through networks of neurons residing in a brain ceaselessly modify the connections of the nodes and the network structures themselves, resulting in concurrent computing and memorizing. Inspired by the biological computing systems, akin computing architectures, including the ones involving memristors as artificial synapses, are intensely being developed. Going back to the desire paths, the key to construct such systems is on positive feedback mechanisms together with gradual restoration. Such a mechanism seems ubiquitous in nature, especially in flow systems, which evolve to provide easier access to the imposed currents [1].

In this study, we examined a random network of single-walled carbon nanotubes (SWCNTs) as a network system evolving through conducting electrons. MEIJO eDIPS SWCNTs sonicated in sulphuric acid/nitric acid to give around 100 nm in length were suspended in polyacrylamide hydrogel, which were expected to support the network structures as well as to allow plasticity for adjusting conditions of the electric contacts between the tubes. Then, voltage pulses were applied between wire electrodes spaced 1.0 mm apart in the gel thus prepared. The conductivity of the gel was found to increase until 1.0 wt% of the SWCNTs concentration, while it stays nearly constant above it, indicating the percolation threshold. Fig. 1 shows the variations of the currents with time at pulsewidth, frequency, and voltage of 50 ms, 500 Hz, and 5 V, respectively, which flow the gels with 0.1, 1.0, and 2.0 wt% SWCNTs. In each case, initial increase and subsequent saturation of the current starting at around 400 s was observed with no noticeable electrophoretic behavior. An interval more than 15 min allowed the gel to revert to the low conductive states, which presumably demonstrates improvement of electric contacts driven by the flowing electrons and thermal perturbation. Furthermore, the networks of debundled short SWCNTs were also investigated using different types of dispersants.

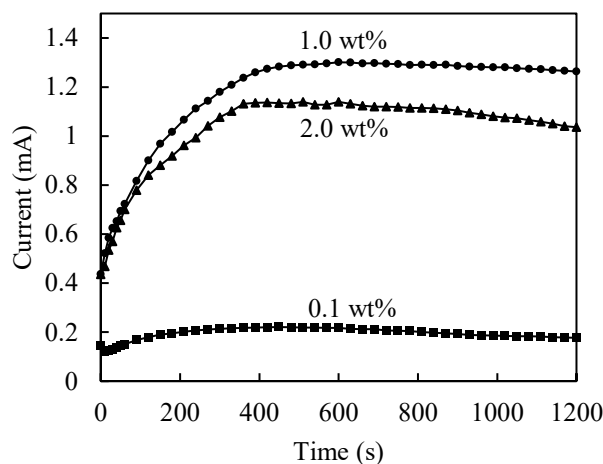


Fig. 1 Variations of the currents flowing through the gels containing 0.2, 1.0, and 2.0 wt% of SWCNTs.

[1] A. Bejan, *Int. J. Heat. Mass. Transfer*, **40**, 799 (1997).

Corresponding Author: M. Ozawa

Tel: +81-52-838-2410, Fax: +81-52-832-1179,

E-mail: mozawa@meijo-u.ac.jp

Temperature Dependence of the Thermoelectric Conductivity L_{12} in Semiconducting SWCNTs with Controlled Chemical Potential

○Yota Ichinose¹, Akari Yoshida¹, Manaho Matsubara², Shigeki Saito¹, Kan Ueji¹, Yohei Yomogida¹, Takahiro Yamamoto², and Kazuhiro Yanagi¹

¹Department of Physics, Tokyo Metropolitan University, Tokyo, Japan

²Department of Physics, Tokyo University of Science, Shinjuku, Tokyo, Japan

One-dimensional (1D) materials are expected to exhibit the highest thermoelectric (TE) performance due to their unique electronic structures [1]. Single-walled carbon nanotubes (SWCNTs) are an ideal 1D model; thus, we have investigated the relationship between their TE properties and the location of the chemical potential, μ [2]. Previously, we pointed out the importance of the thermoelectric conductivity, L_{12} , to clarify the influence of the line shape of density of state on the TE properties of semiconducting SWCNTs [3]. Currently, we are investigating the behaviors of the temperature dependence of the properties because the mechanisms of the TE generation can be understood through temperature dependence. Here, in this study, we investigate the temperature dependence of L_{12} , precisely controlling the chemical potential, μ , from the conduction (or valence) band to within the bandgap using an ionic liquid-based electric double-layer technique.

We prepared semiconducting SWCNTs with a diameter of 1.4 nm. In addition, as shown in Fig. 1, we constructed a new measurement device system combining the electric double layer carrier injection method and the on-tip thermometer method, which can measure the temperature of the sample with the resistance of gold wires to measure the temperature dependence.

Figure 2 shows the temperature dependence of S when μ is located in the conduction band, at the band edge, and within the bandgap of semiconducting SWCNTs. While the behavior of S within the bandgap is non-degenerate semiconductor-like, the other two show a clearly different behavior seems to be variable range hopping. However, L_{12} ($=S\sigma T$) behaved quite differently among the three parties. Figure 3 is a logarithmic plot of L_{12} and T . The slope of L_{12} ($\propto T^a$) was found to be systematically different. Thus, we found that L_{12} can show apparent changes in TE properties that cannot be seen by just looking at S as μ shifts. In this presentation, we will discuss the physical background in more detail.

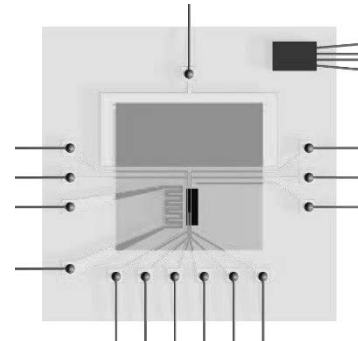


Fig. 1. Device image.

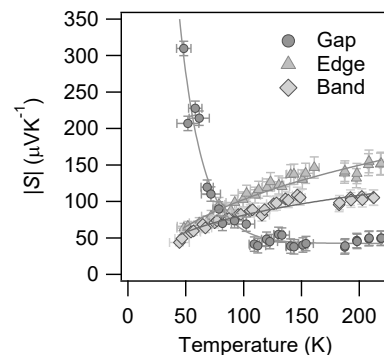


Fig. 2. Temperature dependence of S .

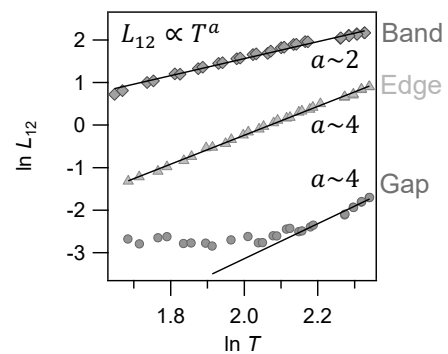


Fig. 3. Temperature dependence of L_{12} .

[1] Hicks & Dresselhaus, *PRB* **47**, 16631 (1993). [2] K. Yanagi et al., *Nano Letters* **14** (11), 6437 (2014).

[3] Y. Ichinose et al., *PRM* **5**, 025404 (2021).

Corresponding Author: K. Yanagi, +81-42-677-2494, yanagi-kazuhiro@tmu.ac.jp

Heat and charge-carrier flows in single-walled carbon nanotube film during a vertical electrolyte-gating

○Nobuhiro Muto¹, Kan Ueji¹, Yuya Matsuoka¹, Yota Ichinose¹,
Yohei Yomogida¹, Takashi Yagi¹, Jana Zaumseil¹, Kazuhiro Yanagi¹

¹ Department of Physics, Tokyo Metropolitan University, Tokyo 192-0372, Japan

² National Metrology Institute of Japan, National Institute of Advanced Industrial Science and Technology, Tsukuba, Ibaraki 305-8563, Japan

³ Institute for Physical Chemistry and Centre for Advanced Materials, Universität Heidelberg, D-69120 Heidelberg, Germany

Along with the rapid development of the Internet-of-Things society, an integrated circuit for electronics is miniaturized on a nanoscale over the years. In addition, improving the performance of electronic elements generates a large amount of heat, which causes damage to the circuit. Accordingly, thermal management is important to avoid thermal problems [1]. Flexible materials such as carbon nanotubes are attracting attention to address this problem. Time-domain thermoreflectance (TDTR) method is an ultrafast laser-based technique (pump-probe method) that can measure the thermal conductivity of nanoscale materials. In our system, a transducer for TDTR is a gold (Au) layer and the use of Au enables electrolyte gating. Thus, we can clarify the thermal conductivity (κ) and the electrical conductivity (σ) in nanoscale materials, such as single-walled carbon nanotube (SWCNT) and transition metal dichalcogenides, with different gate voltage. The previous [2] elucidated the κ - σ relationship of semiconducting SWCNT film but measurement directions are different: σ and κ correspond to lateral and vertical directions, respectively. For intuitive understanding, we employ a vertical electrolyte-gated transistor [3] where the channel direction corresponds to the film thickness, to match the measurement directions. In this study, we attempt to evaluate the κ - σ relationship of semiconducting SWCNT film with different Fermi levels to construct a thermal switch driven by electricity.

The electrolyte gating system involving (6,5) SWCNT film used an ionic gel as the gate dielectric under a high vacuum. The electrical characteristics were determined by a source-meter and a digital multimeter. The film exhibits ambipolar behavior with a clear on/off ratio of $\sim 10^5$ (Fig. 1), indicating that the electrolyte fully penetrated through SWCNT film, and then carrier injection can be tuned even in vertical transistor. Accordingly, the thermal conductivity of the SWCNT films with varying doping levels when heat and carrier flows match can be evaluated by our TDTR system. The details of this study will be further discussed during the presentation.

[1] A. L. Moore *et al.*, *Materials today* **17**, 163–174 (2014)

[2] K. Ueji *et al.*, *Applied Physics Letters* **117**, 133104 (2020)

[3] M. Rother *et al.*, *ACS Appl. Nano Mater* **1**, 3616–3624 (2018)

Corresponding Author: K. Ueji and K. Yanagi

E-mail: kueji@tmu.ac.jp (K.U.), yanagi-kazuhiro@tmu.ac.jp (K.Y.)

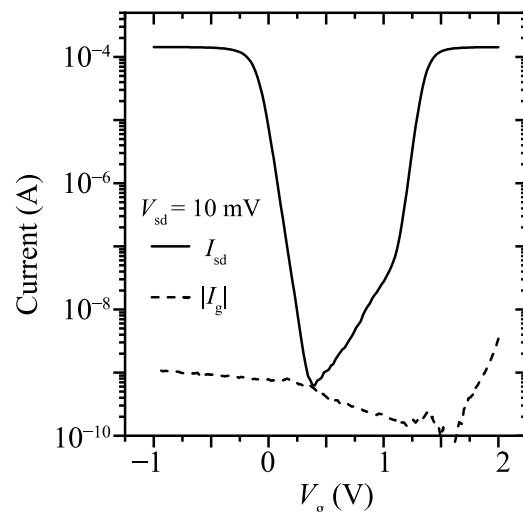


Fig. 1 Transfer characteristic of (6,5) SWCNT film in the vertical device.

Dry Functionalization of Carbon Nanotubes While Retaining Intrinsic Properties

Dewu Lin¹, Don N. Futaba¹, Kazufumi Kobashi¹, Kenji Hata¹

¹ CNT-Application Research Center, AIST, Ibaraki 305-8565, Japan

Because of the chemical stable surface made of sp^2 carbons, functionalization of CNTs has been widely explored to modify the interfacial properties for advanced performance in specific applications. Adding functional groups through solution-based wet chemistry has enabled researchers to achieve abundant modification, however, the time-consuming and destructive processes, including separation, purification, and collection, make it challenging to directly functionalize pre-assembled CNTs without degrading the intrinsic properties.

Herein, we propose a convenient, solvent-free approach to perform interfacial modification of CNTs without degrading the intrinsic properties. Briefly, controlled oxidation is carried out to introduce oxygen-contained polar groups on the surface of the CNTs [1], then by the activation with thermal heating, carbon free radicals are generated for the following grafting with various monomers in gas phase (Figure 1A). Thermogravimetric analysis (TGA) showed 3.4 wt.% of monomer methyl methacrylate (MMA) was chemically bonded to the CNTs (Figure 1B). More characterization by FTIR spectroscopy, contact angle, etc. confirmed the covalent bonding of the MMA. Further investigation revealed that the oxidation treatment was the destructive step due to the forming and growth of carbon vacancy defects. Therefore, by a controlled and slow oxidation [2], we finally achieved dry functionalization of CNTs while retaining intrinsic crystallinity, electrical conductivity, and mechanical strength, which was confirmed by multiple characterization results (Figure 1C).

Such solvent-free interfacial modification is applicable to other graphitic nanocarbons with any pre-assembled structures. Further development will be focus on the improvement of efficiency, including creating active sites and grafting.

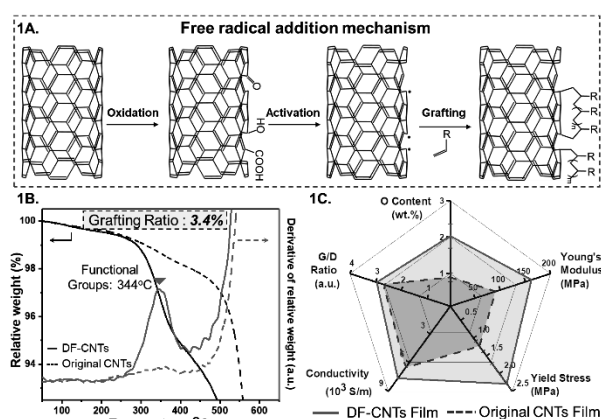


Figure 1. (a) Free radical addition mechanism of dry functionalization; (b) TGA profiles of dry functionalized CNTs (DF-CNTs) and original CNTs; (c) Comparison of crystallinity, conductivity, and mechanical properties.

[1] R. Menzel *et al.* Chem. Sci., **1**, 603 (2010).

[2] T. Hiraoki *et al.* Adv. Funct. Mater., **20**, 422 (2010).

Corresponding Author 1: Kenji Hata

Tel: +81-29-861-4551,

E-mail: kenji-hata@aist.go.jp

Corresponding Author 2: Don N. Futaba

Tel: +81-29-861-4402,

E-mail: d-futaba@aist.go.jp

Aromaphilicity: the affinity for graphene and carbon nanotubes determined by experiments and simulations

○Atsushi Hirano¹, Tomoshi Kameda², Momoyo Wada¹, Takeshi Tanaka¹, Hiromichi Kataura¹

¹ Nanomaterials Research Institute, National Institute of Advanced Industrial Science and Technology (AIST), Ibaraki 305-8565, Japan

² Artificial Intelligence Research Center, National Institute of Advanced Industrial Science and Technology (AIST), Tokyo 135-0064, Japan

Molecular adsorption onto aromatic carbon nanomaterials is generally involved in various phenomena, including physical and chemical reactions of these materials. Particularly in biological systems, nonspecific protein adsorption is associated with their bioavailability and cytotoxicity. It is necessary to elucidate the molecular mechanism of protein–nanomaterial interactions for understanding and predicting such biological impacts of the aromatic carbon nanomaterials. We have ever examined the interactions of the carbon nanomaterials with proteins, polypeptides and amino acids [1–3]. Recently, a new concept ‘aromaphilicity’ was proposed, which reflects the affinity for aromatic surfaces of the carbon nanomaterials [4]. The aromaphilicity was determined for 20 amino acids contained in protein structures on the basis of their binding free energy onto graphene using molecular dynamics simulations. We here show that experimental results obtained from liquid chromatographic analyses were consistent with the simulation data. These findings are useful for predicting binding sites of proteins to aromatic carbon nanomaterial surfaces.

The aromaphilicity is indexed as the normalized value of the binding free energy of amino acids onto graphene (Fig. 1a). High aromaphilicity is observed not only for aromatic amino acids—tryptophan (Trp), tyrosine (Tyr) and phenylalanine (Phe)—but also for arginine (Arg). We can draw protein surface profiles of the aromaphilicity using the aromaphilicity index (Fig. 1b). Some proteins have affinity hot spots (high-aromaphilicity regions).

We performed liquid chromatography of *N*-acetyl amino acid amide compounds with an aromatic side chain on a immobilized graphene column. The retention data of these compounds were consistent with the aromaphilicity trend (Fig. 2), which supports the validity of the aromaphilicity index obtained from the molecular dynamics simulations.

- [1] A. Hirano *et al.* Chem. Eur. J. **20**, 4922–4930 (2014).
 [2] K. Iwashita *et al.* Langmuir **31**, 8923–8929 (2015).
 [3] K. Iwashita *et al.* Chem. Lett. **45**, 952–954 (2016).
 [4] A. Hirano and T. Kameda. ACS Appl. Nano Mater., **4**, 2486–2495 (2021).

Corresponding Author: A. Hirano

Tel: +81-29-849-1064, Fax: +81-29-861-2786,

E-mail: hirano-a@aist.go.jp

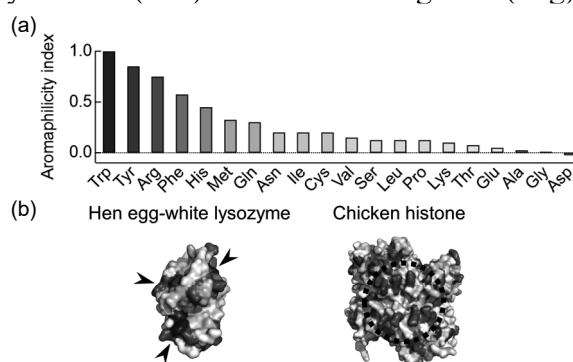


Fig. 1 (a) Aromaphilicity index of amino acids. (b) Surface profiles of the aromaphilicity of the hen egg-white lysozyme (left) and chicken histone (right). The arrows and the dotted circle depict affinity hot spots.

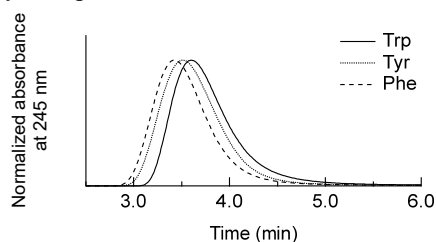


Fig. 2 Liquid chromatography of *N*-acetyl amino acid amides on a immobilized graphene column.

Photo-enhanced Responses of Gas Sensor Based on MoS₂ Monolayers to Various Biogas Species

○T. Goto, R. Inao, H. Tabata, O. Kubo, M. Katayama

Division of Electrical, Electronic and Infocommunications Engineering, Graduate School of
Engineering, Osaka University, JAPAN
E-mail: goto@nmc.eei.eng.osaka-u.ac.jp

Thin layers of molybdenum disulfide (MoS₂) have been attracting attention as an excellent gas sensing material, because they have a unique property to exhibit an effective photoactivated gas response under visible light, resulting in excellent sensitivity and a fast response / recovery at room temperature [1]. Recently, we have reported that gas sensors based on MoS₂ monolayer under the visible light showed excellent performance to NO₂ gas, with a sensitivity of 8.6%/ppb, and respond quickly to the changes in gas concentration [2]. However, the photoactivated response of the MoS₂ sensor has yet to be investigated for only a few gas species. In this study, we explore the responses of the MoS₂ sensor under light illumination to various biogas species such as NH₃, H₂, CH₄, and ethanol and acetone vapors, which are beneficial to be monitored for human health care or medical diagnostics, and aim to clarify the effect of light illumination on their responses and their mechanism.

Figure 1 shows the dynamic responses of the drain current of the monolayer MoS₂ sensor upon the exposure of various NH₃ concentrations under light and dark conditions. A blue LED (peak wavelength:470 nm) was used as the light source, with a typical irradiance of 50 mw/cm². Since NH₃ acts as an electron donor, the drain current increased upon the NH₃ exposure. Sensor response S_G defined as $S_G = 100 \Delta I / I_0$, where ΔI is change in drain current during NH₃ exposure, and I_0 is the initial drain current just before NH₃ exposure, drastically increased under the light condition. Similar trends were observed for the other four gas species. Table 1 summarized the sensor response in the dark and light conditions for each gas species. For all gas species measured, the sensor showed a response of increasing current, which may mean that they are reducing gases. Even for the gas species which cannot be detected in dark condition, the gas sensor clearly showed response to them under the light condition. To explain the result, we proposed a model that the response was mediated by oxygen in air.

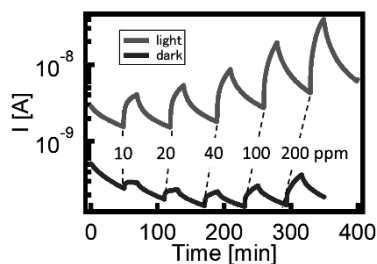


Figure 1. Dynamic response of the drain current upon the exposure of various NH₃ concentrations under light and dark condition.

	Sensor response (%)	
	light	dark
NH ₃ (200 ppm)	811	147
H ₂ (300 ppm)	15	n.d.
CH ₄ (200 ppm)	37	n.d.
EtOH (300 ppm)	87	12
Acetone (300 ppm)	36	n.d.

Table 1. Comparison of sensor response (S_G) in the dark and light conditions for each gas species

- [1] T.Pham *et al.*, ACS Nano **13**, 3196(2019).
[2] H.Tabata *et al.*, ACS Nano **15**, 2542(2021).

Geometric structure and piezoelectric polarization of MoS₂ nanoribbons under uniaxial strain

○Susumu Okada, Yanlin Gao, Mina Maruyama

Department of Physics, University of Tsukuba, Tsukuba 305-8571, Japan

According to their chemically inert surfaces owing to the two-dimensional covalent networks, two-dimensional materials could be emerging materials for various functional devices, such as electronics, photonics, optoelectronics, and piezoelectric devices. Because of the absence of the inversion symmetry in MoS₂ sheet and the chemical difference between Mo and S, an open boundary condition intrinsically causes the electron polarization in MoS₂ nanostructures. Furthermore, the mechanical strains cause the modulation of the polarization. Thus, in this manuscript, we aim to elucidate the correlation between the atomic structure and the electric property of MoS₂ nanoribbon under the uniaxial tensile and compressive strains, using the density functional theory combined with the effective screening medium method.

Piezoelectric polarization is only observed between the zigzag edges of a MoS₂ ribbon under the tensile and compressive strains along the ribbon direction which cause the decrease and increase of the ribbon width (Fig. 1). For the ribbons with chiral edges the piezoelectric polarization is insensitive to the tensile and small compressive strain irrespective of their edge angles, while the large compressive strain causing the edge reconstruction induces the electricity.

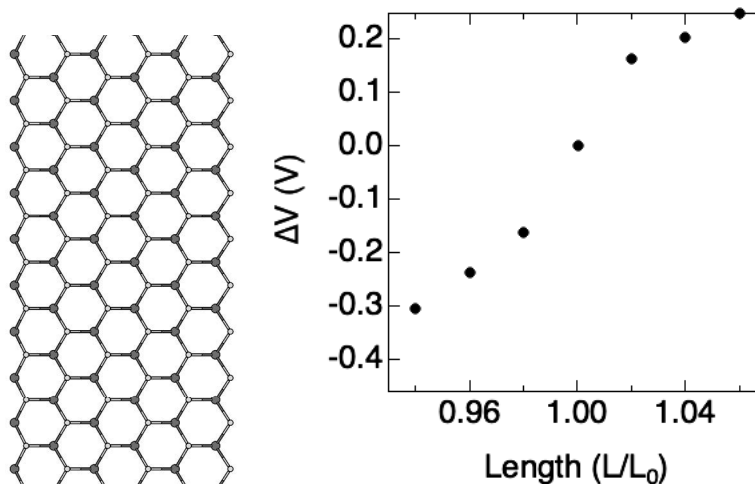


Fig.1 Geometric structure of MoS₂ nanoribbons with zigzag edges. The piezoelectric polarization of MoS₂ nanoribbons under the uniaxial compressive and tensile strain along ribbon direction.

Corresponding Author: Susumu Okada
 TEL: +81-29-853-5921, FAX: +81-29-853-5924
 E-mail: sokada@comas-tsukuba.jp

Raman spectroscopy of Weyl semimetal $\text{Co}_3\text{Sn}_2\text{S}_2$

○Kenya Tanaka¹, Akira Takakura¹, Yasumoto Segawa^{2,3}, Taishi Nishihara¹,
Kazunari Matsuda¹, Yuhei Miyauchi¹

¹*Institute of Advanced Energy, Kyoto University, Uji 611-0011, Japan*

²*Institute for Molecular Science, Okazaki 444-8787, Japan*

³*Department of Structural Molecular Science, SOKENDAI, Okazaki, 444-8787, Japan*

Recently, $\text{Co}_3\text{Sn}_2\text{S}_2$ has attracted much attention as a magnetic Weyl semimetal with a trigonal crystal structure of Kagomé lattice [1-3]. X-ray diffraction (XRD) and energy dispersive X-ray (EDX) spectroscopy techniques have been used to identify the crystal structure of $\text{Co}_3\text{Sn}_2\text{S}_2$. In addition to these techniques, Raman spectroscopy is known as a useful non-destructive optical method for obtaining information of phonon modes that are characteristic to the crystal structure. Once the Raman spectral features of the crystal are identified, the characteristic Raman spectrum can be used as a fingerprint to rapidly identify the crystal structure and confirm successful growth of the crystal without performing time-consuming XRD and EDX measurements. However, Raman spectroscopic study on $\text{Co}_3\text{Sn}_2\text{S}_2$ still remains to be reported.

Here, we report Raman spectra of $\text{Co}_3\text{Sn}_2\text{S}_2$ crystals and their crystal angle dependence. The single crystals of $\text{Co}_3\text{Sn}_2\text{S}_2$ were obtained by vacuum heating of the raw material powders (stoichiometric ratio of powders were Co:Sn:S = 3:2:2). The growth temperature of the crystals was controlled as follows. The mixture sample powders were heated up to 1000 °C over 48 hours and held for 24 hours, and then it was slowly cooled down to 600 °C over 168 hours and kept at 600 °C for 24 hours [4]. The crystal structure of the synthesized material with a distorted hexagonal shape was confirmed as $\text{Co}_3\text{Sn}_2\text{S}_2$ using single crystal XRD and EDX spectroscopy techniques (Figs. 1a and 1b). In the synthesized material, we also found bi-product crystals with elongated shapes that were identified as SnS by XRD and EDX. A plate-type $\text{Co}_3\text{Sn}_2\text{S}_2$ flake (Fig. 1c) was picked up using a sticky polydimethylsiloxane (PDMS) film and transferred to a silicon substrate under an optical microscope. For Raman measurements, we built a home-made optical setup that allows polarization and crystal angle resolved optical measurements with an automated sample rotation stage with a centering mechanism. In the measurements, linear polarized 532 nm continuous laser was mainly used for the polarized excitation. Two major peaks were observed in the wavenumber range from 250 to 400 cm^{-1} . In the presentation, we will discuss the origin of the observed Raman features based on the results of the polarization and angle-resolved measurements.

[1] P. Vaquero *et al.*, *Solid State Sci.* **11**, 513 (2009).

[2] D. Liu *et al.*, *Science* **365**, 1282 (2019).

[3] R. Yang *et al.*, *Phys. Rev. Lett.* **124**, 77403 (2020).

[4] N. Morali *et al.*, *Science* **365**, 1286 (2019).

Corresponding Author: Y. Miyauchi
Tel: +81-774-38-3463,
E-mail: miyauchi@iae.kyoto-u.ac.jp

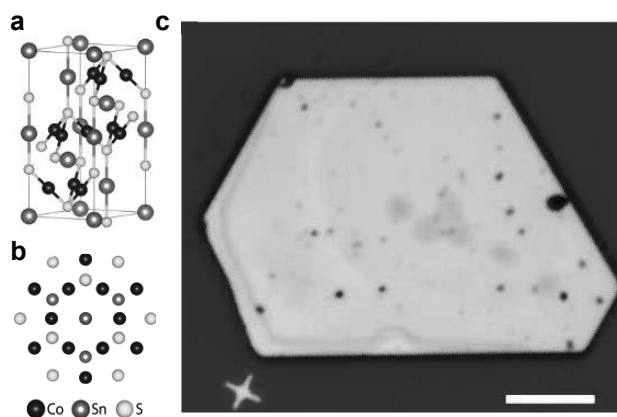


Figure 1. Crystal structure of $\text{Co}_3\text{Sn}_2\text{S}_2$, (a) unit cell and (b) structure viewed from c -axis. (c) Typical optical image of the crystal. Scale bar, 20 μm .

Helicity resolved Raman spectroscopy in MoS₂

○Hirofumi Nema, Yasuhiro Fujii, Shogo Saito, Eiichi Oishi, Akitoshi Koreeda

Department of Physical Sciences, Ritsumeikan University, 1-1-1 Noji-higashi, Kusatsu, Shiga 525-8577, Japan

van Der Waals materials such as graphite and MoS₂ have been widely investigated after the first fabrication of monolayer graphite film (graphene) by Novoselov and Geim et al. For the characterization of van der Waals materials, Raman spectroscopy is a useful and popular tool. Recently, helicity-resolved Raman spectroscopy of graphite films has been carried out to obtain information on interlayer interaction via chiral phonons [1].

Here, we report the helicity-resolved Raman spectroscopy in bulk MoS₂. The in-plane relative motion of transition metal and chalcogen atoms (IMC mode) and the out-of-plane motion involving only chalcogen atoms (OC mode) were observed in our spectra (Fig.1). Similar results were shown by Chen et al. [2].

Below 70 cm⁻¹, two additional Raman peaks appeared (Fig.2). The peak around 33 cm⁻¹ (around 6 cm⁻¹) may correspond to the shear mode (breathing mode) between layers. Compared to the results of 4-layer MoS₂ [2], the peak of the breathing mode shifted to the lower wave number in bulk, while that of the shear mode showed a little or no shift.

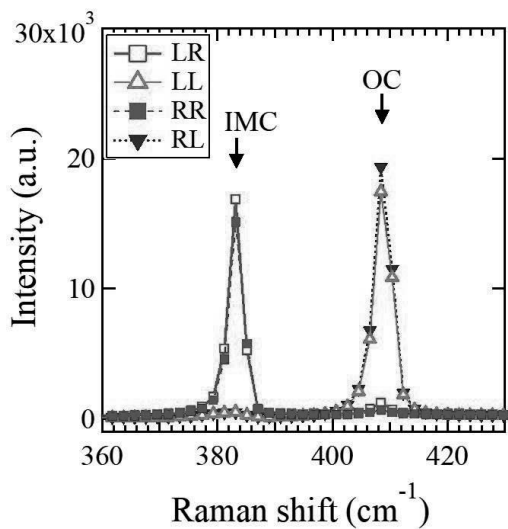


Fig. 1 Helicity resolved Raman spectra in bulk MoS₂ (between 360 cm⁻¹ and 430 cm⁻¹). L (R) represents left-handed (right-handed) circularly polarized light.

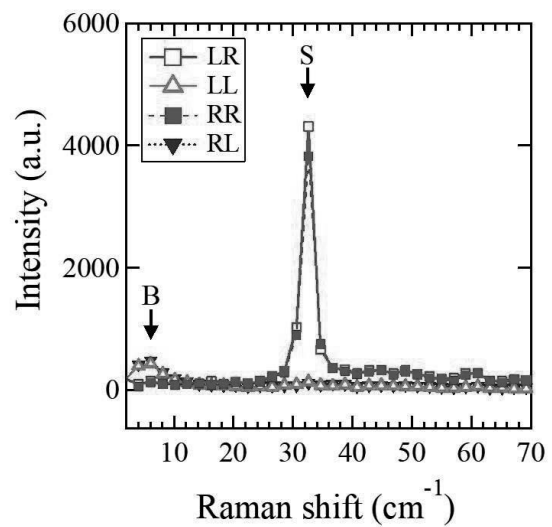


Fig. 2 Helicity resolved Raman spectra in bulk MoS₂ below 70 cm⁻¹.

[1] C. Chen *et al.*, Phys. Rev. B **103**, 035405 (2021).

[2] S.-Y. Chen *et al.*, Nano. Lett. **15**, 2526 (2015).

Corresponding Author: H. Nema

Tel: +81-77-561-5752, Fax: +81-77-561-5752,

E-mail: h-nema@fc.ritsumei.ac.jp

Quasi-ballistic heat transport in graphene elucidated by isotopic interface

○Yoshito Hata, Kuniharu Takei, Seiji Akita, Takayuki Arie

Department of Physics and Electronics, Osaka Prefecture University, Sakai 599-8531, Japan

Due to its outstanding thermal properties, graphene is expected as a candidate for thermal management devices. Since the main heat carrier in graphene is phonon, we investigated the control of heat conduction by introducing isotopes [1] and defects [2]. In this study, we synthesized graphene periodic structures with different isotope regions to control the heat conduction by the number of isotopic interfaces.

We synthesized isotopically separated graphene heterostructures with isotopic interfaces by alternately supplying $^{12}\text{CH}_4$ and $^{13}\text{CH}_4$ as source gases during chemical vapor deposition. The heat conduction in graphene was evaluated by the temperature- and laser power-dependence of Raman peak shifts after fabricating the suspended structures.

Figure 1(a) and 1(b) show the optical microscope and Raman 2D mapping images of graphene isotopic heterostructures. The periodic heterostructures with the width of approximately 500 nm were fabricated. Figure 2 depicts the thermal resistance of suspended graphene with respect of the interface number (N). The thermal resistance increases linearly as N increases up to N=3; the resistance per interface is estimated to be $151.1 \mu\text{m}^2\text{K}/\text{W}$. However, it begins to increase significantly at N greater than 4. The width between interfaces at N=4 is around 560 nm, comparable to the reported phonon mean free path in graphene at room temperature ($\approx 700 \text{ nm}$) [3]. The result implies that the thermal phonons behave in the quasi-ballistic transport regime when the width between interfaces becomes equal to or smaller than phonon mean free path in graphene.

[1] Y. Anno et al., *Phys. Status Solidi RRL* **8**, 692 (2014). [2] Y. Anno et al., *2D Mater.* **4**, 025019 (2017). [3] S. Ghosh et al., *Appl. Phys. Lett.* **92**, 151911 (2008).

Corresponding Author: T. Arie, Phone/Fax: +81-72-254-9265, E-mail: arie@pe.osakafu-u.ac.jp

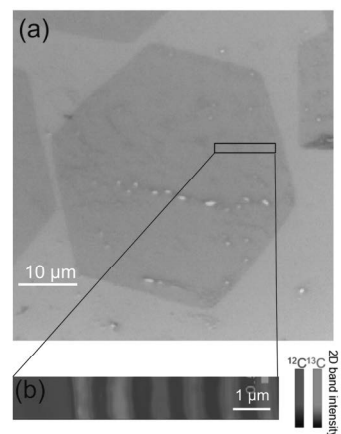


Fig. 1. (a) Optical and (b) Raman 2D mapping images of graphene isotopic heterostructures.

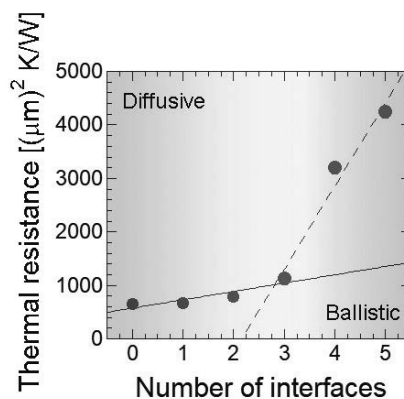


Fig.2. Interface number-dependence of the thermal resistance in graphene.

Switching speed of optically-generated spin current at the graphene edge

○Yuan Tian, M. Shoufie Ukhtary, Riichiro Saito

Department of Physics, Tohoku University, Sendai 980-8578, Japan

Manipulation of spin current is a novel technique in the field of spintronics, which promises new and more effective designs for memory storage and logic circuit [1,2]. Although methods for generating spin current that relies on the either spin Hall effect, spin injection or a spin valve are well established, these conventional methods rely on either complicated structure or magnetic material, which limits the response speed of spintronic devices. Recently, Daigo Oue et.al.[3] theoretically showed that by using the inverse Faraday effect, surface plasmon on the surface of metal can induce a spin current in direction perpendicular to the surface, due to the rotating electric field of the surface plasmon. In our recent paper [4], we further show that through the inverse Faraday effect, a spin current can be generated on graphene via the excitation of the edge plasmon. An edge plasmon is an oscillation of charge accumulation that propagates at the edge of a 2D surface. The edge plasmon induces a spin current that flows in plane, in the direction perpendicular to the edge. The spin current consists of electrons with out-of-plane spin polarization, as is shown in Fig. 1. Here we investigate the switching speed of the spin current generated via the excitation of edge plasmon, which can be used as a tunable spin device with the response speed up to GHz.

In this work, we study the response speed of spin accumulation generated via edge plasmon on graphene. We obtain the analytical and the numerical solutions of the spin diffusion equation as a function of time under a periodic source term representing the edge plasmon to study the switching speed of the device. We find a maximum spin accumulation up to 0.5 neV and the response time of less than 0.2 ns, as are shown in Fig. 2. Since the edge plasmon is generated by light, we can realize optical switching of spin signal with response in GHz.

Reference:

[1] Huai, Yiming, et al., AAPPS bulletin 18.6, 33-40, (2008).

[2] Maekawa, Sadamichi, et al., eds. *Spin current*. Oxford University Press, (2017).

[3] Oue, Daigo, et al., Physical Review B 101.16, 161404, (2020).

[4] M. S. Ukhtary, et al., Phys. Rev. B, 103, 245428-1-8, (2021).

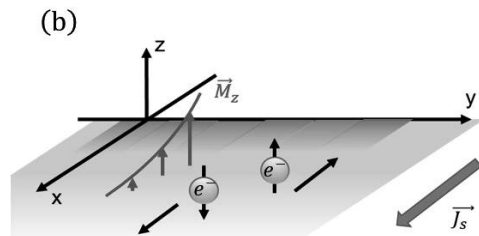


Figure 1: Edge plasmon that propagates along the edge of 2D material (y-axis) which induces the magnetization M_z . The magnetization is localized at the edge, causing spin accumulation near the edge due to the inverse Faraday effect. This distribution of spin accumulation will drive a spin current J_s that flows in x-direction.

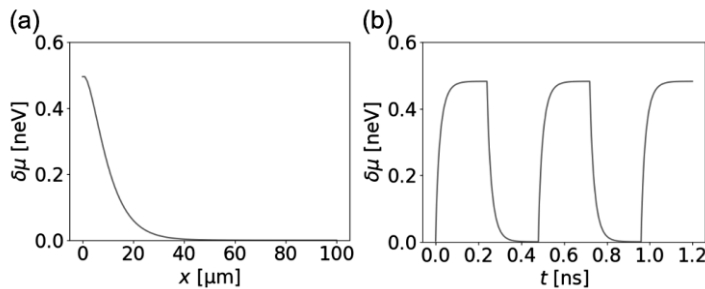


Figure 2: Spin accumulation $\delta\mu$ near the edge (a) as a function of distance from the edge for continuous light. (b) $\delta\mu$ as a function of time for the pulsed light. The edge plasmon is turned on and off in a period of 0.5 ns. The response time of $\delta\mu$ is less than 0.2 ns.

Corresponding Author: Tian Yuan

Email: tian@flex.phys.tohoku.ac.jp

Metal Deposition on a Suspended Graphene Surface

○Kawase Yuta¹, Kenta Matsushima¹, Juntaro Doi¹, Tsutomu Araki¹, Shinichiro Mouri¹

¹ Department of science and engineering, Ritsumeikan University, Shiga 525-8577, Japan

Crystal growth using graphene substrate called van der Waals Epitaxy (vdWE) has been proposed as a way to fabricate transferable compound semiconductors[1,2]. Especially, it is pointed out that potential of ionic substrate under graphene promotes the quasi-homoepitaxial crystal growth, named remote epitaxy [3,4]. These studies suggest the substrate under graphene plays an essential role for vdWE resulting in obscuring the effect of graphene surface itself on the crystal growth including atomic adsorption process. We here propose the platform using suspended graphene to test the net effects of graphene surface on crystal growth or atomic scale adsorption. The dispersion of deposited Indium or Gallium metal on graphene surface was observed using TEM.

Figure 1 show low magnification TEM image of Si₃N₄ grid (EM Japan Co.). Many holes whose diameter is 2.5 μm, are arranged every 5 μm. The bilayer graphene was prepared on it by wet process using the polymer PMMA.

Indium or Gallium metal was deposited on this grid with RF-MBE setup. Figure 2 (a) and (b) show the TEM image of Indium metal dispersed on graphene surface at different temperatures 425°C and 350°C, respectively. The duration of metal supply was five second. The small grain of Indium metal less than 50 nm diameter was dispersed in both cases however its pattern is different reflecting deposited temperature. The grains were aligned in line according to the domain boundary or wrinkles of graphene when the deposition temperature was higher as shown in Fig. 2 (a). The dangling bonds existing in these structures could act as nucleation sites of metal cluster. On the other hand, the grains forms island like clusters when the deposition temperature was lower as shown in Fig. 2 (b). The migration of metal is suppressed, and the nucleation may occur outside the domain boundaries. In the presentation, we would discuss the detailed analysis including the relationship between the number of metals and metal size with changing deposited temperature.

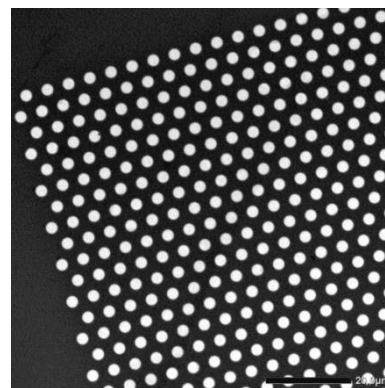


Fig. 1 Low magnification TEM image of the Si₃N₄ grid.

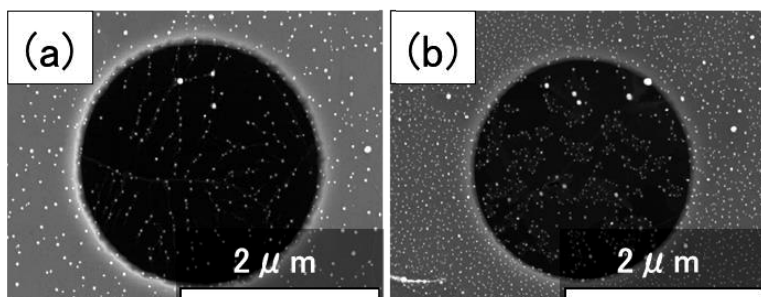


Fig. 2 Distribution of Indium metal of suspended graphene. Deposit temperature of (a) is 425°C, and (b) is 350°C.

References

- [1] J. Kim *et al.*, Nat. Commun. **5**, 4836 (2014).
- [2] W. Kong *et al.*, Nat. Mater. **17**, 999 (2018).
- [3] Y. Kim *et al.*, Nature **544**, 340 (2017).
- [4] D. Dobrovolskas, **S. Mouri, T. Araki**, *et al.*, Nanomaterials **9**, 417 (2019).

This work was supported by JPSJ KAKENHI, #21H01831, #21H01017, #16H06415.

Synthesis of Boron Nitride Nanotubes Using Solid Boron, Water Vapor, and Ammonia

○Takazumi Kaida¹, Hiromu Takahashi¹, Toshio Osawa¹, Hisashi Sugime², Suguru Noda^{1,2,*}

¹ Department of Applied Chemistry, ² Waseda Research Institute for Science and Engineering, Waseda University, Tokyo 169-8555, Japan.

Boron nitride nanotube (BNNT) is a one-dimensional nanomaterial that has high tensile strength with mechanical flexibility, and is thermally and chemically stable, thermally conductive, and electrically insulative [1]. Various applications including thermal interface materials and battery separators are expected, and low-cost production is essential to make those applications practical. BNNTs can be synthesized by high-temperature processes that use thermal plasma or laser to vaporize solid boron or h-BN [2]. However, the BNNTs are still very expensive due to the very high process temperatures and the difficulties in scaling-up. Chemical vapor deposition (CVD) processes at lower temperatures are also researched [1]. Among them, the boron oxide CVD (BOCVD) that uses B₂O₂ vapor formed in the reaction between B and B₂O₃ powders is attractive for the low-cost boron source. However, it is difficult to control the interface reaction between solid B powder and B₂O₃ melt (melting point of ~450 °C).

Here we report the gas-vapor reaction of $2\text{B}(\text{s}) + 2\text{H}_2\text{O}(\text{g}) \rightarrow \text{B}_2\text{O}_2(\text{g}) + 2\text{H}_2(\text{g})$ for the controlled feed of B₂O₂ vapor. We used an externally heated CVD reactor made of a quartz glass tube and set an inner quartz glass tube for the B₂O₂ supply. B powder was set in the inner tube, heated by the reactor furnace, and reacted with H₂O vapor. The Fe catalyst (1.2–3.8 nm)/Al₂O₃ underlayer (1.0 nm)/graphite substrate was prepared by sputter-deposition, set in the CVD reactor, and heated to 1050 °C under an Ar flow. Then H₂O(g) was fed to the inner tube for the B₂O₂ supply for 5 min, and CVD was carried out by flowing NH₃(g) for 10 min. In scanning electron microscope (SEM) images, no tubes were observed for Fe/graphite while many tubes were observed for Fe/Al₂O₃/graphite. The reaction between B(s) and H₂O(g) proved effective for supplying B source and the Al₂O₃ layer proved effective for enhancing catalytic activity of Fe for BNNT growth.

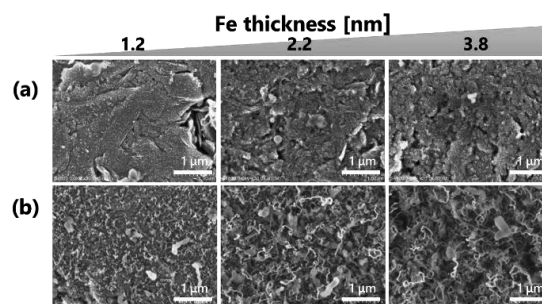


Fig. 1. Plan-view SEM images of the substrates after CVD. (a) Fe/graphite. (b) Fe/Al₂O₃/graphite.

[1] E. Songfeng, *et al.*, Chem. Phys. Lett., **687**, 307 (2017).

[2] K.S. Kim, *et al.*, Semicond. Sci. Technol. **32**, 013003 (2017).

Corresponding Author: S. Noda, Tel: 03-5286-2769, E-mail: noda@waseda.jp

Indium intercalation in bundles of WTe atomic wires

○Hiroshi Shimizu¹, Zheng Liu², Hong En Lim¹, Yusuke Nakanishi¹,
Takahiko Endo¹ and Yasumitsu Miyata¹

¹ *Department of Physics, Tokyo Metropolitan University, Hachioji 192-0397, Japan*

² *Innovative Functional Materials Research Institute, AIST, Nagoya 463-8560, Japan*

One-dimensional (1D) transition metal chalcogenides (TMCs) have recently received significant attention due to their atomically thin wire structure and excellent conductive properties. Recently, we had achieved a scalable growth of highly crystalline, conductive TMC atomic wires using chemical vapor deposition (CVD) [1]. To further improve their conducting properties, highly efficient carrier injection is required. One of the promising ways to realize such purpose is via metal atom intercalation (Fig.1a). However, there is no study on the intercalation for TMC bundles.

In this study, we have investigated the In intercalation into bundles of WTe atomic wires. WTe wires were grown on SiO₂/Si substrates by CVD as reported previously [1]. The intercalation was carried out by vacuum deposition of In thin film. The cross-sectional HAADF-STEM observations reveal the presence of intercalated atoms between individual WTe wires (Fig. 1b). The distance between WTe wires has increased by 1.8% compared to that before the intercalation. In addition, a downshift in the peak at 155 cm⁻¹ has also been observed in the Raman spectra (Fig. 1c). These serve evidences for the realization of In intercalation in WTe bundles. The present results provide an effective approach not only for tuning the electric properties of WTe wires but also for the realization of a novel ternary telluride group.

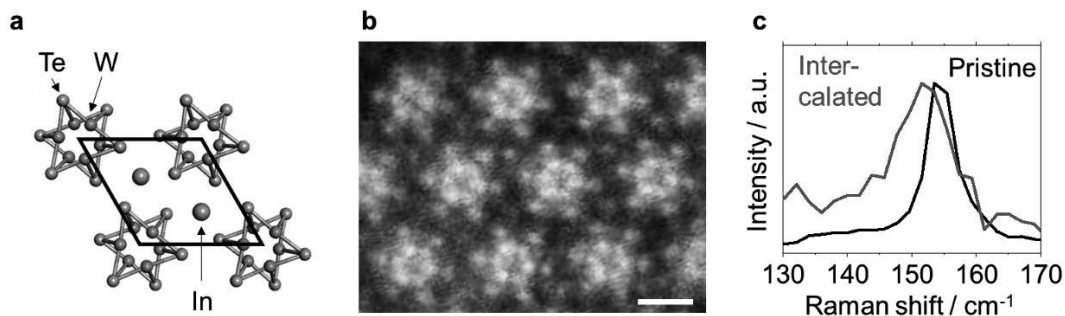


Figure 1 (a) Structure model and (b) Cross-section HAADF-STEM image of In intercalated WTe bundle. Scale bar = 1 nm. (c) Raman spectra for WTe bundle before and after the In intercalation.

[1] H. E. Lim et al., *Nano Lett.*, 21, 1, 243-249 (2021).

Corresponding Author: Y. Miyata, Tel: +81-42-677-2508, E-mail: miyata-yasumitsu@tmu.ac.jp

Carbon nanotube and boron nitride nanotube make battery lighter and safer

○Kentaro Kaneko¹, Keisuke Hori¹, Suguru Noda^{1,2}

¹ Department of Applied Chemistry, Waseda University, Tokyo, Japan.

² Waseda Research Institute for Science & Engineering, Waseda University, Tokyo, Japan

Safety is getting more important for batteries with increasing energy density. We propose inorganic nanotube architecture to develop lighter and safer lithium-ion battery [1]. Differently from the conventional conductive additives such as carbon black and carbon nanofibers, electrically conductive carbon nanotube (CNT) can have multiple roles in battery electrodes. We have previously reported light-weight electrodes, in which 99 wt% active materials were held in the 1 wt% CNT sponge that worked as binder, conductive filler, and current collector [2]. In contrast, boron nitride nanotube (BNNT) is electrically insulative, thus can be used for separator. Both CNT and BNNT have high thermal stability compared to organic polymer.

Self-supporting electrodes were fabricated with submillimeter-long few-wall CNT (prepared by fluidized bed CVD method [3]) and active materials (lithium cobalt oxide or graphite) by dispersion and filtration. Similarly, self-supporting separator (~25 μm thickness) was fabricated via dispersion and filtration of BNNT without using binder. The mass fraction of non-active materials in the electrodes/separator stack decreased to 6.4% with the nanotube-based architecture from 25.0% of the conventional one (Fig. 1).

The thermal stability of the electrodes/separator stack was examined by heating in a N_2 flow for 10 min, and then testing the electrical insulation between the positive and negative electrodes. Differently from the conventional polyolefin separators that melt at ~ 150 $^\circ\text{C}$, no damage was observed in the BNNT separator after heating at 500 $^\circ\text{C}$. Furthermore, the battery made of the heated stack with fresh electrolyte functioned correctly. The nanotube-based architecture makes batteries lighter and safer.

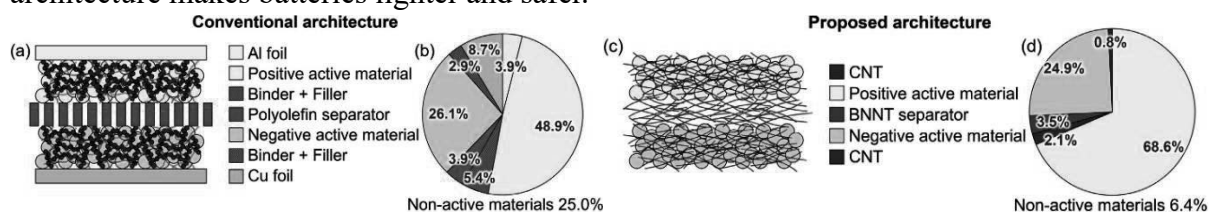


Fig. 1. Structure and mass fraction of conventional and nanotube-based architecture [1].

[1] K. Kaneko, K. Hori, and S. Noda, Carbon **167**, 596 (2020).

[2] K. Hasegawa and S. Noda, J. Power Sources **321**, 155 (2016).

[3] M. Li, M. Risa, T. Osawa, H. Sugime, and S. Noda, Carbon **167**, 256 (2020).

Corresponding Author: S. Noda

Tel: +81352862769, Fax: +81352862769 E-mail: noda@waseda.jp

Chemically-enriched and integrated carbon nanotube photo-thermoelectric scanners for non-sampling, source and label-free chemical monitoring

○Kou Li^{1,2}, Yukio Kawano^{1,2,3}

¹ *Laboratory for Future Interdisciplinary Research of Science and Technology, Tokyo Institute of Technology, 2-12-1 Ookayama, Meguro-ku, Tokyo 152-8552, Japan*

² *Department of Electrical and Electronic Engineering, Tokyo Institute of Technology, 2-12-1 Ookayama, Meguro-ku, Tokyo 152-8550, Japan*

³ *Faculty of Science and Engineering, Chuo University, 1-13-27 Kasuga, Bunkyo-ku, Tokyo 112-8551, Japan*

The use of carbon nanotube (CNT)-based electronics devices accelerates diverse sensing applications. In particular, the photo-thermoelectric (PTE) effect with CNT films makes the most of interesting characteristic of CNTs as broadband electromagnetic-wave sensing with freely deformable configuration[1]. Here, we demonstrate non-sampling, source and label-free chemical monitoring by simply wrapping containers with chemically-enriched and integrated CNT film PTE scanners. The PTE device design on the CNT films enhances photo-induced chemical monitoring sensitivity, and the mechanical flexibility of the device firmly attaches to arbitrary-structured contains. These relax conventional experimental constraints of chemical monitoring, and facilitates future versatile and ubiquitous on-site use.

Fig. 1a depicts the proposed structure of the PTE scanner. The channel of the device consists of multiple series integration of P- and N-type[2] CNT films. This structure enhances photo-detection sensitivity of the device by adding up PTE responses in each pair of P- and N-type CNT films. This device design therefore facilitates non-destructive, non-sampling, source and label-free chemical monitoring as shown in Fig. 1b. Chemical substances, which are dissolved in solvent liquid and circulated by a digital pump, can be examined by simply wrapping outer surface of a soft tube with the proposed device. The use of broadband black-body radiation (BBR) from the solvent develops compact measurement configuration without employing bulky external photo sources. Here, in-liquid chemical substances locally absorbs the BBR from the solvent and passive responses obtained by the proposed device show associated reduction after dissolving glucose (Fig. 1c). This phenomenon advantageously governs concentration monitoring in circulating solvent in a non-sampling and label-free manner.

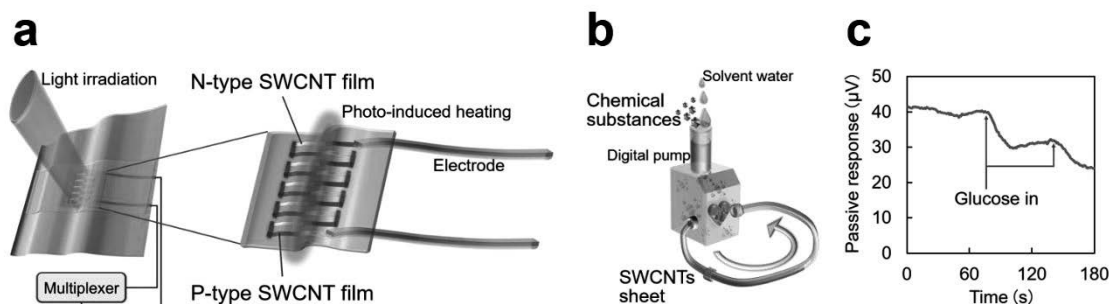


Fig. 1. **a**, Schematic of the proposed device. **b**, Setup of the chemical testing measurement with the proposed device. **c**, Demonstration of the in-liquid glucose detection in a non-sampling, source and label-free manner.

[1] K. Li, et al. *Nat. Commun.*, **12**, 3009 (2021).

[2] Y. Nonoguchi, et al. *Adv. Funct. Mater.*, **26**, 3021–3028 (2016).

Corresponding Author: K. Li

Tel: +81-3-3817-1860

E-mail: lee.k.al@m.titech.ac.jp

Photoluminescence property changes of aryl-modified locally functionalized single-walled carbon nanotubes by *ortho*-substituent effects

○Sadahito Naka¹, Tsuyohiko Fujigaya^{1,2,3}, Tomohiro Shiraki^{1,2}

¹ Graduate School of Engineering, Kyushu University, Fukuoka 819-0395, Japan

² WPI-I2CNER, Kyushu University, Fukuoka 819-0395, Japan

³ Center for Molecular Systems, Kyushu Univ, Fukuoka 819-0395, Japan

Single-walled carbon nanotubes (SWCNTs) with semiconducting features show near infrared photoluminescence (PL), which is applicable to various optical applications including bioimaging probes and telecom devices. In particular, locally functionalized SWCNTs (lf-SWCNTs), which are synthesized by slight amount of chemical modification have been reported to show E_{11}^* PL with red-shifted wavelengths and enhanced quantum yields compared to E_{11} PL of pristine SWCNTs [1,2]. E_{11}^* PL is generated by the formation of luminescent doped sites with narrow band gaps based on sp^3 carbon defect doping to sp^2 carbon network structures of SWCNTs. As a characteristic of lf-SWCNTs, the wavelengths of E_{11}^* PL sensitively change depending on chemical structures of modifier molecules. We have reported that substituted aryl modification for lf-SWCNTs synthesis largely changed PL emission properties. Especially, the lf-SWCNTs synthesized using *ortho*-substituted aryldiazonium salts (*o*ADs) showed remarkably red-shifted PL by ~150 nm than E_{11}^* PL peaks for typical lf-SWCNTs [3]. In this study, we investigate *ortho* substituent effects on the newly observed PL of the aryl-modified lf-SWCNTs based on substituent structure changes.

The synthesized modifiers are *o*AD with different aliphatic substituents (*o*AD-R; R = methyl (Me), ethyl (Et), isopropyl (*i*Pr)). For local chemical functionalization, *o*AD-R was mixed with solubilized SWCNTs in an aqueous micelle solution.

Fig. 1 shows a PL spectrum of SWCNTs reacted with *o*AD-*i*Pr (lf-SWCNTs-*o*iPr). Three PL peaks were observed at 980, 1156, 1306 nm. The emissions at 980 nm and 1156 nm are assigned to E_{11} PL from the pristine sites and E_{11}^* PL from the typical doped sites of lf-SWCNTs. The emission at 1306 nm appeared at a similar wavelength region to PL specifically observed for our previous lf-SWCNTs synthesized by *ortho*-substituted aryl modifications [3]. Interestingly, the wavelength of this peak was red-shifted by changing the substituent structures from Me to *i*Pr. In molecular mechanics simulations, the crystalline lattice structures of SWCNTs tended to be slightly distorted (ca. 0.70 %) due to steric hindrance with the *ortho*-substituents. Therefore, the *ortho*-substituted aryl modification could provide a new tool to modulate the near infrared PL wavelengths of lf-SWCNTs based on strain engineering approaches.

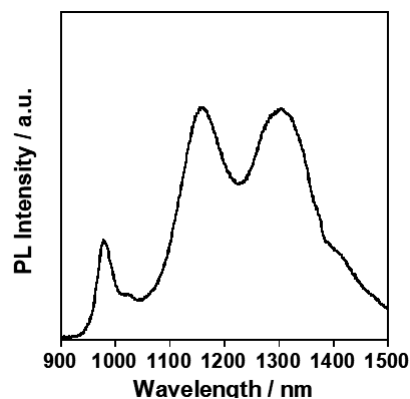


Fig. 1 PL spectrum of lf-SWCNTs-*o*iPr. $\lambda_{\text{ex}} = 570$ nm.

[1] T. Shiraki et al., *Acc. Chem. Res.* **2020**, *53*, 1846. [2] Y. Wang et al., *Nat. Rev. Chem.* **2019**, *3*, 375

[3] T. Shiraki et al., *Chem. Commun.* **2017**, *53*, 12544.

Corresponding Author: T. Shiraki

Tel/Fax: +81-92-802-2841/ +81-92-802-2841

Web: <http://www.chem.kyushu-u.ac.jp/~fifth/jp/>

E-mail: shiraki.tomohiro.992@m.kyushu-u.ac.jp

Pure and Efficient Single-Photon Sources by Shortening and Functionalizing Air-Suspended Carbon Nanotubes

Shuma Oya¹, Rintaro Kawabe¹, Hiroshi Takaki¹, Takayuki Ibi¹, Yutaka Maeda², Kenta Nakagawa^{1,3}, and Hideyuki Maki^{1,4}

¹ Department of Applied Physics and Physico-Informatics, Keio University, Hiyoshi, Yokohama 223-8522, Japan

² Department of Chemistry, Tokyo Gakugei University, Koganei, Tokyo 184-8501, Japan

³ Kanagawa Institute of Industrial Science and Technology (KISTEC), Ebina, Japan

⁴ Center for Spintronics Research Network, Keio University, Yokohama 223-8522, Japan.

Room temperature operating on-chip single photon source (SPS), is a desired nanophotonic device which widens the application of quantum information technologies such as quantum communication. Single-walled carbon nanotube (SWCNT) has been thought to be a good candidate for such devices, for its stable exciton characteristics with telecommunication emission wavelength [1]. In this study, we theoretically propose high-performance SPSs that exhibits both high-purity and high-efficiency single-photon generation by using short and functionalized air-suspended SWCNTs [2].

We investigated the dynamics of excitons, such as exciton diffusion, exciton–exciton annihilation (EEA), and end quenching, on a single, pristine or functionalized, SWCNT by Monte Carlo simulations. As shown in Fig.1, we found out that shortening of SWCNT enhances end quenching, and together with exciton confinement by functionalization, high probability of single excitation emission can be achieved. In addition, we found that high excitation enables high quantum efficiency, without trade-off of single photon purity, under functionalization. Altogether, our simulation pointed out that approximately 100 nm long functionalized SWCNT under high excitation conditions will emit single photon with purity of 99.87% with efficiency of 99.84%. We expect this ideal SPS to enable high rate and long-distance quantum key distributions at room temperature.

This work was partially financially supported by PRESTO and A-STEP from JST and KAKENHI, KISTEC project, Spintronics Research Network of Japan, the Core-to-Core program from JSPS, and NIMS Nanofabrication Platform in Nanotechnology Platform Project by MEXT.

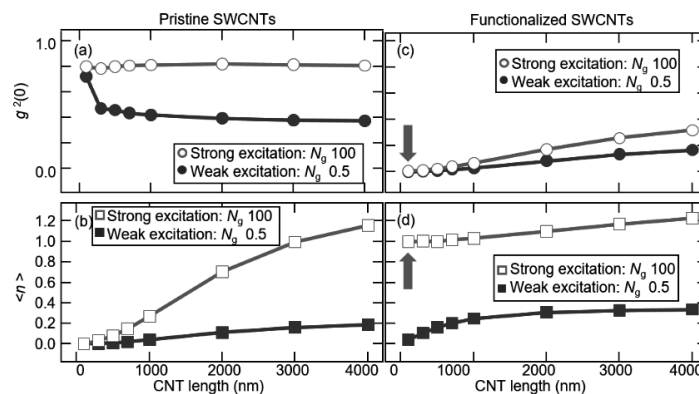


Fig. 1 Simulation results for a single pristine or functionalized SWCNT.

[1] T. Endo, J. I-Hayase, and H. Maki, Appl. Phys. Lett. **106**, 113106 (2015).

[2] R. Kawabe, H. Takaki, T. Ibi, Y. Maeda, K. Nakagawa, and H. Maki, Appl. Nano Mater. **3**, 1, 682 (2020).

Corresponding Author: H. Maki

Tel: +81-045-566-1643, Fax: +81-145-566-1587,

E-mail: maki@appi.keio.ac.jp

In situ XAFS analysis of growth mechanism of single-walled carbon nanotubes from Co-catalyst

Meijo Univ.¹, Meijo Nanomaterial Res. Center²,

[°]Shusaku Karasawa¹, Daiki Yamamoto¹, Kamal P Sharma², Takahiro Saida^{1,2}, Shigeya Naritsuka¹,

Takahiro Maruyama^{1,2}

E-mail: takamaru@meijo-u.ac.jp

Introduction

Single-walled carbon nanotubes (SWCNTs) are expected as next-generation electronic materials. Their electronic states are closely related to the diameter and chirality, therefore, structural control has been an important issue, and it is important to understand the growth mechanism of SWCNTs. However, there are still many unclear points regarding the formation process of SWCNTs from catalyst particles. So far, in situ TEM analyses have been performed to investigate the physical and chemical states of catalyst particles during SWCNT growth [1], but, compared with the conventional growth conditions, they were performed under low pressures and low temperatures. In this study, we performed in situ X-ray absorption fine structure (XAFS) measurement and investigated the chemical state of the Co catalyst during SWCNT growth by conventional CVD.

Experimental Procedure

BN powder and cobalt acetate tetrahydrate were mixed and calcined, and then pellet-molded to prepare a sample for XAFS measurement. Using this sample, we measured Co K edge XAFS spectra during SWCNT growth by alcohol catalytic CVD. The growth temperature and growth time were 800°C and 10 min, respectively. We also investigated the effect of addition of oxygen gas during the increase of sample temperature. The *in situ* XAFS analysis was performed Aichi SR BL5S1 and BL11S2. The grown samples were characterized by Raman, TEM and SEM.

Results and discussion

Fig. 1(a) and 1(b) shows Co K-edge XAFS spectra of the samples during the temperature increase under Ar/H₂ and Ar/O₂ flows, respectively, and Fig. 1(c) and (d) shows Raman spectra of the samples after the XAFS measurements. When oxygen gas was introduced, the absorption edge intensity became stronger, and the reduction of Co particles was suppressed. Raman spectra showed that SWCNT yield was higher and the SWCNT diameter was smaller for the sample heated under Ar/O₂ flow. These results indicate that partially oxidized Co catalysts are suitable to enhance the SWCNT yield.

Acknowledgments

This work was partly supported by the Meijo University Research Branding Project for Cultivation and Invention of New Nanomaterials under the MEXT Private University Research Branding Project. Part of this work was supported by JSPS KAKENHI Grant Number JP19H02563 and the Nanotechnology Platform of MEXT. We thank Prof. Hihara at Nagoya Institute of Technology for performing TEM observation.

References

[1] H. Yoshida et al. Nano Lett. 8 (2008) 2082.

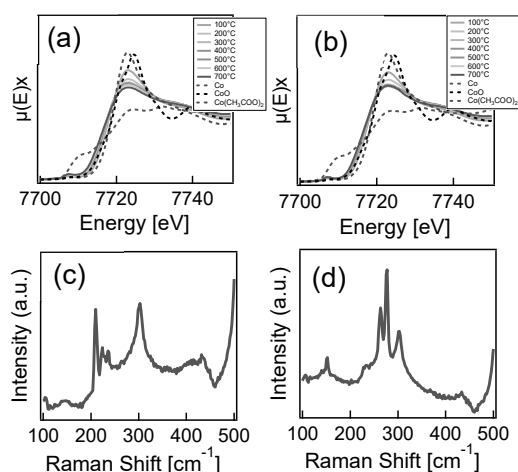


Fig.1 *In situ* XAFS spectra during heating to the growth temperature under (a) Ar/H₂ and (b) Ar/O₂ carrier gases, respectively

Comparison of anisotropic thermal conductivities in bundles of SWCNTs at different temperature regions

○Hiromu Hamasaki¹, Takumi Kawase¹ and Kaori Hirahara²

¹ Dept. of Mechanical Engineering, Osaka University, Osaka 565-0871, Japan

² Dept. of Mechanical Engineering and Center for Atomic and Molecular Technologies, Osaka University, Osaka 565-0871, Japan

For the investigation of the anisotropic thermal conductivity between intra and inter nanotubes, we have focused on the bundles of single-walled carbon nanotubes (SWCNTs) and visualized thermal transport on it by monitoring the evaporation of gold nanoparticles as temperature markers [1]. In order to expand the observable temperature range, the visualization by utilizing solid-liquid phase transition was suggested, instead of the evaporation [2]. Here, we compared the anisotropic thermal conductivities at two different temperature regions by monitoring two types of phase transition of Sn nanoparticles: the phase transition from solid to liquid and liquid to gas.

Figures 1(a) and (c) show transmission electron microscope (TEM) bright and dark field images of the initial state of the bundle, respectively. Fig. 1(b) and (d) show bright and dark field TEM images when particle-A evaporates and melts, respectively. The positions of the evaporated particles whose diameter is 22~25 nm in Fig. 1(b) are indicated as red dots. Corresponding particles in Fig. 1(d) are indicated by red or yellow arrows when the particles are melting or not, respectively. The experimental results indicate that the temperature contours on SWCNTs bundle spread wider along inter-tube direction at higher temperature. The results will be discussed based on the temperature dependence of thermal conductivity along intra and inter nanotube direction.

This work was supported by JST CREST Grant Number JPMJCR17I5, Japan.

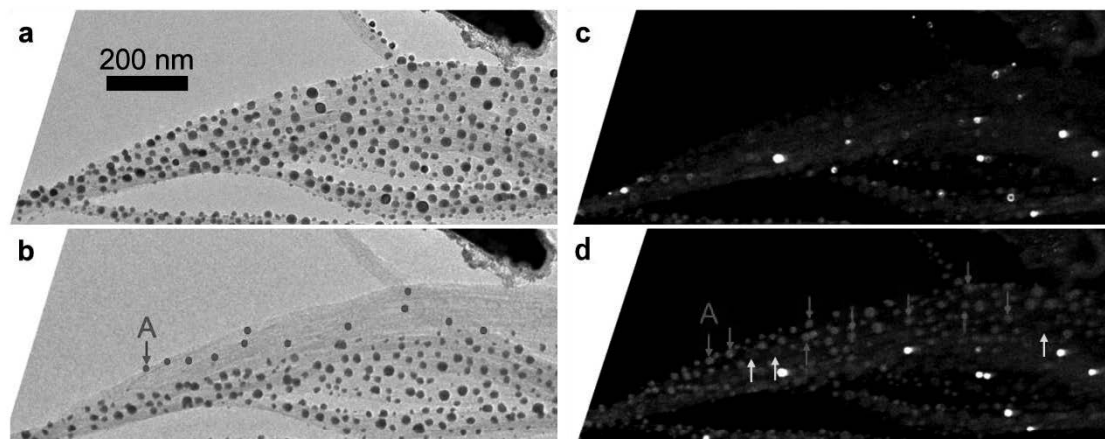


Figure 1 TEM images of a SWCNT bundle decorated by Sn nanoparticles in (a) bright field mode at initial state, (b) bright field mode when particle-A evaporates, (c) dark field mode at initial state and (d) dark field mode when particle-A melts.

[1] H. Hamasaki *et al.* Nano Lett., 2021, 21, 3134-3138.

[2] H. Hamasaki *et al.* the 60th FNTG General Symposium, Mar. 1-3, 2021, online virtual symposium.

Corresponding Author: H. Hamasaki

Tel: +81-6-6879-7307, E-mail: hamasaki@ne.mech.eng.osaka-u.ac.jp

Designing of self-assembled peptides as a molecular scaffold for graphene biosensor

○Shun Shimizu¹, Chishu Honma¹, Yoshiaki Sugizaki²,
Hideyuki Tomizawa, Yuhei Hayamizu¹

¹ Department of Materials Science and Engineering, School of Materials and Chemical Technology, Tokyo Institute of Technology, 2-12-1 Ookayama, Meguro-ku, Tokyo, Japan

² Corporate Research & Development Center, Toshiba Corporation, 1, Komukai-Toshiba-cho, Saiwai-ku, Kawasaki, Japan

Graphene biosensors require to immobilize probe molecules on their surface to achieve a specific binding to target molecules. Pyrene has been widely utilized to immobilize bio-probes on graphene surfaces using their π - π interaction. However, the chemical synthesis of pyrene-conjugated probe molecules may hinder the easy production of a variety of bio-probes. For this sake, self-assembled peptides can be a promising molecular scaffold for immobilizing probe molecules [1]. Recently, our group reported that fibroin-like peptides, which were made by mimicking a silk protein with a stable β -sheet structure, formed a uniform monomolecular thick structure on graphene surface [2]. These peptides have tyrosins at the both ends of the amino-acid sequence as binding sites for graphene surface (YGAGAGAY). In this work, we design a new type of peptides which have the binding site at the side of C-terminal (AGAGAGSYSY) and compare it with the previous peptides in terms of their ability as biomolecular scaffold for biosensing. We expect that the new peptide may have more stability and activity of bio-probes due to their orientation aligned vertically to the graphene surface.

We synthesized two peptides: AGAGAGSYSY and its biotinylated one. The biotin conjugated peptide was used as a bio-probes with peptides to demonstrate the biosensing ability. Aqueous solution of mixture of these peptides was incubated on graphene field effect transistors (GFETs) and was rinsed it by phosphate buffer. Then, electrical measurement of GFETs was performed to detect the binding event of streptavidin at various concentrations. The current between source and drain electrodes was monitored over time during the experiment. As shown in Figure 1, the current decreased as increasing the concentration of streptavidin placed on the GFET. The response fitted well with Langmuir adsorption isotherm and the obtained binding affinity was 40 pM, indicating that the binding event between biotin and streptavidin was successfully monitored by GFET electrically.

This work was supported by the Cabinet Office (CAO), Cross ministerial Strategic Innovation Promotion Program (SIP), “Intelligent Processing Infrastructure of Cyber and Physical Systems” (funding agency: NEDO).

[1] Y. Hayamizu, et al., *Scientific reports*, 2016, 6.1

[2] P. Li, et al., *ACS app. mat. & int.*, 2019, 11.23

Corresponding Author: Y. Hayamizu

Tel: +81-3-5734-3651, Fax: +81-3-5734-2876,

E-mail: shimizu.s.ba@m.titech.ac.jp

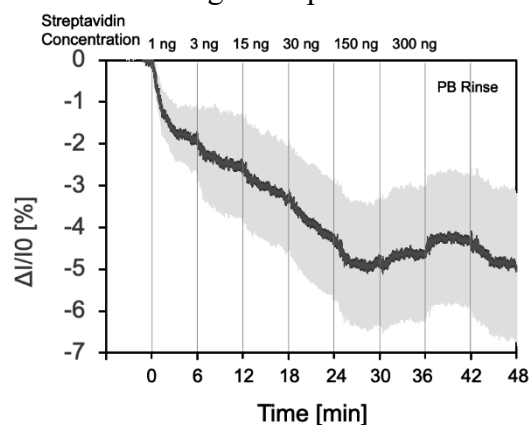


Fig. 1 Current change of GFETs functionalized by peptides over time. 6 FETs were used to determine the error bar (light blue region). The concentration of streptavidin was increased sequentially at every 6 mins and the GFET was rinsed by phosphate buffer after all.

Kelvin probe force microscopy study of MoS₂/MoSe₂ in-plane heterostructures

○Kazuki Hashimoto, Hong En Lim, Yusuke Nakanishi, Takahiko Endo, Yasumitsu Miyata

Department of Physics, Tokyo Metropolitan University, Hachioji, Tokyo 192-0397, Japan

In-plane heterostructures based on transition metal dichalcogenides (TMDCs) have attracted much attention because of their physical properties and future device applications. Recent studies have achieved the continuous epitaxial growth of different TMDC monolayers, resulting in the formation of monolayer nanoribbons and their superlattices with engineered strain [1,2,3]. So far, the local density of states of heterointerface have been mainly studied by scanning tunneling microscopy/spectroscopy [2,3]. However, a facile and quick method is highly desired to characterize the structure and electrical properties of these in-plane heterostructures. In this study, we have studied TMDC-based in-plane heterostructures using Kelvin probe force microscopy (KPFM).

In-plane heterostructure on MoS₂/MoSe₂ was grown using metal organic chemical vapor deposition (MOCVD) system. Topographic and KPFM measurements are acquired simultaneously using Park System NX10 AFM in a non-contact scanning mode. Fig. 1b and c shows topographic and work function images of monolayer MoS₂/MoSe₂/MoS₂/MoSe₂/MoS₂ in-plane heterostructure. The topographic image indicates that the heterostructure has a thickness of 1 nm within the grain. In contrast, a clear contrast can be seen in the work function image between MoS₂ and MoSe₂ (Fig. 1d). In the poster, we will discuss the details of the relationships between local structure and work functions.

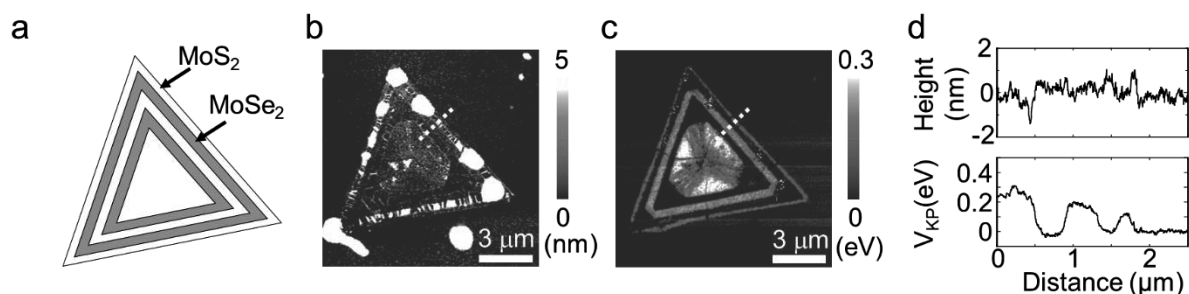


Fig.1 (a) Structure model, (b) topographic and (c) KPFM images of an MoS₂/MoSe₂/MoS₂/MoSe₂/MoS₂ in-plane heterostructure. (d) Height and work function profiles extracted from the white lines marked in b and c.

[1] S. Xie *et al.* Science, **359**, 1131-1136 (2018).

[2] Y. Kobayashi *et al.* ACS Nano, **13**, 7527-7535 (2019)

[3] C. Herbig *et al.* Nano Lett, **21**, 2363-2369 (2021)

Corresponding Author: Y. Miyata

Tel: +81-42-677-2508, Fax: +81-42-677-2483, E-mail : [ymiyata@tmu.ac.jp](mailto:y Miyata@tmu.ac.jp)

Electrolyte-based transition metal dichalcogenide light-emitting devices with microcavity

○Soma Suzuki¹, Tomohiro Ogura¹, Takahiko Endo², Yasumitsu Miyata², Kenichi Yamashita³, Jiang Pu¹, Taishi Takenobu¹

¹Department of Applied Physics, Nagoya University, Nagoya 464-8601, Japan

²Department of Physics, Tokyo Metropolitan University, Tokyo 192-0397, Japan

³Faculty of Electrical Engineering and Electronics, Kyoto Inst. of Tech., Kyoto 606-8585, Japan

Transition metal dichalcogenides (TMDCs) forms stable exciton at room temperature due to its tightly quantum confinement effect, and can provide interesting optoelectronic device functionality combined with microcavity. Specifically, a new quantum bonded state called exciton-polariton, which is strong coupling state of exciton and cavity photon, has been observed at room temperature in TMDCs; so that the ultra-low threshold polariton laser can be expected for future applications [1]. However, previous researches on exciton-polariton of TMDCs have been mostly limited to photoluminescence (PL) measurements [2], and, therefore, the realization of electroluminescence (EL) from microcavity-integrated light-emitting device is remaining challenge toward future device applications, which is hindered by the complicated structures of relevant TMDCs light-emitting devices that are difficult to assemble with microcavities [3]. Here, we proposed a monolayer TMDCs light-emitting device that combines microcavity with simple electrolyte-based light-emitting device structure [4]. We utilize a mixture of insulating polymer and ionic liquid as electrolyte, and it also serves as medium of Fabry-Perot optical cavity using distributed Bragg reflector (DBR). Using this device, we evaluate the cavity mode and exciton-polariton for both PL and EL measurements.

The chemically grown TMDCs monolayer flakes were firstly transferred onto a DBR, and then two gold electrodes were patterned on the surface of TMDCs. Finally, Poly Methyl Methacrylate (PMMA) mixed with an ionic liquid were spin-coated followed by deposition of thin metal film on the PMMA surfaces as a top mirror (Fig. 1). We confirmed that the fabricated device work as a microcavity from the angle-resolved PL spectra, which indicates the cavity mode and exciton-polariton. In addition, when we applied voltages between two electrodes, the ion distributions induce p-n junction inside TMDCs to generate EL. Figure 2 shows optical image of the device and EL image of a WS₂ device, and we clearly observed EL from cavity-integrated device. We will discuss the analysis of the PL and EL characterizations of cavity and exciton-polaritons in these devices.

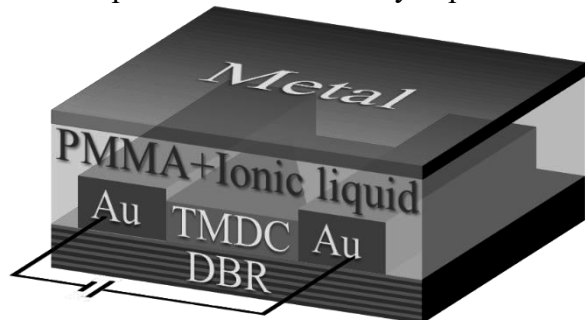


Fig. 1 Electrolyte-based cavity-integrated device

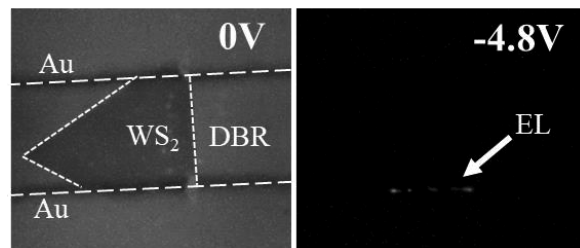


Fig. 2 Optical (left) and EL (right) images

[1] H. Deng et al., PNAS, **100**, 15318 (2003).

[2] N. Lundt et al., Nat. Commun. **7**, 13328 (2016).

[3] F. Withers et al., Nat. Mater., **14**, 301 (2015).

[4] J. Pu et al., Adv. Mater. **29**, 1606918 (2017).

Corresponding Author: T. Takenobu, Tel/Fax: 052-789-5165, E-mail: takenobu@nagoya-u.jp

Stacking angle-dependent intercalation in bilayer graphene

○Yuji Araki¹, Pablo Solís-Fernández², Kenji Kawahara², and Hiroki Ago^{1,2,*}

¹Interdisciplinary Graduate School of Engineering Sciences, Kyushu University, Fukuoka 816-8580, Japan

²Global Innovation Center (GIC), Kyushu University, Fukuoka, 816-8580, Japan

Bilayer graphene (BLG) has unique 2D nanospace which can be utilized to intercalate molecules and ions to alter the electronic properties while maintaining high optical transparency. The intercalation of MoCl₅ molecules significantly reduced the sheet resistance of BLG, and even superconductivity was observed for Ca-intercalated BLG [1,2]. By using large-area BLG grown on a Cu-Ni(111) alloy film, we demonstrated that twisted BLG is more facile to the intercalation as compared with AB-stacked BLG. However, it was not clear how the stacking angle influences the intercalation, because the CVD-grown BLG has various stacking angles [1]. In this work, we fabricated artificially stacked BLG grains with controlled stacking angles and studied the influence of the stacking angle on metal chloride intercalation.

First, large hexagonal graphene grains grown on Cu(111)/sapphire [3] were transferred on another graphene batch on Cu(111)/sapphire while controlling the stacking angle during the transfer process. Then, we transferred this artificially stacked BLG on a SiO₂ substrate. The hexagonal shape of the SLG grains allowed us to define the stacking angle by optical microscope. We sealed this artificial BLG and a mixture of AlCl₃ and CuCl₂ in a glass tube, followed by heating for the intercalation. The ratio of the intercalation was calculated based on the Raman G-band shift [1]. As shown in Figure 1, we discovered a clear correlation between the stacking angle and the intercalation, with intercalation being more efficient for larger stacking angles. In this graph, we also show the full width at half maximum (FWHM) of 2D band of the pristine BLG. The FWHM_{2D} is sensitive to the interlayer coupling in BLG, with large FWHM corresponding to stronger coupling. Therefore, Figure 1 indicates that the interlayer coupling is essential for proceeding the intercalation. Our result deepens the understanding of the intercalation mechanism as well as helping the design of BLG for high ratio of the intercalation, which can be useful for many applications, such as ultralow sheet resistance electrodes and batteries with extraordinarily high capacity.

References: [1] H. Kinoshita *et al.*, *Adv. Mater.*, **29**, 1702141 (2017). [2] S. Ichinokura *et al.*, *ACS Nano*, **10**, 2761 (2016). [3] H. Ago *et al.*, *Appl. Phys. Express*, **6**, 75101 (2013).

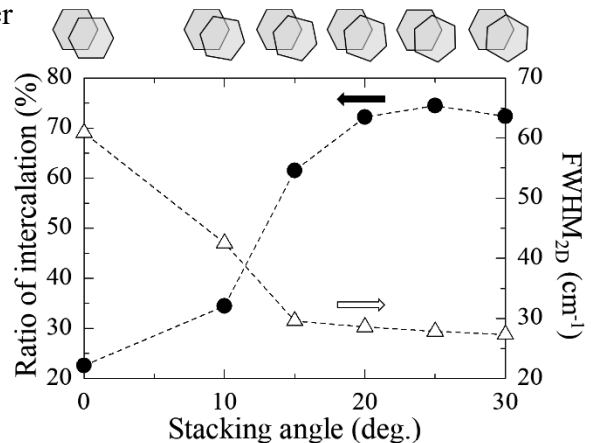


Figure 1. Relationship between the stacking angle and intercalation in BLG. The FWHM of 2D band of the pristine BLG is also plotted.

Organic solar cells with semiconducting carbon nanotubes in the hole transport layer

○Daisuke Miyata¹, Hao-sheng Lin¹, Soma Ishikawa¹, Takeshi Hashimoto², Satoru Hashimoto² Yutaka Matsuo¹

¹ Department of Chemical System Engineering, Nagoya University, Furo-chou, Chikusa-ku, Nagoya 464-8603, Japan

² Meijo Nano Carbon, Nagoya 463-0003, Japan

1. Organic solar cells attention because of their flexibility and the possibility of mass production at lower cost. On the other hand, the conversion efficiency of organic solar cells is lower than that of inorganic cells, which is a major issue that needs to be improved. And to improve power generation efficiency, it is essential to improve the performance of the hole transport layer.

Table 1. Photovoltaic parameters of OSCs

s-CNT(wt%)	0wt%	5wt%	10wt%	15wt%	100wt%
$J_{sc}(\text{mA}/\text{cm}^2)$	6.51	6.26	6.39	6.13	1.97
$V_{oc}(\text{V})$	0.593	0.603	0.594	0.602	0.386
FF	0.585	0.601	0.609	0.607	0.388
$R_s(\Omega)$	99.1	95.3	75.0	97.5	775.3
$R_{sh}(\Omega)$	9983	11190	9923	11703	5597
$\eta(\%)$	2.26	2.29	2.31	2.24	0.29

2. Therefore, in our research, we tried to improve the performance by semiconducting carbon nanotubes to PEDOT:PSS [poly(3,4-ethylenedioxythiophene) poly(styrene sulfonate)], which is mainly used as a hole transport layer.

3. In the experiment, the ratio of s-CNTs (made by Meijo NanoCarbon) aqueous solution to PEDOT:PSS was varied, and the J-V curve, SEM image of the device cross-section, AFM image of the hole transport layer, and Raman spectrum of the hole transport layer surface were measured. mix-PCBM:P3HT (0.95 :1) for the active layer, Ca for the electron transport layer, and Al for the electrode.

4. As shown in the results, the PCE of the reference device was 2.26%, that of the device with 5 wt% s-CNT was 2.29%, and that of the device with 10 wt% s-CNT was 2.31%. The addition of s-CNT decreased the series resistance and slightly increased the PCE efficiency.

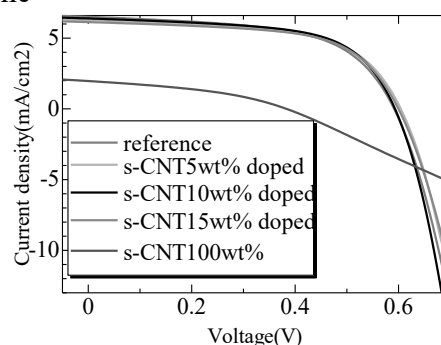


Figure 1 J-V curve of s-CNT doped OSC

Corresponding Author: Y. Matsuo

Tel: +81-52-747-6722

E-mail: yutaka.matsuo@chem.material.nagoya-u.ac.jp

Electrical characterization of carbon-nanotube thin film transistor based on direct deposition method

○Shugo Kogure¹, Ryo Mizuno¹, Hiromichi Kataura², and Yutaka Ohno^{1,3}

¹Department of Electronics, Nagoya University, Nagoya 464-8603, Japan

²Nanomaterials Research Institute, National Institute of Advanced Industrial Science and Technology 305-8565, Japan

³Institute of Material and Systems for Sustainability, Nagoya University, Nagoya 464-8601, Japan

Carbon nanotubes (CNTs) are often bundled in their thin films due to hydrophobic interactions, which degrades the gating action in CNT thin-film transistors (TFTs). In particular, there arises a tradeoff between on-current and on/off ratio of CNT TFTs due to the bundling issue. In this study, we have achieved superior on-current and on/off ratio simultaneously with a CNT thin film deposited by a direct deposition method to previous ones based on the filtration and transfer process. [1]

Bottom-gate CNT TFTs with an Al₂O₃ gate insulator (45nm) were fabricated on a PEN film. Semiconducting CNTs purified by the gel-chromatography was used in this study. A CNT thin film was deposited on the gate insulator layer by immersing the sample in the dispersion of semiconducting CNTs. The Al₂O₃ surface was functionalized with poly-L-lysine (PLL) (Sigma-Aldrich) prior to the CNT deposition. We also fabricated TFTs with CNT thin films formed by previous filtration and transfer process for comparison. [1]

Figure 1 shows AFM images of CNT thin films. The CNTs are more dense and less bundled in the CNT thin film deposited by the direct deposition method, compared to the case of the filtration and transfer process. Figure 2 shows the channel length dependence of on-currents and on/off ratios of the TFTs. Both on-current and on/off ratio were improved by introducing the direct deposition method. In particular, high on-current over 2.5 mA/mm and on/off ratio of 10⁴ were simultaneously obtained at a short channel length of 5 μm. This result is promising for enhancing high-speed operation of CNT TFTs.

[1] J. Hirotsu et al. *Nanoscale Adv.* **1**, 636 (2019).

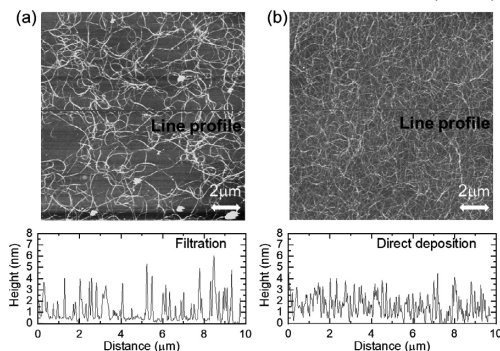


Fig. 1 AFM images. (a) filtration and transfer, (b) direct deposition methods.

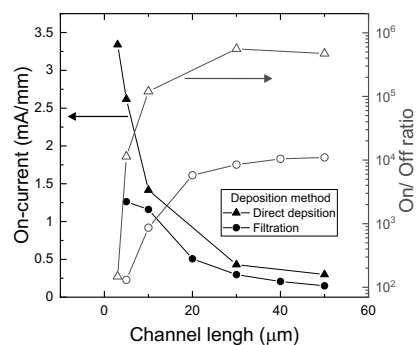


Fig. 2 On-current at V_{DS} and V_{GS} of -5 V and on-off ratio V_{DS} of -2 V versus channel length.

Corresponding Author: Yutaka Ohno, Phone: +81-52-789-5387, E-mail: yohn@nagoya-u.jp

Fabrication of SWCNT-BNNT field-effect transistors and evaluation of contact resistance

Taiki Sugihara¹, Satoru Matsushita¹, Shu Sato¹, Keigo Otsuka¹, Taiki Inoue², Shohei Chiashi¹, Shigeo Maruyama¹

¹ *Department of Mechanical Engineering, The University of Tokyo, Tokyo 113-8656, Japan*

² *Department of Applied Physics, Osaka University, Osaka 565-0871, Japan*

Single-walled carbon nanotube field-effect transistors (SWCNT-FETs) satisfy the demands for miniaturization of FETs. SWCNT-FETs are easily affected by external environments, which causes hysteresis and deterioration of subthreshold swing (SS). High- κ materials[1], for example, can minimize SS values by increasing the gate capacitance, but there remains the trade-off between increased gate leakage and small SS at a reduced insulator thickness. Coaxial wrapping of SWCNTs with boron nitride nanotubes (BNNTs), which has been recently achieved[2], could eliminate interface traps and lead to the simultaneous suppression of the leakage and SS. In this research, we fabricate FETs with single SWCNT-BNNTs as a channel and measure their performance to evaluate the potential of such heterostructures in next-generation electronics.

Air-suspended SWCNT-BNNTs are synthesized on pillar substrates and their synthesis is confirmed by Raman spectroscopy and scanning-electron microscopy. We transfer the SWCNT-BNNTs from the pillar substrates to flat SiO₂ substrates using a polymer stamp. A back-gate FETs are fabricated by depositing Au on SWCNT-BNNTs by electron beam lithography and vacuum evaporation. We investigate the transport properties of these FETs. Although SWCNT FETs usually show p-type properties, some of the FETs with SWCNT-BNNT channels exhibit near-bipolar properties (Fig. 1(a)). We also find that the on-state drain current of each FET varies over several orders of magnitude. By assuming the tunnel resistance of two-dimensional BN flakes with well-defined layer numbers[3], a simple series circuit model yields rather discrete values for the estimated number of BN layers (Fig. 1(b)). Since the BN layer-derived contact resistance is unfavorable in electronic devices, we apply a high bias voltage between the source and drain to selectively induce dielectric breakdown of the BN layers under the metal contact. Figure 1 (c) shows the V_G - I_D characteristics before and after the breakdown, confirming the increased on-current without degrading other characteristics.

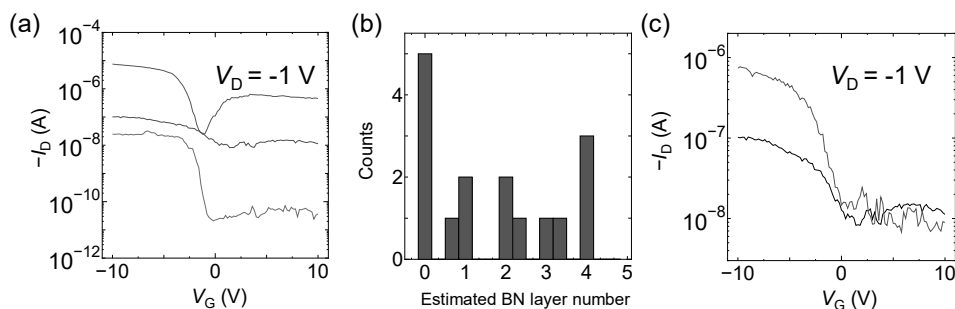


Fig. 1 (a) Typical V_G - I_D characteristic of SWCNT-BNNT FETs. (b) Histogram of estimated BN layer number. (c) V_G - I_D before (black) and after (red) dielectric breakdown of the BN layer.

[1] C. Zhao *et al.*, *Appl. Phys. Lett.* **112**, 053102 (2018). [2] R. Xiang *et al.*, *Science* **367**, 537 (2020).

[3] L. Britnell *et al.*, *Nano Lett.* **12**, 1707 (2012).

Corresponding Author: Shigeo Maruyama, Tel: +81-3-5841-6421, Fax: +81-3-5800-6983,

E-mail: maruyama@photon.t.u-tokyo.ac.jp

Modulating selectivity of 1,3-dipolar cycloaddition by carbon nanotube confinements: A dispersion-corrected density functional theory study

○Shuta Fukuura¹, Takashi Yumura¹

¹*Innovative Materials, Kyoto Institute of Technology, Kyoto 606-8585, Japan*

When molecules inside a carbon nanotube react with each other, the chemical reactions would be influenced by tube confinements. For example, Miners *et al* [1] have experimentally demonstrated that selectivity of 1,3-dipolar cycloaddition reactions inside nanotubes changes depending on the tube diameters. However, how the tube confinement modulates the selectivity has not been elucidated, and thus further computational investigation is required. For this purpose, the current computational study aims to investigate the potential energy surface (PES) of 1,3-dipolar cycloaddition with and without nanotube surroundings. Following ref. [1], we traced 1,3-dipolar cycloaddition between phenylacetylene and phenyl azide (entry 1) or phenylacetylene and benzyl azide (entry 2) inside armchair (*m,m*) nanotubes ($8 \leq m \leq 10$) by obtaining local minima and transition states (TSs) using QM/MM ONIOM methods where dispersion-corrected B97D DFT calculations were used as QM, followed by single-point B97D calculations to evaluate the energy for the optimized geometries. In entry 1 or 2, two N–C bonds are formed between acetylene and azide moieties to yield 1,4- or 1,5-triazole products along 1,4- or 1,5-approach reaction.

DFT calculations found that the degrees of nanotube-confinement-effects in modulating selectivity of the reaction vary between entries 1 and 2. Nanotube confinements have a strong impact on PESs in entry 1 to enhance selectivity of forming the 1,4-triazole product rather than the 1,5-triazole product. In particular, more significant confinement effects to change PES can be found in smaller-diameter tubes, because the 1,4-triazole product is substantially stabilized rather than the 1,5-triazole product, as well as the activation energy to form the 1,5-triazole product is increased. These changes are understood, because two phenyl rings of phenylacetylene and phenyl azide shortly overlap in the TS and product in the 1,5-approach to operate repulsive π – π interactions. On the other hand, PESs in entry 2 with the nanotube environment have remained almost unchanged from those in the gas phase. These differences between entries 1 and 2 come from the presence of a methylene group between phenyl and acetylene moieties.

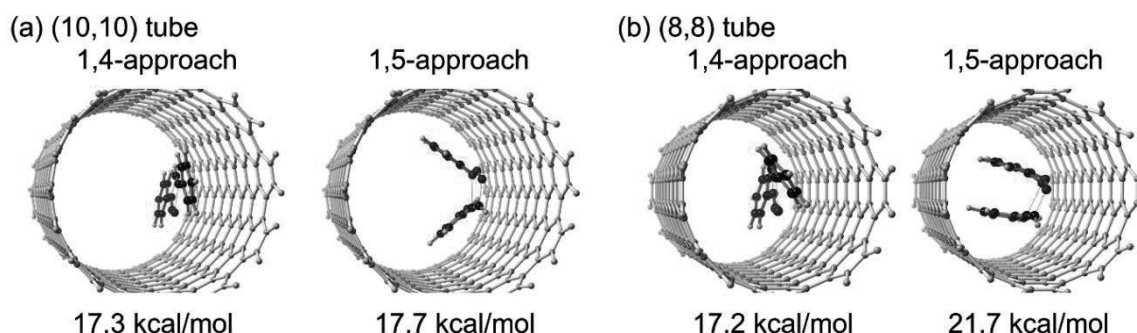


Fig. 1 Optimized structures of transition states in entry 1 inside (a) (10,10) and (b) (8,8) tubes. The energy values are activation energy relative to the reactant complex.

[1] S. A. Miners *et al.* *J. Phys. Chem. C*, **123**, 6294 (2019).

Corresponding Author: S. Fukuura
E-mail: m0671021@edu.kit.ac.jp

Growth of high-density CNT forest by a self-assembled monolayer of iron oxide nanoparticles

○Yuga Kono, Kento Tabata, Takayuki Nakano, Yoku Inoue

Department of Electronics and Materials Science, Shizuoka Univ., Hamamatsu 432-8561, Japan

In the synthesis of carbon nanotube (CNTs) forest, a thin Fe film is generally formed on a substrate for catalyst by sputtering or electron beam deposition. When a thin film of Fe is melted at a high temperature to form nanoparticles, the thickness of the film uniquely determines the size and density of the particles. Therefore, the particles are located at a certain distance, and the maximum density is lower than the closest packing. On the other hand, densely spreading spherical nanoparticles on a substrate allows for hexagonal closest packing. Therefore, if the nanoparticles are formed densely on the substrate, CNTs can be synthesized at a higher density. In the past CNT synthesis using colloidal iron oxide nanoparticles, the CNT forest was not densely packed due to problems such as the inability to uniformly load the particles on the substrate and aggregation when many particles are loaded. In this study, the catalytic particles were anchored to the substrate with self-assembled monolayer (SAM) molecules to increase the loading density of nanoparticles and improve the mass density of the CNT forest.

The catalyst nanoparticles were synthesized using the polyol method. The particle size was controlled by the amount of Fe precursor and the nucleation temperature. The average diameters of the iron oxide nanoparticles prepared were 2.3 nm, 4.8 nm, 7.2 nm, and 11.4 nm. An Al₂O₃ layer was deposited by sputtering on a thermally oxidized Si substrate. Next, the carboxylic acid polymer was dissolved in ethanol with a concentration of 2 mM. The solution was heated to 50 °C, and the substrate was immersed for 24 hours. After that, iron oxide nanoparticles were spin-coated and annealed in air at 375 °C for 1 h. The synthesis of CNTs was carried out by chemical vapor deposition method using C₂H₂ as carbon source, H₂ as reducing agent for catalyst particles, and Ar as carrier gas.

Figure 1 is a scanning electron microscopy (SEM) image of a CNT forest. The high magnification image shows that the CNTs are very dense. Figure 2 shows the relationship between the mass density and length of CNTs. It also plots the mass density vs. length data of high-density CNT forests reported so far. It is found that the density tends to decrease with increasing length. This is due to the deactivation of the catalyst as the synthesis time progresses. In this study, by forming SAMs and fixing iron oxide nanoparticles, very dense forests of up to 211 μm and 101 μg/cm³ were obtained. This density is very high, as high as the upper limit of the density of CNT forests reported so far.

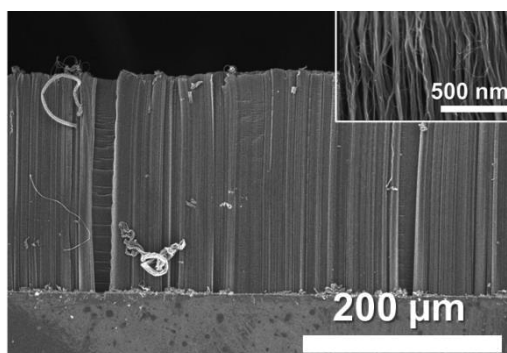


Fig.1 SEM image of CNT forest. Inset shows the magnified image.

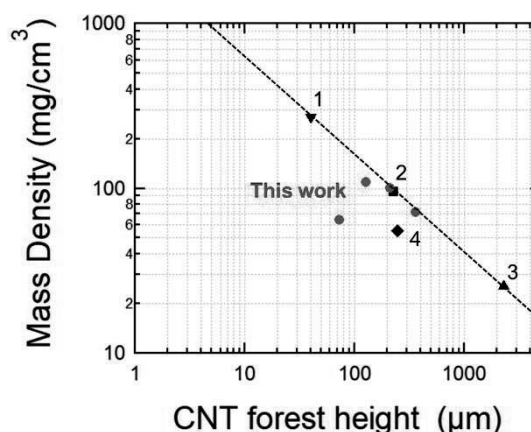


Fig.2 The relationship between mass density and length of our CNT forests are plotted in comparison to the reported high-density CNT forests [1-4].

Corresponding Author: Yoku Inoue
Tel: +81-53-478-1356
E-mail: inoue.yoku@shizuoka.ac.jp
Web: <https://cnt.eng.shizuoka.ac.jp/>

- [1] A. Kawabata, et. al, Appl. Phys. 54, 045101(2015)
- [2] Nicholas T, Dee, et al., Carbon 153, 196-205 (2019)
- [3] H. Inoue, et al., Carbon 158, 662-671 (2020)
- [4] H.Nishino, et al., J. Phys. Chem.111, 17961-17965 (2007)

Chemical vapor deposition growth of carbon layers on boron nitride nanotubes

○Taiki Inoue¹, Masakiyo Kato¹, Yungkai Chou¹, Yoshihiro Kobayashi¹

¹ *Department of Applied Physics, Osaka University, Osaka 565-0871, Japan*

The recent realization of coaxial heteronanotubes consisting of different atomic layers offers novel opportunities to integrate functions into one multi-walled nanotube by controlling nesting order [1,2]. Among candidate nanotubes which can be incorporated into heteronanotubes, carbon nanotubes (CNTs) are known as semiconducting or metallic depending on their chirality, whereas boron nitride nanotubes (BNNTs) are an insulator with a wide bandgap. Although BNNT growth on CNTs was achieved in the previous study [1], CNT growth on BNNTs has not been realized so far, which hinders the formation of complex heteronanotubes with arbitrary nesting order. In this study, we performed carbon layer growth on a BNNT template by chemical vapor deposition toward obtaining coaxial heteronanotubes composed of inner BNNTs and outer CNTs. Commercial few-walled BNNT powders were dispersed in solvent and formed into thin films by vacuum filtration. The BNNT films were loaded in an infrared radiation furnace and used as a template for carbon layer growth. Growth temperature ranged 1150–1350 °C. Ethanol and Ar were used as a carbon source and carrier gas, respectively. The growth conditions were determined by referring to a previous study of overlayer graphene growth on a graphene template [3]. The obtained samples were characterized by Raman spectroscopy, UV-vis-NIR absorption spectroscopy, X-ray photoelectron spectroscopy, and transmission electron microscopy (TEM). The appearance of G-band and D-band in Raman spectra indicates the formation of carbon layers on BNNTs. TEM observation confirmed the preservation of the few-walled structure. Absorption spectra shows an increase of absorbance in a wide wavelength range and a decrease of a BNNT-derived absorption peak around 200 nm after carbon layer growth. This implies the possibility of partial substitution of boron nitride networks with carbon atoms [4], which should be suppressed in a future study.

[1] R. Xiang *et al.* *Science*, **367**, 537 (2020).

[2] Y. Feng *et al.*, *ACS Nano* **15**, 5600 (2021).

[3] R. Negishi *et al.*, *Phys. Status Solidi B*. **257**, 1900437 (2019).

[4] L. Ci *et al.*, *Nat. Mater.* **9**, 430 (2010).

Corresponding Author: T. Inoue

Tel: +81-6-6879-4684,

E-mail: inoue.taiki@ap.eng.osaka-u.ac.jp

Double-walled carbon nanotube transparent conductor overcoming performance–yield tradeoff

○ Jeong-Seok Nam¹, Qiang Zhang², Jiye Han¹, Sukanta Datta², Nan Wei², Er-Xiong Ding², Aqeel Hussain², Saeed Ahmad², Taher Khan², Yong-Ping Liao², Tavakkoli Mohammad², Bo Peng², Shigeo Maruyama³, Hua Jiang², Il Jeon¹, Esko I. Kauppinen²

¹ Department of of Chemical Materials, Pusan national University, Busan 46241, Republic of Korea

² Department of Applied Physics, Aalto University School of Science, FI-00076 Aalto, Finland.

³ Department of Mechanical Engineering, School of Engineering, The University of Tokyo, Tokyo 113-8656, Japan

The floating catalyst chemical vapor deposition (FCCVD) method for producing single-wall carbon nanotubes (SWNTs) has demonstrated great potential in transparent conductive film (TCF) application. In FCCVD, reducing the number of carbon nanotubes (CNTs) is the most well-known method of improving the conductivity of SWNT TCF, achieved by producing thinner and longer CNT bundles.[1] However, this CNT reduction dramatically reduces the yield by orders of magnitude. Here, we report a new FCCVD method of producing highly transparent and conductive TCFs that overcomes the performance-yield tradeoff. In our ferrocene-sulfur-methane system, large-diameter double-walled CNT (DWNT) TCFs were produced with a DC-to-optical conductivity ratio that is on par with the high-performing SWNT TCFs. The optimal FeCp₂ evaporation temperature was determined to be 35°C, which produced DWNT TCFs that exhibited 35 Ω/sq at 90% transmittance and a specific yield of *ca.* 2.6*10⁻³ m²/(h*slm). The device application of DWNT TCFs is tested in perovskite solar cells, which exhibit a power conversion efficiency of 17.4%.

[1] Q. Zhang *et al.* Top. Curr. Chem, 99-128 (2017)

Corresponding Author: I. Jeon

E-mail: il.jeon@spc.oxon.org

Molecular Dynamics Simulation of Single-Walled Carbon Nanotube Growth from Metal Carbide Nanoparticles

○Ikuma Kohata¹, Ryo Yoshikawa¹, Kaoru Hisama², Keigo Ostuka¹, Shohei Chiashi¹ and Shigeo Maruyama¹

¹ *Department of Mechanical Engineering, The University of Tokyo, Tokyo 113-8656, Japan*

² *Department of Physics, University of Tsukuba, Tsukuba 305-8571, Japan*

To achieve the chirality-specific growth of single-walled carbon nanotubes (SWCNTs), it is essential to understand its atomistic growth mechanism. Although it is well-known that catalyst metal nanoparticles play important roles in the growth process, it is still unclear what state and structure of the nanoparticles are optimal for SWCNT growth and how they affect the chirality distribution. Molecular dynamics (MD) simulations are a powerful tool to observe the SWCNT growth from metal nanoparticles, as we have observed the “Octopus growth” and the chirality definable growth [1] by using our original force field [2]. In this study, we employed larger Co catalysts Co₈₀-Co₁₂₀ compared with our previous simulations, Co₆₀ [1,2]. Surprisingly, we observed the formation of two kinds of Co₂C carbide structures and the growth of SWCNTs. Our findings are consistent with recent experimental results with an environmental TEM observation that shows the nucleation of SWCNTs from metal nanoparticles in Co₂C carbide form [3]. We will discuss if the chirality of SWCNT is predefined by the facet geometry of carbide structure.

Figure 1 (a) shows a (11,8) SWCNT growing from Co₁₀₀ catalyst. The structure of the catalyst shows the cubic carbide lattice shown in Fig. 1(c). In contrast, a (14,5) SWCNT grows from the Co₁₀₀ catalyst that has a different catalyst carbide structure with a hexagonal lattice [Fig. 1(b,d)]. The growth from cubic carbide nanoparticles is significantly slower because the carbon chains on the cubic structure entangle each other as shown in Fig. 1(a), resulting in less mobile carbon atoms on the catalyst. On the other hand, the growth from hexagonal nanoparticles is much faster because the straight carbon chains are formed on the catalyst, which can be smoothly converted into SWCNT.

[1] R. Yoshikawa *et al.*, *ACS Nano*, **13**, 6506 (2019).

[2] K. Hisama *et al.*, *J. Phys. Chem. C*, **122**, 9648 (2018).

[3] M. Picher *et al.*, *Nano Lett.*, **14**, 6104 (2014).

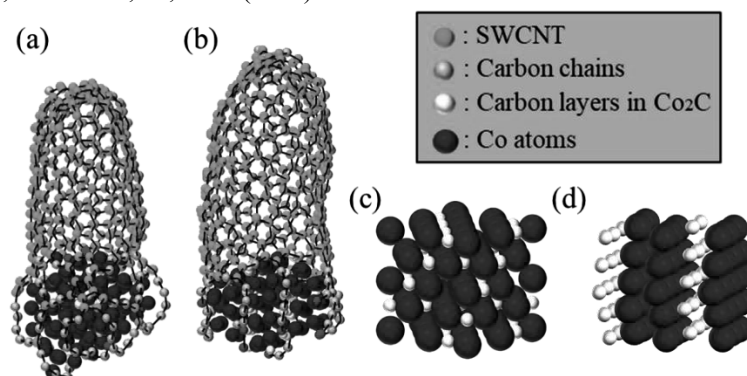


Fig. 1 (a) (11,8) SWCNT growth from hexagonal carbide (b) (14,5) SWCNT growth from cubic carbide (c) Cubic Co₂C structure and (d) Hexagonal Co₂C structure

Corresponding Author: S. Maruyama E-mail: maruyama@photon.t.u-tokyo.ac.jp

Synthesis of g-C₃N₄-[C₆₀] fullerene nanowhisker composites and their photocatalytic activity for degradation of rhodamine B

○Jeong Won Ko¹, Se Hwan Park², Sugyeong Jeon², Weon Bae Ko^{2,3,4}

¹ Department of Animal Life Resources, Chemistry Major, ² Department of Convergence Science, Graduate School, ³ Nanomaterials Research Institute, ⁴ Department of Chemistry, Sahmyook University, 815, Hwarang-ro, Nowon-gu, Seoul 01795, Republic of Korea

Graphitic carbon nitride (g-C₃N₄) was prepared from melamine (C₃H₆N₆) dissolved into distilled water, and the resulting solution was refluxed for 1 h. The precipitate was collected by centrifugation and then dried at 80 °C for 12 h, followed by annealed under an electric furnace at 550 °C for 3 h to obtain solid state g-C₃N₄ [1]. The g-C₃N₄ solution was prepared by dissolving powdered g-C₃N₄ in an aqueous solution with polyvinyl pyrrolidone (PVP). The g-C₃N₄-[C₆₀] fullerene nanowhisker composites were synthesized by the liquid-liquid interfacial precipitation (LLIP) method using the g-C₃N₄ solution, C₆₀-saturated toluene, and isopropyl alcohol [2]. The product of the g-C₃N₄-[C₆₀] fullerene nanowhisker composites were characterized by X-ray diffraction, scanning electron microscopy, Raman spectroscopy, and transmission electron microscopy. The photocatalytic activity of the g-C₃N₄-[C₆₀] fullerene nanowhisker composites assessed through degradation of rhodamine B (RhB) was confirmed by UV-vis spectroscopy.

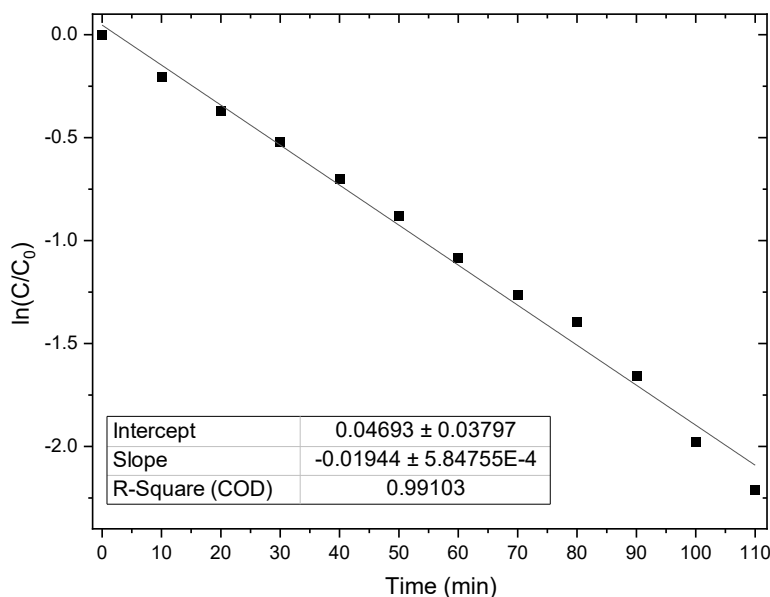


Fig.1 Kinetics study for RhB degradation with g-C₃N₄-[C₆₀] fullerene nanowhisker composites under UV irradiation at 254 nm.

[1] J. Wang, C. Liu, S. Yang, X. Lin, W. Shi, *Journal of Physics and Chemistry of Solids*, **123**, 109164 (2020).

[2] K. Miyazawa, *Journal of Nanoscience and Nanotechnology*, **9**, 41 (2009).

Corresponding Author: W. B. Ko

Tel: +82-2-3399-1700, Fax: +82-2-979-5318,

E-mail: kowb@syu.ac.kr

Synthesis and Characterization of Li-Encapsulated PCBM (Li@PCBM): the First Li@C₆₀ Derivative

○Hiroshi Ueno^{1,2}, Daiki Kitabatake², Hao-Sheng Lin^{3,4}, Yue Ma⁵, Il Jeon⁶,
Fuminori Misaizu^{2,7}, Shigeo Maruyama⁴, Yutaka Matsuo^{3,4,5}

¹ Creative Interdisciplinary Research Division, Frontier Research Institute for Interdisciplinary Sciences (FRIS), Tohoku University, Sendai 980-8578, Japan

² Department of Chemistry, Graduate School of Science, Tohoku University, Sendai 980-8578, Japan

³ Department of Chemical System Engineering, Graduate School of Engineering, Nagoya University

⁴ Department of Mechanical Engineering, School of Engineering, The University of Tokyo

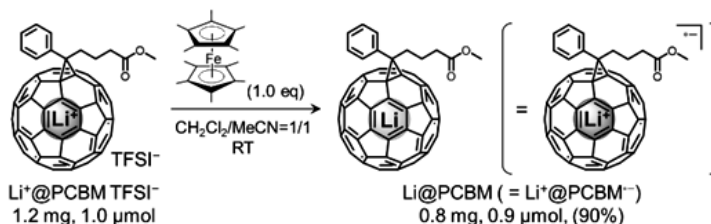
⁵ Hefei National Laboratory for Physical Science at the Microscale, University of Science and Technology of China

⁶ Department of Chemistry Education, Graduate School of Chemical Materials, Institute for Plastic Information and Energy Materials, Sustainable Utilization of Photovoltaic Energy Research Center (ERC) Pusan National University

⁷ New Industry Creation Hatchery Center, Tohoku University

Lithium-encapsulated [60]fullerene (Li@C₆₀) has attracted growing interest owing to its predicted electronic properties arising from the superatomic electronic structure originated in electron transfer from the encapsulated metal to the external carbon cage. Previously we reported chemical synthesis of Li@C₆₀ and its conclusive characterization by X-ray structure analysis, which triggered deeper studies and applications of the C₆₀-based endohedral metallofullerene.^[1,2] However, poor solubility of Li@C₆₀ has been a heavy drawback for its application. Aiming at the application of the material in various research fields, tuning of its properties by chemical functionalization has been strongly awaited.

In this work, we synthesized lithium-encapsulated PCBM (Li@PCBM), the first Li@C₆₀ derivative, by chemical reduction of previously reported cationic Li⁺@PCBM TFSI⁻ (Scheme 1).^[3,4] The structure and its open-shell character was confirmed by spectroscopic analyses and theoretical calculation. Dynamic light scattering measurements revealed that Li@PCBM is highly soluble and can be dispersed as single molecules in common organic solvents such as chlorobenzene in contrast to the poor dispersibility of pristine Li@C₆₀. According to our previously developed superatomic doping concept,^[5] inverted perovskite solar cells were fabricated using Li@PCBM:PCBM as an electron transporting layer. The 1% Li@PCBM:PCBM-used device showed a power conversion efficiency of 9.6% with clearly improved photovoltaic parameters, outperforming the control device (5.7%).



[1] Ueno, H. *et al.*, *Chem. Sci.* **2016**, 7, 5770.

[2] Okada, H. *et al.*, *Carbon* **2019**, 153, 467.

[3] Matsuo, Y. *et al.*, *Org. Lett.* **2012**, 14, 3784.

[4] Ma, Y. *et al.*, *Org. Lett.* **2020**, 22, 7239.

[5] Ueno, H. *et al.*, *Chem. Commun.* **2019**, 55, 11837.

Corresponding Author: H. Ueno, Tel: +81-22-795-7645, E-mail: E-mail: hiroshi.ueno.d5@tohoku.ac.jp

Molecular IR emission of C₆₀ and C₇₀ thin plates

○Tomonari Wakabayashi¹, Kazuki Wakebe¹, Miho Hatanaka², Takeshi Kodama³

¹ Department of Chemistry, Kindai University, Higashi-Osaka 577-8502, Japan

² Department of Chemistry, Keio University, Yokohama 223-8522, Japan

³ Center for Basic Education and Integrated Learning, Kanagawa Institute of Technology, Atsugi 243-0292, Japan

Molecular infrared (IR) emission of fullerene C₆₀ and C₇₀ has been detected in planetary nebulae as evidence for the abundance of these molecules in space [1]. They are thought to be formed in the process of heating and cooling of carbonaceous dust particles in the envelope of the stellar objects. For a quantitative estimate of the abundance of fullerenes in space, physical properties of the molecular IR emission are to be understood in more detail. We planned to observe IR emission spectra of solid C₆₀ and C₇₀ samples at elevated temperatures [2].

Tens of milligrams of fullerene C₆₀ or C₇₀ were pressurized up to 300 kgf/cm² to make a thin plate of thickness less than 0.1 mm. The sample plate was held on a copper slab heated up in a range of 40 - 95°C to observe power profiles of the IR emission from the surface of the sample. The IR radiation was collected by using a gold-coated concave mirror, then conducted to the interferometer in an FTIR spectrometer (Nicolet Magna 750, 0.5 cm⁻¹ resolution) equipped with a DTGS detector. To diminish water vapor absorption lines, the whole system was contained in an acrylic box and purged with dry nitrogen (Iwatani GN-20, 20 L/min).

Figure 1 shows typical IR emission profiles of C₆₀ and C₇₀ thin plates at 80°C. In the upper trace of C₆₀, four signals of the IR-active T_{1u} modes of the icosahedral molecule are clearly seen at 530, 578, 1185, and 1432 cm⁻¹. Besides the four saturating T_{1u}-mode signals, numerous emission lines are discernible between and above the frequencies for the IR-active modes. The weaker signals are mostly ascribed to combinations and overtones of the molecular vibrational modes of C₆₀ [3]. Lower panel shows the emission spectrum of a thin plate of C₇₀. The increased number of strong emission bands proves lower symmetry of the molecule. Temperature dependence of the IR emission intensity will also be discussed.

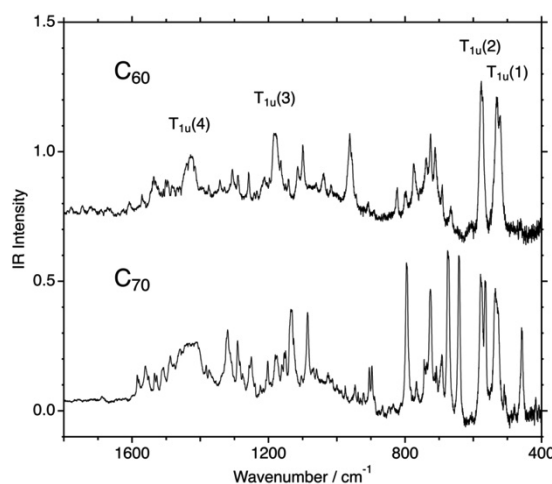


Fig. 1. IR emission spectra of thin plates of C₆₀ and C₇₀ at elevated temperature of 80°C.

[1] J. Cami, J. Bernard-Salas, E. Peebles, and S. E. Malek, *Science* **329**, 1180 (2010).

[2] T. Wakabayashi, Y. Mukai, K. Tanaka, K. Fukumoto, M. Hatanaka, and T. Kodama, *The 60th Anniversary Fullerenes-Nanotubes-Graphene General Symposium*, **2P-12** (2021).

[3] K.-A. Wang, A. M. Rao, P. C. Eklund, M. S. Dresselhaus, and G. Dresselhaus, *Phys. Rev. B* **48**, 11375 (1993).

Corresponding Author: T. Wakabayashi

Tel: +81-6-4307-3408, Fax: +81-6-6723-2721,

E-mail: wakaba@chem.kindai.ac.jp

Spin current generation by edge plasmon in graphene ribbon

○M Shoufie Ukhtary^{1,2}, Yuan Tian², Riichiro Saito²

¹ *Research Center for Physics, Indonesian Institute of Sciences (LIPI), Indonesia*

² *Department of Physics, Tohoku University, Sendai 980-8578, Japan*

Spin current is defined as the difference between charge currents of the spin up and down [1]. The conventional method to generate spin current is by applying voltage on a stack of a ferromagnetic material and normal metal, or by using spin-Hall effect on a two-dimensional (2D) material [1]. However, the magnetic material is needed to generate the spin current and the spin current is tunable only by changing the magnetization, which is not convenient for a nano-scale device. A new optical method for generating the spin current without magnetic material was proposed by Oue and Matsuo, in which they showed that surface plasmon (SP) on a surface of non-magnetic, three-dimensional (3D) metal generates spin current because the rotating electric field of the SP induces spatial dependence of spin accumulation [2]. They found a resonant condition that enhances the generated spin current. However, the spin current flows in the direction perpendicular to the surface and the spins are polarized in the planar direction.

In this work, we discuss the generation of spin current by edge plasmon (EP) on a graphene ribbon. EP is an electromagnetic wave that propagates along the edges of the ribbon and the electric field is localized near the edges. In contrast with the SP on 3D metal, the electric field of EP rotates on the plane of graphene that corresponds to the transverse and out-of-plane optical spin [3]. We found that the spin current J_s flows on the surface of graphene with spin-polarization in the out-of-plane direction as illustrated in Fig. 1 [4]. Further, the spin current induced by EP is tunable not only by the frequency, but also by the Fermi energy of graphene, which enables application for a spin-switching device controlled by light and gate voltage.

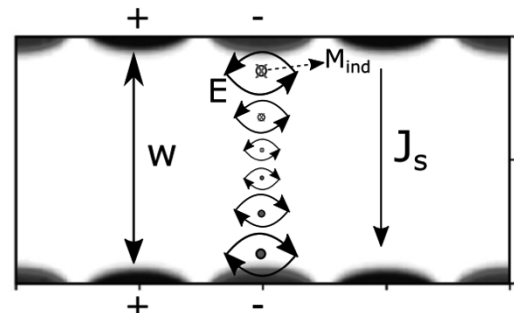


Figure 1 EP (red and blue shows oscillation of induced charges) and the induced magnetization (M). The spin current J_s flows on the surface due to the inhomogeneously distributed M_{ind} , which is induced by the rotating electric field (E) of the EP.

[1] S. Maekawa, et al., Spin Current (Oxford University Press, New York, 2017).

[2] Oue and Matsuo. PRB 101, 161404R (2020)

[3] Bliokh et al. PRL 119, 073901 (2017)

[4] Ukhtary et al. PRB 103, 245428 (2021)

Corresponding Author: M Shoufie Ukhtary

E-mail: shoufiet@flex.phys.tohoku.ac.jp

One-step synthesis of Mo₂C/C composite film on Mo substrate and evaluation of HER catalytic activities

○Shunsuke Numata¹ and Hironori Ogata^{1,2}

¹ *Department of Chemical Science and Technology, Hosei University*

² *Research Center for Micro-Nano Technology, Hosei University*

Electrocatalytic water splitting is one of the suitable methods for hydrogen production. However, this process relies on the electrocatalysis of the hydrogen evolution reaction (HER).

It is well known that Pt-based electrocatalysts show high current density at low overvoltages and are efficient HER electrocatalysts. However, since they are rare and expensive, transition metal carbide (TMC) such as molybdenum carbide has been proposed as an alternative to Pt, and much research has been done so far. It has been reported that the penetration of carbon atoms into the transition metal lattice increases the density of d-band electrons at the Fermi level, leading to Pt-like properties. In addition, it has been reported that HER and conductivity are improved by synthesizing TMC using nanocarbon materials [1].

In this study, Mo₂C/C composite films were fabricated directly on molybdenum substrate by the microwave plasma chemical vapor deposition (MPCVD) method and the HER catalytic activity were investigated. We have investigated the effects surface treatments on the starting molybdenum substrate on the local structure and HER catalytic activity of the Mo₂C/C composite films. We have also investigated the HER catalytic activities of metal carbide / C composite films on other metal substrates.

Detailed experimental results will be reported on the meeting.

[1] Dezhi Wang *et al.*, *ACS Sustainable Chem Eng*, **6**, 13995 (2018).

Corresponding Author: H. Ogata
Tel: +81-42-387-6229, Fax: +81-42-387-6229,
E-mail: hogata@hosei.ac.jp

Schottky barrier height control by reducing Fermi level pinning effect between the single-layer WS₂ and ITO electrodes for high-performance transparent solar cells

○X. He, T. Kaneko, and T. Kato

Graduate School of Engineering, Tohoku University, Sendai 980-8579, Japan

Transition metal dichalcogenides (TMD) is one of the most attractive materials for future transparent and flexible optoelectrical devices due to their atomically thin structure, band gap in visible light range, and high optical transparency. Those merits of TMD have not been applied for transparent and flexible solar cell, which is attracting intense attention as a next-generation energy harvesting technology. Recently, we have developed a new fabrication process of TMD-based solar cell [1]. In our process, Schottky type device configuration is utilized, which can be simply formed by asymmetrically contacting electrodes and TMD (Fig. 1). The power conversion efficiency (PCE) can be reached up to 0.7 %, which is the highest value for solar cell with similar TMD thickness [1].

In order to improve the PCE of transparent Schottky solar cells (TSSC), it is important to understand Schottky junction contacts between ITO and monolayer WS₂. In previous studies, we modified the ITO surface with thin metals (M_x = Ag, Au, Cu, Ni) and directly measured Schottky barrier height (SBH). It was proved that M_x = Cu includes weaker Fermi level pinning (FLP) effect and higher SBH, resulting in better PCE compared with other metals (M_x = Ni, Ag, Au). However, the Fermi level pinning factor (S) of Cu is about 0.25, which means that there still exist inevitable Fermi pinning effect in contact.

Reducing the FLP effect and further increasing SBH is very important for improving the PCE of TSSC. Then, in this study, we attempted to insert an insulating oxide film material WO₃ to reduce the FLP. As a result, the SBH and the PCE of TSSC was found to be greatly improved by inserting WO₃ between Cu and TMD. This finding is important for understanding the contact between TMD and ITO electrodes, and improving the PCE of TSSC.

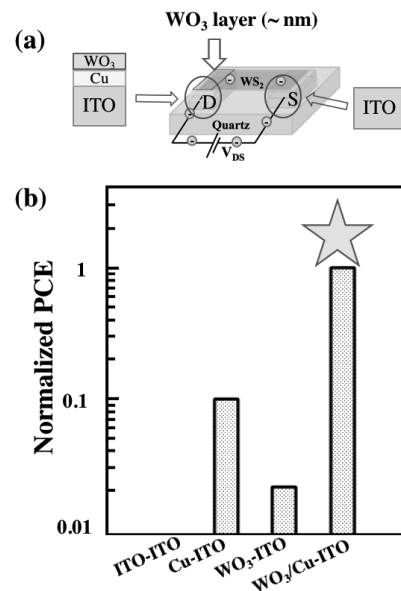


Figure 1: (a) Structure of TMD TSSC, (b) normalized PCE of TMD TSSC with different electrodes.

[1] T. Akama, W. Okita, R. Nagai, C. Li, T. Kaneko, and T. Kato, *Sci. Reports* **7**, 11967 (2017).

Corresponding Author: Toshiaki Kato

Tel: +81-22-795-7046, Fax: +81-22-263-9225, E-mail: kato12@ecei.tohoku.ac.jp

Confinement of Hydrogen Nanobubble between Graphene and Au Surface by Electrocatalytic Hydrogen Evolution Reaction

○Tomohiro Fukushima, Takaha Komai, Ruifeng Zhou, Kei Murakoshi

Department of Chemistry, Faculty of Science, Hokkaido University, Sapporo 060-0810, Japan

The utilization of hydrogen is on demand for the next-generation energy resources, and the control of the proton permeation membrane is required for the stable electrochemical devices. Recently, graphene can be uniquely used as proton permeable membrane.[1] Our theoretical study also supported the proton permeation of the pristine graphene surface through the penetration.[2] However, the experimental study of proton permeation behavior is of still interest. Here we evaluated the proton permeation behavior of graphene from hydrogen nanobubble formation by electrocatalytic hydrogen evolution reaction.

Au (111) surface was prepared through the Cavalier method. Graphene on Au surface (G/Au) was prepared through the chemical vapor deposition. Raman spectroscopy of as-prepared G/Au electrode revealed that high crystallinity of graphene by observation of G band (1580 cm^{-1}) and 2D band (2700 cm^{-1}).

A linear sweep voltammogram (LSV) of G/Au in 0.1 M KOH electrolyte was shown in Figure (a). Cathodic current was observed from -1.3 V , which is due to the hydrogen evolution reaction from G/Au electrode. Noteworthy, a small peak was also observed at -1.13 V , which is absent in neither Au or graphene electrode. Electrochemical Raman spectroscopy showed shift of G band and 2D band, suggesting that G/Au interaction was modulated through the intercalation of atomic species depending on the electrochemical potential. In order to observe the morphology of the G/Au surface, scanning electron microscopy (SEM) images were obtained after the potentiostatic polarization at different electrochemical potential as shown in Figure (b) and (c). After potentiostatic polarization at -1.1 V , a flat G/Au surface was observed. Noteworthy the potentiostatic polarization at -1.2 V induces the hydrogen nanobubble as shown in Figure (c). The control experiment revealed that the peak is due to the proton permeation through the graphene, including proton tunneling process. This study demonstrates the electrochemical hydrogen nanobubble formation enabled by the electrochemical potential modulation.

[1] T. Fukushima, K. Murakoshi, *Current Opinion in Electrochemistry*, **17**, 158 (2019).

[2] T. Fukushima, H. Hasebe, K. Murakoshi, *Chem. Lett.*, in press (2021).

Corresponding Author: T. Fukushima

Tel: +81-11-706-4811, Fax: +81-11-706-4810,

E-mail: tfuku@sci.hokudai.ac.jp

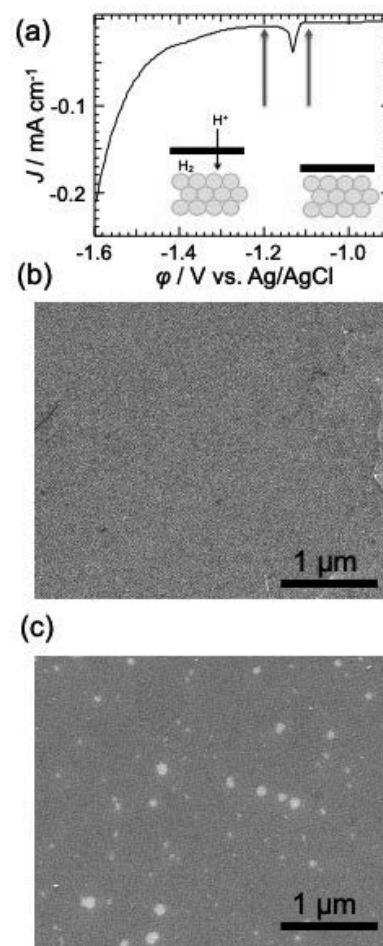


Figure. (a) LSV of G/Au beads electrode in 0.1 M KOH electrolyte (sweep rate = 5 mV/s). SEM image of G/Au surface after potentiostatic polarization at (b) -1.1 V and (c) -1.2 V for 60 sec.

Lateral growth of twisted graphene on graphene/SiC template in a continuous vacuum environment

Yao Yao¹, Taiki Inoue¹, Royta Negishi^{1,2}, Makoto Takamura³, Yoshitaka Taniyasu³ and Yoshihiro Kobayashi¹

¹ Osaka University, Osaka 565-0871, Japan

² Toyo University, Tokyo 112-0001, Japan

³ NTT Basic Research Laboratories, Kanagawa 243-0124, Japan

Twisted few layer graphene (FLG) has recently attracted great attention due to the appearance of the exotic electrical properties [1]. In previous study, we reported that the FLG was synthesized by overlayer growth of graphene on a monolayer graphene template (MLGT) using a chemical vapor deposition (CVD) method. We found that moiré pattern appears in the lattice structure of the grown graphene 2-dimensional (2D) island and the grown 2D graphene islands have the random twisted angles. Coalescence process of graphene island with various twist angles was indicated by temperature and pressure dependence of graphene island size [2]. In this study, based on understanding the growth mechanism of twisted FLG, we further optimized the MLGT. By reducing the nucleation sites on the MLGT, large-area lateral growth of twisted graphene can be realized.

The MLGT used in previous studies were possibly contaminated with adsorbates due to air exposure during the step-by-step processes of MLGT formation and overlayer graphene growth in different vacuum chambers. In order to obtain the cleaner MLGT surface with less nucleation sites, the two processes were continuously performed in an argon atmosphere in an IR heating furnace. Atomic force and scanning tunneling microscope (AFM/STM) are used to evaluate the surface morphology.

The CVD growth mechanism of twisted FLG on MLGT was proposed by the analysis of STM/AFM images (Fig. 1). Moiré pattern in an STM image with different lattice structure indicates the diverse twisted angles and the coalescence growth process. It is typically shown in initial nucleation stage that graphene islands nucleate very closely. Then, graphene islands gradually approach to each other in lateral directions as they grow. Based on the knowledge of CVD growth mechanism, we reduced the nucleation sites during the initial nucleation by cleaner MLGT surface to provide enough space for the further lateral growth (Fig. 2). By comparing Fig. 2a and 2c, the flat surface of MLGT under continuous growth is verified. Fig. 2b and 2d illustrate the twisted FLG grown on MLGT with the same conditions via CVD growth, which shows a significant reduction in nucleation sites and nucleation on step edges. It is further expected to make progress in the large-area lateral growth of twisted graphene.

[1] R. Negishi et al., *Physical Status Solidi B* **257**, 1900437 (2020).

[2] Y. Yao et al., 68th Japan Society of Applied Physics Spring Academic Lecture.

Corresponding Author: Y. Kobayashi

E-mail: kobayashi@ap.eng.osaka-u.ac.jp

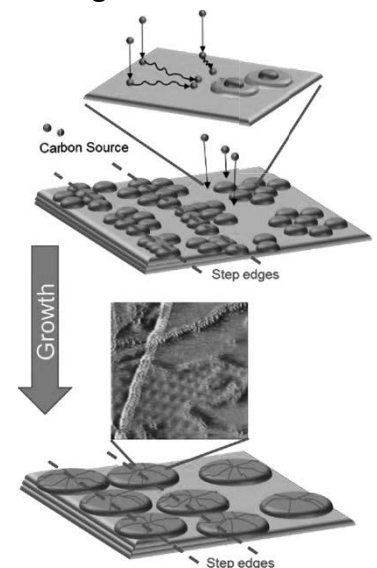


Fig. 1 Initial nucleation stage and later growth stage.

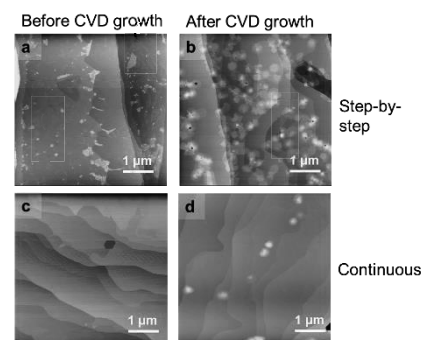


Fig. 2 Optimized results for continuous growth.

Wire-to-Ribbon Conversion in Transition Metal Chalcogenides

○Hong En Lim^{1,*}, Zheng Liu², Jiang Pu³, Hiroshi Shimizu¹, Takahiko Endo¹, Yusuke Nakanishi¹, Taishi Takenobu³, Yasumitsu Miyata^{1,*}

¹ Department of Physics, Tokyo Metropolitan University, Hachioji 192-0397, Japan

² Innovative Functional Materials Research Institute, National Institute of Advanced Industrial Science and Technology (AIST), Nagoya, Aichi 463-8560, Japan

³ Department of Applied Physics, Nagoya University, Chikusa, Nagoya 464-8603, Japan

The unique electronic and magnetic properties predicted in 1D transition metal dichalcogenides (TMDCs) nanoribbons have attracted a rapid growing interest in their fabrication along with the 2D counterpart. [1, 2] Numerous synthetic methods have been developed thus far using chemical vapor deposition, molecular beam epitaxy, and templated growth. [3-6] Nonetheless, it has been challenging to accomplish a controllable growth of their geometry, structure, and orientation. For that, a constant search for an improved fabrication approach with new precursor materials is hence required.

By using tungsten telluride, WTe atomic wires as template precursors, we demonstrate a predefined growth of horizontally or vertically aligned TMDC nanoribbons in this study. The ability to synthesize and control the fine geometrical structure of WTe has not been possible until recently. [7, 8] Using these well-defined nanowires, 1D nanoribbons of WS₂, WSe₂ or WTe₂ were prepared by chalcogenization, in which the WTe was annealed in the respective chalcogen vapors. Horizontally or vertically aligned, layered structures of the nanoribbon fabricated were observed using high-angle annular dark field scanning electron microscopy (HAADF-STEM) and TEM. In addition, randomly organized or unidirectionally oriented network of these ribbons were formed with the different growth substrates used. Polarized Raman measurements revealed a strongly anisotropic optical response. The field effect transistors (FETs) fabricated based on such 1D WSe₂ network showed an ambipolar electronic behavior, implying its potential as 1D channel material for nanoelectronics.

References

- [1] Y. Li *et al.*, J. Am. Chem. Soc. **130**, 16739-16744 (2008).
 [2] P. Cui *et al.*, Nano Lett. **17**, 1097-1101 (2017).
 [3] Z. Wang *et al.*, J. Am. Chem. Soc. **132**, 13840-13847 (2010).
 [4] J.-B. Wu *et al.*, Adv. Opt. Mater. **4**, 756-762 (2016).
 [5] S. Li *et al.*, Nat. Mater. **17**, 535-542 (2018).
 [6] T. Chowdhury *et al.*, Nat. Nanotechnol. **15**, 29-34 (2020).
 [7] M. Nagata *et al.*, Nano Lett. **19**, 4845-4851 (2019).
 [8] H. E. Lim *et al.*, Nano Lett. **21**, 243-249 (2021).

Corresponding Authors:

H.E. Lim, Y. Miyata

Tel: +81-42-677-2508

E-mail: lim@tmu.ac.jp; ymiyata@tmu.ac.jp

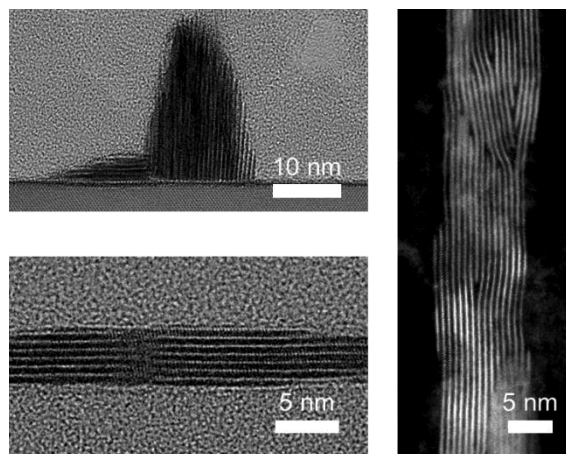


Figure 1 (Left) Cross-section TEM images of the vertically and horizontally aligned WSe₂ nanoribbons. (Right) HAADF-STEM image of a suspended WSe₂ nanoribbon.

Improved synthesis of WS₂ nanotubes with relatively small diameters by tuning sulfurization timing and reaction temperature

○ Md. Ashiqur Rahman^{1,2}, Yohei Yomogida¹, Mai Nagano¹, Ryoga Tanaka¹, Yasumitsu Miyata¹, and Kazuhiro Yanagi¹

¹Department of Physics, Tokyo Metropolitan University, Hachioji, Tokyo 192-0397, Japan.

²Department of Physics, Comilla University, Cumilla-3506, Bangladesh.

Tungsten disulfide (WS₂) nanotubes are cylindrical multiwall nanotubes of WS₂ sheets. As opposed to carbon nanotubes, WS₂ nanotubes possess only semiconducting characteristics regardless of how they are rolled and have advantages for semiconductor applications. WS₂ nanotubes are also scientifically interesting because of their unique properties caused by chiral nanotube structure, such as non-reciprocal conduction [1] and photovoltaic properties [2]. Their properties depend on their diameter and wall number, and thus synthesis of uniform WS₂ nanotubes are great important for correct understanding of their properties. Previously [3], relatively small-diameter WS₂ nanotubes were synthesized using solvothermally synthesized nanowires as precursors. The obtained samples exhibited relatively uniform nanotube structures, but in the samples, there were a lot of degraded nanoparticles and nanoflakes as by-products, which impede understanding of the physical properties of WS₂ nanotubes and their applications. In this study, we removed such by-products by precisely controlling reaction temperature and tuning the sulfurization timing and succeeded to produce the uniform nanotube sample with relatively small diameters.

Tungsten oxide nanowire precursors were synthesized via solvothermal reaction of WCl₆ in ethanol, carried out in a Teflon-lined stainless-steel autoclave at 180°C for 24 h. Then, the obtained nanowires were reacted with sulfur precursor at various temperatures ranging from 750 to 860°C for 1 h in Ar flow by precise control of temperature and adjusting the timing of vaporization of sulfur in the two different synthesis conditions (Method 1 and 2). The annealing time of the nanowire precursors for Method 2 is shorter than that for the Method 1.

Fig. 1 shows a typical TEM image of WS₂ nanotubes synthesized by Method 1. We observed the nanotube and non-nanotube structures (such as particle-like (nanoparticles) and flake-like structures (nanoflakes) simultaneously under all conditions of Method 1. On the other hand, we observed very uniform nanotube samples with well removed nanoflake structures by reducing the annealing time of the nanowire precursors which shows in Fig. 2. Thus, the chalcogenization timing and reaction temperature are considered to be important in the synthesis of inorganic nanotubes.

[1] F. Qin *et al.*, Nat. Commun. 8, 14465 (2017).

[2] Y. J. Zhang *et al.*, Nature 570, 349-353 (2019)

[3] Y. Yomogida *et al.*, Appl. Phys. Express 12, 085001(2019).

Corresponding Author: K. Yanagi, Tel: +81-42-677-2494,

Fax: +81-42-677-2483, E-mail: yanagi-kazuhiro@tmu.ac.jp

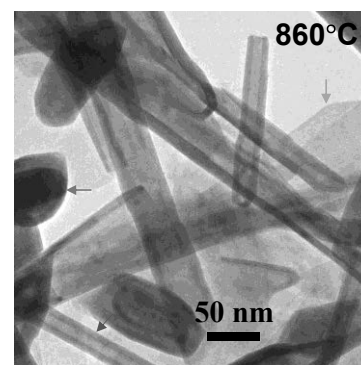


Fig. 1. TEM image of synthesized WS₂ nanotubes by Method 1. The red, blue, and green arrows represent typical samples of nanotubes, nanoparticles and nanoflakes, respectively.

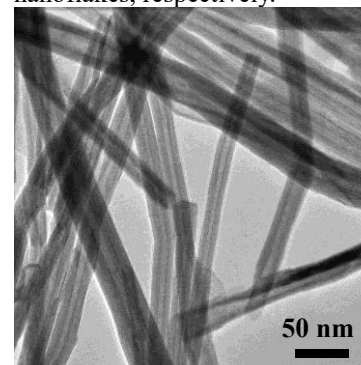


Fig. 2. TEM image of synthesized WS₂ nanotubes by Method 2.

Molecular dynamics study on open-edge growth of boron nitride nanotubes from single-walled carbon nanotube template

○Kaoru Hisama^{1,2}, Ksenia V. Bets³, Nitant Gupta³, Yongjia Zheng¹, Rong Xiang¹,
Keigo Otsuka¹, Shohei Chiashi¹, Boris I. Yakobson³ and Shigeo Maruyama^{1*}

¹ Department of Mechanical Engineering, The University of Tokyo, Tokyo 113-8656, Japan

² Department of Physics, University of Tsukuba, Tsukuba 305-8571, Japan

³ Department of Materials Science & NanoEngineering, Rice University, Houston TX 77005, USA

Recent advances in chemical vapor deposition (CVD) technique for low-dimensional materials have realized syntheses of single-walled carbon nanotube (SWCNT) encapsulated in boron nitride nanotube (BNNT) experimentally [1]. This SWCNT@BNNT keeps the electronic structure of SWCNT near the Fermi level [2] and is expected as a conducting channel with an atomically thin dielectric layer. However, controlling over the quality, or the crystallinity of BNNT coating around SWCNT by CVD remains difficult to achieve, warranting a deeper exploration using molecular dynamics (MD) simulations with empirical potentials to reveal the growth mechanism of BNNT in SWCNT@BNNT.

A system with (6,6) SWCNT is supplied with B_3N_3 molecules, and floating clusters or isolated B and N atoms are systematically removed, emulating conditions inside a CVD reactor. Lennard-Jones interactions are primarily used between BN and C atoms, and it is found that spontaneous BN nucleation is not likely to occur around the SWCNT, at least until 9 ns of simulation at 1900 K [Fig. 1 (a)]. On the other hand, an elongation growth from initial (20,0) BNNT seed is successfully observed [Fig. 1(b)]. This grown BNNT structure with sharp-cut edges is consistent with experimental observation by transmission electron microscope (TEM) [Fig. 1(c)] [3]. Furthermore, the unrolled snapshot of Fig. 1 (b) shows that predominantly the simulated structure is terminated with zigzag edges of B [Fig. 1 (d)], providing insight into the similarly observed experimental preference of the edge shape in BNNT.

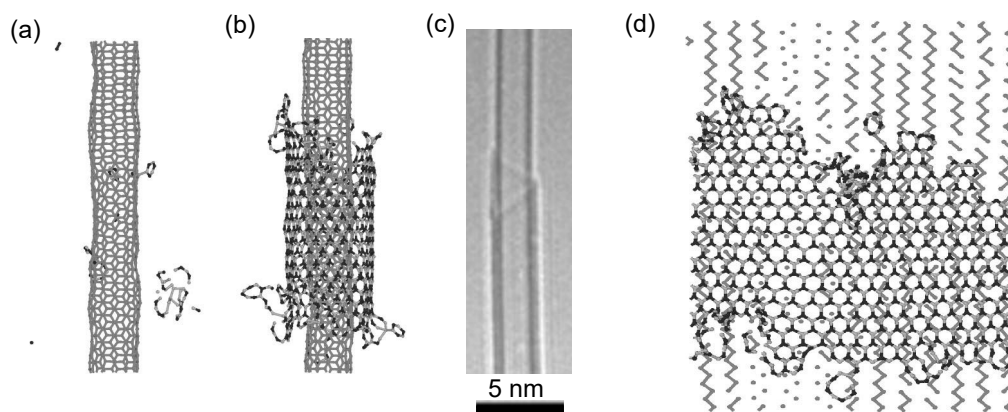


Figure 1 (a) a snapshot of MD simulation with no seed BNNT, after 9 ns at 1900 K. (b) a snapshot with a (20,0) BNNT seed, after 9 ns at 1900 K. (c) Experimental TEM image of SWCNT@BNNT. (d) an unrolled image of Fig. 1 (b). Pink, blue, and green points in snapshots denote B, N and C atoms, respectively.

[1] R. Xiang *et al.*, *Science* **367**, 537 (2020).

[2] K. Hisama *et al.*, *Appl. Phys. Express* **13**, 015004 (2020).

[3] Y. Zheng *et al.*, *Submitted* (2021).

Corresponding Author: Shigeo Maruyama E-mail: maruyama@photon.t.u-tokyo.ac.jp

Avidin-biotin interactions on locally functionalized single-walled carbon nanotubes for photoluminescence wavelength shifts

○Yoshiaki Niidome¹, Rie Wakabayashi¹, Masahiro Goto^{1,2}, Tsuyohiko Fujigaya^{1,3,4}, Tomohiro Shiraki^{1,3}

¹ Department of Applied Chemistry, Kyushu University, Fukuoka 819-0395, Japan

² Center for Future Chemistry, Kyushu University, Fukuoka 819-0395, Japan

³ WPI-ICNER, Kyushu University, Fukuoka 819-0395, Japan

⁴ Center for Molecular Systems, Kyushu University, Fukuoka 819-0395, Japan

Defect doping through local chemical functionalization to single-walled carbon nanotubes (SWCNTs) has produced locally functionalized SWCNTs (lf-SWCNTs) that show enhanced photoluminescence (PL) in near infrared (NIR) regions. [1-3] The doped sites of lf-SWCNTs work as new emissive sites that have narrower bandgaps and trap mobile excitons to be localized states. As a result, lf-SWCNTs emit red-shifted and brighter E_{11}^* PL from localized excitons compared to E_{11} PL of pristine SWCNTs. We have reported small molecule binding at the doped sites of lf-SWCNTs based on supramolecular approaches to selectively shift E_{11}^* PL wavelengths. [3] Recently, microenvironments surrounding lf-SWCNTs have been found as a key factor to modulate E_{11}^* PL properties. [4-6] In particular, larger solvatochromic shifts of E_{11}^* PL occurred than E_{11} PL due to exciton localization effects at the doped sites. [5,6]

Here, we create biomolecule binding systems at the doped sites using avidin-biotin interactions and observe PL wavelength shifts induced by biomolecular interactions. We synthesized biotin-modified lf-SWCNTs (lf-SWCNTs-b) *via* diazonium chemistry. Fig. 1 shows PL spectrum of synthesized lf-SWCNTs-b. Peaks at 980 nm and 1136 nm were observed, which are assigned to E_{11} transition at the pristine sites and E_{11}^* transition at the doped sites for (6,5) lf-SWCNTs-b. Mixing of neutravidin to the lf-SWCNTs-b solution induced red-shifts of E_{11}^* PL by 3 nm. This shift value was larger than that of E_{11}^* PL observed for methoxyaryl-modified lf-SWCNTs that have no biotin units. The result indicates that neutravidin selectively bound on the doped sites of lf-SWCNTs-b and surrounding microenvironments of the doped sites would be changed to affect the localized exciton properties. Thus, protein binding could be useful for exciton PL modulation of lf-SWCNTs and applicable to advanced NIR sensing using the second biological window (1000 – 1350 nm). [7]

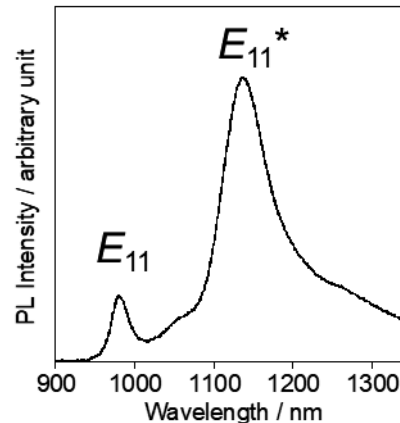


Fig. 1. PL spectrum of lf-SWCNTs-b in a micellar solution of D₂O. $\lambda_{\text{ex}} = 570$ nm.

References

[1] Y. Wang *et al.* *Nat. Rev. Chem.*, **3**, 375 (2019). [2] S. Tretiak *et al.* *Acc. Chem. Res.*, **53**, 1791 (2020). [3] T. Shiraki *et al.* *Acc. Chem. Res.*, **53**, 1846 (2020). [4] S. K. Doorn *et al.* *ACS Nano*, **12**, 8060 (2018). [5] T. Shiraki *et al.* *Chem. Commun.*, **55**, 3662 (2019). [6] T. Shiraki *et al.* *J. Phys. Chem. C*, **125**, 12758 (2021). [7] T. Okazaki *et al.* *Sci. Rep.*, **5**, 840 (2018).

Corresponding Author: T. Shiraki

Tel/Fax: +81-92-802-2841

E-mail: shiraki.tomohiro.992@m.kyushu-u.ac.jp

Circular dichroism spectra of Helicity-sorted Single-wall Carbon Nanotubes with Controlled Chemical Potential

○Yuuya Hosokawa, Yohei Yomogida, Kazuhiro Yanagi

Department of Physics, Tokyo Metropolitan University, Tokyo 192-0397, Japan

Chiral structure of nanotube materials can exhibit very unique physical properties such as bulk photovoltaic, unconventional superconductivity, and so on [1]. Single-wall carbon nanotubes (SWCNTs) exhibit unique chiral structure, and theoretical studies suggest that their chiral structures will induce unique physical phenomena such as photo galvanic effect, gigantic circular dichroism, and so on [2]. However, those phenomena have not been experimentally verified yet. Previously, we clarified that when we prepare randomly oriented SWCNT films we can correctly evaluate circular dichroism (CD) character of the helicity-sorted SWCNT thin films without detecting the false CD signals [3]. Thus, in this study, we investigated the CD spectra of the gated (6,5) SWCNT films to clarify whether we can observe the enhancement of the CD signals by carrier doping.

In this study, we combined electrolyte gating technique and CD measurements. We developed a home-made sample chamber to apply electric field on the sample during CD measurements in a commercial CD spectrometer (JASCO, J-1500). We employed ionic gel for electrolyte and applied gate voltage using side-gating device structure. All the measurements were performed in Ar atmosphere.

Figure 1 and 2 exhibit the change of the CD spectra of (6,5) SWCNTs as the shift of gate voltage in visible and near infrared regions, respectively. Here we only plotted the spectra when hole carriers were injected. As shown here, we observed significant changes in CD spectra as the shift of gate voltages. When the gate was returned to the charge neutral point, the spectrum is well returned to the initial spectrum, and thus the observed changes in CD spectra were returnable and repetitive phenomena. The CD signal caused by E_{11} peak significantly was significantly suppressed by the carrier injection, and we observed the increase of CD signal in some region. The details will be discussed in the poster.

References:

- [1] Qin et al., nature comm. 8, 14465 (2017), Zhang et al., Nature 570, 349 (2019), [2] Ivchenko & Spivak, PRB 66, 155404 (2002), Satco et al., PRB 99, 075403 (2019)
[3] Hosokawa et al, The abstract of the 60th FNTG symposium (2021).

Corresponding Author: K. Yanagi

Tel: +81-42-677-2494 e-mail: yanagi-kazuhiro@tmu.ac.jp

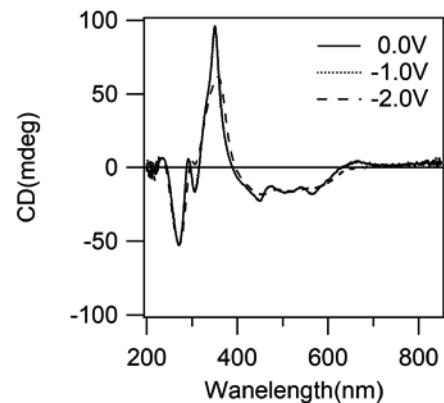


Figure. 1 CD spectra in the visible light region.

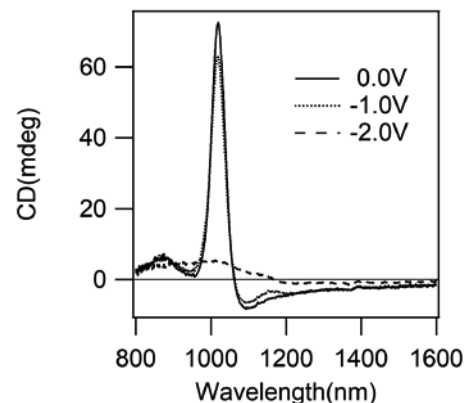


Figure 2 CD spectra in the near infrared region.

Growth mechanism and handedness relation of

1D SWCNT-BNNT van der Waals heterostructures

Yongjia Zheng¹, Akihito Kumamoto², Kaoru Hisama¹, Keigo Otsuka¹, Yuta Sato³, Taiki Inoue^{1,4}, Shohei Chiashi¹, Daiming Tang⁵, Qiang Zhang⁶, Anton Anisimov⁷, Esko I. Kauppinen⁶, Kazu Suenaga⁸, Yuichi Ikuhara², Rong Xiang¹, Shigeo Maruyama¹

¹ Department of Mechanical Engineering, The University of Tokyo, Tokyo 113-8656, Japan

² Institute of Engineering Innovation, The University of Tokyo, Tokyo 113-8656, Japan

³ Nanomaterials Research Institute, AIST, Tsukuba 305-8565, Japan

⁴ Department of Applied Physics, Osaka University, Osaka 565-0871, Japan

⁵ International Center for Materials Nanoarchitectonics (WPI-MANA), NIMS, Namiki 1-1, Tsukuba 3050044, Japan

⁶ Department of Applied Physics, Aalto University School of Science, Tiilenlyöjänkuja 9A SF-01720 Vantaa, Finland

⁷ Canatu Ltd., Helsinki FI - 00390, Finland

⁸ The Institute of Scientific and Industrial Research (ISIR), Osaka University, Osaka 567-0047, Japan

Recently, we presented one-dimensional (1D) van der Waals (vdW) heterostructure that includes single-walled carbon nanotubes (SWCNTs), boron nitride nanotubes (BNNTs) and molybdenum disulfide (MoS₂) [1]. The shell-by-shell growth of this heteronanotube is different from conventional growth of 1D homo-material nanotubes where multiple walls are formed simultaneously from a nanoparticle. Therefore, nucleation and crystal growth behaviors on these highly curved surfaces are of fundamental research interest but is challenging as all processes occur on tiny (only a couple of nm) and highly curved surfaces. Here we would like to reveal the formation process and growth mechanism of outer BNNTs, which can be achieved by directly growing 1D structures on the thermally stable micro-grid so that transmission electron microscopy (TEM) measurement can be performed directly without any treatment. This strategy allows heterostructures to keep in the most intrinsic morphology, and many structure details can be clearly visualized. Furthermore, their handedness relation will also be investigated.

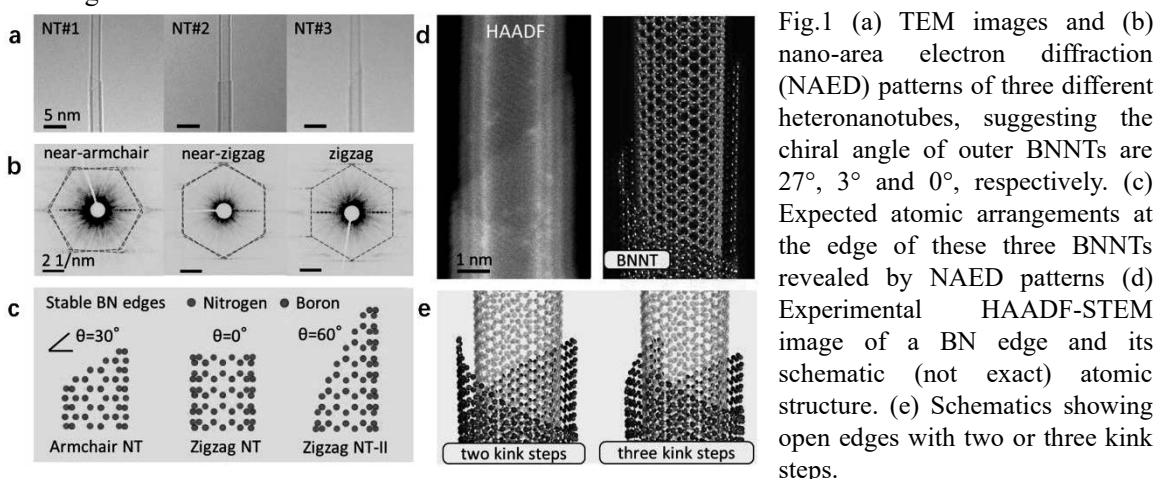


Fig.1 (a) TEM images and (b) nano-area electron diffraction (NAED) patterns of three different heteronanotubes, suggesting the chiral angle of outer BNNTs are 27°, 3° and 0°, respectively. (c) Expected atomic arrangements at the edge of these three BNNTs revealed by NAED patterns (d) Experimental HAADF-STEM image of a BN edge and its schematic (not exact) atomic structure. (e) Schematics showing open edges with two or three kink steps.

[1] R. Xiang *et al.*, *Science*, **367**, 537 (2020).

[2] Y. Zheng *et al.*, *PNAS*, in revision (2021).

Corresponding Author: S. Maruyama

Tel: +81-3-5841-6421,

Fax: +81-3-5841-6983,

E-mail: maruyama@photon.t.u-tokyo.ac.jp

Electrical conductivity and magnetoresistance of SWCNT thin films under ionic-liquid gating

○Hiroki Date¹, Takenori Fujii², Taiki Inoue³, Esko I. Kauppinen⁴,
Shigeo Maruyama¹, and Shohei Chiashi¹

¹ Department of Mechanical Engineering, The University of Tokyo, Tokyo 113-8656, Japan

² Cryogenic Research Center, The University of Tokyo, Tokyo 113-0032, Japan

³ Department of Applied Physics, Osaka University, Osaka 565-0871, Japan

⁴ Department of Applied Physics, Aalto University, Aalto FI-00076, Finland

Macroscale single-walled carbon nanotube (SWCNT) materials such as thin films and yarns are excellent candidates for next generation electronic devices due to their high stability, flexibility, and electrical conductivity. While each individual SWCNTs have a very high electrical conductivity [1], macroscale SWCNT materials which are composed of bundled SWCNTs, have low electrical conductivity [2]. The researches on the electrical properties of macroscale SWCNT materials have been extensively performed so far, but since their properties are influenced by the surrounding environment, the geometric structure of the sample, impurities, etc. [3], the mechanism of electrical conduction and the cause of low electrical conductivity of macroscale SWCNTs are still unknown. In this study, in order to understand the intrinsic electrical properties of SWCNT samples, we fabricated the device based on the electric-double-layer transistor (EDLT) as shown in Fig. 1, and measured the temperature, magnetic field and gate voltage dependences of resistance of SWCNT thin films [4]. The resistance was changed by the gating voltage, and it showed bipolar characteristics (Fig. 2). The resistance decreased with temperature rise at wide temperature range for all gating voltages (Fig. 3). Based on Mott's variable range hopping (VRH) model and fluctuation-induced tunneling (FIT) model, the conduction mechanism of SWCNT thin film will be discussed. The Hall effect was very small except for $V_g=0$ V, which suggests that Hall effect was influenced by the geometry of the sample. The magnetoresistance was negative at 200 K for all gating voltage and magnetic field range (Fig. 4).

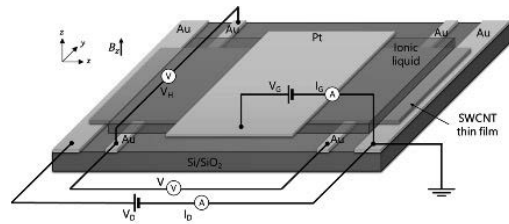


Fig. 1 Schematic image of device.

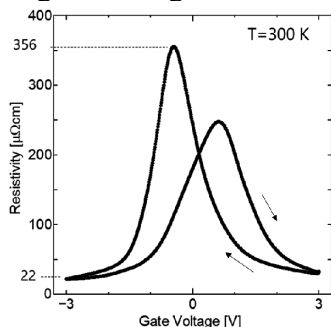


Fig. 2 Gate voltage dependence of resistivity.

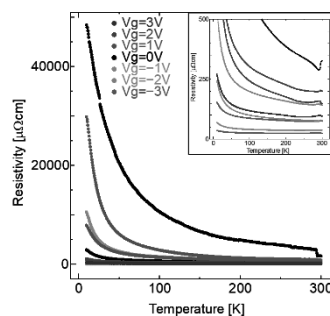


Fig. 3 Temperature dependence of resistivity.

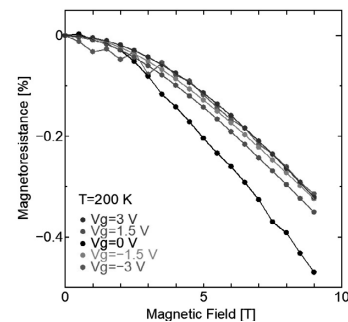


Fig. 4 Magnetic field dependence of magnetoresistance.

[1] T.W. Ebbesen *et al.*, Nature, **382**, 54 (1996). [2] N. Behabtu *et al.*, Science, **339**, 182 (2013).

[3] P.G. Collins *et al.*, Science, **287**, 1801 (2000). [4] A.G. Nasibulin *et al.*, ACS Nano, **5**, 3214 (2011).

Corresponding Author: S. Chiashi

E-mail: chiashi@photon.t.u-tokyo.ac.jp

Optical Spin Hall Effect in Few-Layered NbSe₂: Spin Hall Angle and Temperature Effect

○Ren Habara, Katsunori Wakabayashi

*Department of Nanotechnology for Sustainable Energy, School of Science and Technology,
Kwansei Gakuin University, Sanda Hyogo, Japan*

Transition-metal dichalcogenide (TMDC) is a new class of two-dimensional (2D) electronic system and provides a platform to design functional opt-electronic devices. In TMDCs, electronic properties crucially depend on the combination of metal and chalcogen atoms. Monolayer NbSe₂ is a metallic 2D TMDC material. Figure 1(a) shows the top and side views of the lattice structure of monolayer NbSe₂, which has no spatial inversion symmetry, but respects out-of-plane mirror symmetry. Owing to the lattice structure and the strong atomic spin-orbit coupling (SOC) field, monolayer NbSe₂ possesses Ising-type SOC [1] which acts as an effective Zeeman field, leading to the unconventional topological spin properties.

In this work, we numerically calculate spin-dependent optical conductivity of monolayer NbSe₂ using Kubo formula based on an effective tight-binding model which includes d_{z^2} , $d_{x^2-y^2}$ and d_{xy} orbitals of Nb atoms [1, 2, 3]. Figure 1(b) shows results of spin-dependent optical Hall conductivity σ_{xy}^{spin} (see left figure) and spin Hall angle (SHA) θ^{spin} (see right figure) for several different SOC parameters. These numerical calculations indicate the photo-induced generation of pure spin Hall current in monolayer NbSe₂. The optically induced spin Hall current persists even at room temperature as shown in Fig. 1(c). Also, we discuss layer-number dependence of optical spin Hall conductivity of NbSe₂.

Our results will serve to design opt-spintronics devices such as *spin current harvesting by light irradiation* on the basis of 2D materials.

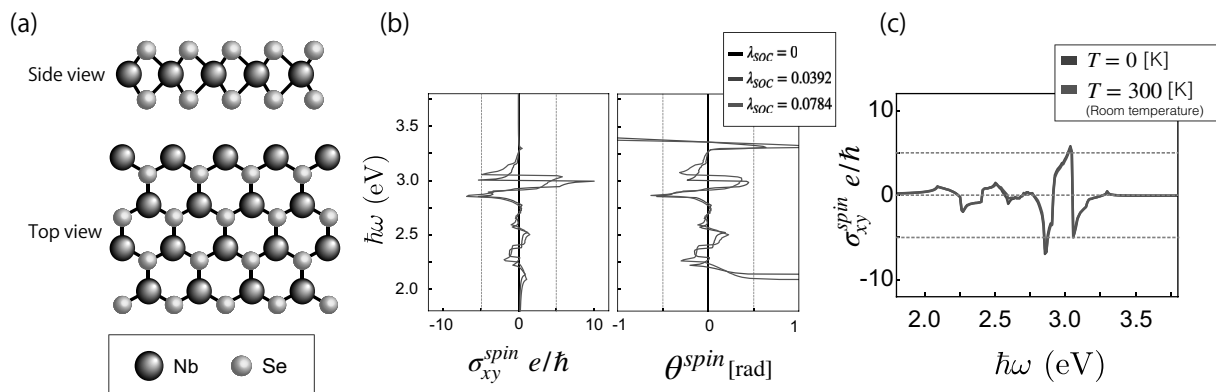


Fig. 1(a) The lattice structure of monolayer NbSe₂. (b) Spin-dependent optical Hall conductivity σ_{xy}^{spin} (left) and spin Hall angle θ^{spin} (right) for several different SOC parameters λ_{SOC} . (c) Temperature dependence of spin-dependent Hall conductivity σ_{xy}^{spin} of monolayer NbSe₂ with SOC parameter $\lambda_{SOC} = 0.0784$ eV.

[1] W.-Y. He, *et.al.*, Commun. Phys. **1**, 40 (2018).

[2] R. Habara, *et.al.*, Phys. Rev. B **103**, L161410 (2021).

[3] G.-B. Liu, *et.al.*, Phys. Rev. B **88**, 085433 (2013).

Corresponding Author: K. Wakabayashi, E-mail: waka@kwansei.ac.jp

Anomalous Photovoltaic Effect in Strained Monolayer WS₂

○Togo Takahashi¹, Jiang Pu¹, Takahiko Endo², Yasumitsu Miyata², Taishi Takenobu¹

¹Department of Applied Physics, Nagoya University, Nagoya, 464-8603, Japan

²Department of Physics, Tokyo Metropolitan University, Tokyo, 192-0397, Japan

The bulk photovoltaic effect (BPVE) has been attracting attention because it does not require p-n junction formation and has a potential to conquer the performance limit of current solar cells [1]. However, this effect originates from the broken spatial inversion symmetry in the crystal and the applicable materials are still limited. For example, although monolayer WS₂ has a non-centrosymmetric crystal structure, the three rotational symmetry in the plane cancels out the electromotive force, and, therefore, one needs the linear polarized light to generate BPVE. Recently, the enhanced BPVE based on WS₂ have been demonstrated using their nanotubes and heterostructures [2,3], concluding that artificial symmetry control is a powerful way to realize BPVE. Here, we focus on the structural deformation by strain as a method to reduce and control the symmetry, and try to clarify the relationship between the symmetry and BPVE in strained monolayer WS₂.

To induce strains, we utilized the difference in the thermal expansion coefficients between the substrate and sample during chemical vapor deposition (CVD) [4]. After CVD synthesis of monolayer WS₂ on SiO₂ substrate, Au / Ni electrodes were deposited as shown in Fig. 1(a), and electromotive force measurements were performed by irradiating a laser with a wavelength of 532 nm. Figure 1(b) shows the current-voltage characteristics with and without light irradiation. Although the device shows high resistance without light irradiation (dashed line), upon light irradiation (solid line), the device shows a spontaneous photocurrent at zero voltage in addition to the slope change (resistance decrease) due to photoexcited carriers. The effect of the Schottky junction between the electrode and WS₂ was removed by irradiating the light on the crystal sufficiently far from the electrode (Fig. 1). Because the CVD-grown WS₂ on SiO₂ substrate naturally implants strains [4], we considered that the observed BPVE is due to strain induced symmetry breaking effect. Therefore, we also investigated the relationship between symmetry control and BPVE in monolayer WS₂ based on the results on SiO₂ substrate, sapphire substrate with local strains, and flexible substrate that can manipulate intentional strains.

[1] Y. Nakamura *et al.*, OYO BUTURI, **90**, 2 (2021)

[2] Y. J. Zhang *et al.*, Nature, **570**, 349 (2019)

[3] T. Akamatsu *et al.*, Science, **372**, 68 (2021)

[4] G. H. Ahn *et al.*, Nat. Commun. **8**, 608 (2017)

Corresponding Author: J. Pu, T. Takenobu

Tel/Fax: +81-52-789-5165

E-mail: jiang.pu@ngoya-u.jp, takenobu@nagoya-u.jp

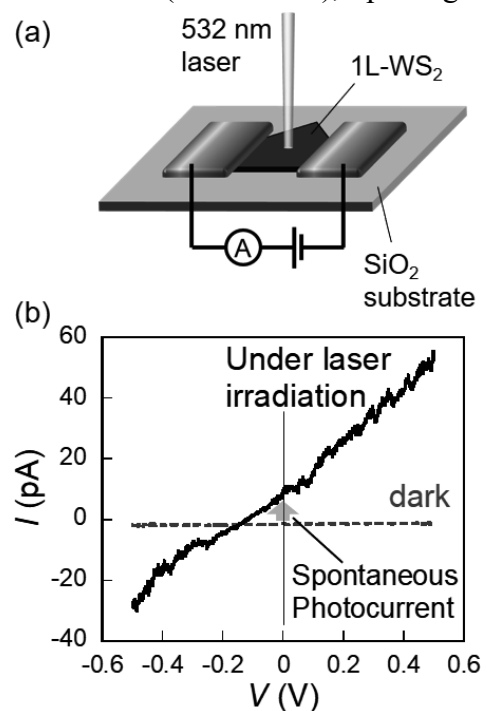


Fig. 1. (a) Device image and measurement method. (b) I - V characteristics with and without light irradiation.

Controlled surface etching of multilayer hBN

Yi Hsin¹, Pablo Solís-Fernández^{1,2}, and Hiroki Ago^{1,2,*}

¹Interdisciplinary Graduate School of Engineering Sciences, Kyushu University, Fukuoka, 816-8680, Japan, ²Global Innovation Center (GIC), Kyushu University, Fukuoka, 816-8680, Japan

Hexagonal boron nitride (hBN) has been in the spotlight, owing to the wide range of applications, such as insulating substrate for 2D materials, tunnel barrier layers, gas barrier films, and ultraviolet/quantum light emitters. Although CVD growth of hBN has been widely studied, there is a limited number of literature reporting etching of hBN. Compared with graphene, etching of hBN is more difficult due to its chemical stability. Spherical nanoparticles of Pt and Ni were reported to etch hBN by moving on its surface, leaving the nanoscale etched trenches [1]. Here, we have studied the hBN etching at lower temperatures with Sn metal and found that Sn forms unique triangular nanoplates and etch only the top layer of multilayer hBN. Moreover, annealing in Ar further etched the hBN layer based on a different mechanism.

Being different from the previous works which used exfoliated hBN, CVD-grown multilayer hBN was employed because it allows large-area investigation. Figure 1(a) shows an AFM image of the multilayer hBN after etching in the presence of Sn vapor at 1000 °C. We observed triangular Sn nanoplates which created nano-trenches in the hBN while moving on its surface. The depth of these nano-trenches was ~0.3 nm, indicating that the etching occurs only at the top layer of the multilayer hBN (Figure 1(b)). We also found that the etching occurs preferentially along the armchair directions of the hBN. According to our knowledge, this is the first time that such triangular nanoplates show the etching of 2D materials. Furthermore, as shown in Figure 1(c), the trenches became wider when annealed in Ar, suggesting that heat treatment induces metal-free etching to form zigzag edges. Our work demonstrates unique etching behaviors of hBN, which provides the surface etching while controlling edge structures that is applicable to 2D nanoelectronics.

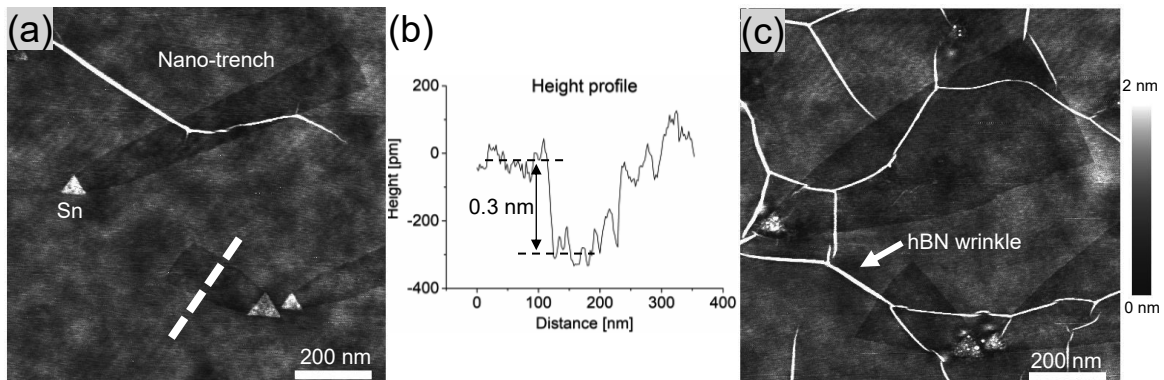


Fig. 1. (a,b) AFM image of multilayer hBN after Sn-assisted etching and height profile of the nano-trench. (c) AFM image of the identical position after Ar annealing.

Reference: [1] H. S. Wang *et al. Nat. Mater.* **20**, 202 (2021).

Nano ~ sub-nanometer-width one-dimensional quantum wells embedded in two-dimensional semiconductors

○Nanami Ichinose¹, Liu Zheng², Takashi Taniguchi³, Kenji Watanabe³, and Ryo Kitaura¹

¹ Department of Chemistry, Nagoya University, Nagoya 464-8602, Japan

² Innovative Functional Materials Research Institute, AIST Nagoya 463-8560, Japan

³ National Institute for Materials Science, Tsukuba 305-0044, Japan

Two-dimensional (2D) heterostructures have attracted plenty of attention. [1] [2] To fully explore the enormous potential of 2D heterostructures, developing a highly controllable fabrication technique is crucial. Although 2D van der Waals stackings have been intensively studied [3] [4], the research on the lateral heterostructures is still limited due to the difficulty in fabrication. In this work, we have focused on heterostructures, in which different 2D materials are laterally integrated side-by-side with a periodicity of down to nanometer scale. These are atomically thin 2D layers with one-dimensional (1D) stripes, namely 1D quantum wells (QWs), that align periodically, providing a novel 1-2D mixed-dimensional platform for exploring crossover from 2D to 1D.

In this study, we focused on heterostructures composed of transition metal dichalcogenide (TMD). Since various TMDs, including metals, semiconductors, superconductors, and topological insulators, are available, it is possible to realize novel 2D heterostructures with various electronic states. The metal-organic chemical vapor deposition (MOCVD) equipment used in this work can rapidly switch the supply of source materials on the order of seconds to realize nanometer-scale 1D QWs. In addition, the MOCVD setup is a cold-wall type, which can prevent metal/chalcogen sources from re-evaporation, ensuring stable source supply throughout a growth process.

In this study, we fabricated 2D lateral heterostructures of WS₂/MoS₂ on hexagonal boron nitride by sequential growth of WS₂ and MoS₂ through rapid switching of supply of W and Mo source. Figure 1 shows a high-resolution High Angle Annular Dark-Field Scanning Transmission Electron Microscopy (HAADF-STEM) image of lateral heterostructures WS₂/MoS₂. In the HAADF-STEM images, W atoms are imaged as bright spots, whereas Mo and S atoms are imaged as much darker spots. As seen, the MOCVD-grown lateral superstructure possesses atomically steep interfaces with a width down to 0.8 nm. This is the narrowest 1D QW of TMDs with atomically sharp edges ever reported. In the presentation, we will give details of the growth process and optical properties of grown heterostructures.

[1] A. K. Geim et al. Nature, 499, 419 (2013).

[2] Y. Kong et al. Nature materials, 13, 1135 (2014).

[3] C. Zhu et al. Nature communication, 11, 772 (2020).

[4] Y. Kobayashi et al. ACS Nano, 13, 7527 (2019).

Corresponding Author: R. Kitaura

Tel: +81-52-789-2482, Fax: +81-52-747-6442

Web: <http://nano.chem.nagoya-u.ac.jp/>

E-mail: r.kitaura@nagoya-u.jp

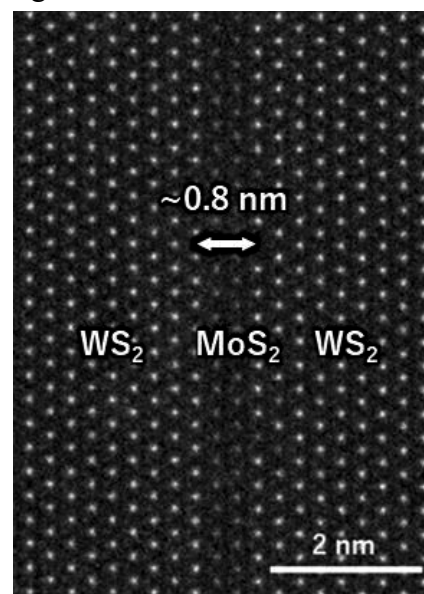


Fig. 1 A High-magnification HAADF-STEM image of a WS₂/MoS₂ hetero structure.

N-type polar transition of p-type MoS₂ by chemical doping

○Hiroto Ogura¹, Yoshiyuki Nonoguchi², Shaochun Zhang³, Yusuke Nakanishi¹,
Hong En Lim¹, Ryo Kitaura³, Kosuke Nagashio⁴, Yasumitsu Miyata¹

¹ Department of Physics, Tokyo Metropolitan University, Hachioji, 192-0397, Japan

² Kyoto Institute of Technology, Kyoto 606-8585, Japan

³ Department of Chemistry, Nagoya University, Nagoya 464-8602, Japan.

⁴ Department of Materials Engineering, The University of Tokyo, Tokyo, 113-8656, Japan

Two-dimensional (2D) transition metal dichalcogenides (TMDCs) have attracted much attention because of their unique physical properties and future device applications. To realize various devices in electronics, it is essential to control the polarity in TMDC devices. For this purpose, surface charge transfer by chemical doping provides a powerful way to control the carrier type of TMDCs [1, 2]. Recently, we have demonstrated the highly efficient and air-stable electron doping of monolayer MoS₂ using a series of potassium salts with crown ethers [3]. In this study, we have applied this technique to achieve the n-type polar transition of p-type TMDCs.

P-type MoS₂ flakes were prepared by the mechanical exfoliation of Nb-doped bulk MoS₂ crystals. Back-gated field-effect transistors (FETs) of the exfoliated flakes were then fabricated onto an SiO₂/Si substrate. Electron doping was conducted by spin coating the butanol solution of KOH/benzo-18-crown-6 on MoS₂ (Fig. 1a). The transfer curve of pristine MoS₂ shows p-type semiconducting behavior (Fig. 1b). After the doping, the polarity of MoS₂ changed from p-type to n-type. Similar tendency was also observed for p-type monolayer MoSe₂. We also demonstrated the spatially controlled n-type doping of partially masked MoS₂. The doped device shows a clear rectifying behavior, suggesting the formation of p-n junction (Fig. 1c). The present results provide an effective way for the control of the polarity in TMDC-based devices, benefiting the development of advanced electronics.

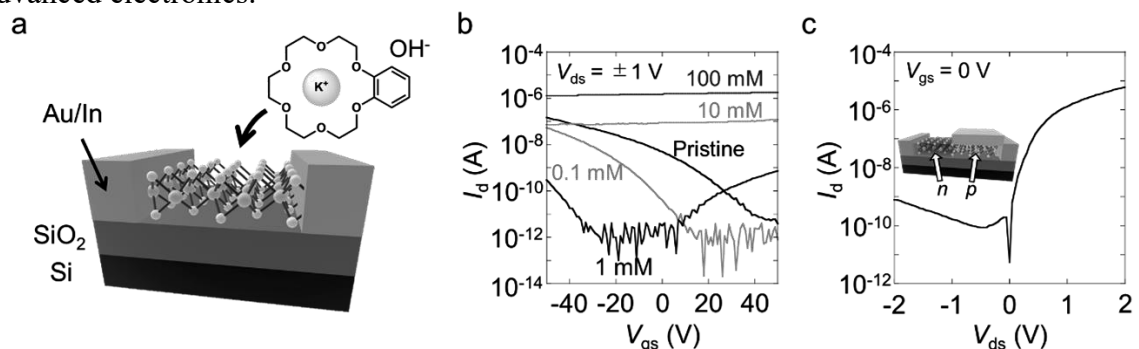


Figure 1 (a) Schematic illustration of the MoS₂ FET and benzo-18-crown-6 with K⁺ ion. (b) Transfer curves of the pristine and doped MoS₂ with different dopant concentrations from 0.1 to 100 mM. (c) *I*-*V* curve of the partially doped MoS₂ with 100 mM dopant solution. The inset is a schematic diagram of a patterned device.

[1] X. Liu *et al.*, *Adv. Mater.*, **28**, 2345-2351 (2016). [2] H. G. Ji *et al.*, *Adv. Mater.*, **31**, 1903613 (2019).

[3] H. Ogura *et al.*, *Nanoscale*, **13**, 8784-8789 (2021).

Corresponding Author: Y. Miyata, Tel: +81-042-677-2508, E-mail: miyata-yasumitsu@tmu.ac.jp

Nonlinear anomalous Hall effect in trigonal superconductor PbTaSe₂

○Yuki Itahashi¹, Toshiya Ideue¹, Shintaro Hoshino²,
Chihiro Goto¹, H. Namiki³, T. Sasagawa³, Yoshihiro Iwasa^{1,4}

¹ *Quantum-Phase Electronics Center (QPEC) and Department of Applied Physics,
The University of Tokyo, Tokyo 113-8656, Japan*

² *Department of Physics, Saitama University, Saitama 338-8570, Japan*

³ *Laboratory for Materials and Structures, Tokyo Institute of Technology, Kanagawa 226-8503, Japan*

⁴ *RIKEN Center for Emergent Matter Science (CEMS), Wako 351-0198, Japan*

Symmetry breaking in solids is one of the central issues of condensed matter physics. To date, a large number of unique physical properties and novel functionalities have been explored in noncentrosymmetric crystals. Among them, nonlinear anomalous Hall effect, which indicates the directional dependent spontaneous Hall effect under time reversal symmetry (Fig. 1 left), is an emerging nonlinear quantum transport [1]. So far, it has been investigated in low-symmetric materials such as WTe₂ and TaIrTe₄ with only one mirror plane and resultant Berry curvature dipole [2-4]. In principle, however, noncentrosymmetric crystals with higher symmetry (trigonal crystals, for example) can also host nonlinear anomalous Hall effect with distinctive origin [5] despite the lack of Berry curvature dipole. Moreover, the search for anomalous Hall effect in exotic quantum phases including superconductivity has been missing and important challenge.

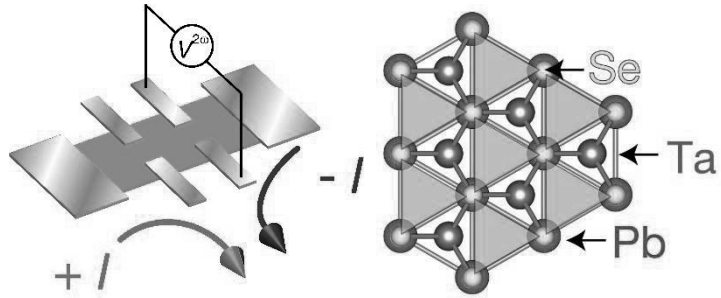


Fig. 1. Schematic image of nonlinear anomalous Hall effect (left) and crystal structure of PbTaSe₂ (right).

In this work, we report nonlinear anomalous Hall effect in noncentrosymmetric trigonal superconductor PbTaSe₂ (Fig. 1 right). We observed nonlinear transport signals, which show the characteristic directional dependence reflecting the trigonal crystal symmetry in both normal and superconducting states. Importantly, nonlinear signals are largely enhanced in superconducting fluctuation region. The present result offers a new aspect of nonlinear transport and superconducting properties.

[1] I. Sodemann and L. Fu, *Phys. Rev. Lett.* **115**, 216806 (2015).

[2] Q. Ma *et al.*, *Nature* **565**, 337–342 (2019).

[3] K. Kang *et al.*, *Nat. Mater.* **18**, 324–328 (2019).

[4] D. Kumar *et al.*, *Nat. Nanotechnol.* **16**, 421–425 (2021).

[5] H. Isobe *et al.*, *Sci. Adv.* **6**, eaay2497 (2020).

Corresponding Author: Y. Iwasa

Tel: +81-3-5841-6822

E-mail: ideue@ap.t.u-tokyo.ac.jp

If the format of this page is broken, Select Printing Layout in “Display” tab.

Thermal properties of MWNT coatings for solar collector

○Hiroshi Furuta^{1,2}, Shimon Honda¹, Md. Saiful Islam¹, and Akimitsu Hatta^{1,2}

¹ School of Systems Engineering, Kochi University of Technology, Kochi 782-8502, Japan

² Center for Nanotechnology, Research Institute, Kochi University of Technology, Kochi 782-8502, Japan

Low cost and high-efficient thermal absorber are expected to be applied in the solar collector [1] or water desalination systems especially in the field of hard-to-reach area, mountain villages in Japan and the developing countries. Black carbon nanotube materials of high-IR absorbance are candidates to compose the thermal absorption coatings in the solar collector systems [2], and the nano-fluids in the solar collector carrier liquids [1].

In this presentation, we report the halogen lamp heating properties of carbon nanotube film coatings on the IR-transparent thermal CVD SiO₂ substrates (th-SiO). The substrate size is 3cm square. Figure 1(a) #1-#3 shows the temperature profiles of MWNTs (Meijo nanocarbon, MW-I) coated th-SiO substrates by the halogen lamp heating at the 20V-3.7A(74W) for the repeated measurements [1]. It is confirmed the baking at 300 °C for 30min in the air of MW-I coated samples increased the lamp heating temperature ratio and radiation ratio after lamp heating, which indicates the increase of emissivity of the CNT coating films after the baking process.

Figure 1(b) shows commercially available solar paint (Okitsumo GSP-1), being utilized in solar water heating panels, painted in this experiment on th-SiO profiles. The maximum temperature increased with the increase of the thickness of the coating films. It was found MWNT films have the potential to be high-efficient heat absorption films for the solar collector. In the presentations, we will discuss the analysis of the lamp heating properties and structures in detail for the MWNT films.

The part of this work was supported by JSPS KAKENHI Grant Numbers 17K06205.

[1] C. Chen, Y. Kuang, L. Hu, *Joule* 3 (3) (2019) 683–718.

[2] K. Nomura, Y. Sawada, H. Nishimori, A. Hatta, H. Furuta, 16p-Z30-3, the 68th JSAP spring meeting (Mar 16-19, 2021, online)

Corresponding Author: H. Furuta

Tel: +81-887-57-2211,

E-mail: furuta.hiroshi@kochi-tech.ac.jp

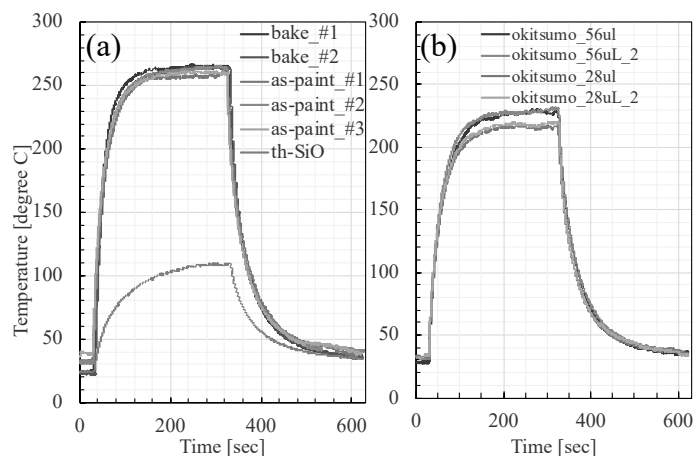


Fig. 1. Temperature profiles of (a) MWNT (Meijo Nanocarbon, MW-I) coating films before #1-3 and after baking bake-#1, 2, and (b) Okitsumo black paint coated th-SiO substrates. The profile of th-SiO substrate is inserted for comparison.

Electrical and mechanical property of homogeneous CNT/Cu composite wire made from copper nanoparticles decorated spin capable CNT forest

○Kosuke Tanaka, Takayuki Nakano, Yoku Inoue

Department of Electronics and Materials Science, Shizuoka University, Hamamatsu 432-8561, Japan

CNT yarns are expected to replace the widely used metallic wires as the lightweight wires of the future. Although CNT yarn have a high mechanical property, their electrical property is much lower than that of metallic wires. Therefore, mixing CNTs with copper is an effective way to solve this problem [1,2]. To maximize the synergy effect, the homogeneous composition of CNT and copper is required. In this study, we fabricated homogeneous CNT/Cu composite wires with various CNT diameters and investigated the mixing effects in electrical and mechanical properties.

Two types of CNTs with diameters of 10 nm and 40 nm were synthesized using CVD. Then, Cu nanoparticles were wholly deposited on CNTs by decomposing Cu precursor at high temperatures. A CNT web was then drawn out from a CNT forest to prepare a CNT yarn. CNTs are decorated with Cu nanoparticles, and therefore, Cu nanoparticles were incorporated inside the yarn. Then, the CNT yarn was dipped in a copper sulfate aqueous solution and subjected to electroplating treatment to fabricate a CNT/Cu composite wire. The composite wire was finally reduced with hydrogen.

Figure 1 shows the relationship between current-carrying capacity (ampacity) and the volume fraction of CNT. The ampacity of the homogeneous CNT/Cu composite wire exceeded that of the Cu wire. Since CNTs have a large contact area with the Cu matrix, joule heating at the Cu is effectively dissipated, lowering the Cu's temperature even under high current and suppressing the electrical current breakdown. Figure 2 shows the stress-strain curves of the composite wires. We found that the homogeneous composite wire has higher tensile strength and Young's modulus than Cu and CNT yarn. This result is attributed to the mixing effect of Cu and CNT.

[1] R. Sundaram *et al.*, *Jpn. J. Appl. Phys.* **57**, 04FP08 (2018), [2] B Han *et al.*, *Carbon*, **123**, 593-604 (2017)

Corresponding Author: Yoku Inoue

Tel: +81-53-478-1356, Web: <http://cnt.eng.shizuoka.ac.jp/>, E-mail: inoue.yoku@shizuoka.ac.jp

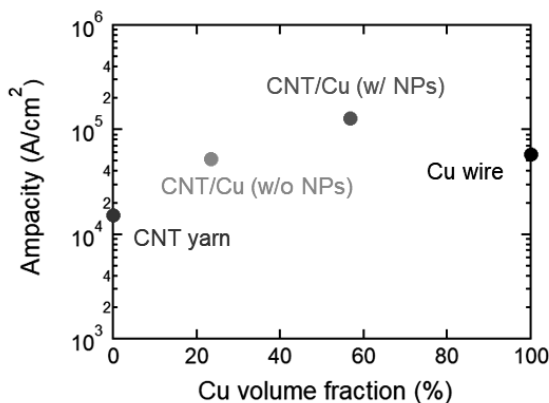


Fig.1 Ampacity of CNT yarn, Cu wire, and CNT/Cu yarns (w/ and w/o NPs)

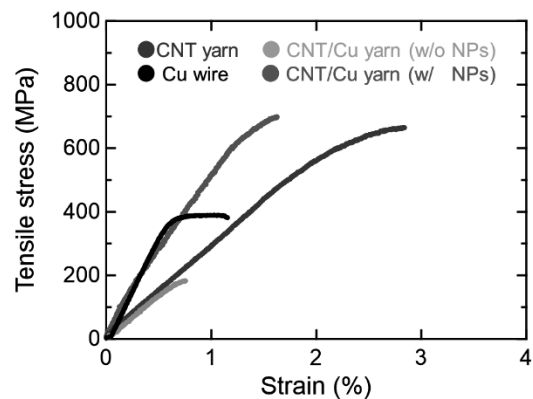


Fig.2 Stress-strain curves of CNT yarn, Cu wire, and CNT/Cu yarns (w/ and w/o NPs)

Spectroscopic ellipsometry on single-chirality-enriched carbon nanotube membranes

○Hengkai Wu¹, Taishi Nishihara¹, Akira Takakura¹, Kazunari Matsuda¹, Takeshi Tanaka²,
Hiromichi Kataura², Yuhei Miyauchi^{1*}

¹ *Institute of Advanced Energy, Kyoto University, Uji, Kyoto 611-0011, Japan*

² *Nanomaterials Research Institute, AIST, Tsukuba, Ibaraki 305-8565, Japan*

Single-walled carbon nanotubes (SWCNTs) have been expected to be future functional materials for various applications because of their distinct physical properties. As their electrical [1], optical [2,3], and mechanical [4] properties strongly depend on their chiral structures, the development of macroscale SWCNT-based devices demands SWCNTs enriched with a single chiral structure and fundamental knowledge on their macroscopic assemblies. Toward the usage of them as opto-thermo functional materials [5,6], recently, we have reported optical spectra of single-chirality-enriched SWCNT membranes fabricated via filtration methods [7]. In these membranes, the orientations of SWCNTs were nearly parallel to the membrane surface (random in-plane orientation), and rarely oriented perpendicular to the surface. Although such orientation of SWCNTs in the membrane implies that their optical response depends on the angle of light propagation to the surface, incident angle dependence of the optical response of single-chirality-enriched SWCNT membranes remains to be addressed experimentally.

In this work, we report the spectroscopic ellipsometry of single-chirality-enriched SWCNT membranes. SWCNT membranes enriched with (6,5) chirality were fabricated on the sapphire substrate via the filtration of nanotube solution prepared by separation method using gel chromatography [8]. The thicknesses of the membranes were determined as a few tens of nanometers using a stylus profilometer. We measured the normal-incident transmittance and angle dependent reflectance spectra (15–70°) around the first subband (S_{11}) exciton resonance using a Fourier-transform infrared spectrometer and a home-made ellipsometer with an InGaAs detector. In the incident angle range of 15–50°, the reflectance peak arising from the S_{11} exciton was insensitive to the incident angle and the polarization, which cannot be explained assuming isotropic refractive index of the media. The incident angle dependence of p -polarized light deviated from the simulations assuming isotropic refractive index, which indicates that the refractive index depends on the incident angle, i.e., the index is anisotropic. In the presentation, we will discuss the refractive index ellipsoid of single-chirality-enriched SWCNT membranes.

[1] R. Saito, M. Fujita, G. Dresselhaus, M. S. Dresselhaus, *Appl. Phys. Lett.*, **60**, 2204 (1992).

[2] H. Kataura *et al.*, *Synth. Met.*, **103**, 2555 (1999).

[3] R. Saito, G. Dresselhaus, M. S. Dresselhaus, *Phys. Rev. B*, **61**, 2981 (2000).

[4] A. Takakura, T. Nishihara, Y. Miyauchi *et al.*, *Nat. Commun.*, **10**, 3040 (2019).

[5] T. Nishihara, A. Takakura, Y. Miyauchi, K. Itami, *Nat. Commun.*, **9**, 3144 (2018).

[6] S. Konabe, T. Nishihara, Y. Miyauchi, *Opt. Lett.*, **46**, 3021 (2021).

[7] T. Nishihara *et al.*, The 59th FNTG general symposium.

[8] Y. Yomogida, T. Tanaka, H. Kataura *et al.*, *Nat. Commun.*, **7**, 12056 (2016).

Corresponding Author: Y. Miyauchi

Tel: +81-774-38-3463

E-mail: miyauchi@iae.kyoto-u.ac.jp

Comparison between high harmonic generation in metallic single-walled carbon nanotubes and graphene

○Hiroyuki Nishidome¹, Kohei Nagai², Kento Uchida², Kenji Kawahara³, Junko Eda¹,
Hitomi Okubo¹, Yohei Yomogida¹, Hiroki Ago^{3,4}, Koichiro Tanaka^{2,5}, Kazuhiro Yanagi¹

¹ Department of Physics, Tokyo Metropolitan University, Tokyo 192-0397, Japan

² Department of Physics, Kyoto University, Kyoto 606-8502, Japan

³ Global Innovation Center (GIC), Kyushu University, Fukuoka 816-8580, Japan

⁴ IGSES, Kyushu University, Fukuoka 816-8580, Japan

⁵ Institute for Integrated Cell-Material Sciences, Kyoto University, Kyoto 606-8501, Japan

The recent development of the intense mid-infrared laser source enables us to investigate high-harmonic generation (HHG) in solid, which is a nonlinear optical but non-perturbative phenomenon [1]. The following two mechanisms are suggested for HHG in solid: the intraband current and the interband polarization due to carriers driven by the laser field. In particular, the intraband current strongly depends on the anharmonicity of the band dispersion, and thus materials with highly anharmonic dispersion like a Dirac point, such as graphene and metallic single-walled carbon nanotubes (m-SWCNTs), are expected to generate unique high harmonics. Theoretically, HHG intensity in graphene would increase by tuning Fermi-level [2], and thus it is important to investigate the Fermi-level dependence of HHG in these materials for understanding the mechanism of HHG. We have studied the relationship between the electronic structure, Fermi level, and HHG in semiconducting single-walled carbon nanotubes [3]. Based on this, in this study, we investigated HHG for m-SWCNTs and graphene with controlled Fermi-level and compared their behaviors.

For the measurements, we used aligned films of m-SWCNTs and mono-layer graphene synthesized by chemical vapor deposition. These were made into electrolyte-gate devices to control Fermi level through the application of gate voltage V_G . These samples were irradiated with a 0.26 eV mid-infrared pulse laser to investigate the relationship between HHG and carrier injection. Figure 1 shows HHG intensity and source-drain current as a function of V_G in (a) m-SWCNTs and (b) graphene. Figure 1(a) shows carrier injection would significantly suppress the 5th harmonics and slightly decrease the 3rd in m-SWCNTs. On the other hand, as shown in Fig. 1(b), HHG in graphene does not change at all. We will discuss the background of these behaviors, including the results of theoretical calculations.

[1] S. Ghimire *et al.* Nat. Phys., 15, 10 (2019).
[2] J. D. Cox *et al.* Nat. Commun., 8, 14380 (2017)
[3] Nishidome *et al.*, Nano Lett 20, 6215 (2020)
Corresponding Author: K. Yanagi,
Tel: +81-42-677-2494, Fax: +81-42-677-2483,
E-mail: yanagi-kazuhiro@tmu.ac.jp

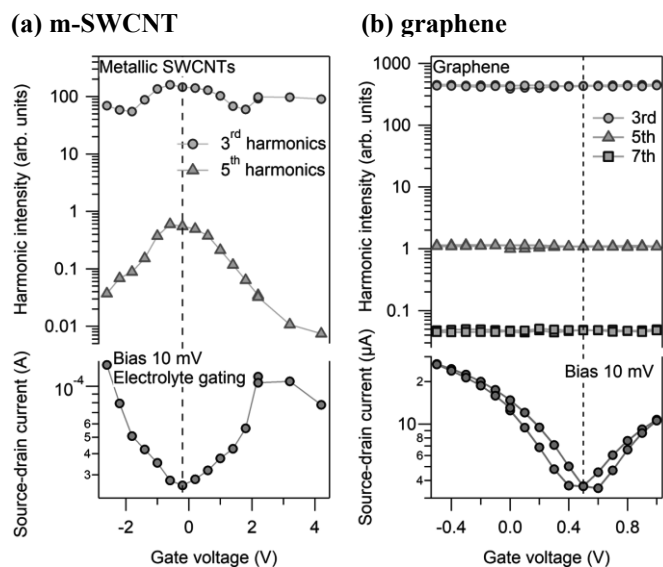


Fig.1 HHG intensity (top) and source-drain current(bottom) as a function of gate voltage

Near infrared photoluminescence from locally functionalized single-walled carbon nanotubes synthesized using bisaryl modifiers with short linkage structures

○ Tomohiro Shiraki^{1,2}, Haruka Aoki¹, Tsuyohiko Fujigaya^{1,2,3}

¹ Department of Applied Chemistry, Kyushu University, Fukuoka 819-0395, Japan

² WPI-I2CNER, Kyushu University, Fukuoka 819-0395, Japan

³ CMS, Kyushu University, Fukuoka 819-0395, Japan

Local chemical functionalization of single-walled carbon nanotubes (SWCNTs) has been developed to enhance their photoluminescence (PL) appearing in the near infrared (NIR) region.[1-4] This functionalization dopes local defects such as sp^3 carbons to the semiconducting crystalline sp^2 carbon networks of SWCNTs for the creation of locally functionalized SWCNTs (lf-SWCNTs). Accordingly, emissive doped sites that have narrower band gaps and exciton trapping features are formed in lf-SWCNTs and E_{11}^* PL appears with red-shifted wavelengths and increased PL quantum yields compared to original E_{11} PL of pristine SWCNTs. To date, diazonium chemistry using aryldiazonium salts have allowed us to modify various molecules on the doped sites, by which wavelength modulation in the NIR regions has been achieved based on the chemical structure variation of the functionalized molecules.[1,2,4] In particular, bisaryldiazonium salts, which have two reactive aryldiazonium groups linked with a spacer moiety, have been designed for proximal defect doping and found to produce E_{11}^{2*} PL over 1250 nm regions for the lf-SWCNTs.

In this study, we newly design bisaryldiazonium salts with a short linkage structure of a naphthalene unit (NbAD) instead of previously used methylene chain linkers. NbAD was synthesized using diodonaphthalene through Suzuki-Miyaura coupling followed by diazotization. The local chemical functionalization was conducted by mixing solubilized SWCNTs (CoMoCAT, (6,5) enriched) in an aqueous micelle solution and NbAD. Fig. 1 shows PL spectrum of SWCNTs reacted with NbAD. A distinct PL peak appeared at 1142 nm, which was red-shifted compared to E_{11} PL (986 nm) of pristine (6,5) SWCNTs and was recognized as E_{11}^* PL generated by the functionalization. Interestingly, the wavelength of PL originating from the NbAD functionalization appeared in shorter wavelength regions than E_{11}^{2*} PL observed for previous bisary-functionalized lf-SWCNTs.[1,2] The result indicates that the positions of the proximal sp^3 carbon defects would be varied depending on the linker structure differences and significantly change PL wavelengths of lf-SWCNTs.

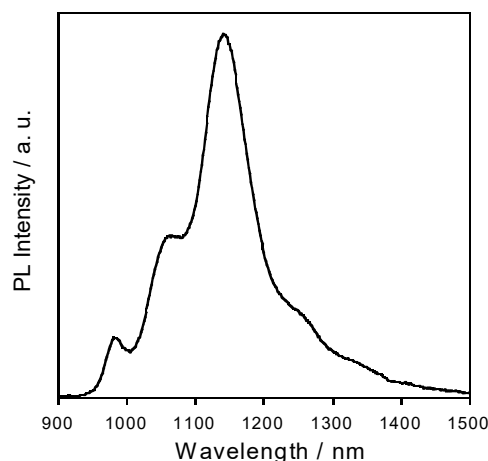


Fig. 1 PL spectrum of SWCNTs reacted with NbAD, $\lambda_{\text{ex}} = 570$ nm.

[1] T. Shiraki, Chem. Lett., **50**, 394 (2021).

[2] T. Shiraki *et al.*, Acc. Chem. Res., **53**, 1846 (2020).

[3] S. Tretiak *et al.*, Acc. Chem. Res., **53**, 1791 (2020).

[4] Y. Wang *et al.*, Nat. Rev. Chem., **3**, 375 (2019).

Corresponding Author: T. Shiraki

Tel/Fax: +81-92-802-2841,

E-mail: shiraki.tomohiro.992@m.kyushu-u.ac.jp

Growth of single-walled carbon nanotubes from Ir catalyst on alumina buffer layer prepared by dip-coating process

○Shu Kondo¹, Daiki Yamamoto¹, Kamal P Sharma², Takahiro Saida^{1,2}, Shigeya Naritsuka³, Takahiro Maruyama^{1,2}

¹ Department of Applied Chemistry, Meijo University, Nagoya 468-8502, Japan

² Meijo Nanomaterial Research Center, Nagoya 468-8502, Japan

³ Department of Materials Science and Engineering, Meijo University, Nagoya 468-8502, Japan

1. Introduction

Our group has succeeded in growing vertically aligned small-diameter single-walled carbon nanotubes (SWCNTs) on a SiO₂/Si substrate [1] and Al₂O₃/SUS foils [2] by the alcohol-catalytic CVD (ACCVD) method using an Ir catalyst. However, the formation of Al₂O₃ layers by the sputtering deposition is not suitable for mass production because it uses a vacuum system. Here, we have attempted to grow SWCNTs using an Al₂O₃ buffer layer which were prepared by the dip-coating technique using an Al chloride.

2. Experimental Procedure

To form alumina buffer layers, the SUS 304 foils were immersed in a 0.2 M aluminum chloride-containing ethanol solution, withdrew at a rate of 1 mm/sec, and then heated at 200 °C for 15 min in air. After repeating this dip-coating process 1 - 4 times, the foils were annealed at 300 °C for 1 h. Then, an Ir catalyst was deposited by pulsed arc plasma discharge. SWCNT growth was carried out in a hot-wall CVD apparatus. The substrate temperature was raised to 850 °C in an Ar/H₂ atmosphere at a flow rate of 100 sccm, then, ethanol of 500 sccm was supplied for 10 min to grow SWCNTs. The samples were characterized by FE-SEM and Raman spectroscopy.

3. Results and discussion

Fig.1 shows Raman spectra for SWCNTs grown on an alumina buffer layer (The number of dip-coating process is 1). Both RBM peaks and G band peaks were observed. The SWCNT diameters estimated from the wavenumbers of RBM peaks were distributed between 0.8 and 1.6 nm. Our results showed that SWCNTs can be grown using alumina buffer layers formed on SUS foils by the dip-coating method.

Acknowledgments

Part of this research was supported by the private university research branding project "Meijo University Brand Building Program by Creating New Nanomaterials" and JSPS Bilateral International Joint Research Projects.

[1] T. Maruyama et al. Appl. Surf. Sci., **509** (2020) 145340.

[2] S. Kondo et al., JSAP Spring Meeting, 19p-P02-2.

Corresponding Author: T. Maruyama

Phone: +81-52-838-2386, Fax: +81-52-832-1172

E-mail: takamaru@meijo-u.ac.jp

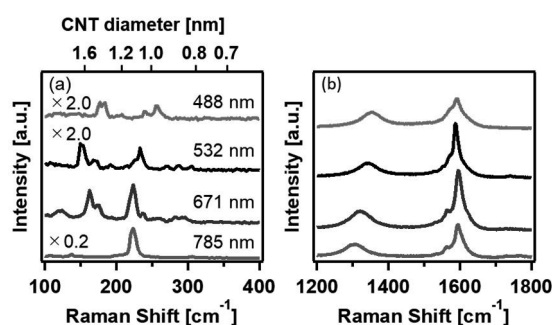


Fig. 1 Raman spectra in (a) the RBM region and (b) the high frequency region of SWCNTs grown on alumina buffer layers prepared by a dip-coating method.

Comparison of single-walled carbon nanotube growth with Ir catalyst on SiO₂ layer prepared by different methods: Sputtering method vs thermal oxidation

○Daiki Yamamoto¹, Shu Kondo¹, Kamal P Sharma¹, Takahiro Saida^{1,2},
Shigeya Naritsuka³, Takahiro Maruyama^{1,2}

¹Department of Applied Chemistry, Meijo University, Japan

²Nanomaterials Research Center, Meijo University, Japan

³Department of Materials Science and Engineering, Meijo University, Japan

1. Introduction

Single-walled carbon nanotubes (SWCNTs) are one-dimensional materials, having various potential for future nanoelectronics. So far, we have succeeded in growing vertically aligned small-diameter SWCNTs on SiO₂/Si substrates by alcohol catalytic chemical vapor deposition (ACCVD) with Ir catalyst [1]. However, there have been few studies on SWCNT growth using Ir catalysts, particularly, the effect of structural property of SiO₂ layers. In this study, to investigate the effect of structural properties of SiO₂ layers, we performed SWCNT growth by ACCVD using Ir catalysts on SiO₂ layers prepared by different methods.

2. Experimental procedure

Ir catalysts were deposited on a SiO₂/Si substrate prepared by thermal oxidation of Si substrates and on a SiO₂ layer prepared by the sputtering deposition on a Si substrate. The thickness of deposited SiO₂ was 20 nm. The nominal thickness of the Ir catalyst deposited was 0.3 nm. SWCNT growth was performed by an ultra-high vacuum (UHV) CVD system. Ethanol gas was supplied through nozzle onto the substrates [1]. The growth time was 60 min. The grown SWCNTs were analyzed by Raman spectroscopy.

3. Result and Discussion

Fig. 1 (a) and (b) shows Raman spectra of the SWCNTs grown on the thermally oxidized SiO₂ substrate and the sputtered SiO₂ layer just under the nozzle at an ethanol pressure 1×10^{-2} Pa, respectively. Fig. 1 (c) and (d) shows Raman spectra of the area on the sample surface with the highest SWCNT yield. Irrespective of the surface area, the diameter distributions were similar for both samples, but the diameters of SWCNTs grown on the sputtered SiO₂ were slightly smaller. We will discuss the effect of surface roughness and surface composition on the SWCNT yield.

This work was supported in part by Private University Research Branding Project from the Ministry of Education, Culture, Sports, Science and Technology (MEXT), Japan.

[1] T. Maruyama et al. Appl. Surf. Sci. 509 (2020) 145340.

Corresponding Author: T. Maruyama

Phone: +81-52-838-2386, Fax: +81-52-832-1172

E-mail: takamaru@meijo-u.ac.jp

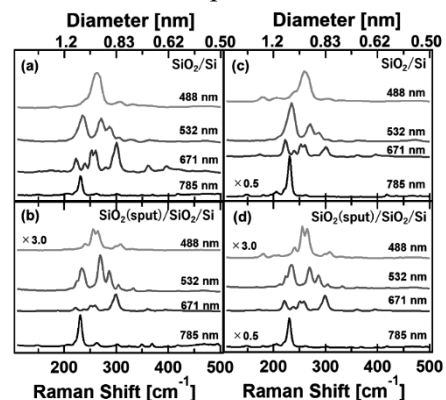


Figure 1 Raman spectra of SWCNTs grown on (a, c) thermally oxidized SiO₂ substrate and (b, d) sputtered SiO₂ layer. (a, b) shows Raman spectra of the area just under the nozzle, and (c, d) shows for the area with highest yield.

Quantitative crystallinity investigation of carbon nanotubes produced by plasma-assisted gas-phase synthesis using far-infrared spectroscopy

○Takashi Tsuji¹, Kazufumi Kobashi¹, Guohai Chen¹, Jaeho Kim², Hajime Sakakita², Yoshiaki Shimizu^{3,4}, Kenji Hata¹, Don N. Futaba¹, Shunsuke Sakurai¹

¹*CNT-Application Research Center, AIST, Ibaraki 305-8565, Japan*

²*Innovative Plasma Processing Group, Research Institute for Advanced electronics and Photonics, AIST, Ibaraki 305-8568, Japan*

³*Nanomaterials Research Institute, AIST, Tsukuba, Ibaraki 305-8565, Japan*

⁴*AIST-UTokyo Advanced Operando-Measurement Technology Open Innovation Laboratory (OPERANDO-OIL), AIST, Kashiwa, Chiba 227-8589, Japan*

Crystallinity of carbon nanotubes (CNTs) is important for CNT-based devices and materials as it strongly affects their properties, such as electric/thermal conductivity and mechanical strength. In addition, crystallinity plays a role in the transfer of properties from the nanometer to millimeter length scales. Therefore, synthesizing highly crystalline CNTs and quantitatively demonstrating their crystallinity are desired. One of the common parameters to evaluate CNT crystallinity is the Raman G/D ratio. However, the richness of Raman spectra renders this approach to be quantitatively inaccurate for this purpose as the signal is dependent on the defect density in CNT graphitic walls and also on CNT diameter and amount of carbon impurities in the sample. Transmission electron microscopy (TEM) of the graphitic structure is exceptionally powerful in visualizing the defects at the atomic level but less quantitative. Recently, a method for estimating the length of CNTs by far-infrared (FIR) spectroscopy have been reported [1]. The length of the crystalline CNT section between defects (so called “effective length”) can be estimated from the FIR absorption peak using one-dimensional plasmon model. Because “effective length” is less sensitive to the diameter and impurities, it can be a quantitative indicator for the crystallinity of CNTs.

Here, we report a quantitative examination of crystallinity of CNTs produced by newly developed plasma-assisted gas-phase synthesis method. For the synthesis of CNTs, Fe catalyst nanoparticles were produced by the decomposition of Fe(CO)₅ using the recently developed microplasma reactor [2,3] and then mixed with carbon source (C₂H₄) in a thermal reactor (925 °C) to initiate nucleation and growth of CNTs. FIR spectroscopy was used to characterize the “effective length” of the CNTs, thus providing an objective and quantitative analysis method on an absolute scale. Our results showed that the “effective length” of our CNT product determined was ~700 nm, which was limited by the physical length of the CNTs. Comparison with FIR measurements of other commercially available single-walled and few-walled CNTs showed that this “effective length” fell within the range of other gas phase synthesis techniques. In addition, this comparison further showed a clear tendency expected from stress-related effects on the “effective length” intrinsic to the synthetic method.

[1] T. Morimoto *et al.* ACS Nano **8**, 9897 (2014).

[2] T. Tsuji *et al.* Carbon, **173**, 448-453 (2020).

[3] T. Tsuji *et al.* ACS Omega, DOI:10.1021/acsomega.1c01822.

Corresponding Author: T. Tsuji

Tel: +81-29-861-0254, Fax: +81-29-861-4851

E-mail: takashi.tsuji@aist.go.jp

The effect of oxidants on SWCNT growth analyzed by isotope labeling technique

○Ryoya Ishimaru¹, Keigo Otsuka¹, Taiki Inoue², Shohei Chiashi¹, Shigeo Maruyama¹

¹ Department of Mechanical Engineering, The University of Tokyo, Tokyo 113-8656, Japan

² Department of Applied Physics, Osaka University, Osaka 565-0871, Japan

Single-walled carbon nanotube (SWCNT) is the most expected material for next-generation high-performance electronics. To grow long, dense SWCNTs suitable for the applications, the understanding of growth mechanisms, especially growth termination and incubation is necessary. Previous studies succeeded in growing long, dense SWCNTs by oxidant-assisted synthesis and suggested that oxidants keep catalysts active by preventing carbon coating [1,2]. For a better understanding of oxidant effects on SWCNT growth, we analyzed SWCNT growth with a recently proposed isotope labeling technique [3,4], which allows us to trace the growth process of individual tubes, including their termination and incubation time.

As an oxidant, water was chosen and added from the middle of the growth. In addition to ¹²C ethanol, main carbon source, ¹³C ethanol was introduced every 1 min, serving as isotope labels inserted into SWCNTs. Total flow rate of ethanol was fixed as the water to ethanol ratio being 0.07. For the post-synthesis analysis, we used Raman mapping images to detect the labels and obtained growth curves of SWCNTs synthesized with the additive water (Fig. 1). SWCNTs continued growing and the growth rate did not change at this water/ethanol ratio. We also compared the growth termination time of SWCNTs synthesized with and without water (Fig. 2(a-b)). Much more SWCNTs synthesized with water kept growing until the carbon supply was stopped (12 min). We also focused on the effect of air leak in the CVD system, which could serve as another oxidant. Two experiments were conducted using ¹³C gas piping with low and high leakage, yielding the distributions of incubation time in Fig. 3(a) and (b), respectively. As we added a maximum amount of ¹³C ethanol every 3 min, corresponding to the biased distributions in Fig. 3(b), the growth incubation assisted by the air leak is suggested.

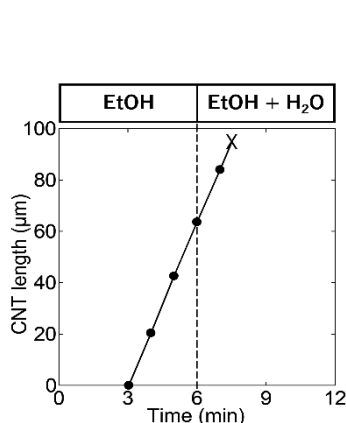


Fig. 1 Growth curve of an SWCNT grown with water addition from the middle of the experiment.

[1] T. Yamada *et al.*, *Nano Lett.*, **8**, 4288 (2008).
[3] K. Otsuka *et al.*, *ACS Nano*, **12**, 3994 (2018).

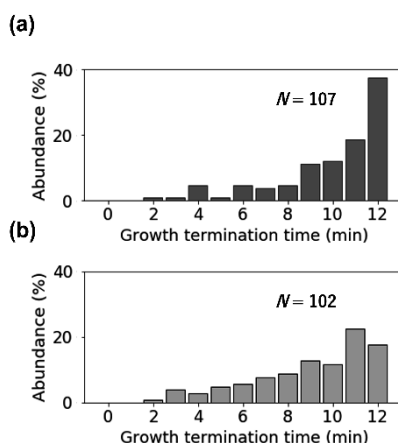


Fig. 2 Growth termination time distributions of SWCNTs grown (a) with water and (b) without water.

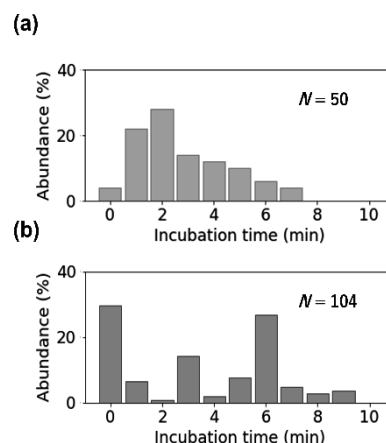


Fig. 3 Incubation time distributions of SWCNTs grown with (a) low and (b) high leakage.

[2] D. N. Futaba *et al.*, *Adv. Mater.*, **21**, 4811 (2009).
[4] B. Koyano *et al.*, *Carbon*, **155**, 635 (2019).

Corresponding Author: S. Maruyama

E-mail: maruyama@photon.t.u-tokyo.ac.jp

Production of atom-encapsulated C₆₀ by ns laser induced breakdown

○Moeno Maejima¹, Haruo Shiromaru¹, Tomonari Wakabayashi²,
Koichi Kikuchi¹, Yohji Achiba¹, Takeshi Kodama³

¹Department of Chemistry, Tokyo Metropolitan University, Tokyo 192-0397, Japan

²Department of Chemistry, Kindai University, Higashi-Osaka 577-8502, Japan

³Center for Basic Education and Integrated Learning, Kanagawa Institute of Technology,
Kanagawa 243-0292, Japan

C₆₀ can encapsulate an atom, typically group V elements and noble gas elements, inside its cage. The encapsulated atom is located in the center of C₆₀ and is shielded from the outside. So far, various approaches have been developed for producing atom-encapsulated C₆₀, for example, ion implantation method for group V elements and high temperature/pressure method for noble gas elements [1]. In the former method, ions with appropriate energies are implanted to C₆₀, and several different techniques have been used to provide ions: a Kaufman ion source [2], a glow discharge [3], an RF discharge [4] and a laser ablation [5]. In this study, we tried to synthesize N@C₆₀ by the novel and relatively simple way, using ns laser induced breakdown (LIB) in nitrogen gas flow.

The experiments were performed with the setup schematically shown in Fig. 1. First, C₆₀ was sublimed to form a C₆₀ film on the upper electrode plate. Next, low-pressure nitrogen gas was introduced to the cell and ns laser was tightly focused at the center, confirming that the LIB plasma was visible. Formed cationic species were accelerated toward the C₆₀ film by the electric field and collided with C₆₀.

Figure 2 shows the ESR spectrum of the solution that ion-bombarded C₆₀ film was dissolved into CS₂. The triplet signal was assigned to the internal atomic nitrogen of N@C₆₀, S=3/2 coupled with nuclear spins ¹⁴N (I=1). In the symposium, the production yield for N@C₆₀ at various experimental conditions will be presented and its dependence on the conditions also discussed.

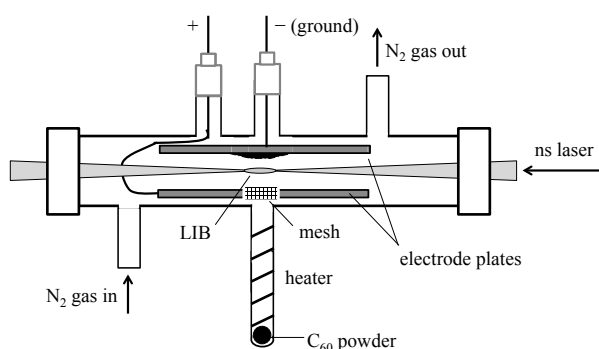


Fig. 1 The schematic view of the experimental setup.

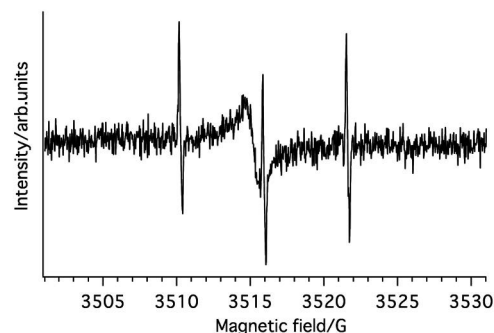


Fig. 2 The ESR spectrum of produced N@C₆₀. Broad signal was assigned to impurity.

[1] M. Saunders, *et al. J. Am. Chem. Soc.* **116**, 2193 (1994).

[2] B. Pietzak, *et al. Carbon* **36**, 613 (1998).

[3] B. Pietzak, *et al. Chem. Phys. Lett.* **279**, 259 (1997).

[4] T. Wakabayashi and T. Kuroda, *The 35th Commemorative Fullerene-Nanotubes General Symposium*, 3P-8 (2008).

[5] H. Itagaki, *et al. AIP Adv.* **9**, 075324 (2019).

Corresponding Author: Takeshi Kodama

Tel: +81-46-206-0222, E-mail: kodama-takeshi@gen.kanagawa-it.ac.jp

Study of magnetic properties of Er-dimetallofullerene anions

○Naoya Fujita¹, Aichi Yamashita², Yoshikazu Mizuguchi², Koichi Kikuchi¹, Yohji Achiba¹,
Takeshi Kodama³

¹Department of Chemistry, Tokyo Metropolitan University, Tokyo 192-0397, Japan

²Department of Physics, Tokyo Metropolitan University, Tokyo 192-0397, Japan

³Center for Basic Education and Integrated Learning, Kanagawa Institute of Technology, Kanagawa 243-0292, Japan

Er (Er^{3+}) has emission in the near-infrared region of about 1.5 μm . In the previous symposium [1], we reported the production and isolation of $[\text{Er}_2@\text{C}_{80}(\text{I}_h)]^-$ and $[\text{Er}_2@\text{C}_{78}(\text{D}_{3h})]^-$, and the emission from the encapsulated Er^{3+} at around 1.5 μm .

In addition, Er^{3+} has a rather large magnetic moment, and its magnetism has also been interested. The magnetism of metallofullerenes containing Er was studied for $\text{Er}@\text{C}_{82}$ and $\text{Er}_2\text{C}_2@\text{C}_{82}$ [2], and it was found that the magnetic behavior changes depending on the encapsulated species. On the other hand, it was reported that $[\text{Dy}_2@\text{C}_{80}(\text{I}_h)]^-$, $[\text{Dy}_2@\text{C}_{78}(\text{D}_{3h})]^-$ [3], $[\text{Tb}_2@\text{C}_{80}(\text{I}_h)]^-$, and $[\text{Tb}_2@\text{C}_{78}(\text{D}_{3h})]^-$ [4] behave as a single molecule magnet. Therefore, in this work, magnetic properties of $[\text{Er}_2@\text{C}_{80}(\text{I}_h)]^-$ and $[\text{Er}_2@\text{C}_{78}(\text{D}_{3h})]^-$ were investigated.

Fig. 1 shows the results of FC/ZFC measurements by SQUID for $[\text{Er}_2@\text{C}_{80}(\text{I}_h)]^-$ and $[\text{Er}_2@\text{C}_{78}(\text{D}_{3h})]^-$. In both cases, there was no difference between FC/ZFC curves down to low temperature. These are in contrast to $[\text{Dy}_2@\text{C}_{80}(\text{I}_h)]^-$, $[\text{Dy}_2@\text{C}_{78}(\text{D}_{3h})]^-$, $[\text{Tb}_2@\text{C}_{80}(\text{I}_h)]^-$, and $[\text{Tb}_2@\text{C}_{78}(\text{D}_{3h})]^-$, and it indicates the relaxation times of magnetic moments of $[\text{Er}_2@\text{C}_{80}(\text{I}_h)]^-$ and $[\text{Er}_2@\text{C}_{78}(\text{D}_{3h})]^-$ are rather shorter than those of Dy or Tb analogues.

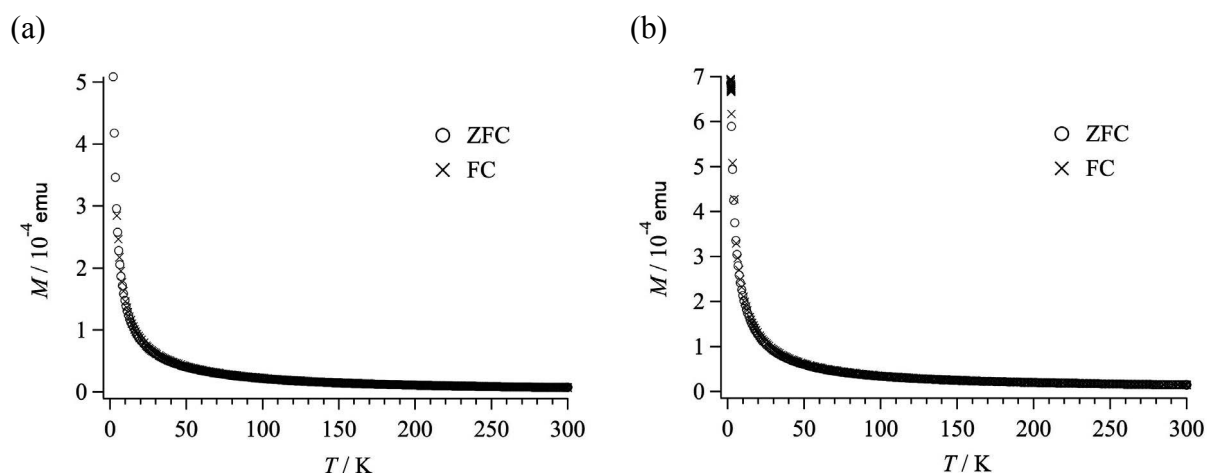


Fig. 1 Zero-field cooled (ZFC) and field cooled (FC) magnetization of (a) $[\text{Er}_2@\text{C}_{80}(\text{I}_h)]^-$ and (b) $[\text{Er}_2@\text{C}_{78}(\text{D}_{3h})]^-$ (Field: 0.2 T, Sweep rate: 5 K/min).

[1] S. Nishimoto, et al. *The 56th Fullerenes-Nanotubes-Graphene General symposium* 98 (2019).

[2] H. Okimoto, et al. *J. Phys, Chem C*, **112**, 6103-6109 (2008).

[3] R. Takai, et al. *The 58th Fullerenes-Nanotubes-Graphene General symposium* 28 (2020).

[4] K. Yamagishi, et al. *The 58th Fullerenes-Nanotubes-Graphene General symposium* 120 (2020).

Corresponding Author: Takeshi Kodama

Tel: +81-46-206-0222, E-mail: kodama-takeshi@gen.kanagawa-it.ac.jp

The cage dependence of single molecule magnet properties of Tb-dimetallofullerene anions: $[\text{Tb}_2@C_{80}(\text{I}_h)]^-$ and $[\text{Tb}_2@C_{78}(\text{D}_{3h})]^-$

○Kazuki Yamagishi¹, Aichi Yamashita², Yoshikazu Mizuguchi², Ryuji Higashinaka², Yuji Aoki², Koichi Kikuchi¹, Yohji Achiba¹, Takeshi Kodama³

¹Department of Chemistry, Tokyo Metropolitan University, Tokyo 192-0397, Japan

²Department of Physics, Tokyo Metropolitan University, Tokyo 192-0397, Japan

³Center for Basic Education and Integrated Learning, Kanagawa Institute of Technology, Kanagawa 243-0292, Japan

Tb-dimetallofullerenes, $\text{Tb}_2@C_{79}\text{N}$ [1] and $\text{Tb}_2@C_{80}(\text{CH}_2\text{Ph})$ [2], have been attracting attention as single molecule magnets (SMMs) containing two lanthanide metal ions in a fullerene cage. The SMM properties of them originate from the ferromagnetically coupled spin system inside the cage, $[\text{Tb}^{3+} - e^- - \text{Tb}^{3+}]$ and the theoretical calculation [1] suggested that the symmetry of the electrostatic field in the fullerene cage affects the SMM properties.

In the previous symposium [3], we reported the synthesis and isolation of $[\text{Tb}_2@C_{80}(\text{I}_h)]^-$ and $[\text{Tb}_2@C_{78}(\text{D}_{3h})]^-$, which have carbon cages with no N-substitution and no additional group, and the measured M-H curves of them exhibited the magnetic hysteresis. In this work, to investigate SMM properties of them in detail, we measured Field Cooled (FC) / Zero-Field Cooled (ZFC) curves and the relaxation time (τ_m) of magnetization.

Fig. 1 and Fig. 2 show FC/ZFC curves of $[\text{Tb}_2@C_{80}(\text{I}_h)]^-$ and $[\text{Tb}_2@C_{78}(\text{D}_{3h})]^-$ in the field of 0.2 T with a sweep rate 5 K min^{-1} . T_B was determined to be 29 K and 10 K, respectively. T_B of $[\text{Tb}_2@C_{80}(\text{I}_h)]^-$ is almost identical with those of $\text{Tb}_2@C_{79}\text{N}$ and $\text{Tb}_2@C_{80}(\text{CH}_2\text{Ph})$ although their symmetry of the electrostatic field in the fullerene cage is different. On the other hand, $[\text{Tb}_2@C_{80}(\text{I}_h)]^-$ and $[\text{Tb}_2@C_{78}(\text{D}_{3h})]^-$ have rather different T_B . The same tendency was observed for M-H curves [3].

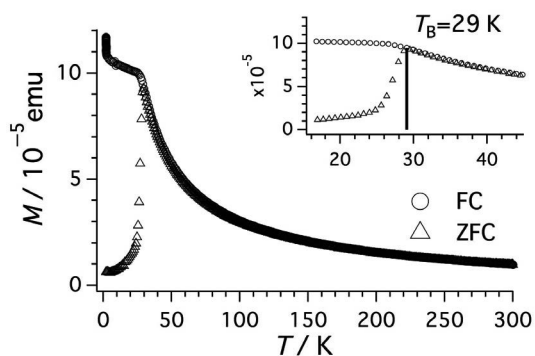


Fig. 1 FC/ZFC curves of $[\text{Tb}_2@C_{80}(\text{I}_h)]^-$.

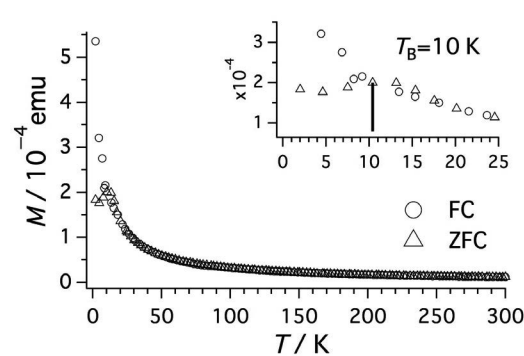


Fig. 2 FC/ZFC curves of $[\text{Tb}_2@C_{78}(\text{D}_{3h})]^-$.

[1] G. Velkos, *et al.* *Angew. Chem. Int. Ed.* **58**, 5891 (2019).

[2] F. Liu, *et al.* *Nature Communications* **10**, 571 (2019).

[3] K. Yamagishi, *et al.* The 58th Fullerenes-Nanotubes-Graphene General Symposium 120 (2020).

Corresponding Author: Takeshi Kodama

Tel: +81-46-206-0222

E-mail: kodama-takeshi@gen.kanagawa-it.ac.jp

Modulation of electronic states in two-dimensional semiconductors by bowl-shaped molecules.

○S. Yotsuya¹, A. Fukui¹, A. Tsurusaki², T. Yoshimura¹, N. Fujimura¹, D. Kiriya¹

¹ Graduate School of Engineering, Osaka Pref. University, Osaka 591-8531, Japan

² Graduate School of Science, Osaka Pref. University, Osaka 591-8531, Japan

It is known that the electronic states in two-dimensional semiconducting materials can be modulated by polar molecules facing on the surface along the out-of-plane direction. It is usually difficult to induce strong carrier modulation by the effect of the polarization in molecules. In this study, we examined the modulation of the electronic state of a two-dimensional semiconducting material, MoS₂, by the effect of polarization of dibenzo[b,e]phosphindolizine, bowl-shaped asymmetric molecule (Fig. 1)[1].

The molecule was deposited on single-layer MoS₂ exfoliated on a 260 nm SiO₂ substrate. The Raman and photoluminescence (PL) spectra (Fig. 2) were measured before and after the deposition of the molecules. The red-shift of the out-of-plane vibrational mode (A_{1g}) in Raman spectrum and the red-shift in the PL spectrum were observed. These trends in the spectra suggest an increase of the electron density in the monolayer MoS₂.

From the relationship in energy levels of the conduction band minimum (CBM) of MoS₂ and the highest occupied molecular orbital (HOMO) of the deposited molecule, surface electron transfer doping would not happen. Therefore, we believe that the asymmetric molecules would align on MoS₂ surface spontaneously, which induces the modulation of the electronic state in the monolayer MoS₂. Furthermore, a clear negative shift of the threshold voltage on a MOSFET with a single-layer MoS₂ was observed after the molecular treatment (Fig. 3). In the presentation, we will discuss the details of the mechanism of the doping with the relationship of the asymmetric structure and polarization of molecules.

Reference

[1] A. Tsurusaki *et al.*, Chem. Commun. **55**, 4909-4912 (2019)

Corresponding Author: D. Kiriya

Tel: +81-72-254-9327, Fax: +81-72-254-9327,

E-mail: kiriya@pe.osakafu-u.ac.jp

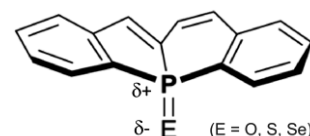


Fig. 1 Chemical structure of dibenzo[b,e]phosphindolizine. In this work, the molecule of E=O is mainly used.

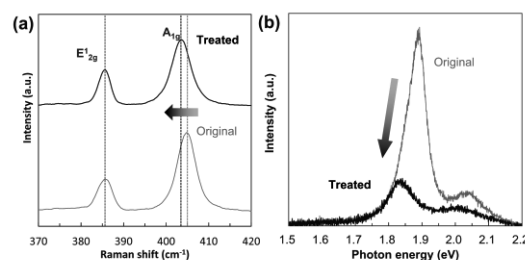


Fig.2 (a) Raman spectra and (b) PL spectra of the original and molecular treated monolayer MoS₂. Raman shift is about 1 cm⁻¹.

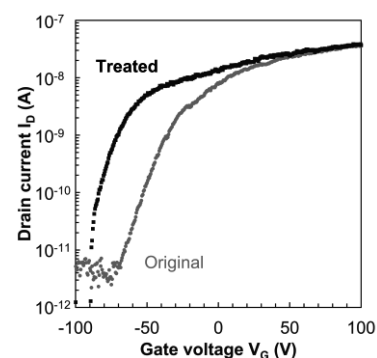


Fig.3 Transfer characteristics of the original and molecular treated monolayer MoS₂.

Diffusion of Oxygen Atom on Single Layer of Graphene Sheet with Atomic Vacancy V_6 for Graphene Oxide as ReRAM devices

○Takazumi Kawai¹

¹ Graduate School of Integrative Science and Engineering, Tokyo City University,
Tokyo 158-8557, Japan

Among various 2D materials graphene oxide attract much attentions due to its fascinating properties such as a flexibility, easy fabrication, low cost, transparency and so on, especially, as a non-volatile resistive switching random-access-memory (Re-RAM). Basically the mechanism for the ReRAM device is considered to be breakdown of conducting strips caused by the diffusion of oxygen atoms on the graphene sheet [1-4].

Here, we consider the global diffusion of oxygen atoms, where the atoms are required to diffuse from one side of graphene sheet to the other side, and go through an atomic vacancy on edges. In this paper, we consider the single atom diffusion through V_6 defect by ab initio electronic state calculations using the quantum espresso code [5]. Since the V_6 defect is large enough for oxygen atom to diffuse, the diffusion barrier would be similar for that through graphene edges.

Optimized path for oxygen diffusion through the V_6 defect is shown in Fig.1(a)-(d) and variation of total energy Fig.1(e), where we took the total energy of most stable structure as 0 eV. From the graph (Fig.1(e)) we found that the energy of initial structure is higher than that at edge of V_6 defect and diffusion barrier is around 0.5 eV, which is much lower than that without V_6 defect. Thus, the oxygen atom is easily trapped by the defect/edge on the graphene.

For the diffusion from the edge of V_6 on one side to the other, the diffusion barrier is around 4 eV, where the oxygen atom break into the C-C bond. From the energy variation between epoxide at the edge (Fig.1(b) to (d)), there is only one peak for the oxygen break into CC-bond. Then the oxygen atom approach to the V_6 defect break into C-C bond without any energy barrier. However the energy barrier for the diffusion is 4 eV, which indicate that the diffusion rarely occur under room temperature. At the presentation, we will show the effect of external electric fields by applying the voltage using Effective Screening Medium Method (ESM).

- [1] H. Tian, *et al.*, Nano Letters, 14 (2014) 3214.
 [2] A. Rani, *et al.*, small, 12 (2016) 6167.
 [3] H. Liua, *et al.*, Mater. Today Commun. 25 (2020) 101537.
 [4] M. Brzhezinskaya, *et al.*, J. Alloys Compd. 849 (2020) 156699.
 [5] P. Giannozzi et al., J. Phys.:Condens. Matter 21 395502 (2009); P. Giannozzi et al., J. Phys.:Condens. Matter 29 465901 (2017); P. Giannozzi et al., J. Chem. Phys. 152 154105 (2020); URL <http://www.quantum-espresso.org>".

Corresponding Author: T. Kawai,
 Tel: +81-3-5707-0104,
 E-mail: tkawait@tcu.ac.jp

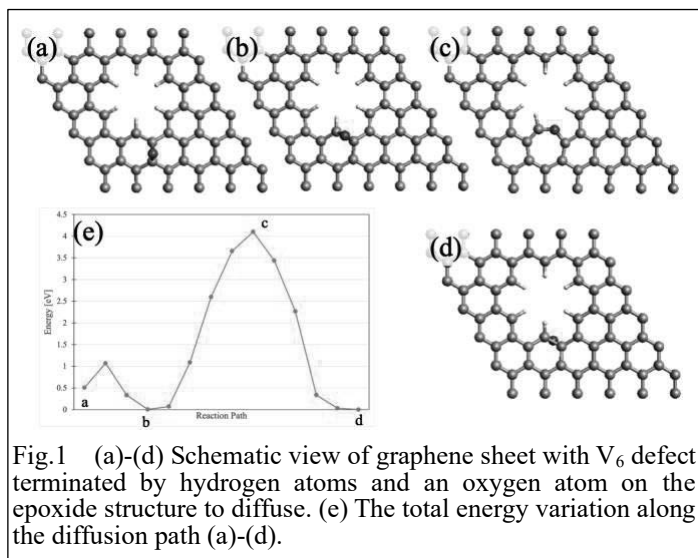


Fig.1 (a)-(d) Schematic view of graphene sheet with V_6 defect terminated by hydrogen atoms and an oxygen atom on the epoxide structure to diffuse. (e) The total energy variation along the diffusion path (a)-(d).

Modulation of electronic properties of graphene by B⁺ / N⁺ beam irradiation

○Takumi Hidaka^{1,3}, Yasushi Ishiguro², Kosuke Nakamura¹,
Tomoaki Nishimura³, Kazuyuki Takai^{1,3}

¹ Graduate School of Science and Engineering, Hosei University, Tokyo 184-8584, Japan

² Department of Electrical and Electronic Engineering, Tokyo Denki University,
Tokyo 120-8551, Japan

³ Research Center for Ion Beam Technology, Hosei University, Tokyo 184-8584, Japan

Effects of the environment and the presence of defects / impurities are crucial in the electronic properties of 2D materials. Especially in graphene, different responses are expected for introducing of B and N atoms in view of doping and scattering of carriers. In this study, B⁺ and N⁺ beams were irradiated into graphene as a quantitative method for introducing impurities, and their effects on the electron transport were investigated. To distribute B⁺ and N⁺ on the graphene surface, we applied NaCl to a sacrificial layer upon ion beam irradiation [1].

Cr (10 nm) / NaCl (1200, 1000 nm) layers were deposited as sacrificial layer on the graphene obtained by the cleavage method on SiO₂ / Si substrates. The film thickness of the sacrificial layer was optimized using Monte Carlo simulation for the ion distribution by SRIM2013. B⁺ and N⁺ irradiation to the sample was performed at an acceleration voltage of 200 keV with a dose of 10¹³ cm⁻². The gate voltage dependence of the conductivity is evaluated by using field effect transistor (FET) of graphene before / after the irradiation.

The charge neutral point of the graphene FET shifted to the positive side in the gate voltage after B⁺ irradiation on graphene (**Fig.1**). On the other hand, the charge neutral point of the FET shifted to the negative voltage side after N⁺ irradiation on graphene (**Fig.2**). These indicate that the introduced B⁺ and N⁺ cause hole doping and electron doping in graphene, respectively.

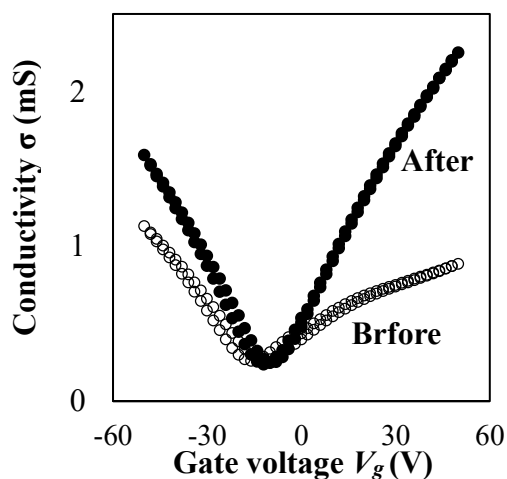


Fig.1 Conductivity of graphene before and after B⁺ irradiation

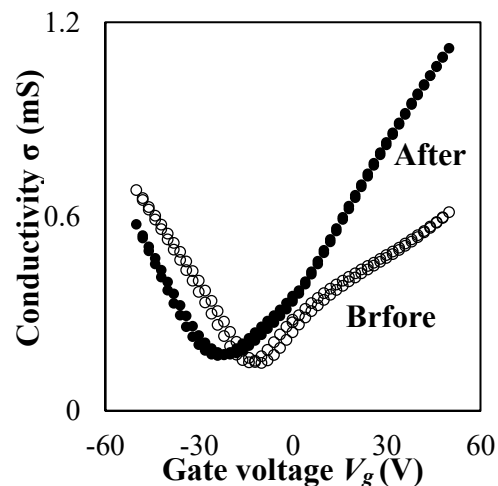


Fig.2 Conductivity of graphene before and after N⁺ irradiation

[1] K. Nakamura *et al.* FNTG symposium (2018).

Corresponding Author: K. Takai

E-mail: takai@hosei.ac.jp

Application of the energy exchange eHEX algorithm to thermal transport in 2 layers hBN system in molecular dynamics calculations

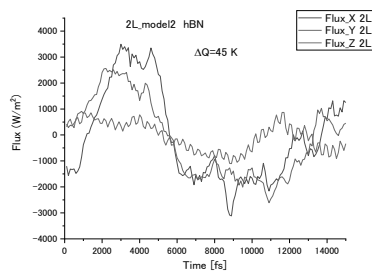
○Tatiana Zolotoukhina¹, Yusuke Michisuji¹, Wataru Yuhara¹

¹ Department of Mechanical Engineering, University of Toyama, Toyama 930-8555, Japan

Interest in the application of layered hexagonal boron nitride (hBN) has recently increased, due to its superior physicochemical properties compared to that of typical two-dimensional material. hBN can be utilized in power chips as both an insulating layer as well as a heat spreader for local hotspots with high heat flux [1-3]. The advantage of hBN films and even single layers is that they might be integrated into the semiconductor circuitry and be placed directly on top or below the hotspot without any insulating SiO₂ layers. We investigate an out-of-plane energy transfer channel as it couples to the in-plane transfer, its efficiency as well as dependence on the sample size. To that end, the 2 layers hBN sample with AA stacking was used to test the eHEX [4] energy exchange algorithm in molecular dynamics simulation of heat flow in the 2-layered system.

The hBN layers were of the 1440 x 173.52 Å size with AA stacking and $\Delta z=3.3$ Å distance between layers. We tested the eHEX energy exchange algorithm in application to the 2D structures at conditions of periodic boundary in x & y-direction. Calculations were carried in LAMMPS. Definition of the cross-sectional area for the flux was taken as $2\Delta z$ to accumulate interlayer distance. The conduction area for flux evaluation was $L_x/2$ in the x-direction, heating and cooling areas were taken to be 8 Å size in the x-direction. Fluctuation of flux x,y,z components with time (15 ps) was found at the constant heat exchange scheme of non-equilibrium eHEX heating. Heat propagation in each direction has a different fluctuation scale at the same heating time, with the highest frequency of fluctuations in z.

(a) averaged heat flux, conduction area



(b) heat flux in x & z directions by layers

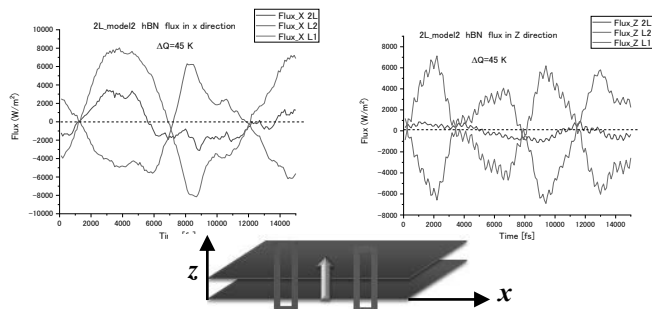


Fig1 Heat flux in hBN 2 layer interacting system (T=300 K, conduction area in x)

[1] B. Zhao, B. Guizal, Z. M. Zhang, S. Fan, and M. Antezza, *Phys. Rev. B*, 95, 245437, (2017).

[2] I. C. Choi, K. Lee, C.-R. Lee, J. S. Lee, S. M. Kim, K.-U. Jeong, and J. S. Kim, *ACS Appl. Mater. Interfaces*, 11, 20, (2019).

[3] K.-J. Tielrooij, N C. H. Hesp, A. Principi., *et. al.*, *Nature Nanotechnology*, 13, 41–46, (2018).

[4] P. Wirsberger, D. Frenkel, C. Dellago, *J. Chem. Phys.*, 143, 124104 (2015).

Corresponding Author: T. Zolotoukhina

Tel: +81-76-445-6739, Fax: +81-76-445-6739, E-mail: zolotu@eng.u-toyama.ac.jp

Aggregates of Elementary Diamond Nanoparticles in Their Aqueous Colloidal Solutions Induced by Trace Ions

- Masaya Nemoto^{1,2}, Toshihiko Tanaka^{1,2}, Yasuhiro F. Miura³, Tetsuya Aoyama², Kazunori Miyamoto⁴, Atsuya Muranaka², Masanobu Uchiyama^{2,4}, Eiji Osawa⁵

¹Department of Chemistry and Biochemistry, National Institute of Technology, Fukushima College, 30 Aza-nagao, Tairakamiarakawa, Iwaki, Fukushima, 970-8034, Japan

²Elements Chemistry Laboratory, RIKEN CPR, 2-1 Hirosawa, Wako, Saitama, Japan

³Hamamatsu University School of Medicine, 1-20-1 Handayama, Higashi-ku, Hamamatsu City, Shizuoka, Japan

⁴Graduate School of Pharmaceutical Sciences, the University of Tokyo, 7-3-1 Hongo, Bunkyo-ku, Tokyo, Japan

⁵Nano Carbon Research Institute Ltd., Asama Research Extension Center, Shinshu University, 3-15-1 Tokida, Ueda, Nagano, Japan

Elementary diamond nanoparticles (EDIANs)¹ are aggregated by trace ions in their aqueous colloidal solutions and we have to consider that trace carbonate or bicarbonate ions contaminate pure water and that the ions often make them aggregate when diluting the solutions with it.² Taking rich ions of biological organs into account, hence we also have to consider that they also aggregate through their success of drug delivery systems³. Perhaps the aggregates showed so-called EPR effect, which should contribute much to the success. We demonstrate here their aggregates by various kinds of thin salt aqueous solutions in our recent experiments under nitrogen atmosphere ($O_2 < 0.2\%$). Do the aggregation depend on ion species?

We diluted nanodiamond(ND) solutions (NanoAmando[®], NanoCarbon Research Institute Ltd., containing EDIANs) from 2.5 to 0.25wt% with various thin salt solutions (using ultrapure water) in the N₂ atmosphere. Their particle sizes were measured with a DLS, thus showing their dependence on salt concentration (Fig.1). However their

dependence on the species were obscure while Hofmeister-like dependence^{2,4} was observed through their sedimentation with ions. The observed aggregation is an early stage of sedimentation and we consider that different kinds of mechanism take place between ions and EDIANs in each process. We also will mention reversibility of aggregation: some aggregated EDIANs can be dispersed again by ultrasonic waves.

[1] A. S. Barnard, E. Osawa; *Nanoscale* 6, 1188 (2014); [2] Nemoto, et al., FNTG 60th Abstract Book (2021); [3] E.K.Chow, X.-Q. Zhang, M. Chen, R. Lam, E. Robinson, H. Huang, D. Schaffer, E. Osawa, A. Goga, D. Ho, *Sci. Trans. Med.*, 3, 73 (2011); [4] N.O. Mchedlov-Petrosyan, N. N. Kamneva, A. I. Marynin, A. P. Kryshstal, E. Osawa, *Phys. Chem. Chem. Phys.*, 17, 16186 (2015).

Corresponding Author: Toshihiko Tanaka / Tel: +81-246-46-0810 / E-mail: ttanaka@fukushima-nct.ac.jp

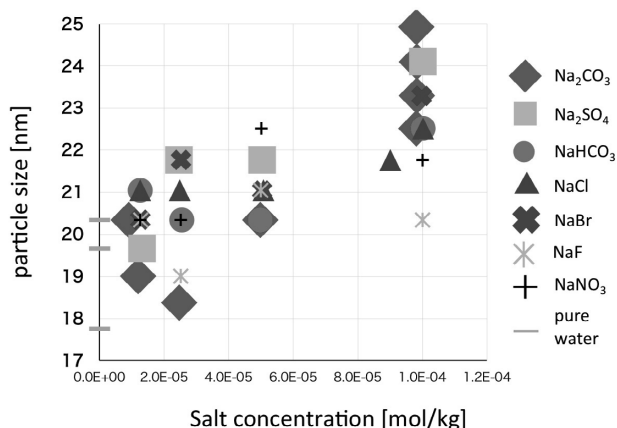


Figure 1. DLS size measurements of EDIANs' solutions diluted with water or various aqueous salt solutions shown above. Samples are prepared in the N₂ atmosphere.

Synthesis and properties of fluorescent carbon quantum dots using lignin

○Takaki Yoda¹ and Hironori Ogata^{1,2,3}

¹Grad. Sch. Sci. and Engin., Hosei Univ.

²Dept. Chem. Sci. and Technol., Hosei Univ.

³Research Center for Micro-Nano Technol., Hosei Univ.

Carbon quantum dots (C-QDs) are one of the nanomaterials that have attracted much attention in recent years. C-QDs have many advantages over conventional semiconductor quantum dots and organic dyes, including chemical stability, dispersibility, fluorescence properties, hydrophilicity, and high resistance to photodegradation [1]. Currently, there are two main synthesis approaches for the preparation of C-QDs; "top-down" and "bottom-up" approaches. In the top-down approach, large carbon materials are decomposed by arc discharge, laser ablation, or chemical oxidation [2]. On the other hand, the bottom-up approach is synthesis of C-QDs create carbon molecules via precursors such as the hydrothermal method [3], pyrolysis method, and the microwaves method [4]. These methods have been reported to have complicated procedures, relatively large particle sizes (30-50 nm), and low quantum yields of fluorescence.

In recent years, biomass has been attracting attention as a material for C-QDs. In particular, synthesis of C-QDs have been reported from groceries such as soymilk [5] and plant seeds [6] *et al.* They use a simple heating process and can be synthesized at low cost. We clarified that C-QDs can be synthesized from lignin by pyrolysis. In this study, we investigated the structure and optical properties of C-QDs synthesized from lignin, and their differences from C-QDs synthesized by other methods.

Figure 1 shows a TEM image of C-QD synthesized from lignin.

Detailed results will be reported at the meeting.

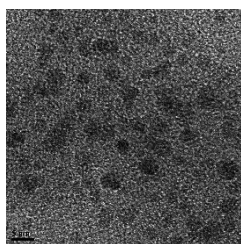


Fig.1 TEM images of Lignin C-QDs.

References:

- [1] Wang, Y. *et al.*, *J.Mater.Chem.C*, **2**,6921(2014).
- [2] Zhao, Q.L. *et al.*, *Chem.C*, **41**,5116(2008).
- [3] Pan, D. *et al.*, *Adv.Mater.*, **22**,6,734(2010).
- [4] Liu, R. *et al.*, *J.Am.Chem.Soc.*, **133**,39,15221(2011).
- [5] Chengzhou, Z. *et al.*, *Chem.C*, **48**,9367(2012).
- [6] Akansha, D. *et al.*, *Sci.Rep.*, **9**,14004(2019).

Corresponding Author: H.Ogata

Tel: +81-42-387-6229, Fax: +81-42-387-6229,

E-mail: hogata@hosei.ac.jp

Synthesis of Boron Nitride Nanotubes Using Mist of Boric Acid Aqueous Solution as a Low-Cost Boron Source

○Sota Ebisu¹, Tetsuro Sawada¹, Toshio Osawa¹, Hisashi Sugime², Suguru Noda^{1,2*}

¹ Department of Applied Chemistry, ² Waseda Research Institute for Science and Engineering, Waseda University, Tokyo 169-8555, Japan.

Boron nitride nanotubes (BNNTs) are mechanically, thermally, and chemically stable similarly to carbon nanotubes (CNTs) and optically transparent and electrically insulative oppositely to CNTs, thus have rich opportunities for application including glass composites [1] and battery separators [2]. BNNTs, produced from solid boron or h-BN powder as boron source, are now commercially available from start-up companies. Temperatures as high as several thousand degree C are needed to yield vapors from these solid sources [3], resulting in the BNNTs as expensive as a few hundred USD per gram. Moreover, the BNNTs contain boron and/or h-BN particles at high content. BNNTs can also be synthesized via chemical vapor deposition (CVD). The process temperature is as low as 1000–1400 °C or less, thus low cost production can be expected. Ammonia can be used as a gaseous nitrogen source. But expensive boron sources such as borazine or solid sources such as boron oxide are used by now. Finding low-cost and safe boron-containing compound for gaseous boron source is a key issue.

We have reported boric acid, which is widely used for disinfectants, as a low-cost boron source, and realized the BNNT synthesis by feeding its vapor via sublimation [4]. But the sublimation was unstable due to the sintering and dehydration of the boric acid powder. In this work, we studied another method that uses mist of the boric acid aqueous solution.

BNNT synthesis was examined using Fe/graphite combinatorial catalyst library as shown in Fig. 1. Graphite was selected as the substrate because it does not react with Fe at high temperature. Fe was sputter-deposited onto graphite with a thickness gradient of 0.49–3.2 nm using a physical filter. BNNTs were synthesized on the Fe/graphite substrate in a quartz glass tube reactor for 10 min by feeding NH₃/Ar gas and mist of boric acid aqueous solution using an ultrasonic nebulizer. Scanning electron microscope (SEM) images show the formation of nanotubes on the substrates (Fig. 1). With decreasing Fe thickness, nanotubes decreased the yield and got more straight.

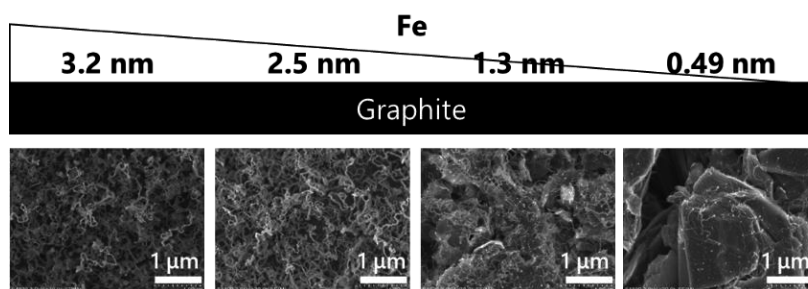


Fig. 1. Plan-view SEM images of BNNTs grown on Fe/graphite substrate with various Fe thicknesses.

- [1] N.P. Bansal, et al., *J. Am. Ceram. Soc.*, **89**, 1 (2006).
- [2] K., Kentaro, et al., *Carbon*, **167**, 596 (2020).
- [3] M.W. Smith, et al., *Nanotechnology*, **20**, 50 (2009).
- [4] T. Sawada, et al., *The 58th FNTG General Symposium*, 2P-23 (2020).

Corresponding Author: S. Noda, Tel: 03-5286-2769, E-mail: noda@waseda.jp

発表者索引
Author Index

Author index

A

Abe, Ryo 3-7
Abe, Yuho *1P-12
Achiba, Yohji 1P-78, 1P-79, 1P-80
Adachi, Yusuke *3-17
Ago, Hiroki 1P-39, 1P-65, 1P-72
Ahmad, Saeed 1P-46
Akita, Seiji 1P-25, 3-17
Anisimov, Anton 1P-61
Aoki, Haruka 1P-73
Aoki, Yuji 1P-80
Aoyama, Tetsuya 1P-85
Araki, Tsutomu 1P-27
Araki, Yuji *1P-39
Arie, Takayuki 1P-25, 3-17
Arifuku, Michiharu 1P-14

B

Barnard, Amanda 3-10
Bets, Ksenia 1P-58
Bianco, Alberto 2-2
Bichara, Christophe *2S-7

C

Chae, Sangwoo 2-1
Chen, Guohai *1P-15, 1P-76, 2-5
Chiashi, Shohei 1P-2, 1P-13, 1P-42,
1P-47, 1P-58, 1P-61,
1P-62, 1P-77, 2-7
Chou, Yungkai 1P-45

D

Dai, Wanyu *2-7
Date, Hiroki *1P-62
Datta, Sukanta 1P-46
Ding, Er-xiong 1P-46
Doi, Juntaro 1P-27

E

Ebisu, Sota *1P-87
Eda, Junko 1P-72
Endo, Takahiko 1P-9, 1P-10, 1P-29,
1P-37, 1P-38, 1P-56,
1P-64, 3-13

F

F. miura, Yasuhiro 1P-85
Fang, Nan 3S-1
Feng, Ya 1P-13
Fujigaya, Tsuyohiko 1P-5, 1P-11, 1P-32,
1P-59, 1P-73, *2I-3
Fujii, Takenori 1P-62
Fujii, Yasuhiro 1P-24
Fujimura, Norifumi 1P-81
Fujita, Naoya *1P-79
Fukui, Akito 1P-81
Fukunishi, Yasuhiro 3-20
Fukushima, Tomohiro *1P-54
Fukuura, Shuta *1P-43
Furuta, Hiroshi *1P-69
Futaba, Don 1P-19, 1P-76, 2-5
Futaba, Don n. 1P-15

G

Gao, Weilu 3-8
Gao, Yanlin 1P-22, 3-12, 3-18
Goto, Chihiro 1P-68
Goto, Masahiro 1P-59
Goto, Taishi *1P-21
Gupta, Nitant 1P-58

H

Habara, Ren *1P-63
Hamasaki, Hiromu *1P-35
Hamasuna, Aoi *1P-5
Han, Jiye 1P-46, 3-5
Harano, Koji *3-11
Hashimoto, Kazuki *1P-37
Hashimoto, Satoru 1P-40
Hashimoto, Takeshi 1P-40
Hata, Kenji 1P-4, 1P-15, 1P-19,
1P-76, 2-5
Hata, Yoshito *1P-25
Hatanaka, Miho 1P-50
Hatta, Akimitsu 1P-69
Hayamizu, Yuhei 1P-36, 2-3
Hayashi, Kenjiro 3-19
He, Xing *1P-53
Hidaka, Takumi *1P-83
Higashinaka, Ryuji 1P-80

Higuchi, Naoto	1P-3	Kataura, Hiromichi	1P-20, 1P-41, 1P-71, 2-4
Hirahara, Kaori	1P-35	Katayama, Mitsuhiro	1P-21
Hirano, Atsushi	*1P-20	Kato, Masakiyo	1P-45
Hirotsu, Jun	3-6	Kato, Toshiaki	1P-53, 3-16
Hisama, Kaoru	1P-47, *1P-58, 1P-61, *3-12	Kato, Yuichiro k.	3S-1
Homma, Chishu	*2-3	Kauppinen, Esko	1P-62
Honda, Shimon	1P-69	Kauppinen, Esko i	1P-13
Honma, Chishu	1P-36	Kauppinen, Esko i.	1P-46, 1P-61, 3-5
Hori, Keisuke	1P-30	Kawabe, Rintaro	1P-33
Horiuchi, Kanako	3-8	Kawahara, Kenji	1P-39, 1P-72
Hoshino, Shintaro	1P-68	Kawai, Hideki	3-8
Hosokawa, Yuuya	*1P-60	Kawai, Takazumi	*1P-82
Hussain, Aqeel	1P-46	Kawano, Yukio	1P-31
Huyghebaert, Cedric	*2S-5	Kawase, Takumi	1P-35
I		Kawase, Yuta	1P-27
Ibi, Takayuki	1P-33	Khan, Taher	1P-46
Ichinose, Nanami	*1P-66	Kikkawa, Masahide	3-11
Ichinose, Yota	*1P-17, 1P-18, 3-8, 3-9	Kikuchi, Iori	*1P-10
Ideue, Toshiya	1P-68	Kikuchi, Koichi	1P-78, 1P-79, 1P-80
Iijima, Sumio	*2S-1	Kim, Jaeho	1P-15, 1P-76, 2-5
Ikuhara, Yuichi	1P-61	Kiriya, Daisuke	1P-81
Imafuku, Ryohei	*1P-3	Kitabatake, Daiki	1P-49
Inao, Ryota	1P-21	Kitada, Takahito	3-16
Inoue, Taiki	1P-2, 1P-14, 1P-42, *1P-45, 1P-55, 1P-61, 1P-62, 1P-77	Kitaura, Ryo	1P-2, 1P-66, 1P-67, 3-12
Inoue, Yoku	1P-44, 1P-70	Kiyoyanagi, Noriko	1P-14
Ishiguro, Yasushi	1P-83	Ko, Jeong won	1P-48
Ishikawa, Soma	1P-40, 2-1	Ko, Weon bae	1P-48
Ishimaru, Ryoya	*1P-77	Kobashi, Kazufumi	1P-19, 1P-76
Islam, Md. saiful	1P-69	Kobayashi, Masaya	2-6
Itahashi, Yuki	*1P-68	Kobayashi, Mikio	*1P-9
Iwasa, Yoshihiro	1P-68	Kobayashi, Yoshihiro	1P-14, 1P-45, 1P-55
J		Kodama, Takeshi	1P-50, 1P-78, 1P-79, 1P-80
Jeon, Il	1P-46, 1P-49, 3-4, 3-5	Koga, Naoki	*1P-16
Jeon, Sugyeong	1P-48	Kogure, Shugo	*1P-41
Jiang, Hua	1P-46	Kohata, Ikuma	*1P-47
K		Komai, Takaha	1P-54
Kaida, Takazumi	*1P-28	Komatsu, Natsumi	3-8
Kameda, Tomoshi	1P-20	Kondo, Daiyu	*3-19
Kaneko, Kentaro	*1P-30	Kondo, Shu	*1P-74, 1P-75
Kaneko, Takuhei	2-1	Kono, Junichiro	3-8
Kaneko, Toshiro	1P-53, 3-16	Kono, Yuga	*1P-44
Karasawa, Shusaku	*1P-34	Koreeda, Akitoshi	1P-24
Kashio, Tatsuya	3-20	Kubo, Osamu	1P-21
Kataoka, Masako	3-19	Kumamoto, Akihito	1P-61
		Kumari, Nikita	*3-7
		Kuwahara, Shota	*3-1
		Kuwahara, Yuki	3-1

L

Lee, Sangsu *3-5
 Li, Kou *1P-31
 Liao, Yong-ping 1P-46
 Lim, Hong en 1P-10, 1P-29, 1P-37,
 1P-56, 1P-67, 3-13
 Lin, Dewu *1P-19
 Lin, Hao-sheng 1P-40, 1P-49, 2-1
 Liu, Chao 3-11
 Liu, Ming 1P-13
 Liu, Zheng 1P-29, 1P-56

M

Ma, Yue 1P-49
 Maeda, Yutaka 1P-33
 Maejima, Moeno *1P-78
 Maki, Hideyuki 1P-3, 1P-33
 Maruyama, Mina 1P-7, 1P-22, 3-12, 3-15,
 3-18
 Maruyama, Shigeo 1P-2, 1P-13, 1P-42,
 1P-46, 1P-47, 1P-49,
 1P-58, 1P-61, 1P-62,
 1P-77, *2S-4, 2-7, 3-4
 Maruyama, Takahiro 1P-34, 1P-74, 1P-75,
 2-6, 3-20
 Matsubara, Manaho 1P-17
 Matsuda, Kazunari 1P-9, 1P-23, 1P-71, 3-3
 Matsui, Keisuke *1P-6
 Matsunaga, Masahiro *3-6
 Matsuo, Yutaka 1P-40, 1P-49, 2-1, 3-4
 Matsuoka, Yuya 1P-18, 3-9
 Matsushima, Kenta 1P-27
 Matsushita, Satoru 1P-42
 Matsuura, Yuuma 1P-16
 Michisuji, Yusuke 1P-84
 Misaizu, Fuminori 1P-49
 Mita, Kazuki 3-20
 Miyamoto, Kazunori 1P-85
 Miyata, Daisuke *1P-40
 Miyata, Yasumitsu 1P-9, 1P-10, 1P-29,
 1P-37, 1P-38, 1P-56,
 1P-57, 1P-64, 1P-67,
 3-13
 Miyauchi, Yuhei 1P-23, 1P-71, 3-3
 Mizuguchi, Yoshikazu 1P-79, 1P-80
 Mizuno, Ryo 1P-41
 Mohammad, Tavakkoli 1P-46
 Mouri, Shinichiro 1P-27
 Murahashi, Tomoaki 3-20
 Murakoshi, Kei 1P-54

Muranaka, Atsuya 1P-85
 Murera, Diane 2-2
 Muroga, Shun *1P-4
 Muto, Nobuhiro *1P-18, 3-9

N

Nagai, Kohei 1P-72
 Nagai, Yukiko *1P-11
 Nagano, Mai 1P-57
 Nagashio, Kosuke 1P-67
 Naka, Sadahito *1P-32
 Nakagawa, Kenta 1P-3, 1P-33
 Nakajima, Haruna *1P-2
 Nakamura, Eiichi 3-11
 Nakamura, Kenta 1P-11
 Nakamura, Kosuke 1P-83
 Nakamura, Masakazu 3-7
 Nakanishi, Yusuke 1P-10, 1P-29, 1P-37,
 1P-56, 1P-67
 Nakano, Takayuki 1P-44, 1P-70
 Nakashima, Asato 3-20
 Nam, Jeong-seok 1P-46, 3-4, 3-5
 Namiki, Hiromasa 1P-68
 Naritsuka, Shigeya 1P-34, 1P-74, *3-20
 Narituka, Shigeya 1P-75
 Negishi, Royta 1P-55
 Nema, Hirofumi *1P-24
 Nemoto, Masaya 1P-85
 Niidome, Yoshiaki *1P-59
 Niiyama, Hiroto 1P-3
 Nishidome, Hiroyuki *1P-72, 3-8
 Nishihara, Taishi 1P-23, 1P-71
 Nishikiori, Yuichi 1P-1
 Nishimura, Tomoaki 1P-83
 Nishina, Yuta 2-2, 3-14
 Noda, Suguru 1P-1, 1P-28, 1P-30,
 1P-87, *2I-2
 Nonoguchi, Yoshiyuki 1P-67
 Numata, Shunsuke *1P-52

O

Ochi, Hayato 1P-1
 Ogata, Hironori 1P-12, 1P-52, 1P-86
 Ogura, Hiroto *1P-67
 Ogura, Tomohiro 1P-38
 Ohno, Jun 1P-11
 Ohno, Yutaka 1P-41, 3-6
 Oishi, Eiichi 1P-24
 Okada, Ryotaro 3-8

Okada, Susumu	1P-7, *1P-22, 3-12, 3-15, *3-18	Seo, Seungju	3-4
Okamoto, Naofumi	3-7	Sharma, Kamal	1P-34, 1P-74, 1P-75
Okazaki, Toshiya	1P-4	Sharma, Kamal prasad	2-6
Okubo, Hitomi	1P-72	Shawky, Ahmed	3-4
Osawa, Eiji	1P-85, *3-10	Shimizu, Hiroshi	1P-10, *1P-29, 1P-56
Osawa, Toshio	1P-28, 1P-87	Shimizu, Shun	*1P-36
Otsuka, Keigo	1P-13, 1P-42, 1P-47, 1P-58, 1P-61, 1P-77, 2-7, 3S-1	Shimizu, Yoshiki	1P-15, 1P-76, 2-5
Otuka, Tomohiro	3-16	Shimura, Eriko	3-1
Oya, Shuma	*1P-33	Shinokita, Keisuke	1P-9, *3-3
Ozawa, Masaki	1P-16	Shiraki, Tomohiro	1P-32, 1P-59, *1P-73
P		Shiromaru, Haruo	1P-78
Pandey, Manish	3-7	Solís-fernández, Pablo	1P-39, 1P-65
Park, Se hwan	1P-48	Suenaga, Kazu	1P-61
Peng, Bo	1P-46	Sugai, Toshiki	3-1
Peng, Lian-mao	2S-2	Sugihara, Taiki	*1P-42
Prassides, Kosmas	1P-6	Sugime, Hisashi	1P-1, 1P-28, 1P-87
Pu, Jiang	1P-10, 1P-38, 1P-56, 1P-64	Sugizaki, Yoshiaki	1P-36, 2-3
R		Suzuki, Daichi	*3-2
Rahman, Md. ashiquar	1P-57	Suzuki, Soma	*1P-38
Ravat, Prince	3-11	T	
Reina, Giacomo	*2-2	Tabata, Hiroshi	1P-21
Ruiz, Amalia	2-2	Tabata, Kento	1P-44
S		Takahashi, Hiromu	1P-28
Saida, Takahiro	1P-34, 1P-74, 1P-75	Takai, Kazuyuki	1P-83
Saito, Nagahiro	2-1	Takaki, Hiroshi	1P-33
Saito, Riichiro	1P-26, 1P-51, *2S-3	Takakura, Akira	1P-23, 1P-71
Saito, Shigeki	1P-17	Takamura, Makoto	1P-55
Saito, Shogo	1P-24	Takei, Kuniharu	1P-25, 3-17
Saito, Takeshi	3-1	Takenobu, Taishi	1P-10, 1P-38, 1P-56, 1P-64
Saito, Yahachi	*3-14	Tanaka, Kenya	*1P-23
Sakakita, Hajime	1P-15, 1P-76, 2-5	Tanaka, Koichiro	1P-72
Sakano, Masato	*3S-2	Tanaka, Kosuke	*1P-70
Sakurai, Shunsuke	1P-15, 1P-76, *2-5	Tanaka, Naoki	1P-5
Sasagawa, Takao	1P-68, *3S-3	Tanaka, Ryoga	1P-57
Satake, Masamitsu	1P-14	Tanaka, Takeshi	1P-20, 1P-71, 2-4, *2I-1
Sato, Naofumi	*3-16	Tanaka, Tomomi	3-1
Sato, Shintaro	3-19	Tanaka, Toshihiko	1P-85, 3-10
Sato, Shu	1P-42	Tang, Daiming	1P-61
Sato, Yuta	1P-61	Taniguchi, Takashi	1P-2, 1P-66, 3-3, 3S-1
Sawada, Tetsuro	1P-87	Taniyasu, Yoshitaka	1P-55
Segawa, Yasumoto	1P-23	Terasaki, Nao	3-2
Sekine, Ryosuke	3-11	Thanh cuong, Nguyene	3-18
Seo, Mizuki	3-16	Tian, Yuan	*1P-26, 1P-51
		Togo, Takahashi	*1P-64
		Toko, Kaoru	*2S-6
		Tomizawa, Hideyuki	1P-36, 2-3
		Tsuji, Takashi	1P-15, *1P-76, 2-5
		Tsurusaki, Akihiro	1P-81

Tsuzuki, Mayumi	2-4	Yasui, Kotaro	*1P-1
U		Yi, Hsin	*1P-65
Uchida, Kento	1P-72	Yoda, Takaki	*1P-86
Uchiyama, Masanobu	1P-85	Yomogida, Yohei	1P-17, 1P-18, 1P-57, 1P-60, 1P-72, *3-8, 3-9, 3-13
Ueji, Kan	1P-17, 1P-18, 3-8, *3-9, 3-13	Yoshida, Akari	1P-17
Ueno, Hiroshi	1P-49	Yoshikawa, Ryo	1P-47
Ueno, Keiji	1P-2	Yoshimura, Takeshi	1P-81
Ukhtary, M. shoufie	1P-26	Yotsuya, Shotaro	*1P-81
Ukhtary, Muhammad shoufie	1P-51	Yuan, Wenyu	3-13
Usami, Rei	*1P-8	Yuhara, Wataru	1P-84
W		Yumura, Takashi	1P-43
Wada, Momoyo	1P-20	Z	
Wada, Naoki	1P-9	Zaumseil, Jana	1P-18, 3-9
Wakabayashi, Katsunori	1P-63	Zhang, Qiang	1P-46, 1P-61, 3-5
Wakabayashi, Rie	1P-59	Zhang, Shaochun	1P-67
Wakabayashi, Tomonari	*1P-50, 1P-78	Zheng, Liu	1P-66
Wakebe, Kazuki	1P-50	Zheng, Yongjia	1P-58, *1P-61, 2-7
Wang, Mengyue	*1P-14	Zhou, Ruifeng	1P-54
Wang, Shuhui	*1P-13	Zhou, Ying	1P-4
Watanabe, Kenji	1P-2, 1P-66, 3-3, 3S-1	Zolotoukhina, Tatiana	1P-84
Wei, Nan	1P-46		
Wu, Hengkai	*1P-71		
X			
Xiang, Rong	1P-13, 1P-58, 1P-61, 2-7, 3-4		
Y			
Yagi, Takashi	1P-18, 3-9, 3-13		
Yakobson, Boris	1P-58		
Yamada, Maho	2-5		
Yamada, Takeo	1P-4		
Yamada-takamura, Yukiko	3S-4		
Yamagishi, Kazuki	*1P-80		
Yamamoto, Daiki	1P-34, 1P-74, *1P-75, 2-6		
Yamamoto, Takahiro	1P-17		
Yamashita, Aichi	1P-79, 1P-80		
Yamashita, Daiki	3S-1		
Yamashita, Kenichi	1P-38		
Yana, Takumi	2-1		
Yanagi, Kazuhiro	1P-17, 1P-18, 1P-57, 1P-60, 1P-72, 3-8, 3-9, *3-13		
Yanagisawa, Haruaki	3-11		
Yao, Yao	*1P-55		

複写をご希望の方へ

フラーレン・ナノチューブ・グラフェン学会では、複写複製および転載複製に係る著作権を学術著作権協会に委託しています。当該利用をご希望の方は、学術著作権協会 (<https://www.jaacc.org/>) が提供している複製利用許諾システムもしくは転載許諾システムを通じて申請ください。

注意: 著作物の引用、翻訳等に関しては、(社)学術著作権協会に委託致しておりません。直接、フラーレン・ナノチューブ・グラフェン学会へお問い合わせください。

Reprographic Reproduction outside Japan

Fullerenes, Nanotubes and Graphene Research Society authorized Japan Academic Association For Copyright Clearance (JAC) to license our reproduction rights and reuse rights of copyrighted works. If you wish to obtain permissions of these rights in the countries or regions outside Japan, please refer to the homepage of JAC (<http://www.jaacc.org/>) and confirm appropriate organizations to request permission.

In order to obtain permission to quote and/or translate, please contact the copyright holder directly.

2021年8月25日発行

第61回フラーレン・ナノチューブ・グラフェン総合シンポジウム 講演要旨集

《フラーレン・ナノチューブ・グラフェン学会》

〒464-8601 愛知県名古屋市千種区不老町

名古屋大学 未来材料・システム研究所

未来・エレクトロニクス集積研究センター 大野研究室内

Phone/Fax: 03-3830-4848

E-mail: secretariat@fntg.jp

URL: https://fntg.jp/jp_new/

印刷 / 製本 中西印刷株式会社

高感度近赤外線
2次元 InGaAs ハイスピードカメラ

NIRvana® HS

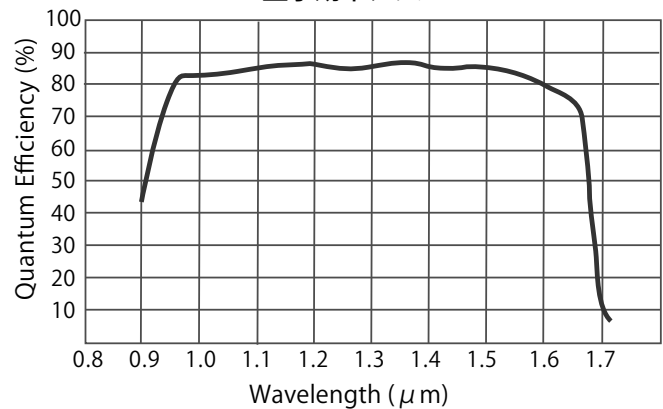
- ハイスピード
250 fps (full 640x512 pixels)
1200 fps (200x200 pixels)
- 多彩な読み出しモード
Integrate While Read (IWR) mode搭載
マルチROI
- 低読み出しノイズ
- USB3.0接続



アプリケーション例

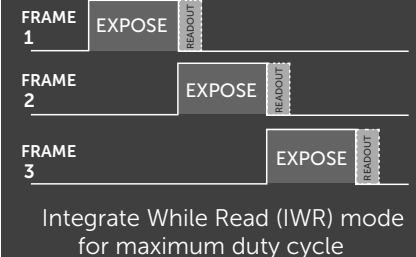
- ・フォトニック結晶PLイメージング及びスペクトル
- ・一重項酸素イメージング及びスペクトル
- ・太陽電池PLイメージング及びスペクトル
- ・天体観測微弱光イメージング
- ・食品断面イメージング
- ・In-Vivoイメージング など

量子効率グラフ



仕様

モデル	NIRvana HS	NIRvana:640	NIRvana:640LN
センサー	640 x 512 x InGaAs		
素子サイズ	20 μm x 20 μm		
波長範囲	0.9 ~ 1.7 μm		
冷却温度	-55°C (-50°C空冷)	-80°C	-190°C
ダークチャージ	700 e-/p/sec	300 e-/p/sec	<8 e-/p/sec
読み出しノイズ	<60 e-rms	<120 e-rms	15 e-rms
ダイナミックレンジ	16 Bit (>15Bit@1 素子)		
フレームレート	250 fps	110 fps	2.77 fps@250KHz
インターフェース	USB3.0	Gig E	



www.pi-j.co.jp

テレダイン・ジャパン株式会社 プリンストンインスツルメンツ

〒170-0013 東京都豊島区東池袋 3-4-3 池袋イースト TEL 03-6709-0631 FAX 03-6709-0632



原子分解能分析電子顕微鏡
JEM-ARM300F2 GRAND ARM™2

40.5 pm

新しく開発された原子分解能分析電子顕微鏡 (GRAND ARM™2) では、
新ポールピース "FHP2" の導入に加え、防音・耐震・レンズ安定度の強化を行い、
世界最高峰の分解能を実現しています。
この世界最高峰の分解能とEDS性能を両立させ、さまざまな研究に対応できます。

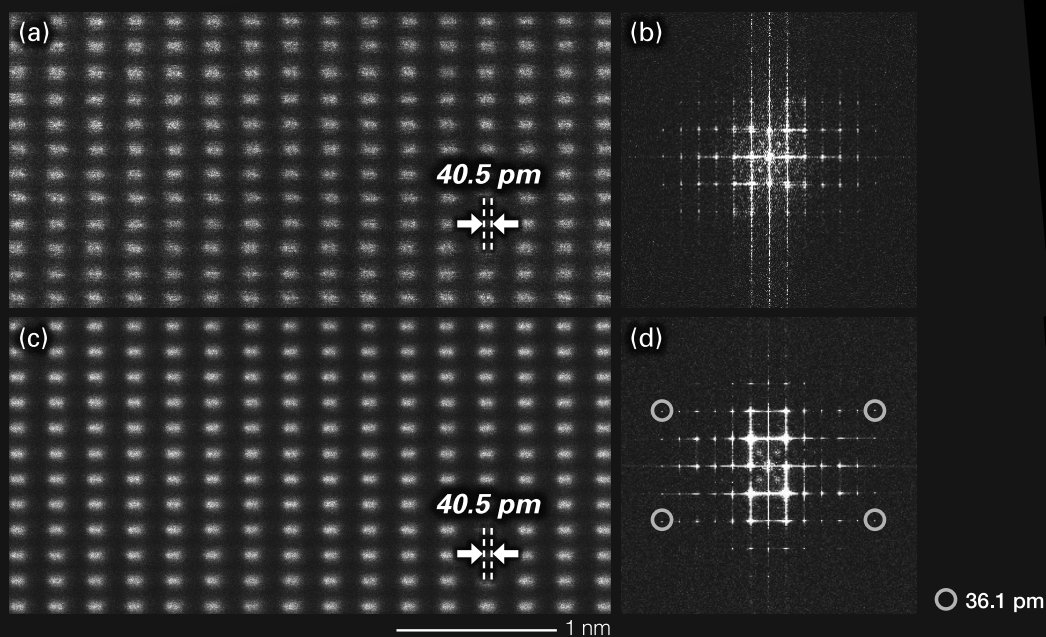


図1 (a) 1フレームで得られたGaN[212]のSTEM-HAADF像とそのFFTパターン(b)。
(c) 20フレーム積算で得られたGaN[212]のSTEM-HAADF像とそのFFTパターン(d)。

JEOL 日本電子株式会社

本社・昭島製作所 〒196-8558 東京都昭島市武蔵野3-1-2 TEL:(042)543-1111 (大代表) FAX:(042)546-3353
www.jeol.co.jp ISO 9001・ISO 14001 認証取得

JEOLグループは、「理科学・計測機器」「産業機器」「医用機器」の3つの事業ドメインにより事業を行っております。
「理科学・計測機器事業」電子光学機器・分析機器・計測検査機器 「産業機器事業」半導体関連機器・産業機器 「医用機器事業」医用機器

モデルチェンジ ～スマートなデザインに簡単操作～

BRANSON 超音波ホモジナイザー

長くご愛顧いただいておりますBRANSON超音波ホモジナイザーで新たなモデルが誕生しました。

主な特長

- 1.電気エネルギーから超音波振動への変換効率が95%以上
→ 無駄なエネルギーロスが小さく、安定した振幅が得られる。
- 2.通常では、液体の種類によって振幅が安定し難い。
→ 条件を変えても一定の振幅を保つ機能がついている。
- 3.ジュール (watt×sec) による発振制御が可能
→ Total何ジュールでこの処理が完了するという情報が論文に掲載できる。

20kHz超音波ホモジナイザー
BRANSON SONIFIER SFX250,550

40kHz超音波ホモジナイザー
BRANSON SONIFIER SFX150HH



主なアプリケーション

分散

カーボンナノチューブ 有機顔料 無機顔料 セラミック セメント 感光体 記録材料
磁性粉 粉末冶金 酸化鉄 金属酸化物 シリカ アルミナ カーボンブラック
ポリマー ラテックス 製紙 ファンデーション
研磨剤 電池 フィラー 光触媒 触媒 ワクチン 体外診断薬 歯磨き粉 シャンプー
半導体 電子基盤 液晶 貴金属 金属 宝石 タイヤ 発酵菌類 その他

乳化

エマルジョン製剤 農薬 トナー ラテックス 界面活性剤 クリーム 乳液 その他

日本国内販売総代理店



株式
会社

セントラル科学貿易

東京本社: 〒136-0071 東京都江東区亀戸1-28-6 タニビル3F

TEL 03-5627-8150 FAX 03-5627-8151

技術物流センター: 〒272-0146 千葉県市川市広尾2-1-9

TEL 047-701-6100 FAX 047-701-6116

大阪支店: 〒533-0031 大阪府大阪市東淀川区西淡路1-1-36 新大阪ビル

TEL 06-6325-3171 FAX 03-6325-5180

福岡営業所: 〒812-0016 福岡県福岡市博多区博多駅南1-2-15 事務機ビル

TEL 092-482-4000 FAX 092-482-3797

札幌出張所: 〒001-0911 北海道札幌市北区新琴似11条13-7-13-2

TEL 011-764-3611 FAX 011-764-3612

<https://www.cscjp.co.jp>

グラフェンの量産化に向けて...

Neutron



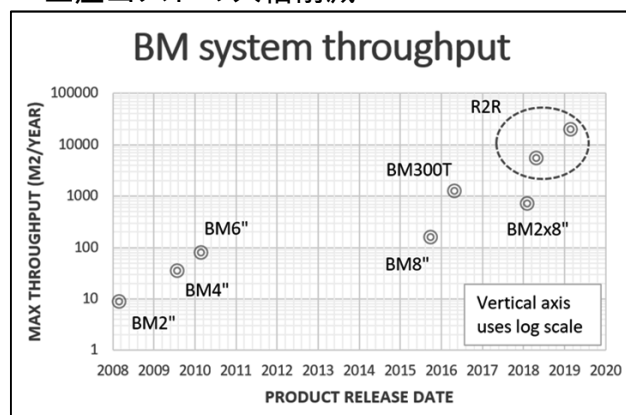
▼概要▼

Roll-to-Roll (R2R)

ロール状に巻いた金属ホイルを、巻き取りながら連続的にグラフェンを成長可能な量産用装置

◆特徴◆

- 連続成長
- 生産能力 **20,000 m² / year**
- Cuホイル及びSteelホイルの両方に対応
- 大気環境で成長可能で、真空チャンバ不要
- 生産コストの大幅削減



CCS 2D & NOVO



▼概要▼

2D材料及びグラフェンの成長装置

◆特徴◆

- Closed Coupled Showerhead(CCS) 技術を適用
- 成長温度は**1400°C**まで昇温可能
- **基板に直接**2D材料またはグラフェンを成長可能
- プラズマ機能装備
- 多種原料を搭載可能(hBN, MoS₂, WSe₂)

BM300T



▼概要▼

ウェハ基板上CNT及びグラフェン成長装置

◆特徴◆

- 12"及び8" wafer 自動搬送対応
- プラズマ機能装備
- High 2D/G > 2.5の高品質を達成

GEMINI 超高安定性 干渉計



時間分解蛍光スペクトル、コヒーレントラマン分光、ポンププローブ測定、単一分子分光など幅広い用途に有用。堅牢・コンパクトな干渉計

- ・高効率、高感度
- ・1秒以内の高速スキャン
- ・コンパクト、定価価格
- ・優れた耐振動性能
- ・波長範囲 250 ~ 3500 nm
- ・外形寸法 100 x 110 x 65 mm

アプリケーション

- ・時間分解蛍光スペクトル測定
- ・EEM 測定
- ・ポンププローブ過渡吸収測定 他



MultiHarp TCSPC (時間相関単一光子検出)



時間相関単一光子計数 (TCSPC)、マルチチャンネルでのスケールリング (MCS) 等
ピコ秒~ミリ秒分解能 イベント・タイミングモジュール

- ・独立入力チャンネル：最大 64 ch. *
- ・デッドタイム 最短 650 ps *
- ・チャンネル間のデッドタイム 無
- ・最小基本分解能：5 ps *
- ・データスループット：200M cps *
- ・時間タグ時間分解 (TTTR) モード

* Multi Harp 160 での値

アプリケーション

- ・時間分解蛍光スペクトル測定
- ・蛍光寿命イメージング (FLIM)
- ・時間分解フォトルミネセンス計測 (TRPL)
- ・アンチバンチング
- ・量子暗号・量子通信
- ・蛍光相関分光 (FCS)
- ・フェルスター共鳴エネルギー移動 (FRET)
- ・誘導放出抑制顕微鏡 (STED)
- ・ポンププローブ過渡吸収測定 他

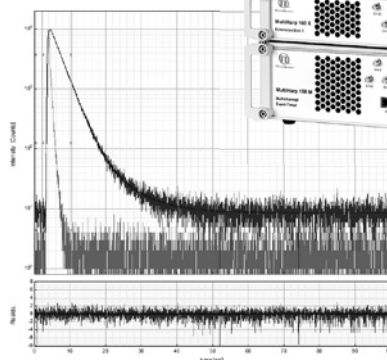


MultiHarp 150

MultiHarp 150
デモ機
あります



MultiHarp 160



<https://www.japanlaser.co.jp/>

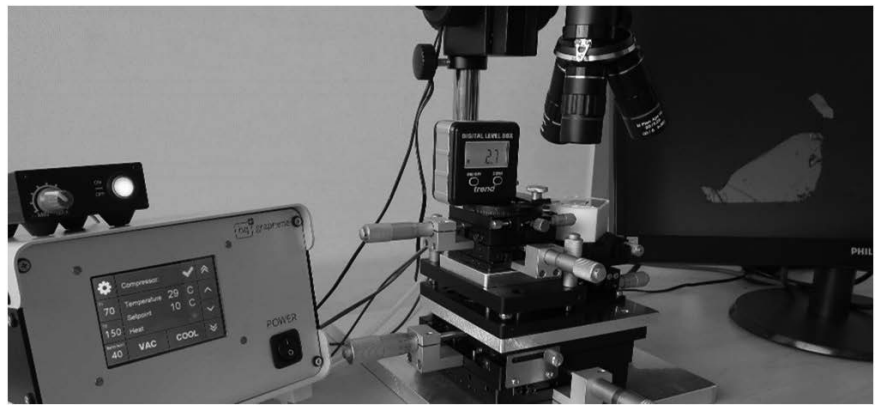
E-mail: jlc@japanlaser.co.jp

JLC 株式会社日本レーザー

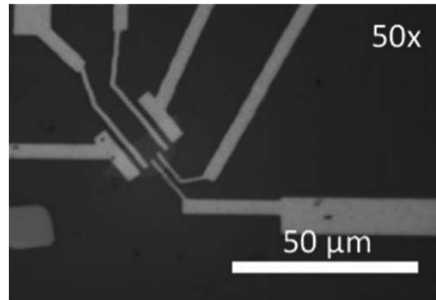
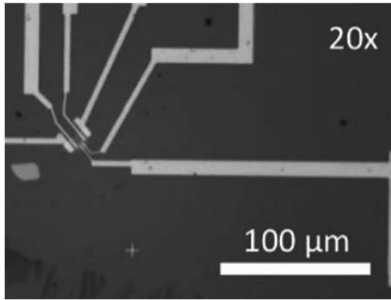
東京本社 東京都新宿区西早稲田2-14-1 TEL 03-5285-0861
大阪支店 大阪市東淀川区東中島1-20-12 TEL 06-6323-7286
名古屋支店 名古屋市中区錦3-1-30 TEL 052-205-9711

設計 & 生産

hq⁺ graphene



2D Heterostructure Transfer System



NEW!!

fully motorized
transfer systems !!

高品質の2D結晶ヘテロ構造を作製するのに必要なすべての機能が含まれています！！

- PDMSスタンプの正確な配置
- Ready to Useのシステム構成
- コンパクト設計
- パソコンによる操作は不要
- 1℃単位での加温設定が可能

デモ機の
貸し出し可能

*HQ Graphene社は高品質の2D単結晶を提供している業界トップクラスのメーカーです。

Abalonyx社品:酸化グラフェン(GO)

modified Hummers法で生成されたGOをペーストor乾燥粉末で提供！

- ・ 20%水性GOペースト(酸性) / 水性10%GO水溶液(酸性度低下)
- ・ <35 meshのGO乾燥粉末、超音波処理で脱イオン水に完全に分散

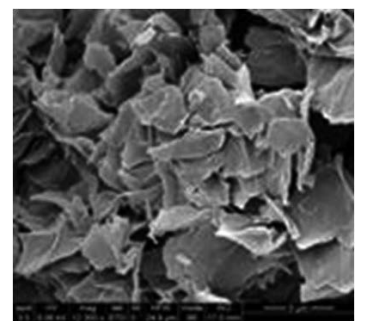
Abalonyx社品:還元酸化グラフェン(rGO)

酸化グラフェンを熱還元して生産したrGOを提供！

- ・ 導電性および疎水性/両親媒性の部分的に還元された rGO
- ・ 独自の圧縮プロセスで製造されたポリマー分散用 rGO

*Abalonyx社: 酸化グラフェン&還元グラフェン製品のリーディングカンパニー

Abalonyx
Innovative materials



無料サンプルあり

Grolltex社品: CVDグラフェン/hBN

高品質なCVDグラフェンおよびhBNを提供！

- ・ 大面積の単層グラフェン/hBNを実現
- ・ 銅フォイル/Si基板以外への転写が可能



GROLLTEX
Graphene-rolling-technologies

Filgen[®]
biosciences & nanosciences

輸入販売元

フィルジェン 株式会社

【お問い合わせ】 TEL : 052-624-4388 FAX : 052-624-4389

メール : biosupport@filgen.jp URL : https://filgen.jp/